

## Some Problems of the Electrical Double Layer

by Roger Parsons

Gates and Crellin Laboratories of Chemistry  
California Institute of Technology  
Pasadena, California 91109

### Introduction

Detailed results for the adsorption of ions at mercury electrodes are now available for a number of different systems. Results for the potassium halides in water are summarized elsewhere.<sup>1</sup> Li,<sup>2</sup> Rb,<sup>2</sup> and Cs<sup>2,3</sup> chlorides have also been studied in water. Surface excesses at the mercury-water interphase have also been obtained for NaCNS,<sup>2,4</sup> NaCN,<sup>2</sup> NaClO<sub>4</sub>,<sup>2</sup> NH<sub>4</sub>ClO<sub>4</sub> in NH<sub>4</sub>F,<sup>5</sup> HClO<sub>4</sub>,<sup>6</sup> NaNO<sub>3</sub>,<sup>7</sup> NH<sub>4</sub>NO<sub>3</sub> in NH<sub>4</sub>F,<sup>8</sup> NaClO<sub>3</sub>,<sup>2</sup> NaBrO<sub>3</sub>,<sup>2</sup> NaN<sub>3</sub>,<sup>9</sup> NaH<sub>2</sub>PO<sub>4</sub>,<sup>10</sup> TlF,<sup>11</sup> TlNO<sub>3</sub>,<sup>12</sup> sodium p-toluene sulphonate,<sup>13</sup> sodium benzene-m-disulphonate,<sup>14</sup> sodium formate,<sup>15</sup> sodium acetate,<sup>15</sup> sodium propionate,<sup>15</sup> concentrated solutions of strong acids,<sup>16</sup> tetra-alkyl ammonium iodides,<sup>17</sup> long chain ions,<sup>18</sup> and aromatic cations.<sup>19,20,21</sup> The adsorption of ions on mercury from non-aqueous solution has been studied to a smaller extent but results are available for KI in KF in methanol,<sup>22</sup> KCl,<sup>23</sup> NaCl,<sup>24</sup> CsCl,<sup>24</sup> and KI<sup>25</sup> in formamide, LiCl, KCl, and CsCl in N-methyl formamide, alkali formates, phosphates, and sulphates in formic acid.<sup>15</sup> The adsorption of thiourea has been studied in detail also in water,<sup>27</sup> methanol,<sup>22</sup> and formamide.<sup>28</sup> The adsorption of other non-electrolytes has been reviewed thoroughly by Damaskin and Frumkin.<sup>29</sup> Adsorption on solid metals has also been studied in a more quantitative way in recent years.<sup>30</sup> Although the results are of considerable interest, they are in general not sufficiently accurate to be useful in the examination of the detailed structure of the double layer.

### The Diffuse Layer

The adsorption of ions at an electrode is usefully classified as specific or non-specific. This is an operational classification which in practice depends on the simple model of non-specific adsorption introduced by Gouy<sup>31</sup> and Chapman.<sup>32</sup> This model is analogous to the Debye-Hückel theory of electrolytes. In this model<sup>33,34,35</sup> adsorption arises as a result of the electrostatic interaction between point charge ions and the charge on the electrode. The size of the ions is introduced only as a distance of closest approach to the electrode ( $x_2$ ). This results in an ionic atmosphere or diffuse layer extending from  $x_2$  and decaying out into the bulk of the solution, the net charge on this diffuse layer being equal and opposite to that on the metal surface. Specific adsorption is then all adsorption which cannot be accounted for by the Gouy-Chapman theory. Most obviously it will occur when ions can approach the electrode more closely than  $x_2$  and specific 'chemical' interaction occurs between ion and electrode, but other effects, such as the 'squeezing out' of a structure-breaking ion from the bulk of the solution may also contribute to the specific interaction. Because such specific forces are short-range, specifically adsorbed ions are usually located in a monolayer with their centers in a plane at  $X_1$  from the electrode ( $x_1 < x_2$ ).

This is not a very sophisticated model, but as in the case of electrolyte theory, progress beyond the first approximation is difficult. Numerous attempts to improve the theory of the diffuse layer have not resulted in a widely used model for two reasons: first, the theories suggest that modifications are small under practical conditions, and their use is much more complicated than the Gouy-Chapman theory; second, there have been very few experimental tests of the theory under conditions where deviations from it might be expected; i. e., at high concentrations and high electrode charges. Such tests are difficult because under these conditions the diffuse layer makes an insignificant contribution to the electrode capacity. Measurements in mixed electrolytes<sup>36</sup> and of the kinetics of electrode reactions<sup>35,37</sup> provide the most critical tests, but interpretation is not unambiguous. For the limited object of defining specific adsorption, recent theoretical work<sup>38</sup> suggests that the relation between cationic and anionic charge contributions in the diffuse

layer is unchanged by improvements in the model; hence, continued use of the Gouy-Chapman theory may be justified. On the other hand, the simple theory probably gives an inaccurate potential distribution in the diffuse layer.

### The Inner Layer

The theory of the inner layer is more difficult than that of the diffuse layer because it is a region of very small thickness, probably one solvent molecule thick, and its composition varies within wide limits. It is very doubtful whether macroscopic concepts such as dielectric constant have real meaning for this region although they continue to be used. The problem of electrostatic interaction in the inner layer has been extensively discussed in two recent reviews.<sup>39,40</sup> As mentioned above, short-range forces between adsorbed particles and between particles and electrode are at least as important in this region as are the electrostatic forces. It seems likely<sup>14,41</sup> that the two types of forces can be meaningfully separated, at least to a first approximation, in the way first proposed by Stern.<sup>39</sup> That is, the non-electrostatic particle-electrode interaction energy is approximately independent of the charge on the electrode. This 'chemical' adsorption energy is clearly<sup>40</sup> a difference between the energy of interaction of the adsorbing particle with the electrode and that of the solvent particle. A detailed calculation<sup>41</sup> for simple ionic (particularly halide) adsorption has suggested that the observed behavior can be explained without invoking the formation of a chemical bond between the adsorbing particle and the electrode. However, it seems more probable that chemical bond formation occurs to a different extent with different species ranging from thiocyanate ion and thiourea where sulphur is undoubtedly bonded to the mercury electrode through to aliphatic sulphonates and carboxylates where bond formation seems very unlikely. Since the two extremes behave in a generally similar way it is unlikely that a very definite conclusion can be made for intermediate cases as to whether bond formation occurs. On the other hand, there seems to be little doubt about the importance of solvation effects<sup>44</sup> in solution and in the double layer.

The energy of interaction of the adsorbing species with the electrode would be obtained most unambiguously from measurements at very small adsorbed amounts, but these are difficult to make reliably. Consequently, the usual procedure is to use measurements at higher adsorbed densities and to allow for the particle-particle interactions by theoretical calculation or to extrapolate to zero adsorbed density using an adsorption isotherm. This procedure at present introduces uncertainty because accurate calculations of the interaction are not possible and the correct form of the adsorption isotherm is not known, because it depends on a knowledge of the free energy of one component in a dense two-dimensional non-ideal liquid mixture. Nevertheless, an empirical extension<sup>44, 45, 46</sup> of the Zhukovitskii-Flory-Huggins model seems to satisfy a number of limiting criteria and to be capable of useful interpretation: allowance for difference of size of adsorbate and solvent, approach to saturation, etc. At sufficiently low densities the interaction coefficient may be simply related to a two-dimensional second virial coefficient. In a number of ionic systems this is found to be extremely large, possibly reflecting the strong repulsive forces between ions of like sign. However, these forces are to a large extent screened<sup>34</sup> by the presence of conducting walls (metal and diffuse layer) on either side of the inner layer. Further, the magnitude of the second virial coefficient of iodide ion is strongly solvent dependent.<sup>22, 25</sup> This does not seem to be readily explicable in simple electrostatic terms since the effective dielectric constant in the inner layer should vary very little with the solvent. In contrast, the second virial coefficient of thiourea has almost the same value in the three solvents studied<sup>22, 27, 28</sup> and this value is about that to be expected from a simple electrostatic model.<sup>47</sup> It is possible that the behavior of ions is due to solvation in the inner layer.<sup>8</sup>

The problem of solvent properties in the inner layer has been frequently related to the appearance of a 'hump' in the capacity-potential curve.<sup>48</sup> On the other hand, the 'hump' has been attributed entirely to the result of ionic specific adsorption.<sup>43</sup> There is no doubt that the latter can cause humps; in the simplest case the capacity is proportional to the slope of the adsorption isotherm which must pass through a maximum between zero coverage and saturation; the benzene-disulphonate

ion<sup>14</sup> is a good illustration of such behavior. Nevertheless, there is little doubt that the hump in formamide<sup>49</sup> and in N-methylformamide<sup>50</sup> is attributable to solvent reorientation and it is probable that this effect is also present in water. Until recently it seemed that humps were absent in solvents of lower dielectric constant than water. Now, however, it is known that they also occur in propylene carbonate,<sup>51</sup> ethylene carbonate,<sup>52</sup> dimethyl sulphoxide,<sup>53</sup> sulpholane,<sup>51</sup> 4-butylolactone,<sup>52</sup> and 4-valerolactone.<sup>52</sup> However, the nature of the hump in these solvents remains to be investigated. The simultaneous presence of an adsorption hump and a solvent hump can be discerned in the capacity curve of thiourea in a formamide solution of KF (Fig. 1). It has also been suggested<sup>54</sup> that the presence of adsorbed ions may enhance or reduce a hump due to solvent reorientation by interacting with the solvent molecules in the inner layer. Some support for this view may be obtained from a consideration of the isoelectronic series:  $\text{ClO}_4^-$ ,  $\text{HSO}_4^-$ , and  $\text{H}_2\text{PO}_4^-$ . These ions are all about the same size but their interaction with bulk water varies considerably:<sup>55</sup>  $\text{ClO}_4^-$  is a structure breaker while  $\text{H}_2\text{PO}_4^-$  is heavily hydrated. This sequence is reflected in their adsorption behavior on mercury. At potentials negative to the point of zero charge the amount of adsorption is in the sequence  $\text{ClO}_4^- > \text{HSO}_4^- > \text{H}_2\text{PO}_4^-$  while at high positive charges the sequence is reversed. The magnitude of the hump is also in the sequence  $\text{ClO}_4^- > \text{HSO}_4^- > \text{H}_2\text{PO}_4^-$  (Fig. 2). It is possible that the presence of  $\text{ClO}_4^-$  in the inner layer facilitates the reorientation of water, while the  $\text{HPO}_4^-$  ion tends to reduce its freedom to reorient.

#### References

1. J. Lawrence, R. Parsons, and R. Payne, This Symposium.
2. H. Wroblowa, Z. Kovac, and J. O'M. Bockris, *Trans. Faraday Soc.*, **61**, 1523 (1965).
3. A. N. Frumkin, R. V. Ivanova, and B. B. Damaskin, *Doklady Akad. Nauk, S.S.S.R.*, **157**, 1202 (1964).
4. R. Parsons and P. C. Symons, unpublished work.
5. R. Payne, *J. Phys. Chem.*, **70**, 204 (1966).
6. R. Parsons and R. Payne, unpublished work.
7. R. Payne, *J. Electrochem. Soc.*, **113**, 999 (1966).
8. R. Payne, *J. Phys. Chem.*, **69**, 4113 (1965).
9. C. d'Alkaine, E. R. Gonzalez, and R. Parsons, unpublished work.
10. R. Parsons and F.G.R. Zobel, *J. Electroanal. Chem.*, **9**, 333 (1965).
11. P. Delahay and G. G. Susbielles, *J. Phys. Chem.*, **70**, 547 (1966).
12. G. G. Susbielles, P. Delahay, and E. Solon, *J. Phys. Chem.*, **70**, 2601 (1966).
13. J. M. Parry and R. Parsons, *J. Electrochem. Soc.*, **113**, 992 (1966).
14. J. M. Parry and R. Parsons, *Trans. Faraday Soc.*, **59**, 241 (1963).
15. J. Lawrence and R. Parsons, unpublished work.
16. Z. A. Iofa and A. N. Frumkin, *Zhur. Fiz. Khim.*, **18**, 268 (1944).
17. M.A.V. Devanathan and M. J. Fernando, *Trans. Faraday Soc.*, **58**, 368 (1962).
18. K. Eda, *Nippon Kagaku Zasshi*, **80**, 343, 349, 461, 465 (1959); **81**, 689, 875, 879 (1960).
19. E. Blomgren and J. O'M. Bockris, *J. Phys. Chem.*, **63**, 1475 (1959).
20. B. E. Conway and R. G. Barradas, *Electrochim. Acta*, **5**, 319, 349 (1961).
21. B. E. Conway, R. G. Barradas, P. G. Hamilton, and J. M. Parry, *J. Electroanal. Chem.*, **10**, 485 (1965).
22. J. D. Garnish and R. Parsons, *Trans. Faraday Soc.*, in press.
23. G. H. Nancollas, D. S. Reid, and C. A. Vincent, *J. Phys. Chem.*, **70**, 3300 (1966).
24. B. B. Damaskin, R. V. Ivanova, and A. A. Survila, *Elektrokhimiya*, **1**, 767 (1966).
25. R. Payne, *J. Chem. Phys.*, **42**, 3371 (1965).
26. B. B. Damaskin and R. V. Ivanova, *Zhur. Fiz. Khim.*, **38**, 92 (1964).
27. F. W. Schapink, M. Oudeman, K. W. Leu, and J. N. Helle, *Trans. Faraday Soc.*, **56**, 415 (1960).
28. E. Dutkiewicz and R. Parsons, *J. Electroanal. Chem.*, **11**, 196 (1966).

29. B. B. Damaskin and A. N. Frumkin, *Modern Aspects of Electrochemistry*, III, ed. J. O'M. Bockris and B. E. Conway, Butterworths, London, 1964.
30. E. Gileadi, *J. Electroanal. Chem.*, 11, 137 (1966).
31. G. Gouy, *J. Phys. Radium*, [4], 9, 457 (1910).
32. D. L. Chapman, *Phil. Mag.*, [3], 25, 475 (1913).
33. D. C. Grahame, *Chem. Rev.*, 41, 441 (1947).
34. R. Parsons, *Modern Aspects of Electrochemistry*, I, ed. J. O'M. Bockris and B. E. Conway, Butterworths, London, 1954.
35. P. Delahay, *Double Layer and Electrode Kinetics*, Interscience, Wiley, New York, 1965.
36. K. M. Joshi and R. Parsons, *Electrochim. Acta*, 4, 129 (1961).
37. L. Gierst, L. Vandenberghe, E. Nicholas, and A. Fraboni, *J. Electrochem. Soc.*, 113, 1025 (1966).
38. H. R. Hurwitz, A. Sanfeld, and A. Steinchen-Sanfeld, *Electrochim. Acta*, 9, 929 (1964).
39. S. Levine, J. Mingins, and G. M. Bell, *J. Electroanal. Chem.*, 13, 280 (1967).
40. C. A. Barlow and J. R. Macdonald, *Advances in Electrochemistry and Electrochemical Engineering*, ed. P. Delahay and C. W. Tobias, Interscience, Wiley, in press.
41. S. Levine, G. M. Bell, and D. Calvert, *Can. J. Chem.*, 40, 518 (1962).
42. O. Stern, *Z. Elektrochem.*, 30, 508 (1924).
43. J. O'M. Bockris, M.A.V. Devanathan, and K. Muller, *Proc. Roy. Soc.*, A274, 55 (1963).
44. T. N. Andersen and J. O'M. Bockris, *Electrochim. Acta*, 9, 347 (1964).
45. B. B. Damaskin, *Electrokhimiya*, 1, 63 (1965).
46. R. Parsons, *J. Electroanal. Chem.*, 8, 93 (1964).
47. R. Parsons, *Proc. Roy. Soc.*, 261A, 79 (1961).
48. D. C. Grahame, *J. Chem. Phys.*, 23, 1725 (1955).
49. S. Minc, J. Jastrzebska, and M. Brzostowska, *J. Electrochem. Soc.*, 108, 1161 (1961).
50. B. B. Damaskin and Yu. M. Povarov, *Doklady Akad. Nauk. S.S.S.R.*, 140, 394 (1961).
51. J. Lawrence, B. Sc. Thesis, Bristol, 1964.
52. R. Payne, unpublished work.
53. R. Payne, *J. Am. Chem. Soc.*, in press.
54. E. Schwartz, B. B. Damaskin, and A. N. Frumkin, *Zhur. Fiz. Khim.*, 36, 2419 (1962).
55. M. Selvaratnam and M. Spiro, *Trans. Faraday Soc.*, 61, 360 (1965).

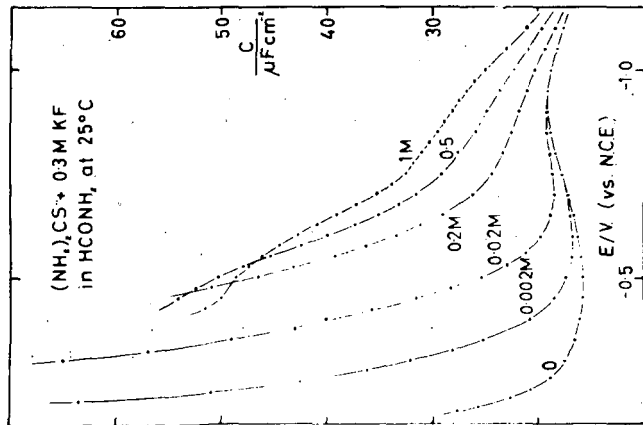


Fig. 1

Capacity of a mercury electrode as a function of potential. The 0.3 M potassium fluoride solution in anhydrous formamide contained thiourea at the concentration shown by each line.

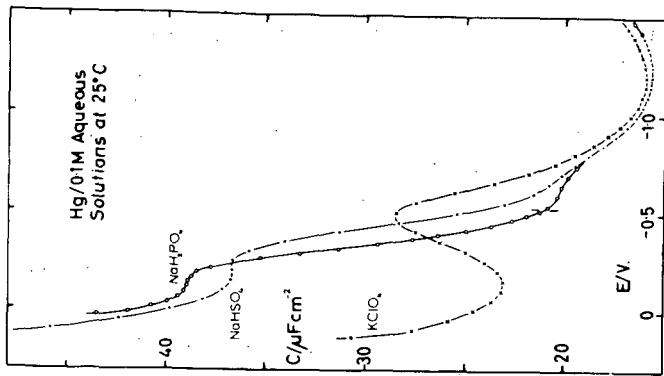


Fig. 2

Capacity of a mercury electrode as a function for 0.1 M aqueous solutions of potassium perchlorate, sodium bisulphate and sodium dihydrogen phosphate.

## THE ESSENTIAL IDEAS OF ELECTRODE KINETICS

Paul Delahay

Department of Chemistry, New York University, Washington Square  
New York, New York 10003

The fundamental concepts in electrode kinetics are introduced. General references in English, or available in translation, include books (1-4), review-volumes (5-6) and reviews (7-8).

Historical (only key ideas)

1. The description of electrode kinetics in terms of current-potential (overvoltage) relationships is primarily based on:
  - (a) the concept of exchange current (Butler, 1924)
  - (b) the introduction of the transfer coefficient (Erdey-Gruz and Volmer, 1930)
  - (c) the correlation between electrode kinetics and double layer structure (Frumkin, 1933)
  - (d) the correlation with adsorption at the electrode (Frumkin and Ershler, 1940; also Temkin)
2. Elucidation of reaction mechanisms involves:
  - (a) the introduction of stoichiometric numbers in the analysis of current - potential relationships (Horiuti and Ikusima, 1939)
  - (b) reaction orders studies (Vetter and Gerischer (1950); also Essin (1940)
  - (c) the detection and, if possible, quantitative estimation of intermediates by various techniques
  - (d) other approaches: double layer effects, detailed analysis of the effect of coupled chemical reactions, isotope effects, etc.
3. "Molecular" interpretation of electrode kinetics requires the development of theories of electron transfer (Marcus (1956)). These had as a precursor the introduction of potential-energy diagrams (Horiuti and Polanyi, 1935; Butler, 1936).

Descriptive Kinetics in Terms of Exchange Current and Transfer Coefficient

1. Introduction of the concept of exchange current by consideration of forward and backward reactions at equilibrium.
2. Discussion of transfer coefficient from potential-energy diagram.
3. Definition of overvoltage and discussion of current-overvoltage characteristics.

Correlation with Double Layer Structure

1. Correction for the concentrations of reactants (and products) in the plane of closest approach.
2. Correction for the drop of potential across the diffuse double layer.
3. Other effects: solvent structure, specific effects, etc.

The first two corrections can be made quite well, in the absence of specific adsorption, on the basis of the theory of the diffuse double layer. Specific adsorption poses problems. Solvent and specific effects do not lend themselves to quantitative analysis at this stage.

### Correlation with Adsorption

The problem is to write current-overvoltage characteristics taking into account the coverage by reactants and/or products. Adsorption equilibrium follows some isotherm, e.g., the Langmuir or Temkin isotherms. The exchange current can then be correlated to the standard free energy of adsorption, and the effect of the nature of the electrode can be investigated. Formulation can be developed for parallel or consecutive reactions.

The effect of potential on adsorption, e.g., organic reactant on mercury, can also be introduced in the current-potential characteristic.

### Elucidation of Mechanisms

Analysis of current-overvoltage variations in terms of stoichiometric numbers, reaction orders, Tafel plots, etc., provides fundamental criteria for the elucidation of reaction mechanisms. These criteria may suffice for simple processes (e.g., overall reaction identical with rate determining step) but in general, they do not allow unambiguous assignment of mechanisms for more complex reactions. Other methods must then be applied (see Historical).

### Mass Transfer

Complication by the finite rate of mass transfer of reactants and products can be avoided when the exchange current is sufficiently low (vigorous stirring, large excess of reactants and products). This complication cannot be avoided with high exchange currents. Diffusion in electrode processes was already understood in the early work of Sand and Cottrell (about 1900) and was extensively studied in polarography (Heyrovsky, 1922; Ilkovic 1934). Combination of kinetics and diffusion has been vigorously studied for the last 20 years (Brdicka and Koutecky, 1947). Hydrodynamic problems can also be attacked (rotating disk electrode, Levich 1942).

### "Molecular" Electrode Kinetics

This is a difficult problem but at least a way to introduce modern chemical physics in electrochemistry (which is mostly prequantum in its present concepts and orientation). Satisfactory treatment has been developed only for processes that do not involve the breaking or making of a bond. Application of theory has been made mostly to homogeneous redox processes, but there are unexploited applications to electrode kinetics. No prediction is ventured about treatments involving a bond-breaking or bond-making process.

### Topics not Treated

The double layer, anodic films, processes with mixed potential (corrosion), semiconductor electrodes, methodology and techniques, etc.

### References

1. G. Kortum, "Treatise on Electrochemistry", 2nd edition, Elsevier, Amsterdam, 1965.
2. K.J. Vetter, "Elektrochemische Kinetik", Springer, Berlin, 1961. English translation by S. Bruckenstein and B. Howard, Academic Press, New York, in press.
3. P. Delahay, "Double Layer and Electrode Kinetics", Interscience-Wiley, New York, 1965.
4. B.E. Conway, "Electrode Processes", Ronald Press, New York, 1965.

5. "Modern Aspects of Electrochemistry", J.O'M. Bockris editor, Butterworths, London, vol.1 (1954), vol.2 (1959), vol.3 (1964).
6. "Advances in Electrochemistry", P. Delahay and C.W. Tobias editors, Interscience-Wiley, New York, vol.1 (1961), vol.2 (1962), vol.3 (1963), vol.4 (1966), vol.5 and 6 in press.
7. Ann. Rev. Phys. Chem., 5, 477 (1954); 6, 337 (1955); 8, 229 (1957); 12, 227 (1961); 15, 155 (1964).
8. Ann. Reports Chem. Soc., 51, 103 (1954); 54, 17 (1957); 55, 67 (1958); 56, 32 (1959); 61, 80 (1964).

ELECTRON TRANSFERS AT ELECTRODES AND IN SOLUTION.  
COMPARISON OF THEORY AND EXPERIMENT

R. A. Marcus

Noyes Chemical Laboratory  
University of Illinois  
Urbana, Illinois 61801

Detailed quantitative information about different theoretical aspects of electron transfer rates in solution and at electrodes can be obtained from appropriate experiments. Recent theoretical work has predicted certain quantitative correlations between rates of crossed-redox reactions and rates of isotopic exchange, and between homogeneous and electrochemical rates. Experimental tests of these predictions yield insight into "intrinsic" and "driving force" factors.

The intrinsic factor is related to differences in properties of oxidized and reduced species (e.g., differences in corresponding bond lengths and differences in solvent orientation polarization). The driving force term is related to the standard free energy of reaction in the homogeneous reaction and to the activation overpotential in the electrode reaction.

Measurements of temperature coefficients of rates in dilute solution provide some information about adiabatic and dielectric saturation effects. Absolute rates, in conjunction with knowledge of bond length differences and bond force constants, provide some insight into the overall picture, though do not disentangle these various factors (intrinsic, adiabatic, unsaturation, etc.).

The present state of experimental information on these theoretical topics will be described.

## Techniques for the Study of Electrode Processes

Ernest Yeager and Frank Ludwig

Department of Chemistry  
Western Reserve University and Case Institute of Technology  
Cleveland, Ohio

The electrochemist is faced with two types of problems in undertaking an experimental study of the kinetics of a particular electrode system.

1. Identification of all of the factors or parameters which must be known and controlled in order to carry out interpretable experiments.
2. Choice of the most promising instrumental techniques for the study.

In conjunction with the first, it can not be emphasized too strongly that the real pitfall in electrochemistry is not the lack of sophisticated instrumental techniques and methods but rather that these techniques do not give adequate knowledge or control over many of the physical and chemical variables which have a major effect on electrode processes. The choice of techniques to be used to study the kinetics of a particular electrode process requires a projection as to the probable mechanism and the magnitude of the corresponding rate constants, the extent of mass transport control and ohmic losses, and then a best matching up of the requirements imposed by these factors to the available techniques. Only then can the experiment be properly designed.

This paper will attempt to identify the critical experimental parameters that must be controlled in electrode kinetic studies and indicate approaches to their control. The various steady-state and transient techniques available for establishing kinetic parameters will then be compared. Some of the features of these methods are summarized in Table 1. Important experimental problems and factors which need to be controlled in electrode kinetic studies are listed in Table 2 together with the procedures or techniques most promising for affecting their control.

Both steady-state and transient techniques have found extensive use in kinetic studies of electrode processes. The most common means for perturbing electrode systems from equilibrium involve the application of some well-defined current or voltage function but such techniques are difficult to apply to electrode systems of high resistivity in the solution or electrode phase (e.g., oxides, organic semiconductors). In such instances changes in temperature, pressure, concentration, or surface area may be used to perturb the electrode system with the relaxation followed by the measurement of the electrode potential--thus avoiding the passage of any appreciable current through the system (see Table 1).

#### Acknowledgment

Some of the experimental aspects of this paper are based on research supported by the Office of Naval Research.

Table 1. Typical electrical methods for the study of electrode kinetics.

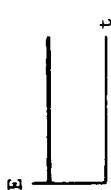
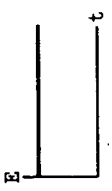
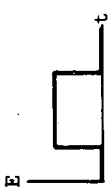
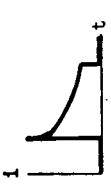
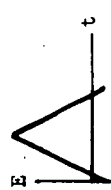
Technique	controlled variable	i-E-time	dependent variable	Maximum $k_s$ (cm/sec)	Remarks
<u>Steady State</u>					
1. direct potentiostatic				$10^{-2}$	Instrumentation simple. Progressive changes in electrode surface cause serious problems in many instances. Can be carried out with very slow voltage sweep (sufficiently slow for capacitive current to be negligible).
2. direct galvanostatic				$10^{-2}$	Instrumentation very simple. Progressive changes in electrode surface cause serious problems in many instances. Can be carried out with ramp function of low slope. Not recommended for systems involving limiting currents or maxima in i vs. E curves.
3. indirect galvanostatic (interrupter)				$10^{-2}$	Yields steady state polarization but also can be used to obtain E vs. t information after interruption of current. Virtually eliminates IR correction problem without use of Luggin capillary. (Other remarks same as for direct galvanostatic method.)
<u>Non-Steady State</u>					
1. voltage step				100	IR drop between working and reference electrodes must be very small. Requires correction at short times for double layer charging. Requires fast action potentiostat plus oscilloscope.
2. cyclic linear sweep voltammetry-slow sweep (<1 V/sec)				$10^{-2}$	Complete analysis very complex. Effective technique for preliminary studies to identify various features. If $dE/dt$ is sufficiently small, may be equivalent to steady state. IR drop between working and reference electrodes must be very small. Requires potentiostat and fast recorder or oscilloscope.

Table 1. Typical electrical methods (continued)

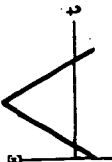
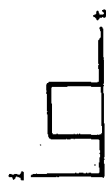
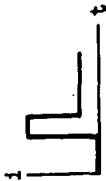
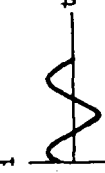
Techniques	controlled variable	i-E-time	dependent variable	Maximum $k_s$ (cm/sec)	Remarks
3. cyclic linear sweep voltammetry-fast sweep (>1 V/sec)			1 cycle	$10^{-1}$	Complete theoretical analysis very complex. Yields information concerning adsorption kinetics (particularly fast). Effective technique for preliminary examination of surface. IR drop between working and reference electrodes must be very small. Requires fast action potentiostat plus oscilloscope.
4. single current step				$10^0$	Instrumentation relatively simple (pulsed galvanostat plus oscilloscope). Relatively easy to correct for IR drop. Requires correction for double layer charging.
5. double current step				$10^1$	Adjust height-width of first current pulse such that $(dE/dt) = 0$ at beginning of second current pulse. Avoids double layer charging correction. Requires more complex instrumentation than single current step method (double current pulse generator plus oscilloscope). Relatively easy to correct for IR drop. For very fast kinetics, must consider diffuse layer-diffusion layer interactions.
6. a-c impedance at reversible potential				$10^1$	Requires measurements over a range of frequencies to separate double layer and kinetic effects. High accuracy possible. Transfer coefficient not determined directly; evaluate from dependence of $i_0$ on concentration. Keep a-c voltage low to avoid non-linear effects. Requires a-c bridge or a-c generator plus oscilloscope.

Table 1. Typical electrical methods (continued)

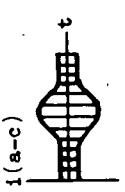
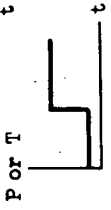
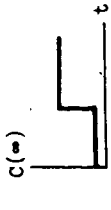
Techniques	controlled variable	i-E-time	dependent variable	Maximum $k_s$ (cm/sec)	Remarks
7. a-c impedance with d-c potential ramp				$10^1$	Theoretical analysis complex. Can yield information concerning adsorption changes in double layer. Instrumentation rather complex (fast action potentiostat with a-c and ramp function generators plus phase meter, detector, and recorder or oscilloscope).
8. Faradaic rectification and distortion				$10^2$	For very fast processes. Requires sophisticated equipment for very fast processes (gated r-f current source capable of providing power). Heat effects can be a problem. Diffuse layer-diffusion layer interactions must be considered for very fast kinetics.
9. Pressure or temperature step techniques				$10^1$ (P step)	After disturbance, relaxation is similar to that with electrical perturbation techniques. Offers advantage that fast kinetics can be studied in systems with insufficient conductivity to pass appreciable current. Pressure step easily obtained with bursting diaphragm ( $10^{-5}$ sec resolution).
10. Concentration perturbation method				$10^{-1}$	After disturbance, relaxation is similar to that with electrical perturbation techniques. Offers advantage that high resistivity can be tolerated. Flow techniques provide convenient means for producing change in bulk concentration ( $10^{-3}$ sec resolution).

Table 2. Typical experimental problems and factors to be controlled in the study of electrode processes in aqueous systems.

Problem or factor	Techniques for controlling or measuring	Remarks
1. Impurity effects a. solution purity	<ol style="list-style-type: none"> <li>1. Use the best of conventional physical and chemical purification procedures (multiple stage distillation, recrystallization, chromatographic purification) followed by <u>in situ</u> adsorption-pre-electrolysis with forced convection at various controlled potentials. Continue adsorption-pre-electrolysis until no further change in kinetics evident.</li> <li>2. Use a minimum volume of solution for a given area of electrodes.</li> </ol>	<p>Probably adequately controlled only in most careful work. Impurities can cause difficulty at small fractions of monolayer coverage if critical sites are blocked or if electronic properties of surface are disturbed in a non-localized manner (e.g., d-orbital poisons). [Monolayer corresponds to 10<sup>-9</sup> moles/cm<sup>2</sup> of true electrode area.] Beware of introducing impurities into solution (e.g., platinum) through pre-electrolysis.</p>
b. electrode phase	<ol style="list-style-type: none"> <li>1. Use easily purified metals whenever possible (but life is not this simple!), e.g., mercury.</li> <li>2. Start with highest purity electrode materials available.</li> <li>3. Where practical, use zone refining, distillation, etc.</li> </ol>	<p>Electrochemists often use metals with low concentrations of spectrographically detectable elements. These metals are often contaminated very substantially with other elements for which emission spectroscopy is not sensitive. Recommend checking impurities with mass spectrometer.</p>
c. gases used to saturation solution and above solution	<ol style="list-style-type: none"> <li>1. H<sub>2</sub> readily ultrapurified with Pd diffuser.</li> <li>2. He readily purified with molecular sieve-diffuser or liquid N<sub>2</sub>-adsorbate trap.</li> </ol>	<p>Gases other than H<sub>2</sub> and He more difficult to purify. When possible, use these. Beware of Teflon or other plastic tubing for connections to cell--O<sub>2</sub> permeable.</p>
d. cell construction materials	<ol style="list-style-type: none"> <li>1. Use high purity glass (low As particularly for H-overpotential) for acid and neutral media; fabricate glass cell with H<sub>2</sub> flame; do not blow directly with breath; treat with solution for prolonged period to leach out dissolvable impurities.</li> <li>2. Use Teflon for alkaline, acid, or neutral media; use great care to minimize contamination in machining; use oxidizing solution to remove organic contaminants; treat with solution for prolonged period.</li> </ol>	<p>Glass is unsatisfactory for alkaline solutions. Teflon is porous and soaks up solution components--difficult to remove; also permeable to O<sub>2</sub>.</p>

Table 2. Typical experimental problems and factors (continued)

Problem or factor	Techniques for controlling or measuring	Remarks
e. atmospheric pollution	<ol style="list-style-type: none"> <li>1. Use high vacuum techniques.</li> <li>2. Where such techniques are unpractical, use controlled atmosphere enclosure with non-contaminating atmosphere.</li> <li>3. Carefully out-gas all solutions to remove last traces of oxygen.</li> </ol>	<p>Small traces of oxygen difficult to keep out of system and to remove from solutions.</p>
f. contamination from counter and reference electrodes	<ol style="list-style-type: none"> <li>1. Choose counter and reference electrode so as to be compatible with system or place in well isolated compartments.</li> </ol>	<p>Pd diffuser hydrogen electrode often attractive for high current density counter electrode.</p>
2. Non-uniform current distribution and non-uniform surface concentrations of reactants and products	<ol style="list-style-type: none"> <li>1. Use spherical electrodes or guard electrode arrangement (e.g., ring-disc assembly).</li> <li>2. Maximize the ratio of differential reaction impedance to solution resistivity.</li> </ol>	<p>Kinetic studies require uniform current distribution. Avoid closely placed Luggin capillary. Beware of porous electrodes.</p>
a. resulting principally from potential gradients in solution	<ol style="list-style-type: none"> <li>1. Redesign electrode.</li> </ol>	<p>Unlikely in properly designed electrodes for kinetic studies. Often encountered in applied electrochemistry.</p>
b. resulting principally from potential gradients in electrode	<ol style="list-style-type: none"> <li>1. Use electro configurations giving uniform Nernst diffusion layer thickness (e.g., rotating disc or ring-disc assembly).</li> <li>2. Use sufficient convection that concentrations at surface are essentially the same as in bulk solution even though Nernst diffusion layer is non-uniform in thickness.</li> <li>3. Avoid convective transfer through use of transient techniques.</li> </ol>	<p>Avoid use of closely placed Luggin capillary.</p>
c. non-uniform mass transport along electrode resulting from differences in boundary layer thickness	<ol style="list-style-type: none"> <li>1. Use Luggin capillary and if necessary, extrapolation technique.</li> <li>2. Increase conductivity through use of supporting electrolyte.</li> <li>3. Use interrupter or similar step function technique to measure overpotential.</li> </ol>	<p>More of a problem in potentiostatic control.</p>
3. Ohmic drops included in measurements		
a. within electrolyte		

Table 2. Typical experimental problems and factors (continued)

Problem or factor	Techniques for controlling or measuring	Remarks
b. within electrode	<ol style="list-style-type: none"> <li>1. Redesign electrode to minimize--if possible.</li> <li>2. Use interrupter or other step function technique to measure.</li> </ol>	A problem in studies with semiconductor electrodes (e.g., oxide, organic semiconductors, etc.).
4. Mass transport control predominant; insensitivity to kinetics	<ol style="list-style-type: none"> <li>1. Use more effective convection (e.g., high speed rotating electrode, ultrasonics).</li> <li>2. Use non-steady state technique better suited to study of fast kinetics (e.g., stepfunction technique, Faradaic rectification, etc.).</li> </ol>	See Table 1 for range of formal rate constants accessible with various techniques.
5. Topographical features of solid electrodes	<ol style="list-style-type: none"> <li>1. Use step function or sweep methods which permit completion of measurements before substantial changes in surface structure have occurred.</li> <li>2. Use great care in mechanical and chemical polishing and annealing.</li> </ol>	A major problem in studies of deposition and dissolution. A major reason for favoring liquid metals for kinetic studies. Single crystals may help somewhat in some instances but do not eliminate problem.
a. time variance and reproducibility problems (area, microcrystallographic orientation of surface, defect concentration, etc.)	<ol style="list-style-type: none"> <li>1. Capacity measurements at a given potential provide indication of relative values for true area.</li> <li>2. Gas adsorption measurements (BET), other adsorption techniques.</li> </ol>	Microcracks, porosity, etc. can cause serious complications. Try to avoid kinetic studies on porous electrodes. Applicable only to systems with relatively high true/apparent area ratio.
b. determination of: true area	<ol style="list-style-type: none"> <li>1. Etch pit studies combined with electron and ordinary optical microscopy and LEED.</li> <li>1. Etch pit studies coupled with electron and optical microscopy.</li> </ol>	Requires experience and facilities which most electrochemical kineticists do not have. Much room for improved techniques.
micro orientation of the surface, defect concentration	<ol style="list-style-type: none"> <li>1. Determine point of zero charge (pzc) from interfacial tension, differential capacity, and/or other methods (hardness, ATR, etc.) and then calculate potential drop across diffuse layer and concentrations in Helmholtz plane from these data. Works well with Hg, more complicated with solid electrodes, particularly with adsorbed hydrogen or oxygen.</li> </ol>	On some limited occasions (particularly at potentials remote to the pzc with concentrated supporting electrolyte), the potential drop across diffuse layer can be assumed approx. constant and the concentration of reacting species in the Helmholtz plane proportional approx. to bulk concentration provided no specific adsorption.
surface defect concentration		
6. Electrical double layer		
a. potential drop across diffuse ionic layer and concentration of species in pre-reaction layer (not specifically adsorbed)		

Table 2. Typical experimental problems and factors (continued)

Problem or factor	Techniques for controlling or measuring	Remarks
<p>b. concentration of specifically adsorbed species--both re-actants and non-reactants</p>	<p>1. Measure directly by <u>in situ</u> optical or radiochemical method.                      2. Determine from voltammetry, charging curves, impedance measurements.                      3. Determine from interfacial tension--capacity measurements--Gibbs adsorption eq.</p>	<p>A necessity in virtually all kinetic studies.</p>
<p>c. potential drop across and carrier concentration in space charge layer in semiconductor electrode</p>	<p>1. Attempt to calculate from capacity measurements and kinetic behavior of redox couples on surface.</p>	<p>With higher carrier concentration, potential drop across space charge layer may be negligible and carrier concentration at surface proportional to bulk concentration. With low carrier concentrations, potential drop across space charge layer may be much larger than drop across interface and changes in carrier concentration at surface of semiconductor may be the predominant factor responsible for the dependence of the current on electrode potential. Space charge layer and non-linear characteristics of metal-semiconductor interface can cause serious complications in interpreting double layer and kinetic studies at semiconductor-electrolyte interfaces.</p>
<p>7. Competing electrode reactions                      a. quantitative information concerning rates</p>	<p>1. Evaluate rates by various analytical methods.</p>	<p>Can cause pH and other changes which must be considered in addition to fact that overall current corresponds to more than one process.</p>
<p>b. suppression</p>	<p>1. When possible, use electrodes and solutions not conducive to the particular competing process (high hydrogen overpotential metals, inert metals, etc.).</p>	<p>Often not possible.</p>
<p>8. Reaction intermediates</p>	<p>a. identification                      1. Use analytical technique to identify in bulk. If very unstable or transient, try ATR, ESR, voltammetry on ring with rotating ring-disc technique, etc.</p>	<p>Very difficult if only present as adsorbed species.</p>

Table 2. Typical experimental problems and factors (continued)

Problem or factor	Techniques for controlling or measuring	Remarks
8. Reaction intermediates (continued) b. measure concentration	Use rotating ring-disc techniques, double pulse or chronopotentiometry with current reversal techniques, ATR, etc.	Rotating ring-disc technique particularly useful.

ELECTROCHEMICAL REACTIONS AT SEMICONDUCTOR ELECTRODES

D. R. Turner

Bell Telephone Laboratories, Inc.  
Whippany, New Jersey

Electrochemical reactions at semiconductor electrodes have been studied in detail only recently. Beginning with the classic paper of Brattain and Garrett<sup>1</sup> in 1955 which laid down many of the basic principles, our understanding of the subject developed very rapidly. Excellent survey papers and original contributions to semiconductor electrochemistry are attributed to Dewald<sup>2</sup>, Green<sup>3</sup>, and Gerischer<sup>4</sup>. Electrochemical processes are now well understood on single-crystal elemental semiconductors such as Ge and Si<sup>5,6</sup>. Some intermetallic semiconductor compounds such as GaAs have been studied and, while the chemistry of the reactions is different, their electronic behavior is the same as for Ge and Si.

Electrochemical reactions at semiconductor electrodes are unique in electrochemistry in that the kinetics of electrode processes may be determined by phenomena which occur within the electrode itself. In order to understand electrochemical reactions at semiconductor electrodes, it is necessary first to recognize how semiconductors differ from metals in their electrical properties. In metals, there is always a large number of electrons associated with valence bonds which have sufficient energy to become conduction electrons. Another way of saying this is that the valence band of electron energy levels overlap with the conduction band. In semiconductors, there is an appreciable energy gap between the top of the valence band and the bottom of the conduction band. This results in a relatively low electronic conductivity since the number of electrons which have enough thermal energy to bridge the gap and provide current carriers is relatively low. Current carriers in semiconductors are of two types--conduction band electrons (electrons free to move through the crystal lattice) and valence band holes (electrons missing from covalent bonds). Electron motion from bond to bond gives the effect of positive charges moving in the opposite direction. These positive charges are called electron holes or simply holes. Each electron that bridges the energy gap produces one hole and one electron current carrier. The product of the concentrations of holes and electrons is a constant at a given temperature. The analogy between the hydrogen ion--hydroxyl ion equilibrium in water and the hole ( $e^+$ )--electron ( $e^-$ ) equilibrium in semiconductors is often made. Both equilibria are controlled by the law of mass action. Increasing one carrier type depresses the concentration of the other. The relative concentrations of holes and electrons in semiconductors are controlled by doping with small amounts of impurities which provide energy levels lying close to the valence band (these accept electrons from the semiconductor and produce p-type material) or close to the conduction band (these donate electrons to the semiconductor and make n-type semiconductors). The terminology n- and p-type indicates the polarity of the major current carrier in the semiconductor--n signifies negative charges

(electrons) while p is for positive charges (holes). Certain electrochemical reactions require specifically holes or electrons from the semiconductor. Hence, reaction rates may become limited by the supply of holes or electrons when they are the minority current carrier in the semiconductor. A complication in clearly defining the concentration of holes and electrons in the surface region of semiconductors is surface states. These are often ill-defined surface phenomena which give rise to allowed energy levels in the normally forbidden region--the energy gap. Surface states can trap electrons and/or holes. They may also act as a source of current carriers. A comprehensive review of the structure of the semiconductor-electrolyte interface has been prepared by Boddy<sup>7</sup>.

### Electrochemical Techniques

A wide variety of experimental techniques has been used to study electrochemical reactions on semiconductor electrodes. Many of these techniques take advantage of the semiconducting properties of the electrode. Photo effects, capacitance measurements, and solid-state pn junction indicator electrodes give information about the charge distribution and/or the charge transfer mechanism at the semiconductor-electrolyte interface.

### Anode Reactions

The important anodic reactions are semiconductor dissolution, film formation, and oxidation of ions in solution.

#### Dissolution

Germanium is dissolved anodically in most electrolyte solutions whereas silicon may be electrolytically dissolved only in fluoride solutions. Brattain and

Garrett<sup>1</sup> showed that the Ge dissolution reaction consumes holes at the anode surface. The same phenomenon has since been demonstrated for the anodic dissolution of all semiconductors. Saturation anodic currents are observed with n-type semiconductors. The limiting anodic current is increased when the surface concentration of holes is increased by any means. Illumination of the anode surface with light of sufficient energy to excite electrons from the valence to the conduction band thus creating hole-electron pairs is the most effective method of increasing the hole concentration in the semiconductor surface. The Ge dissolution valence is four at low current densities and between two and four holes per Ge atom are consumed in the anodic reaction depending on the surface hole concentration. At high current densities, the Ge dissolution valence becomes two. The anodic solution of Si in fluoride solutions is quite different from Ge. The Si dissolution valence is two at low current densities and becomes about four when the current density exceeds a critical value at which fluoride ions are consumed in the anodic reaction as fast as they reach the

surface by mass transport. Divalent silicon is unstable and disproportionates to tetravalent Si and amorphous Si. A thick film of amorphous Si can be built up below the critical current density. The thick film comes off at the critical current density and Si dissolution valence becomes four. Electropolishing also occurs under the conditions of tetravalent dissolution.

### Film Formation

Stable uniform films of oxides or other materials cannot be formed anodically on Ge in aqueous solutions because of their excessive solubility in water. Non-aqueous solutions may be used to produce films on Ge. Anodically formed oxide films are produced on Si in fluoride-free electrolytes.

### Cathodic Reactions

Cathodic reactions of interest at semiconductor electrodes are reduction of surface films, cathodic dissolution of Ge, and reduction of ions in solution. Many cathodic reactions on semiconductor electrodes require conduction band electrons. Therefore, limiting currents are observed at p-type semiconductors where conduction band electrons are the minority current carrier.

### Film Reduction

Surface films such as oxides may be cathodically reduced on Ge but not on Si. This is of practical interest when metal contacts must be electrodeposited directly on an oxide-free semiconductor surface. The plating solution composition and the method of applying current to the cell is important in determining whether or not an intimate contact between deposited metal and semiconductor is formed.

### Cathodic Dissolution of Ge

The discharge of hydrogen ions on electrodes has been studied more than any other electrochemical reaction. This reaction on semiconductor electrodes is unique in two respects: (1) conduction band electrons are required for the electron transfer process and (2) at very high current densities ( $>100 \text{ A/cm}^2$ ), germane ( $\text{GeH}_4$ ) is formed at nearly 100% current efficiency.

### Redox Reactions

The reduction and oxidation of ions in solution at semiconductor electrodes are especially interesting since the electron transfer process is predominantly with valence band or electron band electrons depending on the potential of the redox system.<sup>4</sup> In general, the stronger the oxidizing agent formed or reduced at the semiconductor electrode, the more likely that the reaction will involve the injection or extraction of holes. Conversely, the stronger the reducing agent produced or oxidized on a semiconductor, the greater

is the fraction of the current from electrons extracted from or injected into the conduction band. Practically all the experimental work concerning redox reactions at semiconductor electrodes has been done with Ge. A pn junction indicator electrode is the most convenient method of determining the relative amount of each kind of electron in the redox reaction.

### Practical Applications

An understanding of the basic electrochemical reactions at semiconductor electrodes has led to improvements of many electrochemical processes for semiconductor materials. The most important of these are: "chemical" etching and polishing, electropolishing, metal deposition, metal displacement plating, and staining pn junctions.

### Oxide Semiconductors

Oxide semiconductors were known long before elemental semiconductors yet the oxide materials are not nearly as well understood. Their semiconducting properties stem largely from structural defects in oxides that would be insulators if the crystals were defect-free. These oxides are of considerable practical significance; for example, many battery electrodes and corrosion films are composed of semiconducting oxides. Attempts have been made in recent years to interpret battery and corrosion reactions in terms of semiconductor phenomena with limited success.

### REFERENCES

1. W. H. Brattain and C. G. B. Garrett, Bell System Tech. J., 34 129 (1955).
2. J. F. Dewald in "Semiconductors," ed. N. B. Hannay, A.C.S. Monograph #140, Reinhold, New York (1959).
3. M. Green in "Modern Aspects of Electrochemistry," Vol. II, ed. J. O'M Bockris, Butterworths, London (1959).
4. H. Gerischer in "Advances in Electrochemistry and Electrochemical Engineering," ed. P. Delahay, Interscience Publishers, New York (1961).
5. D. R. Turner in "Electrochemistry of Semiconductors," ed. P. J. Holmes, Academic Press, New York (1962).
6. E. A. Efimov and I. G. Erusalimchik, "Electrochemistry of Germanium and Silicon," Translation by A. Peiperl, The Sigma Press, Washington, D.C. (1963).
7. P. J. Boddy, J. Electroanal. Chem. 10, 199 (1965).

PASSIVATION OF METALS AND ALLOYS

A. C. Makrides

Tyco Laboratories, Inc.  
Waltham, Massachusetts 02154

(Not Available)

Fundamentals of Electrodeposition

J. V. Petrocelli

Ford Motor Company, Dearborn, Michigan

Introduction

Electrodeposition is an extensive and complicated subject. This discussion is confined to the energetics and kinetics of metal deposition from aqueous solutions. The formation of anodic films and the morphology of deposits is briefly mentioned. The elucidation of the atomic mechanisms has made significant progress in the past decade; it is the object here to review the present status. The cited works represent the more available literature and may be consulted for details, particularly the more recent reviews (1,2).

Energetics

The energy of the reaction between a metal and an electrolyte is the difference between the cohesive energy of the metal and the solvation energy of the metal ions. The former is the sum of the mutual potential energy of the valence electrons and the ions, that of the valence electrons, that of the ions and the kinetic energy of the electrons and the ions. The last may be neglected. The cohesive energy per atom may be expressed as

$$E_c = \frac{1}{2}U_{i,i} + \frac{1}{2}U_{e,e} + U_{i,e} + \frac{3}{5}\epsilon_F \quad (1)$$

The mutual potential energy between the electrons and the ions may, on the average, be divided into half for the electrons and half for the ions. We may then express the cohesive energy of the metal in terms of an ionic work function,  $\alpha_+$ , and the electronic work function,  $\alpha_e$ , as follows:

$$\alpha_+ = \frac{1}{2}U_{i,e} + \frac{1}{2}U_{i,i} - \frac{2}{5}\epsilon_F$$

$$\alpha_e = \frac{1}{2}U_{i,e} + \frac{1}{2}U_{e,e} + \epsilon_F$$

and

$$\alpha_+ = E_c - \alpha_e = S + I - \alpha_e$$

where S and I are the sublimation energy and ionization energy per atom, respectively.

The energy of solvation,  $W_+$ , is the energy change for solvating a gaseous ion. These quantities and the relevant potential energy curves are shown in fig. 1.

The standard free energy change for a metal ion to leave the lattice and go into solution is approximately

$$\Delta G_{\text{chem}}^0 \approx \alpha_+ - W_+$$

An electrical potential difference,  $(\phi_M - \phi_S)$ , develops across the interface so that the total free energy change for the transition of ions from metal to solution is the sum of the chemical free energy change,  $\Delta G_{\text{chem}}^0$ , and the electrical

free energy change,  $ZF[\phi_M - \phi_S]$ . At equilibrium the total free energy change is zero and  $\Delta G_{\text{chem}} = -\Delta G_{\text{elec}}$ . At equilibrium the exchange rates of the ions are equal - the exchange current density,  $i_0$ .

The  $\Delta G_{\text{elec}}$  may be varied by an external circuit, disturbing the equilibrium and causing either a net deposition or net dissolution. The change in  $\Delta G_{\text{elec}}$  from the equilibrium value is  $ZF\eta$ , where  $\eta$  is the overvoltage.

The energy  $\alpha_+$  and  $S$  must have the values appropriate to an internal ion. Since ions come from the surface during the reaction, we must look for the representative ion or atom on the surface.

### Crystal Structure

The various surface sites are shown in fig. 2. The binding energy of an atom or ion varies according to its lattice position. The kink atom or kink site (K.S.) on the close packed planes is the representative one. The energy to remove this atom is equal to the average energy per atom, provided the ratio of surface atoms to bulk atoms is very small. At equilibrium the electrochemical potential of this ion is equal to that of an ion in solution. When the crystal is built up by the addition of ions, the ion is incorporated into this site, the "repeatable step." Ions "at ledges" or adsorbed on planar sites have higher potential energies. To form a new surface layer without the presence of steps requires an "excess energy" - nucleation energy. The new cluster of atoms requires a critical radius,  $r_c$ , in order to become a nucleus and grow. The value of  $r_c$  varies inversely with  $\eta_c$ , where  $\eta_c$  is analogous to a supersaturation.

The free energy increase required for the formation of a nucleus with height  $d$  is

$$\Delta G_c = \frac{\pi d V \sigma}{Z \eta}$$

where  $V$  is the atomic volume and  $\sigma$  is the surface energy of the edge. Vermilyea has estimated that an  $\eta_c$  of about 0.1 v would be required for most metals for a significant rate of growth with nucleation. This agreed with his findings for deposition of Cu on Cu whiskers which were bound by atomically flat surfaces (3,4).

Analogous to growth from the vapor, low values of  $\eta_c$  suffice for electrocrystallization in many cases. Following the ideas of Burton, et al (5), it is assumed that growth occurs at the steps of screw dislocation (see fig. 3). A critical radius of curvature is required for the steps at a given  $\eta_c$ , as in the case of nucleation. This leads to a ledge spacing,  $\ell$ , which varies inversely with  $\eta_c$ .

### Kinetics and Deposition Path

Advances in knowledge on mechanisms of crystal growth from the vapor have furnished the background for developments in electrodeposition (5,6). The latter is more complicated, and specific effects of solvation and field strengths must be taken into consideration. As previously indicated, the mechanism must provide for the ultimate incorporation of the ion into the K.S. when reaction proceeds near to equilibrium conditions - very low  $\eta_c$ .

Two alternate paths must be considered: Path I - direct deposition of an ion from the solution to the K.S.; Path II - transfer of the ion from solution to an adsite with subsequent surface diffusion to the K.S. In the latter case either transfer to adsite or surface diffusion may be the rate-determining step (r.d.s.).

Conway, et al (7) calculated the potential energy profiles for the two paths. Their necessarily qualitative results indicate that at low  $\eta$  Path II is energetically more feasible. Mott, et al (8), Vermilyea (3), and Fleischmann, et al (2) have suggested the conditions for either Path I or II to be predominant.

The basic consideration is the mean diffusion distance of an adion, which is determined by its residence time on the surface and the activation energy for surface diffusion. When the jump time on the surface,  $\tau_D$ , is greater than the jump time to the solution,  $\tau$ , Path I will dominate. When  $\tau_D < \tau$ , Path II will be significant.  $\tau_D \cong a^2/D$  where "a" is the distance between the two adsites and D is the surface diffusion constant.

$$\tau = 1 / \frac{i_0}{C_0} \exp \left[ \frac{\beta Z F}{RT} \eta \right]$$

where  $C_0$  is the adion concentration at equilibrium and  $\beta$  the anodic transfer coefficient.  $\eta$  is considered a negative quantity for cathodic polarization. Mott, et al (8) suggest that, if N is the concentration of K.S., surface diffusion will be slow and rate controlling when  $Na^2\tau/\tau_D < 1$ ; and that transfer will be rate controlling when the ratio is greater than one. Since  $\tau$  increases as  $|\eta|$  increases, surface diffusion control would be expected at lower values of  $\eta$  with a shift to transfer control as  $\eta$  increases.

The net current density at a point x distant from the growth site at a time t is given by

$$i(x,t) = i_0 \left[ \exp \left( \frac{-\alpha Z F}{RT} \eta \right) - \frac{C(x,t)}{C_0} \exp \left( \frac{(1-\alpha) Z F}{RT} \eta \right) \right]$$

and

$$\frac{\partial [C(x,t)]}{\partial t} = \frac{i(x,t)}{Z F} + D \frac{\partial^2 [C(x,t)]}{\partial x^2}$$

where C is the adion concentration. In the steady state C(x) becomes constant and adions diffuse from x to growth sites at the same rate as they transfer from solution to adsites at x.

Damjanovic and Bockris (4) have treated the steady state conditions assuming  $C = C_0$  at the growth site and a random distribution of dislocations,  $N/\text{cm}^2$ . The model is shown in fig. 5. Some results of their calculations are given in fig. 6. The ratio

$$ND/i_0 \exp \left( \frac{\beta Z F}{RT} \eta \right)$$

is equivalent to the Mott ratio. As ND increases for a given  $\eta$ , the rate control shifts to transfer and a more uniform current density. For a given ND an increase in  $\eta$  produces the same effect. These authors appear to maintain that even when  $i_x/i_{x_0} \sim 1.0$ , deposition is to an adsite, and not directly to K.S.

The conditions for Path I have been developed by Vermilyea (3), Fleischmann, et al (2), and Hurlen (9). Expressions for i have been determined by considering hemicylindrical diffusion from the solution to ledges and hemispherical diffusion to the K.S. The stirring-independent limiting current predicated by the treatment for certain conditions has not been observed on metals with high  $i_0$ .

The experimental approach to determine mechanisms have used transient behavior. The technique involves the application of current or potential pulses of very short duration ~ milliseconds. The object is to deposit less than a monolayer without changing the existing surface structure. The use of the time dependent terms obtained from the above equations allows the determination of  $C_0$ ,  $i_0$  and  $v_0$ , where  $ZFv_0$  is the "diffusion current" on the surface at equilibrium. The parameters obtained also make it possible to determine the slow step of Path II. (1,2,3,10)

Ag has been studied extensively. The results indicate that  $i_0 \sim 30-100$   $\text{mA/cm}^2$ ,  $C_0 \sim 10^{-9}$  moles/ $\text{cm}^2$  and that surface diffusion is the r.d.s. up to about  $\eta = 50$  Mv. The adion appears to have about 30-50% of its charge in solution (1,2,10).

Bockris, et al (11) studied liquid and solid gallium and showed that surface diffusion is rate controlling on the solid up to about  $\eta \approx 50-100$  Mv; but that transfer was the r.d.s. on the liquid, as expected. On the other hand, Gerischer (10) found transfer rate control on both liquid and solid Hg.

The case for Cu is not so clear cut. Results indicated "mixed" control by both surface diffusion and transfer at low  $\eta$ , with transfer control at higher  $\eta$ . The kinetic parameters show that transfer involves the consecutive reactions, reduction to  $\text{Cu}^+$  in the solution and transfer of  $\text{Cu}^+$  (10,12).

Lorenz (13) showed that surface diffusion is the r.d.s. on Zn at low  $\eta$ .

Bockris, et al (14) found that Fe has the transfer step as rate controlling and that the reaction is catalyzed by  $\text{OH}^-$ . Anions affect the rate where  $\text{ClO}_4^- > \text{SO}_4^{2-} > \text{Cl}^- > \text{Ac}^- > \text{NO}_3^-$ .

Fleischmann, et al (15) deposited a single layer of Ni, one unit cell high, on Hg from thiocyanate solutions. Indications are that deposition is via Path II and that the rates of surface diffusion and transfer are comparable.

Generally the experimental results agree with the theoretical developments and support Path II as the predominant path for the metals with relatively high  $i_0$ . The field is ripe for further experimental work and closer scrutiny of the theories, however.

### Crystal Growth

Theories and many experimental observations on crystal growth are present in the literature (1,2,5,6,16,19). Growth proceeds by flow of steps and kinks on the surface. Macrosteps - visible ones - occur by "bunching" - a clustering of the smaller atomic steps. The morphology of a deposit is very dependent on the presence of adsorbed impurities, current density, and type of electrolyte. Without presence of impurities and at low  $\eta$ , existing steps will spread; their curvature depends upon  $\eta$ . The higher  $\eta$ , the greater the curvature. Formation of multilayers is primarily by rotation of screw-dislocation steps. In the presence of impurities and/or at higher  $\eta$ , new layers nucleate. Growth habits consist of many types; e.g., layers, spirals, blocks, pyramids, and ridges. The spirals are visual evidence of the screw-dislocation mechanism. Pyramids probably develop from spiral growth. Figures 7 and 8 show layer and spiral growth on copper.

### Anodic Films

When the metallic ions can form an insoluble compound with a constituent of the solution (e.g.,  $\text{OH}^-$ ,  $\text{S}^{2-}$ ,  $\text{Cl}^-$ ), the solid compound may form on the surface - usually during anodic dissolution. If the film is continuous, metallic ions and/or

the negative ions migrate through the film as it grows. This is assumed to be the case for many oxide films such as passive films and capacitor films. The ionic transport through the film is usually the r.d.s. Non-continuous films nucleate on or near the surface. Their growth may be by ionic transport through the film or by deposition of the ions from solution and along the surface. The mechanisms of electrocrystallization of these films is basically similar to those of the metal deposits (20).

### References

1. J. O'M. Bockris and A. Damjanovic, "Modern Aspects of Electrochemistry," Vol. 3, eds. Bockris and Conway, Academic Press, New York, 1964, p. 224.
2. M. Fleischmann and H. R. Thirsk, "Advances in Electrochemistry and Electrochemical Engineering," ed. Paul Delahay, Interscience Publ., New York (1963), p. 123.
3. D. A. Vermilyea, *J. Chem. Phys.* **25**, 1254 (1956), *ibid.* **27**, 814 (1957).
4. A. Damjanovic and J. O'M. Bockris, *J. Electrochem. Soc.* **110**, 1035 (1963).
5. W. K. Burton, N. Cabrera and F. C. Frank, *Proc. Roy. Soc. London* **243**, 299 (1951).
6. J. P. Hirth and G. M. Pound, "Condensation and Evaporation," The MacMillan Co., New York (1963).
7. B. E. Conway and J. O'M. Bockris, *Proc. Roy. Soc.* **248**, 394 (1958); *Electrochimica Acta* **3**, 340 (1960).
8. N. F. Mott and R. J. Watts-Tobin, *Electrochimica Acta* **4**, 79 (1961).
9. T. Hurlen, *Electrochimica Acta* **11**, 1205 (1966).
10. H. Ferischer, *Electrochimica Acta* **2**, 1 (1960).  
W. Mehl and J. O'M. Bockris, *J. Chem. Phys.* **27**, 218 (1957); *Can. J. Chem.* **37**, 190 (1959).  
W. Lorenz, *Z. Physik. Chem.* **17**, 136 (1958).
11. J. O'M. Bockris and M. Enyo, *J. Electrochem. Soc.* **109**, 48 (1962).
12. J. O'M. Bockris and M. Enyo, *Trans. Faraday Soc.* **58**, 1187 (1962).  
J. O'M. Bockris and H. Kita, *J. Electrochem. Soc.* **109**, 928 (1962).
13. W. Lorenz, *Z. Physik. Chem.* **19**, 377 (1959).
14. J. O'M. Bockris, D. Drozic and A. R. Despic, *Electrochimica Acta* **7**, 293 (1961).
15. M. F. Fleischmann, J. A. Harrison and H. R. Thirsk, *Trans. Faraday Soc.* **61**, 1742 (1956).
16. O. Knacke and I. Stranski, *Prog. Met. Physics* **6**, 181 (1956).
17. A. Damjanovic, M. Paunovic and J. O'M. Bockris, *J. Electroanal. Chem.* **9**, 93 (1965).
18. Seiter, Fischer and Albert, *Electrochimica Acta* **2**, 167 (1960).
19. H. Fischer, "Elektrolytische Abscheidung und Elektrokristallisation von Metallen," Julius Springer, Berlin (1954).
20. T. P. Hoar, "Modern Aspects of Electrochemistry," Vol. 2, ed. J. O'M. Bockris, Academic Press, New York (1959), p. 262.  
M. Fleischmann and H. R. Thirsk, *Electrochimica Acta* **2**, 22 (1960).  
D. A. Vermilyea, "Advances in Electrochemistry and Electrochemical Engineering," Paul Delahay, ed., Interscience Publishers, New York (1963), p. 211.

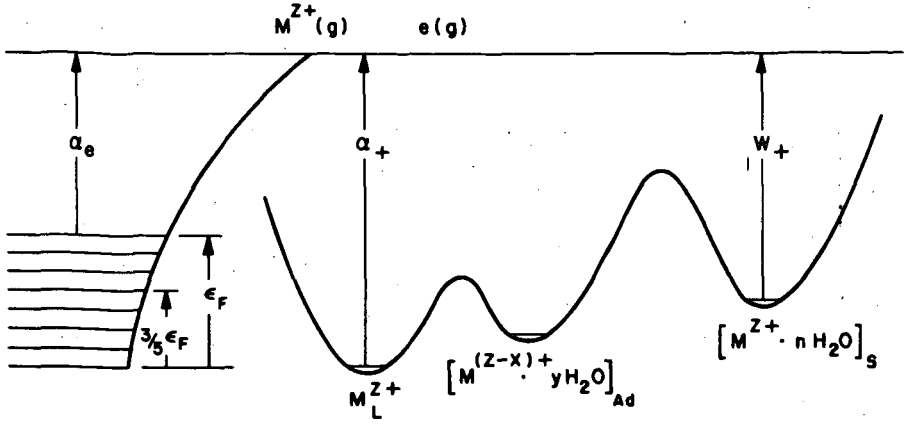


Fig. 1 Potential Energy Curves

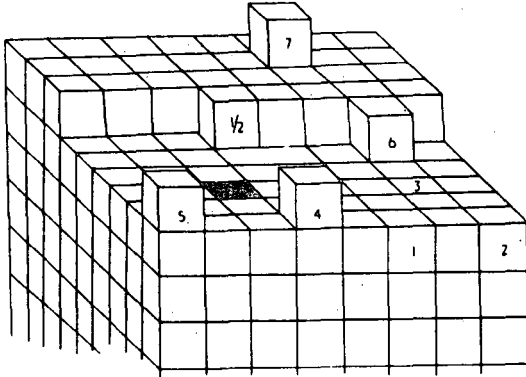


Fig. 2 Crystal Model  
[From Knacke (16)]

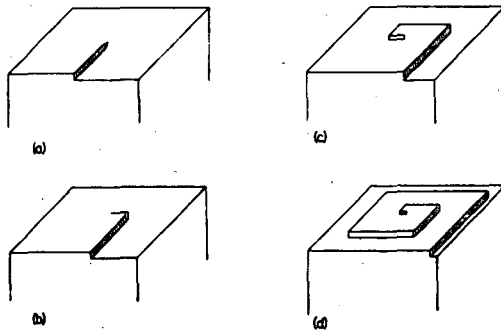
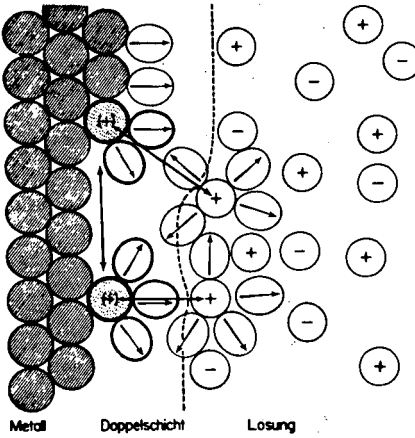
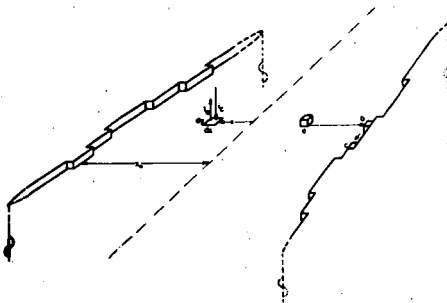


Fig. 3 Screw Dislocation  
[From Gerischer(10)]



**Fig. 4 Double Layer**  
[From Gerischer (10)]



**Fig. 5 Model For Deposition**  
[From Damjanovic(4)]

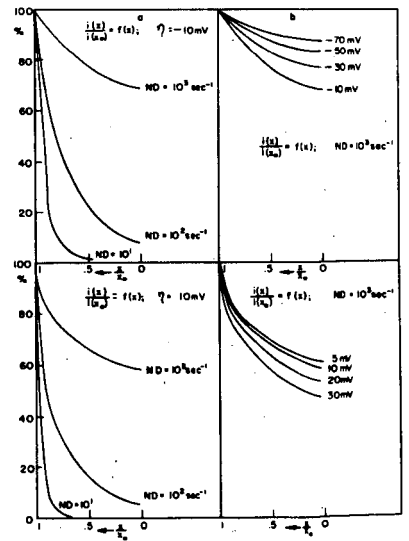


**Fig. 6 Current Density vs Distance**  
[From Damjanovic (4)]



**Fig. 7 Layer Growth-Copper**  
[From Damjanovic (17)]



**Fig. 8 Spiral Growth-Copper**  
[From Seiter (18)]

## ELECTRODE REACTIONS IN MOLTEN SALTS

S. Senderoff

Union Carbide Corporation  
 Consumer Products Division  
 Research Laboratory  
 P. O. Box 6116  
 Cleveland, Ohio

While studies of thermodynamic properties of molten salts, such as equilibrium potentials, molar volumes and phase diagrams, and transport properties, such as conductivity and viscosity, are quite well advanced, the study of the electrode reactions in these media, which is the essence of electrochemistry, is at a very early stage of development. The neglect of electrode reaction studies in molten salts probably arises from two factors common to high temperature heterogeneous reactions. 1) The reaction rate is so high that usual methods of investigation expose only diffusion control and 2) the effects of small impurities may be overwhelming and cause serious irreproducibility of measurements. The latter is particularly serious when one considers the corrosiveness of many molten salts, difficulties with containers, atmospheres, etc. As a result, with a few exceptions, most studies of electrode reactions in molten salts are still semiquantitative, and concerned with identifying the rate-controlling step and the path(s) of reaction, or if diffusion controlled, the intermediates and products of the overall reaction, and diffusion coefficients of the reacting species. Very little has been accomplished in quantitatively determining kinetic parameters of molten salt reactions, such as exchange currents, reaction rate constants, or transmission coefficients. The most important methods by which these are accomplished in aqueous systems at ordinary temperatures are (1):

1) Current-voltage curves in which each point is obtained under a steady state condition of electrolysis. The analysis of the Tafel slopes (i. e., the slope of the plot of overvoltage,  $\eta$ , vs.  $\log i$ , the current density) provides the kinetic data and insight into mechanisms.

2) Transient D. C. techniques or voltammetry, including polarography with slow or rapid scanning procedures and potentiostatic and galvanostatic methods. In all cases equations relating current, voltage and time may be derived, a criterion for diffusion control set up, and departures from diffusion control interpreted in terms of kinetic parameters and mechanisms. The use of these methods in conjunction with the rotating disc electrode has proved to be extremely effective in many cases.

3) A. C. impedance measurements in which the frequency dependence of the impedance is measured to obtain a polarization resistance and pseudocapacity identified with the electrode reaction and from which a rate constant may be calculated and mechanisms deduced. Before this can be done, however, the double layer capacity and resistance of the solution must be determined in the absence of the electrode reaction.

#### Current Voltage Curves and the Oxygen Electrode

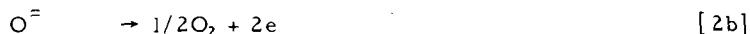
For the first method (steady state current voltage curves) to show any kinetic properties a rather slow reaction is required; and in molten salts only a few gas electrode reactions are slow enough to have been successfully studied by this method. An example of this is the work of Janz et al (2) on the anodic evolution of oxygen from carbonate melts on platinum and gold electrodes in the temperature range of 600° to 900°C. The overall reaction for this system is:



The first question raised by Janz et al was whether the reaction proceeded by direct oxidation of  $\text{CO}_3^-$  ion as in [1] or by a prior dissociation,



followed by electrochemical oxidation of the oxide ion,



From the temperature coefficient of the overvoltage and the effect of gas composition ( $\text{CO}_2/\text{O}_2$  ratio) on the overpotential, it was concluded that prior dissociation was involved. The next question considered was the detailed mechanism of the oxidation of oxide ion shown in [2b]. The processes considered were:



followed by either:

$\text{M-O} + \text{O}^- \rightarrow \text{M} + \text{O}_2 + 2e$  [4a], or  $\text{MO} + \text{MO} \rightarrow 2\text{M} + \text{O}_2$  [4b], where M is the metal of the electrode. If [3] were rate controlling, the Tafel slope would be  $\text{RT}/F^*$ . If [4a] were rate controlling the Tafel slope would be  $\text{RT}/F$  at high current density and  $\text{RT}/3F$  at low current density. If [4b] controlled the rate the Tafel slope would be  $\text{RT}/4F$ . The observed Tafel slopes derived from the polarization curves at  $600^\circ\text{C}$  corresponded closely to the values calculated for step [4a] both at high and low current density. Thus the mechanism for oxygen evolution at this temperature from molten carbonate was identified as dissociation [Reaction 2a], followed successively by surface oxide formation [Reaction 3], and electrochemical oxygen gas formation [Reaction 4a], the last being rate controlling. At higher temperatures (near  $800^\circ\text{C}$ ), the Tafel slopes are not linear and the gas evolution mechanism is not easily ascertained. A change in rate controlling step to oxide formation [Reaction 3] is not ruled out.

On silver electrodes the reaction is apparently much faster than on platinum and gold since almost no polarization was observed by Janz below a current density of  $10^{-4}$  amp/cm<sup>2</sup>, and Kronenberg (3) reports the reaction to be reversible on silver between  $400^\circ$  and  $600^\circ\text{C}$  since he found the potential to obey the Nernst equation with variation of the partial pressure of  $\text{CO}_2$  and  $\text{O}_2$ . In fuel cell applications the frequent use of silver as a catalyst for the oxygen electrode in molten carbonate systems undoubtedly arises from this property.

#### A. C. Impedance Measurements

The third method listed above, A. C. impedance measurements, has proved to be very difficult to apply to molten salt reactions, and with a few exceptions (4), has not been used. Where it has been attempted the results have been difficult to interpret because of the inability to determine the double layer capacity of the solution in an unambiguous manner. The ambiguity of this value arises not only from difficulties with adsorption of trace impurities but from theoretical difficulties regarding the applicability of the value obtained in the absence of the reducible species (5).

#### Rapid-Scan Polarography in Analytical Chemistry

The second method, that involving D. C. transients, has proved to be the most valuable for the study of molten salt systems. The use of rapid-scan polarography and a few other techniques included in this group will now be illustrated in their application to analytical chemistry. The first of the analytical methods to be adapted to molten salts was polarography. This has been expertly reviewed by Laitinen and Osteryoung (4). Except for very low temperature melts, dropping mercury can not be used as an electrode. In most cases either the "dipping"

\*In all calculated Tafel slopes it is assumed that the symmetry factor,  $\beta = 1/2$ .

electrode of Lyalikov and Karmazin (4), or solid microelectrodes have been used. To make a dipping electrode, a wire is sheathed with an insulating tube and inert gas bubbled slowly through the tube. As the liquid rises and falls in the tube, alternately contacting the wire and mixing with the bulk, an action analogous to a dropping electrode is obtained and polarographic waves have been obtained which have been useful in analysis. Solid microelectrodes have been successfully used but difficulties have been encountered with changing of their area due to the dendritic deposits usually obtained from molten salts, and to instability of seals in these media.

Some interesting recent work on analysis in molten systems using rapid-scan polarography and other D. C. transient methods is that of Manning and Mamantov (6). These authors worked mostly in molten fluoride electrolytes at temperatures of 500° to 600°C, and used a pyrolytic graphite indicator electrode and a platinum wire dipped in the melt as a "quasi-reference" electrode. It is hard to say what electrode reaction the "quasi-reference" represents: it is less noble than the Pt,  $Pt^{++}$  electrode potential by at least one volt, which would represent a vanishingly small concentration of  $Pt^{++}$ , certainly insufficient to give a stable and reproducible electrode. It is, however, surprisingly stable, and may represent a redox reaction of an impurity common to the melts, possibly iron. The observed potential is not far from the  $Fe^{3+}/Fe^{2+}$  potential in fluorides, and iron is a common impurity.

Nickel in the alkali fluoride ternary eutectic was determined by rapid-scan polarography and anodic stripping techniques. At high scan rates the limiting current was proportional to concentration in the range studied (10-100 ppm Ni) and the electrode reaction was reversible. Since the reaction appeared to be diffusion controlled at high scan rates, the diffusion coefficients and the activation energy of diffusion (the current limiting process) could be calculated from the linear plots of peak current at known concentration vs. the square root of the scan rate. An activation energy of 18 kcal/mole was found which is about twice the value found by Senderoff and Mellors (7) for transition metal ions in the same solvent, and the diffusion coefficient of  $4.5 \times 10^{-6}$  cm<sup>2</sup>/sec at 600°C is lower by a factor of at least 2 than one would expect. These anomalous values suggest the possibility that the electrode process is not truly diffusion limited and that some kinetic process may be involved as well, or that some experimental difficulties have interfered.

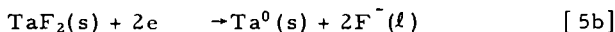
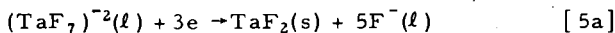
Iron in the same solvent (LiF-NaF-KF) and in the LiF-BeF<sub>2</sub> eutectic was determined by rapid-scan polarography (~ 1V/min) and by chronopotentiometry. Again at high scan rates the reactions appeared to be diffusion controlled and reversible. The diffusion coefficient of  $Fe^{2+}$  obtained by chronopotentiometry was larger than that from polarography and the difference has been ascribed to experimental difficulties with the chronopotentiometry. However, as noted above, the diffusion coefficient obtained by polarography may be too small. The same techniques have been applied to uranium and zirconium in LiF-NaF-KF solvent though in the latter case the relationship between wave height and concentration was erratic. This may have been due to attack on zirconium by the solvent.

#### Chronopotentiometry and Electroplating

Finally, an illustration of the application of galvanostatic transient techniques (commonly called chronopotentiometry) to the study of the mechanisms of the electrode reactions in electroplating of metals from molten fluorides will be presented.

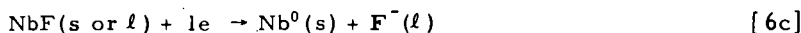
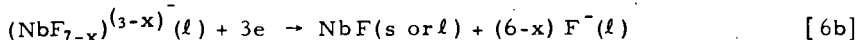
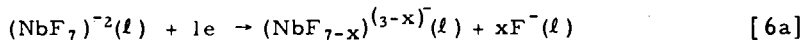
When electrodepositing metals in the solid state from molten salt electrolytes, powders and dendrites are usually obtained. However, it was shown by

Mellors and Senderoff (7) that the electrolysis of pure fluoride melts under certain conditions produces dense, thick, coherent deposits of chromium, molybdenum, tungsten, vanadium, niobium, tantalum, zirconium, and hafnium. In an effort to determine the unique properties of this system a study of the cathode reactions by chronopotentiometry was undertaken. By this method, a pulse of constant current is applied to a cell for a time long compared to the charging time of the double layer, but not long enough for convection to become significant at the electrode. In the molten fluoride at 600° to 800°C this time range was found to be a few tenths of a second to about 1 sec. During the passage of this pulse the potential-time curve is displayed on an oscilloscope and recorded photographically, the potential being taken with respect to a stable reversible reference electrode. The reference electrode used in this work was the Ni/NiF<sub>2</sub>, alkali fluoride // half-cell which was reproducible under these conditions to about ±25mv. Contact between the reference electrode and electrolyte under study was made with a porous alumina bridge impregnated with the solvent which was the KF-NaF-LiF eutectic in most cases. All work was done in an argon atmosphere in a special cell in which all components were suspended from a plastic insulating cover at the top of the cell and allowed to hang in the hot zone without touching each other or the cell envelope. The cell has been thoroughly described elsewhere (7). The indicator electrode was a 1 cm<sup>2</sup> disc of platinum or of the refractory metal under study suspended in the electrolyte by a fine wire without the use of any insulator. The counter electrode was in almost all cases the metal under study. Cathodic chronopotentiograms at various levels of current, temperature, and concentration were run on a solution of K<sub>2</sub>TaF<sub>7</sub> in KF-LiF-NaF eutectic similar to that from which tantalum is plated. They showed that tantalum is reduced to metal in two steps according to the scheme:



The first step is reversible and diffusion controlled. The second step by which the metal is produced, is irreversible and not diffusion controlled. Cathodic-anodic chronopotentiometry, in which a cathodic pulse of a few tenths of a second is followed immediately by an anodic pulse, serves to identify the intermediate, TaF<sub>2</sub>, as a material very slightly soluble in the electrolyte. Its existence as a solid film on the electrode is believed to be the source of the irreversibility of the second step. Since the first step is diffusion controlled, the diffusion coefficient of the reacting species and activation energy for diffusion could be calculated from the data and they were shown to be of magnitude expected for an ion such as (TaF<sub>7</sub>)<sup>-2</sup> which had been shown by IR spectroscopy to be the only significant tantalum-containing species present in solution.

A similar study with a solution of K<sub>2</sub>NbF<sub>7</sub> in the same solvent showed a three step reduction:



The first two steps are diffusion controlled and reversible, the last step is not diffusion controlled and irreversible. Cathodic-anodic chronopotentiometry showed that the intermediate produced in step 2, NbF, is only slightly soluble in a solution in which the mean valence of niobium is close to 4, but is rapidly attacked and dissolves in a solution in which the mean valence of niobium is 5. It is significant that in order to plate niobium, the mean valence of the solution must be less than 4.2, while in the case of tantalum coherent plates can be obtained from a pentavalent solution. In the latter case the intermediate is not attacked or dissolved by the pentavalent solution. As in the case of tantalum, the irreversibility of the metal producing step [6c] is believed to arise from a solid film of NbF on the electrode.

The study of zirconium deposition by chronopotentiometry was made difficult by interference of an alkali metal reduction wave with that of zirconium, but it was shown that the plating occurs as a single 4-electron irreversible reduction. The irreversibility is believed to arise from a corrosion reaction in which potassium metal is produced by attack of the zirconium by the electrolyte: i. e.,  $Zr + 4KF \rightarrow ZrF_4 + 4K(g)$ .

Chronopotentiometric studies of the reduction of molybdenum and tungsten solutions to metal were made difficult by the instability of the very dilute solutions required for chronopotentiometric work. While the plating solutions are stable, the 10- to 50-fold dilutions required for chronopotentiometry are not. However, it was shown that in both cases the metal is produced in single step irreversible reductions. The irreversibility is believed to arise from the slow dissociation of a polynuclear to mononuclear anion preceding the reduction step.

The chronopotentiogram of  $Cr^{3+} \rightarrow Cr^0$  showed a reversible step,  $Cr^{3+} \rightarrow Cr^{2+}$  followed by the irreversible step  $Cr^{2+} \rightarrow Cr^0$ . The origin of the irreversibility has not been ascertained. That for  $Fe^{3+} \rightarrow Fe^0$  showed two diffusion-controlled reversible steps  $Fe^{3+} \rightarrow Fe^{2+} \rightarrow Fe^0$ . It is significant that in the cases of iron and of nickel, coherent deposits cannot be obtained. Only dendrites can be formed over a thin diffusion layer of metal. The nickel reduction is also probably reversible, or very nearly so (6).

These results suggest that the necessary, though not sufficient condition for the electrodeposition of dense, coherent, thick deposits of metals from molten salts is that there be some irreversibility in the metal producing step of the electrode process. It is probable that the solid films, corrosion of the electrode, or slow chemical steps which cause the irreversibility inhibit the continued growth of dendrites and foster nucleation of new crystals.

#### BIBLIOGRAPHY

1. P. Delahay, *New Instrumented Methods in Electrochemistry*, Chap. 8, Interscience, New York (1954).
2. G. J. Janz, F. Colom and F. Saegusa, *J. Electrochem. Soc.*, 107, 581 (1960).  
G. J. Janz and F. Saegusa, *ibid.*, 108, 663 (1961).
3. M. L. Kronenberg, *ibid.*, 109, 753 (1962).
4. H. A. Laitinen and R. A. Osteryoung in "Fused Salts," Ed. B. R. Sundheim, McGraw Hill, N. Y. pp. 265-272 (1964).
5. A. D. Graves, G. J. Hills and D. Inman, "Advances in Electrochemistry and Electrochemical Engineering, Vol. 4, Ed. Paul Delahay, Interscience, N. Y., pp. 162-166 (1966).
6. D. L. Manning, *J. Electroanalyt. Chem.*, 6, 227 (1963); *ibid.*, 7, 302 (1964);  
D. L. Manning and G. Mamantov, *ibid.*, 7, 102 (1964).
7. S. Senderoff and G. W. Mellors, *Science* 153, 1475 (1966); *J. Electrochem. Soc.*, 112, 840 (1965); *ibid.*, 113, 66 (1966).
- G. W. Mellors and S. Senderoff, *ibid.*, 112, 266 (1965); 113, 60 (1966);  
*Can. Pat.* 688,546 (1964).

## ORGANIC ELECTRODE REACTIONS: APPROACHES AND RESULTS

Philip J. Elving

The University of Michigan, Ann Arbor, Michigan

The present paper does not attempt to be exhaustive, but rather to focus attention on certain trends, which seem of major importance for future studies with particular reference to unsolved problems. Consequently, only a minimum number of references are cited.

## INVESTIGATIVE TECHNIQS

Developments in technics of particular relevance for the future investigation and utilization of organic electrode processes, include (1) three-electrode configurations, largely involving operational amplifier control systems, which have minimized the problems associated with the large  $iR$  drop in nonaqueous solutions, (2) reliable indicating electrodes based on graphite, which have extended the potential range available for studying electrochemical oxidations, (3) cyclic voltammetry for the identification of reversible redox couples and frequently of electroactive intermediates formed either chemically or electrolytically (recent papers on the theory of stationary electrode polarography by Shain, Nicholson, et al. (1) may provide the means for quantitatively resolving the electrochemical and associated chemical steps in electrode processes), (4) alternating current polarography and tensammetry, particularly for studying adsorption phenomena, and (5) the use of optical and magnetic resonance spectroscopic technics for identifying electrode reaction products and intermediates, e.g., (a) electron spin resonance to detect transitory free radical intermediates, (b) ellipsometry to investigate electrode surface phenomena including film formation, (c) internal reflectance technics to detect and identify electrode reaction intermediates in the solution-electrode interfacial region during electrolysis, (d) optically transparent electrodes for the concurrent examination of solutions during electrolysis by absorption spectrophotometry or internal reflectance spectroscopy, and (e) examination of luminescence phenomena which accompany the electrolytic generation of certain free radicals.

Electrolysis at controlled electrode potential, although by now a relatively old technic, is still frequently essential in preparing sufficiently large amounts of products to permit their isolation, characterization, identification and determination.

## ROLE OF THE CHEMICAL ENVIRONMENT

Since it is obviously difficult to explain satisfactorily the course of many electrochemical processes unless the relevant environment is sufficiently well characterized, considerable attention has been focused on the locus of the electrode reaction (the solution-electrode interface or the electrical double layer, EDL) and on the role of the test solution composition.

The structure of the EDL and its role in electrochemical kinetics and therefore in determining the potentials of irreversible processes, which include most organic electrode reactions, are well summarized in Delahay's recent book (2). Unfortunately, in the case of organic compounds, insufficient attention is yet being given to the actual effects of adsorption on the electrode and of the potential variation

in the double layer as revealed by the extensive studies by Frumkin, Parsons, Mairanovskii and others. There is little doubt but that, in the future, the definition of the potential variation in the EDL will be a dominant factor in obtaining a more detailed picture of electrode processes. At present, there is an unfortunate tendency by some polarographers to use psi and related potentials as a deus ex machina in explaining phenomena as being due to such potentials, when their actual values either are not known or have been guessed at from other studies, which may or may not be relevant.

Related items include the increasing interest in the differentiation between surface and volume reactions, e.g., work of Mairanovskii, and the revival of interest in the correlation of electrocapillary and current-potential curves.

Nonaqueous Media. Current interest in the electrochemistry of organic compounds in nonaqueous media is due not only to the practical factors of increased solvent power and decreased solvolysis, but also to theoretical considerations, e.g., medium effects on (1) mass transport through viscosity and solvation, and (2) the potential-reaction relationship through its participation directly or via derived species in (a) the primary electrochemical reaction, (b) polarization of the reactant molecules, (c) accompanying and intermediate chemical reactions, including ion-pair formation, and (d) the structure of the EDL.

Of major importance for future work in nonaqueous media is the establishment of potential scales which will permit correlation of data obtained in aqueous and nonaqueous media. The problems involved and some possible solutions have been explored by Kolthoff (3) in a recent comprehensive paper on polarography in organic solvents. There is also a need for more careful elucidation of the reactivity of the solvent and its possible participation in electrode processes, e.g., pyridine would facilitate organic oxidations, which involve removal of protons and/or formation of carbonium ions, by acting as a proton-acceptor and a carbonium ion stabilizer. Better evaluation is desirable of the purity of solvents in respect to the effect of small amounts of impurity, especially surface-active agents and water, e.g., 0.01% water in a typical solvent corresponds to a 4 or 5 mM water solution. The effect of such residual water is commonly overlooked except when the presence of a hydrogen ion source is required to complete a postulated reaction scheme.

Proton Participation. While rationalization of the experimental variation of  $E_{1/2}$  with pH has been quite well done, the theories and equations derived to rationalize such behavior have not been entirely satisfactory, due primarily to (1) uncertainties in the assumptions made and in the terms used in the equations, (2) lack of specificity in respect to the physical process which the equation aims to describe, and (3) uncertainties in the experimental data (4). The nature of pH-dependent processes has been elucidated by their investigation in proton-poor solvents, coupled with the controlled addition of proton donors, e.g., phenol. A problem, which merits further investigation, is that of the role of Lewis acids in facilitating organic reduction processes.

Background Electrolyte. The effects of background electrolyte and other solution components on the observed electrochemical behavior of organic compounds are frequently quite marked and involve, among

others, the following phenomena: (1) composition, structure and potential gradient in the EDL, (2) competitive adsorption on the electrode of electroactive species, its product and other solution components, (3) activities as affected by ionic strength, equilibrium constants, etc., (4) solvation, (5) complexation, including protonation and other Lewis acid-base adduct equilibria, ion-pairing, and charge-transfer complex formation, (6) proton activity and concentrational stability, e.g., buffering, and (7) kinetics of the various equilibria listed as well as of others involving the electroactive species, e.g., its formation from a more stable solution component. Hopefully, future studies will provide more detailed models for the rationalization of electrolyte effects.

#### ELECTRODE REACTION MECHANISMS

Current conceptions of the mechanisms of organic electrode processes have been recently summarized by Perrin (5). Descriptions of such processes frequently still merely involve the listing of the products of the electrode reaction with, in some cases, more or less speculative postulation of intermediates formed during the reaction. Only in a few cases has there been sufficiently detailed experimental evidence to allow the postulation of structures for the transition states involved.

General Mechanistic Path. A mechanistic pattern has been outlined (6) for organic electrode processes, which not only rationalizes the general course of such processes but also the occasional changes in mechanism with experimental conditions or between members of a homologous series, e.g., reduction of a ketone to either pinacol or carbinol by selection of pH and applied potential.

The fundamental process in an organic electrochemical reduction is bond rupture, which requires only one electron to produce a free radical species; addition of a second electron completes rupture of the bond to give a carbanion. Consequently, only  $1e^-$  or  $2e^-$  processes need be considered in mechanism discussion; transfer of more than 2 electrons in a single polarographic wave is due to (1) mechanical fusion of waves and/or (2), more importantly, instability of the species produced as a result of the first electron-transfer step at the potential of its formation and, consequently, its immediate further reduction.

On this basis, one can postulate the general mechanism, outlined in Fig. 1, involving a generalized carbon reaction site, R:X, where R represents the reactive carbon center and X another carbon, oxygen, nitrogen, halogen or other atom. There may be more than one bond between R and X, e.g., in an olefinic or carbonyl group. (Electrochemical reduction is illustrated, since it has been much more extensively studied than electrochemical oxidation; generally analogous patterns can be formulated for the latter.)

In the primary step of the electrode process, the reaction site accepts a single electron to form the electrode activated complex, which can then either revert to the original species or dissociate to give a free radical precursor and an anionic species; if a multiple bond was originally present between R and X, these two species could form a single free radical anion. The exact nature of these species will be modified by the extent of participation of protons, solvent molecules and other solution constituents or even the electrode surface (participation of the latter species in subsequent steps, al-

though not explicitly indicated, may be involved.)

The free radical precursor either immediately on formation can accept a second electron and be reduced to a carbanion or can exist as a stable free radical species. The latter can either dimerize or, at more negative potential, be further reduced to the equivalent of a carbanion. The charge on the carbanion, formed by either path, can be neutralized either by acceptance of a proton from the solution or by electronic rearrangement with the charge being transferred to another part of the molecule where it can be suitably handled.

Chemical reactions preceding, accompanying or following the charge-transfer process may - and often do - play significant roles in the overall process, e.g., the possibly profound effect of the kinetics of such reactions upon the observed polarographic pattern.

The reaction scheme outlined will be illustrated by the complex pattern of five polarographic waves observed in the reduction of pyrimidine in aqueous solution. As an example of a more detailed postulation of an organic electrode process with respect to the site at which electron transfer occurs, the reduction of a ketone in acidic solution, which results in two  $1e$  waves (I: pH-dependent; II: nearly pH-independent) will be considered.

Time will probably not allow discussion of (1) structure in causing steric hindrance, in the steric control of products, and in stereospecific electrode reactions, or (2) the relatively scanty measurements of heterogeneous rate constants and transfer coefficients for organic electrode reactions (cf. effect of adsorption of organic compounds on their electrochemical kinetics).

#### HALF-WAVE POTENTIAL CORRELATION

Correlation of polarographic  $E_{1/2}$  values with numerical structural and reactivity characteristics is usually based on the postulation that the characteristic  $E_{1/2}$  of a compound is a function of electron density and other factors, which, in turn, are also relatively simply related to some biological, physical or chemical property. The frequently resulting linear relationship between  $E_{1/2}$  for a series of more or less closely related compounds and a suitably selected mathematical function of the values of the given property for that series of compounds permits (1) prediction of the magnitude of the property of a compound from its readily measured  $E_{1/2}$  and (2) the rapid comparative evaluation of a property based on comparison of  $E_{1/2}$  values.

The large variety of experimental and theoretical properties and phenomena, which have been compared to polarographically determined potential data, include photoionization potentials, degree of carcinogenesis, wavelengths of spectrophotometric absorption maxima, anti-oxidant ability, quantum mechanically calculated parameters, and structural summation characteristics. The best known and most extensively used correlations have involved various forms of the Hammett  $\sigma$ - $\rho$  equation based on polar substituent quantities and the Taft modification (cf. reviews by Zuman (7) and Perrin).

Correlations of molecular orbital (M.O.) calculations with polarographic data generally involve the quantum mechanically calculated energies for adding an electron to the lowest empty M.O. or removing one from the highest occupied M.O. *A priori*, the optimum approach would seem to involve the use of electrochemical data based on initial

le processes, since the M.O. data apply to such processes. While such le processes can be observed for some organic compounds in aqueous media, in the case of other compounds, measurements in nonaqueous media are necessary. The validity of this approach is shown by the work of Streitwieser and others on the correlation of potentials for the oxidation of organic compounds in nonaqueous media at platinum electrodes with a variety of calculated values based on M.O. theory (cf. review by Zahradnik and Parkanyi (8)).

#### APPLICABILITY OF ORGANIC ELECTROCHEMISTRY

Finally, reference should be made to some applications based on the study of organic electrochemical processes, e.g., the use of polarography in elucidating problems in organic chemistry involving equilibria, rates and mechanisms, synthesis and structure.

The study of interactions is typified by Peover's work on donor-acceptor charge-transfer complexes in nonaqueous media; the formation of intermediate species was detected by polarography, which could not be picked up by spectrophotometry.

The correlation of the mechanisms of electrochemical and biological processes is a provocative possibility, which is related to the fact that electrolytic oxidations and reductions occur under experimental conditions resembling those of enzymatic and other biological transformations. Thus, the electrolytic oxidation of uric acid proceeds by a mechanism analogous to that postulated for the enzymatic oxidation.

Synthesis. The potentialities of preparative organic electrochemistry at controlled potential have, by and large, not yet been realized, being used commercially only for the small-scale production of relatively costly products. The principal limitation has been the difficulty of controlling the applied potential, which generally has to be very large because of the  $iR$  drop encountered for the appreciable current flow desirable in a preparative process.

Frequently, it is possible to control the potential by control of experimental conditions, electrolysis process and/or current drawn. An outstanding example of this approach is the work of Baizer (9), who has extensively investigated inter- and intramolecular electrolytic reductive coupling of unsaturated species to produce a variety of compounds, many of which are not readily accessible by more conventional synthesis. Adiponitrile, used in the manufacture of nylon, is now being made commercially by the electrolytic reductive coupling of acrylonitrile.

An interesting application of electrosynthesis is the generation of free radical species for study by electron spin resonance.

Fuel Cells. A considerable fraction of the research activity on fuel cells during the past decade has been focussed on the electrochemical oxidation of hydrocarbons at catalyst-type electrodes with some attention to that of oxygenated compounds, e.g., alcohols. Although there has been considerable publication of mechanistic studies, the complexity of the electrode process for the oxidation of even as simple a hydrocarbon as propane to carbon dioxide and water has defied satisfactory rationalization. The electrochemical reactions of the hydrocarbon and immediate oxidizable organic products may be masked by the electrochemical oxidation of hydrogen split off from the hydro-

carbon as active hydrogen or in a reforming reaction. The nature of the electrode is such as to favor adsorption as an essential feature of the electrochemical reaction.

Analysis. The value of polarographic and related methods for organic analysis is too well known to merit discussion except to refer to the determination of organic compounds at trace levels, e.g., the analysis of mixtures of maleic and fumaric acids at the  $10^{-7}$  M level by the use of pulse polarography.

#### ACKNOWLEDGMENT

The author thanks the U. S. Atomic Energy Commission, which long supported his work on the polarographic behavior of organic compounds.

#### REFERENCES

- (1) R. S. Nicholson, I. Shain, et al., *Anal. Chem.*, **36**, 706, 1212 (1964); **37**, 178, 190, 1351 (1965); **38**, 150, 542, 1406 (1966).
- (2) P. Delahay, "Double Layer and Electrode Kinetics", Interscience Publishers, New York, 1965.
- (3) I. M. Kolthoff in G. J. Hills, ed., "Polarography 1964", Interscience Publishers, New York, 1966, pp. 1-24.
- (4) P. J. Elving, *Pure Appl. Chem.*, **7**, 423 (1963).
- (5) C. L. Perrin in S. G. Cohen, et al., ed., "Progress in Physical Organic Chemistry", Volume III, Interscience Publishers, New York, 1966.
- (6) P. J. Elving and B. Pullman in I. Prigogine, ed., "Advances in Chemical Physics", Vol. III, Interscience Publishers, New York, 1961, pp. 1-31.
- (7) P. Zuman, "Organic Polarographic Analysis", Pergamon Press, London, 1964.
- (8) R. Zahradnik and C. Parkanyi, *Talanta*, 1289 (1965).
- (9) M. M. Baizer, *J. Electrochem. Soc.*, **111**, 215 (1966); subsequent papers in *J. Electrochem. Soc.* and *J. Org. Chem.*

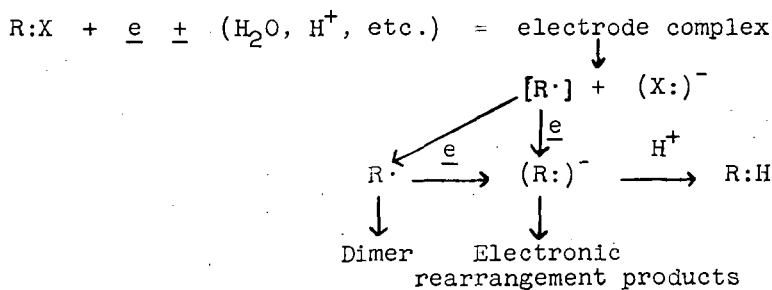


Fig. 1. Generalized reaction mechanism for an organic electrode reaction (R:X represents a generalized reaction site). Allowance has to be made in the above formulation for (a) the participation of protons, solvent, other solution constituents and the electrode surface in various steps, (b) the presence of chemical reactions preceding, accompanying and following charge-transfer processes, and (c) resulting modification of the species shown.

## SURVEY OF MODERN ELECTROANALYTICAL METHODS

Charles N. Reilley  
 Department of Chemistry  
 University of North Carolina  
 Chapel Hill, N. C. 27514

The recent thrust of electroanalytical techniques has been primarily directed toward analysis of the nature of electrode processes rather than toward evaluation of solution concentrations. As an aid in accomplishing this goal, a whole series of new methods have been developed. The first group, involving semi-infinite diffusion, can be classified into two broad categories by the size of the excitation signal ("large" and "small" amplitude), and then each can be further sub-classified according to the form (shape, periodicity, etc.) of the excitation signal and occasionally according to the monitored response. Ideally, the small amplitude cases are those where the excitation signal is sufficiently small that the perturbation introduced can be considered linear. Nevertheless, those cases where the excitation signal is small, but primary attention is given to minute non-linear effects, are considered in this group. The aforementioned excitation signal is an impressed voltage, current, or, in some cases, a combination of these which is experimentally applied over a time interval. This signal, in turn, evokes from the system a response signal of the complimentary electrical variable whose amplitude and time dependency reflects the composition and nature of the electrochemical system under consideration. This response signal, in whole or in part, is then converted into a monitored response by electrical, mechanical, or graphical means and is displayed unchanged, or in differential or integral form, as a function of  $t$ ,  $t^{1/2}$ ,  $E$ , or some other convenient parameter. The presentation is suggested by theory and ameliorated by instrumentation. In this manner, the effect of chemical kinetic complications, such as pre-kinetic, post-kinetic, catalytic, or successive reactions can be exaggerated and the evaluation simplified. Similar principles facilitate the evaluation of adsorption phenomena and electron-transfer rates. The following figures (prepared by William Heineman and Thomas Ridgway of this laboratory) indicate some, but by no means all, of the methods currently available and utilized.

Thin-film and thin-layer electrodes offer several interesting avenues in electrochemical investigations. Both involve diffusion across a thin film or layer; with a thickness of  $10^{-3}$  to  $10^{-2}$  cm., essentially homogeneous mixing is accomplished by simple diffusion in 0.1 to 10 seconds. For the latter technique, a thin layer of sample solution is confined between two boundaries, at least one of which is a working electrode. This system has been applied to rapid controlled-potential coulometry and to the study of adsorption and post-kinetic reactions. When both boundaries are independent working electrodes, several approaches to the study of chemical events occurring in the thin layer are possible. Chemical changes initiated at one electrode may be observed or modified at the other electrode with only a small time lag. Also rapid attainment of steady-state current is achieved where an oxidation occurs at one electrode and the corresponding reduction at the other.

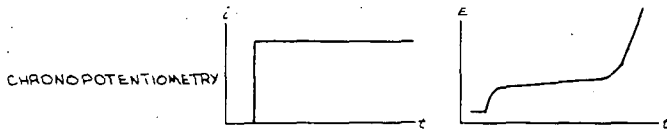
Some interesting applications of the technique are:

1. establishment of diffusion coefficients;
2. steady-state current as a function of the potentials of the two electrodes: steady-state "voltammetry";
3. rapid controlled-current or controlled-potential coulometric titrations in the thin layer;
4. study of the products of electrode reactions; intermediate oxidation states, metastable products, adsorption isotherms of products, etc.;
5. kinetics of chemical reactions in the solution layer;
6. photolysis and spectrophotometry in the thin layer.

I. LARGE AMPLITUDE ELECTROANALYTICAL TECHNIQUES

NAME	EXCITATION SIGNAL	SYSTEM RESPONSE SIGNAL	MONITORED RESPONSE
------	-------------------	------------------------	--------------------

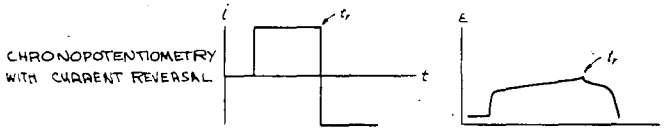
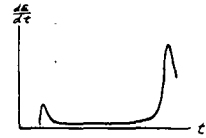
CONTROLLED CURRENT



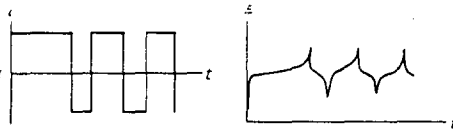
DERIVATIVE CHRONOPOTENTIOMETRY

SAME

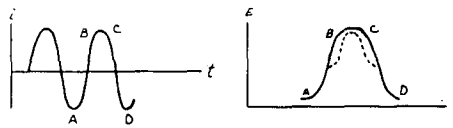
SAME



CYCLIC CHRONOPOTENTIOMETRY



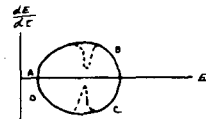
A.C. OSCILLOGRAPHIC POLAROGRAPHY



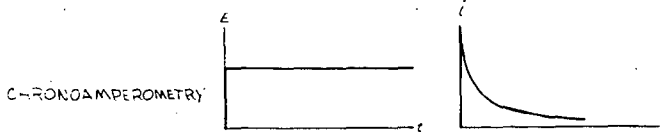
OSCILLOPOLAROGRAPHY

SAME

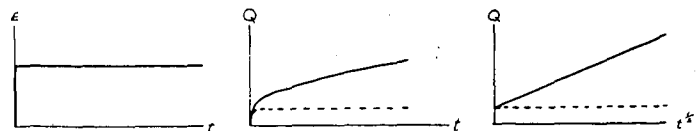
SAME

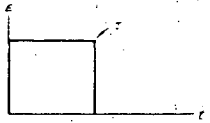
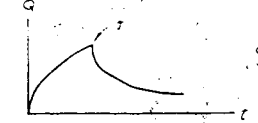
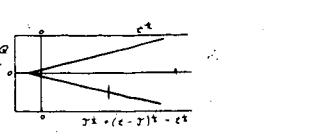
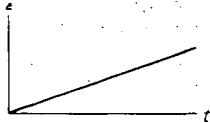
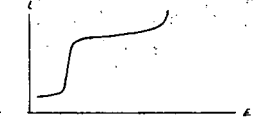
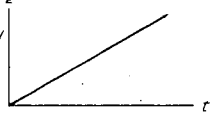
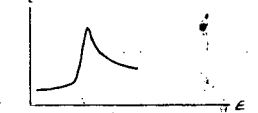
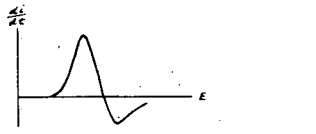
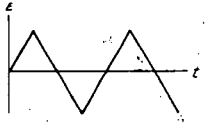
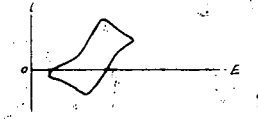
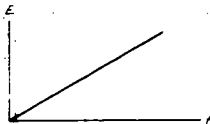
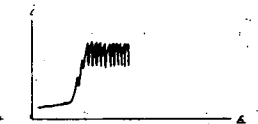
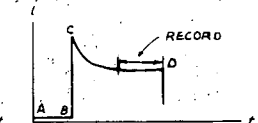
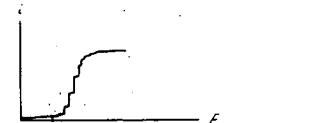
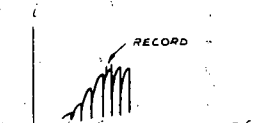
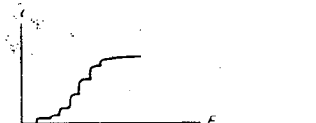
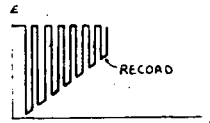
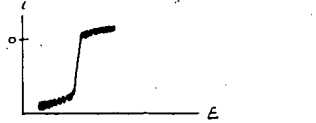


CONTROLLED POTENTIAL



POTENTIAL STEP CHRONOCALCULOMETRY



NAME	EXCITATION SIGNAL	SYSTEM RESPONSE SIGNAL	MONITORED RESPONSE
DOUBLE POTENTIAL STEP CHRONOCOULOMETRY			
VOLTAMMETRY			
CHRONOAMPEROMETRY WITH POTENTIAL SWEEP			
DERIVATIVE VOLTAMMETRY	SAME	SAME	
CYCLIC VOLTAMMETRY			
POLAROGRAPHY			
PULSE POLAROGRAPHY			
FAST POLAROGRAPHY			
CALOUSEK I			

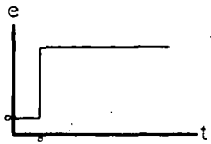
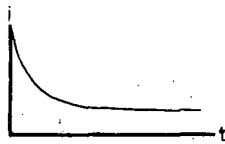
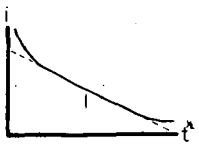
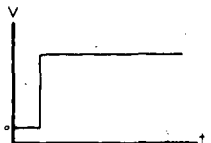
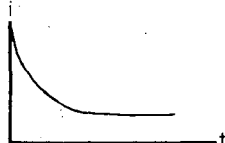
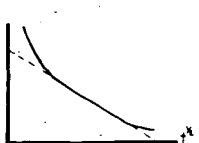
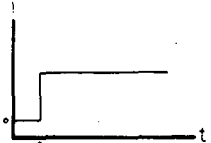
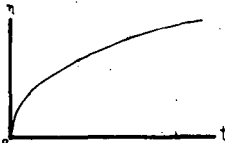
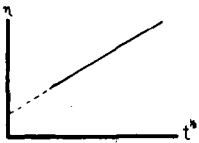
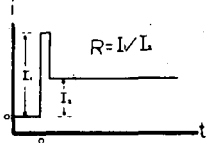
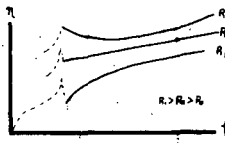
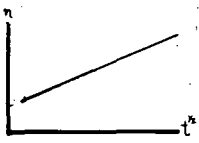
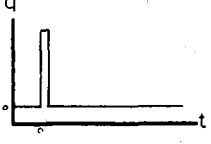
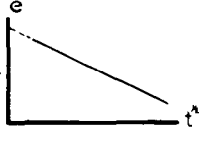
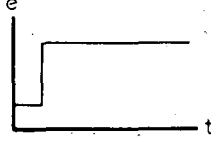
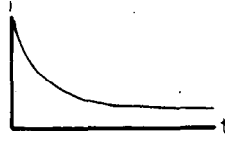
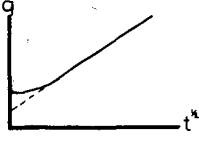
I. [CONTINUED]

NAME	EXCITATION SIGNAL	SYSTEM RESPONSE SIGNAL	MONITORED RESPONSE
KALOUSEK II			
SINGLE - SWEEP OSCILLOGRAPHIC POLAROGRAPHY			
MULTISWEEP OSCILLOGRAPHIC POLAROGRAPHY			
TRIANGULAR - WAVE OSCILLOGRAPHIC POLAROGRAPHY			
CYCLIC TRIANGULAR - WAVE OSCILLOGRAPHIC POLAROGRAPHY			

II. SMALL AMPLITUDE ELECTROANALYTICAL TECHNIQUES

NAME	control ac dc	EXCITATION SIGNAL	SYSTEM RESPONSE SIGNAL	MONITORED RESPONSE
ac polarography	E E			
square wave polarography	E E			
Kalousek III polarography	E E			
triangular wave polarography	E E			
staircase polarography	E E			
derivative pulse polarography	E E			
tensammetry	E E			
ac chronopot	I I			
av polarography	I E			

NAME	control ac dc	EXCITATION SIGNAL	SYSTEM RESPONSE SIGNAL	MONITORED RESPONSE
av chronopot	E I			
intermodulation polarography	E E			
rf polarography	E E			
higher harmonic ac polarography	E E			
faradaic rectification	I I=0			
faradaic rectification	E I=0			
faradaic rectification	E E=E <sub>c</sub>			
faradaic rectification	I E=E <sub>c</sub>			
sawtooth sweep	E E			

NAME control dc	EXCITATION SIGNAL	SYSTEM RESPONSE SIGNAL	MONITORED RESPONSE
E potentiostatic			
V voltastatic			
I galvanostatic single pulse			
I galvanostatic double pulse			
Q coulostatic			
E integral potential step			

## Current Distribution and Mass Transfer in Electrochemical Systems

John Newman

Inorganic Materials Research Division, Lawrence Radiation Laboratory, and  
Department of Chemical Engineering, University of California, Berkeley

Fundamental equations describing transport in dilute electrolytic solutions have been known since the turn of the century. In an electrochemical system, many processes occur simultaneously, and the treatment of such systems involves consideration of the ohmic potential drop, concentration changes near electrodes, and the kinetics of the heterogeneous electrode reaction.

Application of these principles has followed two main courses. There are systems where the ohmic potential drop can be neglected. The current distribution is then determined by the same principles which apply to heat transfer and non-electrolytic mass transfer. This usually involves systems operated at the limiting current with an excess of supporting electrolyte. Let us call these "convective-transport problems."

At currents much below the limiting current it is possible to neglect concentration variations near the electrodes. The current distribution is then determined by the ohmic potential drop in the solution and by electrode overpotentials. Mathematically, this means that the potential satisfies Laplace's equation, and many results of potential theory, developed in electrostatics, the flow of inviscid fluids, and steady heat conduction in solids, are directly applicable. Let us call these "potential-theory problems." The electrode kinetics provide boundary conditions which are usually different from those encountered in other applications of potential theory.

Problems have been treated which do not fall within either of these two classes. First, there are "intermediate problems," where convective transport is essential but neither concentration variations near the electrode nor the ohmic potential drop in the solution can be neglected. These involve currents below, but at an appreciable fraction of, the limiting current.

Some problems are not so general, but can be regarded as an extension of the convective-transport problems. At the limiting current the ohmic potential drop in the bulk of the solution may still be negligible, but the electric field in the diffusion layer near electrodes may lead to an enhancement of the limiting current. The current may then be distributed in a similar fashion, but the magnitude is changed.

In porous electrodes convection may not be present, but it is usually necessary to consider the ohmic potential drop, concentration variations, and electrode kinetics. Most treatments adopt a macroscopic model which does not take account of the detailed, random geometry of the porous structure. Results of potential theory are then not applicable since Laplace's equation does not hold.

Transport in electrolytic solutions. The concentration and potential distributions are to be determined from the equations

$$\underline{N}_i = -z_i u_i F c_i \nabla \Phi - D_i \nabla c_i + \underline{v} c_i \quad (1)$$

$$\frac{\partial c_i}{\partial t} = -\nabla \cdot \underline{N}_i, \quad \underline{i} = F \sum_i z_i \underline{N}_i, \quad \sum_i z_i c_i = 0 \quad (2,3,4)$$

The first states that species in the solution can move by migration, diffusion, and convection. The second is a material balance for a species. The third states

that the current arises from the motion of charged particles. The fourth is the condition of electroneutrality. These laws provide the basis for the analysis of electrochemical systems. The fluid velocity is to be determined from the laws of fluid mechanics.

Electrode kinetics. The differential equations describing the electrolytic solution require boundary conditions in order for the behavior of an electrochemical system to be predicted. The most complex of these concerns the kinetics of electrode reactions and relates the normal component of the current density at an electrode to the surface overpotential. The surface overpotential  $\eta_s$  can be defined as the potential of the working electrode relative to a reference electrode of the same kind located just outside the double layer.

There is no completely general expression describing electrode kinetics. However, it is adequate for our present purpose to assume that the current density depends exponentially on the surface overpotential in the following form:

$$i = i_0 \left[ \exp \left\{ \frac{\alpha n F}{RT} \eta_s \right\} - \exp \left\{ - \frac{(1-\alpha) n F}{RT} \eta_s \right\} \right]. \quad (5)$$

Convective-transport problems. For the reaction of minor ionic species in a solution containing excess supporting electrolyte, it should be permissible to neglect the contribution of ionic migration to the flux of the reacting ions, so that equation (1) becomes

$$\underline{N}_i = -D_i \nabla c_i + \underline{v} c_i, \quad (6)$$

and substitution into equation (2) yields

$$\frac{\partial c_i}{\partial t} + \underline{v} \cdot \nabla c_i = D_i \nabla^2 c_i. \quad (7)$$

This may be called the equation of convective diffusion. A similar equation applies to convective heat transfer and convective mass transfer in non-electrolytic solutions. Since these fields have been studied in detail, it is possible to apply many results to electrochemical systems which obey equation (7).

The systems typically studied in heat and mass transfer involve laminar and turbulent flow with various geometric arrangements. The flow may be due to some more or less well characterized stirring (forced convection) or may be the result of density differences created in the solution as part of the transfer process (free convection).

Essential to the understanding of convective-transport problems is the concept of the diffusion layer. Frequently, due to the small value of the diffusion coefficient, the concentrations differ significantly from their bulk values only in a thin region near the surface of an electrode. In this region the velocity is small, and diffusion is important to the transport process. The thinness of this region permits a simplification in the analysis, but it is erroneous to treat the diffusion layer as a stagnant region. Figure 1 shows the concentration profile in the diffusion layer, with the electrode surface at the left. Far from the surface convective transport dominates, while at the surface itself there is only diffusion.

To illustrate the current distribution obtained in this type of problem, consider two plane electrodes of length  $L$  and separated by a distance  $h$  and which form parts of the walls of a flow channel with otherwise insulating walls. For laminar flow from left to right, with an average velocity  $\langle v \rangle$ , the limiting current density has the distribution, as illustrated in figure 2,

$$i = 0.9783 \frac{nF D_i c_\infty}{s_i} \left( \frac{\langle \nu \rangle}{hD_i x} \right)^{1/3}, \quad (8)$$

where  $x$  is the distance along the electrode. The mass-transfer rate is infinite at the upstream edge of the electrode where fresh solution is brought in contact with the electrode. The current decreases with increasing  $x$  since the solution in the diffusion layer has already been depleted by the electrode reaction further upstream. Later it will be instructive to compare this current distribution with that which would be obtained when the ohmic potential drop in the solution is controlling.

Other convective-transport problems which have been treated include flow in a pipe and in annular conduits, a flat plate in a free stream, rotating cylinders, growing mercury drops, rotating disks, and free convection at vertical and horizontal plates and outside spheres and cylinders.

Applications of potential theory. When concentration gradients in the solution can be ignored, equations (3), (1), and (4) yield

$$\underline{i} = -\kappa \nabla \Phi \quad (9)$$

where

$$\kappa = F^2 \sum_i z_i^2 u_i c_i \quad (10)$$

is the conductivity of the solution. Equation (2) when multiplied by  $z_i$  and summed over  $i$  yields

$$\nabla^2 \Phi = 0, \quad (11)$$

that is, the potential satisfies Laplace's equation.

The boundary conditions are determined with equation (9). On insulators

$$\partial \Phi / \partial y = 0, \quad (12)$$

where  $y$  is the normal distance from the surface. On electrodes, equation (9) relates this potential derivative to the surface overpotential through equation (5). If the potential  $\Phi$  in the solution is measured with a reference electrode of the same kind as the working electrode, then the surface overpotential can be eliminated with the relation

$$\eta_s = V - \Phi, \quad (13)$$

where  $V$  is the potential of the metal electrode. The resulting boundary condition is a nonlinear relationship between the potential and the potential derivative and is not commonly encountered in other applications of potential theory.

In so-called primary-current-distribution problems the surface overpotential is neglected altogether, and the solution adjacent to the electrode is taken to be an equipotential surface. The resulting current distribution for the plane electrodes in the flow channel considered earlier is shown in figure 2 for  $L = 2h$ . The distribution is symmetric since convection is not important. The current density is infinite at the ends of the electrodes since the current can flow through the solution beyond the ends of the electrodes. This is a general characteristic of primary current distributions. The current density where an electrode meets an insulator is either infinite or zero unless they form a right angle.

The so-called secondary current distribution takes into account the surface overpotential, although the boundary condition is frequently replaced by a linear or a logarithmic (Tafel) relation between the potential and the potential derivative. The general effect of electrode polarization is to make the secondary current distribution more nearly uniform than the primary current distribution, and an infinite current density at the edge of electrodes is eliminated.

Intermediate problems. The current distribution on a rotating disk electrode<sup>1</sup> and free convection on two vertical electrodes at either end of a rectangular tank<sup>2</sup> have been treated with account taken of concentration variations, ohmic potential drop, and surface overpotential. The results are, as one might expect, intermediate between the two extreme cases. The formulation of the problem so as to take advantage of the thinness of the diffusion layer has also been discussed.<sup>3</sup>

Effect of migration on limiting currents. At the limiting current, the current density is distributed along the electrode in the same manner as when migration is neglected, but the magnitude of the current density at all points is increased or diminished by a constant factor which depends upon the bulk composition of the solution. This effect has been treated<sup>3,4</sup> for the rotating disk, the growing mercury drop, penetration into a semi-infinite medium, the stagnant Nernst diffusion layer, and arbitrary two-dimensional and axisymmetric diffusion layers.

- 
- <sup>1</sup> John Newman. "Current Distribution on a Rotating Disk below the Limiting Current." Journal of the Electrochemical Society, 113, 1235-1241 (1966).
  - <sup>2</sup> Kameo Asada, Fumio Hine, Shiro Yoshizawa, and Shinzo Okada. "Mass Transfer and Current Distribution under Free Convection Conditions." Journal of the Electrochemical Society, 107, 242-246 (1960).
  - <sup>3</sup> John Newman. The Effect of Migration in Laminar Boundary Layers. UCRL-16665-Rev. December, 1966.
  - <sup>4</sup> John Newman. "Effect of Ionic Migration on Limiting Currents." Industrial and Engineering Chemistry Fundamentals, 5, 525-529 (1966).

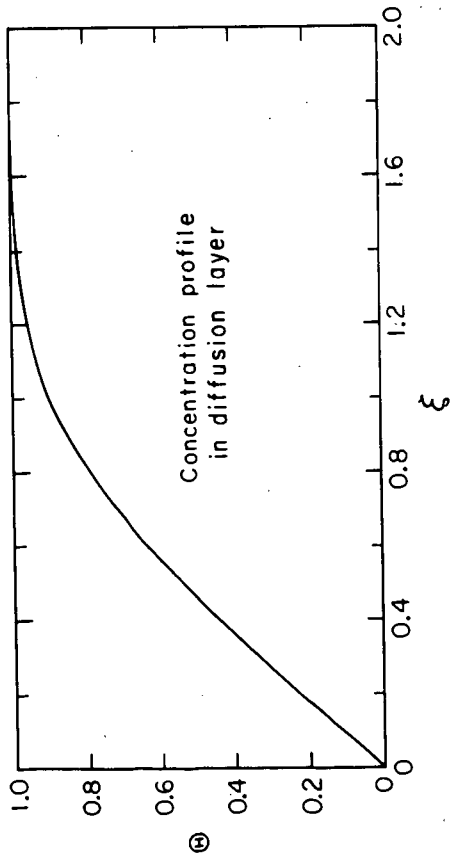
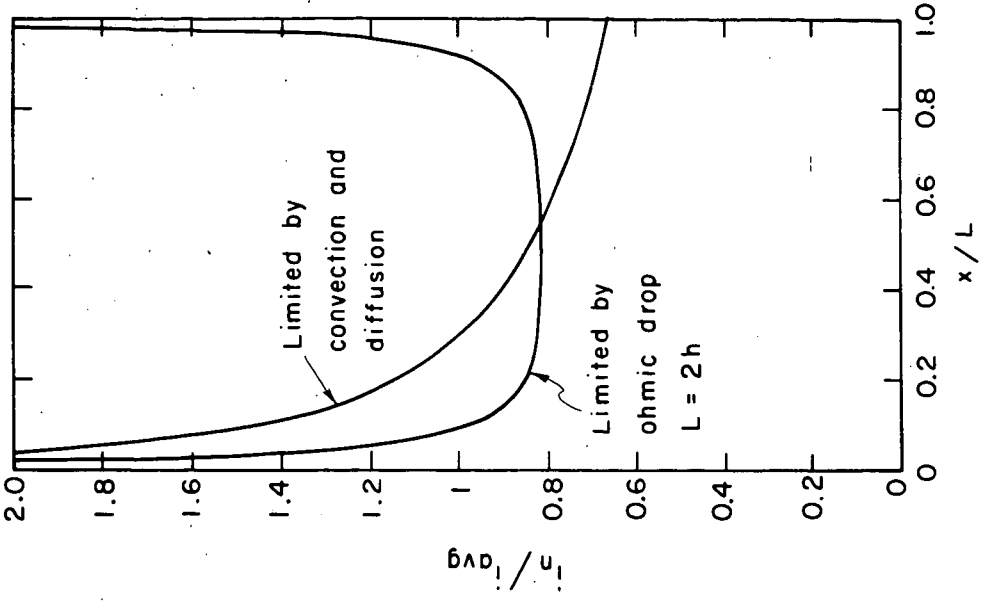


Figure 1.

Figure 1. Current distribution on planar electrodes.

THE EFFECT OF FUNDAMENTAL PROPERTIES OF ELECTRODE  
MATERIALS ON ELECTROCATALYSIS

J. O'M. Bockris, A. Damjanovic and R. J. Mannan

Electrochemistry Laboratory  
University of Pennsylvania  
Philadelphia, Pa. 19104

The most important aspect of electrocatalysis is the mechanism of charge transfer at the metal solution interface and the various factors affecting it. To elucidate major factors affecting the catalysis, the kinetics of  $\text{Fe}^{++}/\text{Fe}^{+++}$ , and also of  $\text{H}^+/\text{H}_2$  reactions were studied on a number of metals and alloy electrodes, as well as on electrodes of some complex compounds. Studies with the  $\text{Fe}^{++}/\text{Fe}^{+++}$  redox system are of particular interest as they provide information about the role of electrodes in a charge transfer reaction in the absence of complicating adsorption. The  $\log i_0$  values at Pt, Rh, Ir, Pd, and Au are found, for this system, to be linearly dependent on the work function. The linearity was also observed with atomic composition in Au-Pd and Au-Pt alloys. Several carbide electrodes ( $\text{TiC}$ ,  $\text{TaC}$ , and  $\text{B}_4\text{C}$ ) and tungsten bronzes with a general formula of  $\text{Na}_x\text{WO}_3$  ( $x < 1$ ) exhibited stability and activity comparable to those of noble metals in the redox reaction. The importance of the electronic factors in electrode catalysis is demonstrated for  $\text{H}^+/\text{H}_2$  reaction by the linear relation established between  $\log i_0$  and per cent d-character in Au-Pd and Au-Pt alloys. The observed changes in the activities for these reactions at different metals or with different alloy compositions are discussed in relationship to the physical properties of metals and alloys.

Electrochemistry in Thin Layers of Solution

FRED C. ANSON

Gates and Crellin Laboratories of Chemistry, California  
Institute of Technology, Pasadena, California 91109

Although the major recent interest in the potentialities of thin layer electrochemical experiments seems to date from a paper published in 1963 (1), the idea that advantages might be inherent in experiments with very

---

(1) C. R. Christiansen and F. C. Anson, *Anal. Chem.*, **35**, 205 (1963).

---

thin layers of solution is older. In 1962, Schmidt and Gygaux (2), for example,

---

(2) G. Schmidt and H. R. Gygaux, *Chimia*, **16**, 165 (1962).

---

discussed the use of a thin layer cell for studies of metal deposition on solid electrodes and presented designs for useful cells.

However, the advent of a micrometer-type thin layer cell (3, 4)

---

(3) A. T. Hubbard and F. C. Anson, *Anal. Chem.*, **36**, 723 (1964).

---

(4) D. M. Oglesby, S. H. Omang, and C. N. Reilley, *ibid.*, **37**, 1312 (1965).

---

has made the exploitation of the technique much easier and, therefore, more rapid.

Figure 1 shows a typical micrometer-type cell. The details of its construction and operation have been given (3, 4) and need not be repeated here. Descriptions of numerous experimental applications of this type of cell have also appeared (5-13) as well as an impressive catalog of suggested experiments for

---

(5) A. T. Hubbard and F. C. Anson, *J. Electroanal. Chem.*, **9**, 163 (1963).

(6) A. T. Hubbard and F. C. Anson, *Anal. Chem.*, **38**, 58 (1966).

(7) *Ibid.*, **38**, 692 (1966).

(8) *Ibid.*, **38**, 1601 (1966).

(9) *Ibid.*, **38**, 1887 (1966).

(10) D. M. Oglesby, L. B. Anderson, B. McDuffie, and C. N. Reilley, *ibid.*, **37**, 1317 (1965).

(11) L. B. Anderson and C. N. Reilley, *J. Electroanal. Chem.*, **10**, 295 (1965).

(12) H. Dahms, *ibid.*, **11**, 62 (1966).

(13) D. M. Oglesby, J. D. Johnson, and C. N. Reilley, *Anal. Chem.*, **38**, 385 (1966).

---

which the results have been predicted if not yet obtained. (14, 15)

(14) L. B. Anderson and C. N. Reilley, *J. Electroanal. Chem.*, **10**, 538 (1965).

(15) L. B. Anderson, B. McDuffie and C. N. Reilley, *ibid.*, **12**, 477 (1966).

One of the major unique advantages of the thin layer approach is the facility it provides for performing fast exhaustive electrolysis. The dimensions of the thin layer can be made small enough so that all of the reactant dissolved in the solution reaches the electrode surface by diffusion within a few seconds. Under these conditions all of the reactant contained in the layer of solution is electrolyzed so that the relation between the amount of electricity,  $Q$  required to consume all of the reactant and its concentration,  $C$ , is given by Faraday's Law:

$$Q = nFA\ell C \quad (1)$$

where  $n$  is the number of electrons involved in the electrode reaction,  $F$  is the Faraday,  $A$  is the electrode area, and  $\ell$  is the solution thickness ( $A \times \ell =$  the solution volume).

Excellent agreement of experimental results with equation 1 have been obtained and advantage has been taken of this property to determine  $n$ -values for electrode reactions.

A particularly simple and yet powerful exploitation of the adherence of thin layer experiments to equation 1 is in studies of reactant adsorption (4). If the faces of the electrodes in the micrometer cell are equilibrated with an excess a solution of potentially adsorbed reactant and then all of the solution except for a thin layer of volume  $A \times \ell$  removed, and an exhaustive electrolysis performed the quantity of electricity required will be given by equation 2

$$Q = nFA\ell C + 2nFA\Gamma \quad (2)$$

where  $\Gamma$  is the amount of adsorbed reactant in moles/cm<sup>2</sup> and the factor of 2 arises because the adsorption occurs on two electrodes of area  $A$ . In favorable cases it is possible to make  $\ell$  so small that  $2nF\Gamma$  is comparable or even greater than  $nFA\ell C$  so that quite accurate measurements of  $\Gamma$  are possible.

Another already exploited use of the thin layer cell is in the detection of intermediates in electrode reactions. By insulating the two platinum pole pieces of the thin layer cell from each other they can be used as independent probes of the same thin layer of solution. Thus, products of a reaction at one electrode can be continuously detected and determined at the opposing electrode which can be independently controlled at whatever potential is characteristic for the determination of particular suspected intermediate.

Advantage has been taken of this feature of thin layer cells to establish that oxygen is not evolved in significant amounts when platinum electrodes are oxidized at potentials below 1.2 volts vs S. C. E. and that considerable ozone is evolved at more anodic potentials (15). It has also been possible by means of the

(15) G. Lauer, Ph. D. Thesis, California Institute of Technology, Pasadena, California, 1966.

thin layer cell to detect directly the presence of "irreducible oxide" on the surface of platinum electrodes which have been oxidized and subsequently reduced. When the thin layer electrodes were treated in this way and then just filled with warm hydrochloric acid, current-potential curves were obtained which matched those

for independently prepared solutions of  $\text{PtCl}_6^-$ . Blank experiments with oxidized, reduced, and "aged" electrodes did not lead to any detectable  $\text{PtCl}_6^-$  (15).

Reilley and co-workers have applied the thin layer approach to twin electrode cells in which one face of a micrometer electrode is an anode and the other a cathode. Steady state currents can be set up with such a configuration and the magnitudes of these currents can be used to measure diffusion coefficients or to study the kinetics of chemical reactions coupled to the electrode reaction. The great simplification in mathematics afforded by the thin layer conditions permits the straightforward treatment of cases that pose considerable difficulty with the usual techniques, e.g. the second order disproportionation of uranium(V) (16).

---

(16) C. N. Reilley and B. McDuffie, *Anal. Chem.*, **38**, 1881, (1966).

---

The list of other potential uses for the thin layer approach is endless and depends only on the ingenuity of the experimenter and his success at constructing improved cells. Especially high on our priority list are the construction of an effective mercury thin layer cell and applications to solutions containing little or no supporting electrolyte.

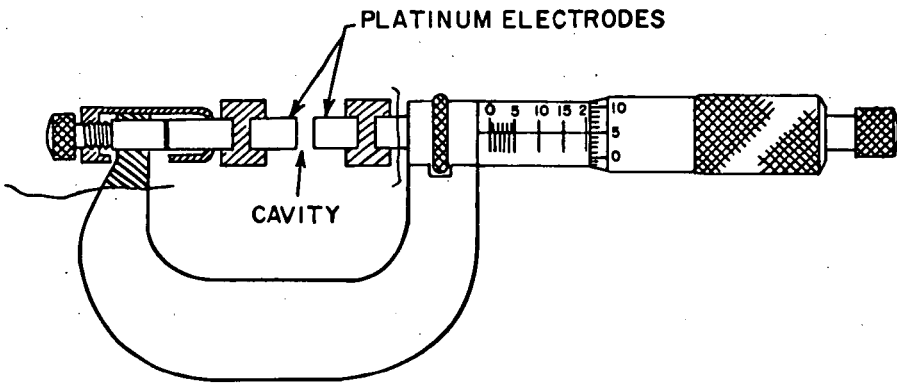


Figure 1 - Micrometer - type  
Thin Layer Cell

Chronocoulometry: Application to the Study of  
Adsorption at an Electrode Solution Interface

Robert A. Osteryoung

North American Aviation Science Center, Thousand Oaks, California 91360

Introduction

Chronocoulometry is a term used to describe a technique, developed jointly at North American Aviation Science Center and California Institute of Technology,<sup>1,8</sup> in which the charge-time behavior of an electrode in a solution is observed. The electrode, initially at some potential  $E_i$  where no current flows, has applied to it either a linear potential ramp or a potential step which results in the passage of charge across the electrode interface. If the resultant potential excursion is sufficient to bring the electrode potential into a region where a faradaic current flows, the charge passed will include coulombs required to charge the electrical double layer,  $Q_{dl}$ , as the potential changed from  $E_i$  to a final potential,  $E_f$ , and the faradaic charge passed,  $Q_F$ , from time the potential excursion is initiated at  $t=0$  until the measurement is made at some later time,  $t$ . Thus, the total charge passed,  $Q_t$ , will be

$$Q_t = Q_F + Q_{dl} \quad (1)$$

The prime assumption in what follows is that the  $Q_{dl}$  is essentially time independent, while  $Q_F$  is a function of time. If  $Q_t$  is measured as a function of time, and  $Q_F(t)$  is known, then the terms may be separated by plotting  $Q_t$  against the proper function of time. In addition, if  $\Gamma$  moles/cm<sup>2</sup> of a species Ox are adsorbed at  $E_i$  and react at  $E_f$ , an additional amount of charge,  $nF\Gamma$ , will pass. If we assume that this charge will likewise be time independent, then

$$Q_t = Q_F + Q_{dl} + nF\Gamma \quad (1')$$

$Q_F$  then arises from a faradaic reaction where the reactant must diffuse to the electrode to result in charge passage.  $Q_{dl}$  and  $nF\Gamma$  represent charge which arises from non-diffusing - hence time independent - sources.  $Q_{dl}$  must be determined, then, by an independent procedure to permit evaluation of  $nF\Gamma$ . For instance, consider an electrode in a supporting electrolyte with species Ox, at a potential  $E_i$ , when no faradaic current flows. The surface charge density,  $Q_{E_i}$  may be determined by using an extruded mercury drop or dropping mercury electrode. Now, consider the solution containing only Red at a concentration in solution or in an amalgam equal to Ox. An electrode potential  $E_f$  is impressed.  $E_f$  is such that the reaction  $Ox + ne \rightarrow Red$  would occur and the surface concentration of Ox would be zero. (This is the condition that would prevail at the electrode surface at  $E_f$  in an experiment where only Ox is initially in solution and the potential is changed to  $E_f$ , with the charge-time behavior recorded.) The charge density,  $Q_{E_f}$  is measured. However, since

$$Q_{dl} = Q_{E_f} - Q_{E_i}$$

then  $Q_{dl}$  is known regardless of how the potential is varied from  $E_i$  to  $E_f$  in the chronocoulometric experiment.

This ability to separate the faradaic and double layer charge, either by time-independence of  $Q_{dl}$  or by direct measurement of surface charge density, makes chronocoulometry particularly useful.

Chronocoulometry has been applied to the study of electrode kinetics,<sup>4,5,9-11</sup> to a study of a catalytic reaction and other reactions in solutions<sup>11-14</sup> and to studies and determinations of the extent of the adsorption of a species which undergoes reaction at the electrode surface.<sup>3,4,6-8,15,17</sup> It is principally to this latter problem that the remainder of the paper is addressed. In particular, we shall consider the use of double-potential step chronocoulometry as a technique which permits an "insitu" double layer correction even in the presence of extensive adsorption.<sup>19,20</sup>

Double Potential Step Chronocoulometry

Consider the redox couple, with standard potential  $E^0$ ,



An electrode at a potential  $E_i$ , sufficiently anodic of  $E^0$  so no current flows, is in a solution containing excess supporting electrolyte and Ox. At  $t=0$ , the potential is stepped to a value  $E_f$  sufficiently cathodic of  $E^0$  so that the surface concentration of Ox is immediately driven to zero. Reaction 2 then proceeds to the right at a rate limited by diffusion of Ox to the electrode. After a time,  $\tau$ , the potential is stepped back to  $E_i$ , which is sufficiently anodic so that the concentration of Red at the electrode surface is driven to zero. Again, the current is limited by the rate of diffusion of Red back to the electrode surface. The  $Q$ - $t$  behavior is observed.

Initially we consider neither Ox nor Red adsorbed. The faradaic charge during the forward step is given by the integral of the Cottrell equation

$$i(t) = nF\sqrt{D_{\text{Ox}}} C_{\text{Ox}} / \sqrt{\pi t}$$

and, adding in  $Q_{d1}$ , we obtain

$$Q(t < \tau) = \frac{2nF\sqrt{D_{\text{Ox}}} C_{\text{Ox}} \sqrt{t}}{\sqrt{\pi}} + Q_{d1} \quad (3)$$

where the symbols have their usual significance. For  $t > \tau$ , the charge  $Q_f$  may be obtained by integration of current-time equations derived by Kambara. This yields

$$Q(t > \tau) = \frac{2nF\sqrt{D_{\text{Ox}}} C_{\text{Ox}}}{\sqrt{\pi}} (\sqrt{t} - \sqrt{t-\tau}) \quad (4)$$

Equation (4) contains no  $Q_{d1}$  term because the electrode potential is back at its initial potential at  $t > \tau$ .

It is convenient, however, to consider the net charge,  $Q_r$ , passed during the interval  $t > \tau$ ,  $Q_r = Q(\tau) - Q(t > \tau)$ . Thus

$$Q_r = \frac{2nF\sqrt{D_{\text{Ox}}} C_{\text{Ox}}}{\sqrt{\pi}} [\sqrt{t-\tau} + \sqrt{\tau} - \sqrt{t}] + Q_{d1}$$

Thus, plots of  $Q(t < \tau)$  vs.  $t^{1/2}$  and  $Q$  vs.  $\Theta = (\sqrt{t-\tau} + \sqrt{\tau} - \sqrt{t})$  will a) be linear, b) have identical slopes ( $2nF\sqrt{D_{\text{Ox}}} C_{\text{Ox}} / \sqrt{\pi}$ ) proportional to  $C_{\text{Ox}}$ , and c) have identical intercepts equal to  $Q_{d1}$ .

If Ox is adsorbed to the extent of  $\Gamma$  moles/cm<sup>2</sup> and reacts at  $E_f$ , then

$$Q(t < \tau) = \frac{2nF\sqrt{D_{\text{Ox}}} C_{\text{Ox}}}{\sqrt{\pi}} \sqrt{t} + Q_{d1} + nF\Gamma \quad (5)$$

A plot of  $Q(t < \tau)$  vs.  $t^{1/2}$  will have the same slope as in the absence of adsorption, but the intercept will now be  $Q_{d1} + nF\Gamma$ . However, during the forward step more Red is formed at the surface,  $d1$ , and starts to diffuse away than in the absence of adsorbed Ox - i.e., Red is formed both from Ox which was adsorbed on the electrode surface and which diffuses to the electrode. This, qualitatively, will make the slope of the reverse step larger than in the absence of adsorption of Ox, hence larger than the forward slope, which is unaffected by adsorption.

Specifically, defining  $Q_r$  as before,<sup>19,20</sup>

$$Q_r = \frac{2nF\sqrt{D_{\text{Ox}}} C_{\text{Ox}}}{\sqrt{\pi}} [\Theta] + nF\Gamma \left[ 1 - \frac{2}{\pi} \sin^{-1} \sqrt{\frac{\tau}{t}} \right] + Q_{d1} \quad (6)$$

This differs from Eq. 4 only by the term  $nF\Gamma [1 - 2/\pi \sin^{-1} \sqrt{\tau/t}]$ , arising from reoxidation of initially adsorbed Ox.  $Q_{d1}$  here is the true double layer charging term in the presence of adsorption.

Equation (6) may be simplified by approximating  $(1 - 2/\pi \sin^{-1} \sqrt{\tau/t})$  with a linear function of the form  $a_1(\Theta/\sqrt{\tau}) + a_0$  to give

$$Q_r = \frac{2nF\sqrt{D_{\text{Ox}}} C_{\text{Ox}}}{\sqrt{\pi}} \left( 1 + \frac{a_1 nF\Gamma}{Q_c} \Theta \right) + a_0 nF\Gamma + Q_{d1} \quad (6')$$

where  $Q_c$  is the charge which has diffused at  $t=\tau$ ,  $(2nF/D C_{ox} \sqrt{\tau})/\pi$ . Hence, from the intercepts of  $Q(t < \tau)$  vs.  $t^{1/2}$  and  $Q_r$  vs.  $\Theta$  plots,  $nF\Gamma$  may be attained.

$$nF\Gamma = \frac{Q_c - Q_r}{1 - a_r} \quad (7)$$

when  $Q_c$  and  $Q_r$  are the intercepts in the Q-axis of the  $Q(t < \tau) - t^{1/2}$  and  $Q_r - \Theta$  plots. The constants  $a_0$  and  $a_1$ , although dependent on the experimental time-ratios used, can be made close to zero and unity, respectively. In short, the intercept of the  $Q_r - \Theta$  plot is quite close to the true  $Q_{dl}$  required.

Further,

$$\frac{S_r}{S_f} = 1 + \frac{a_1 nF\Gamma}{Q_c} \quad (8)$$

where  $S_r$  and  $S_f$  are the slopes of the reverse and forward plots, respectively, ( $Q_c$ , experimentally, is  $Q(t=\tau) - Q_c$ ). This may be used to establish an internal check on the procedure. Further, the double layer charging term is given by

$$Q_{dl} = \frac{Q_r - a_0 Q_c}{1 - a_0} \quad (9)$$

Figure 1 shows, qualitatively, the Q-t behavior expected without (a) and with (b) adsorption.

Figure 2 shows  $Q - t^{1/2}$  and  $Q_r - \Theta$  plots for 1 mM Cd(II) in 1 F KNO<sub>3</sub> and 0.8 F KNO<sub>3</sub> + 0.2 F KSCN.<sup>19,20</sup> A potential step from -200 to -950 mV vs. the SCE was applied. The points labelled Blank in A and B refer to coulombs required to charge the double layer in the Cd(II) - free base solutions. A summary of data is given in Table I. It is seen that a) the amount of Cd(II) adsorbed decreases as the initial potential is made more cathodic and b) the amount of Cd(II) adsorbed rises to a maximum and decreases with increasing thiocyanate concentration.

Figure 3 is a plot of  $nF\Gamma$  vs. E obtained chronocoulometrically for Zn(II) in 0.05 F NaSCN + 0.95 F NaNO<sub>3</sub>. This system is of interest because the potential range for E is such that complete desorption can be achieved at potentials prior to the Zn(II) reduction wave.<sup>22,23</sup> Also included in this figure,<sup>24</sup> is the amount of specifically adsorbed thiocyanate, as determined by Parsons. The straight line in the figure is a plot of the slope of the forward Q-t plot vs. [Zn(II)]. The slope should be, and is, proportional to the concentration of Zn(II).

Figure 4 is  $\Gamma$  vs. electronic charge,<sup>18</sup> rather than potential, for thiourea in 1 M NaNO<sub>3</sub> obtained by Case and Anson. The thiourea does not react, but give rise to an anodic depolarization wave. The open circles are chronocoulometric data, the circles are from classical capacity measurements of Parsons and Symons<sup>25</sup> and the triangles from Schapink et al.<sup>26</sup> This is the first instance where a direct comparison between chronocoulometry and classical methods can be made, and the agreement is overwhelming!

Using essentially a coulometric method, evidence for the validity of the assumption regarding the rapidity of the reaction of adsorbed material has been obtained.<sup>27</sup>

The chronocoulometric procedures appear to offer real advantages in adsorption and kinetic studies. With the aid of sophisticated data acquisition systems, rapid and precise measurements of parameters can be carried out.<sup>28,29</sup> It is hoped that others will attempt to apply to their problems what we consider a very useful approach to studying electrode processes.

#### References

1. R. A. Osteryoung, G. Lauer, and F. C. Anson, Anal. Chem., 34, 1833 (1962).
2. J. H. Christie, G. Lauer, R. A. Osteryoung, and F. C. Anson, Ibid, 35, 1979 (1963).
3. R. A. Osteryoung, G. Lauer, and F. C. Anson, J. Electrochem. Soc., 110, 926 (1963).

4. J. H. Christie, G. Lauer, and R. A. Osteryoung, *J. Electroanal. Chem.*, 7 60 (1964).
5. J. H. Christie, G. Lauer, and R. A. Osteryoung, *J. Electrochem. Soc.*, 111, 1420 (1964).
6. F. C. Anson, *Anal. Chem.*, 36, 932 (1964).
7. R. A. Osteryoung and F. C. Anson, *Ibid* 36, 975 (1964).
8. F. C. Anson, *Ibid* 38, 54 (1966).
9. G. Lauer and R. A. Osteryoung, *Ibid* 38, 1106 (1966).
10. P. J. Lingane and J. H. Christie, *J. Electroanal. Chem.*, 10, 284 (1965).
11. J. H. Christie, *Ibid* - in press.
12. P. J. Lingane and J. H. Christie, *Ibid* - in press.
13. R. Koopmann and H. Gerischer, *Ber. Bunsenges Physik. Chem.*, 70, 118, 127 (1966).
14. R. Koopmann, *Ibid*, 70, 121 (1966).
15. R. W. Murray and D. J. Gross, *Anal. Chem.*, 38, 392 (1966).
16. B. Epstein, Thesis - Univ. of Calif., Riverside (1966).
17. F. C. Anson and D. A. Payne, *J. Electroanal. Chem.* - in press.
18. B. Case and F. C. Anson, *J. Phys. Chem.* - in press.
19. J. H. Christie, R. A. Osteryoung, and F. C. Anson, *J. Electroanal. Chem.*, in press.
20. F. C. Anson, J. H. Christie, and R. A. Osteryoung, *Ibid* - in press.
21. T. Kambara, *Bull. Chem. Soc. Japan*, 27, 529 (1954).
22. R. A. Osteryoung and R. L. Myers - unpublished experiments.
23. J. H. Christie and R. A. Osteryoung - *J. Phys. Chem.* - in press.
24. R. Parsons - Private Communication.
25. P. C. Symons, Thesis, U. of Bristol, England, 1963.
26. F. W. Schapink, M. Oudemans, K. W. Leu, and J. N. Helle, *Trans. Faraday Soc.*, 56, 415 (1960).
27. R. A. Osteryoung and F. C. Anson, unpublished experiments.
28. R. A. Osteryoung and G. Lauer, *Anal. Chem.*, 38, 1137 (1966).
29. G. Lauer, F. C. Anson, and R. A. Osteryoung - unpublished.

Table I

Data Summary for Adsorption of Cd(II) from Thiocyanate Solutions

$nF\Gamma_0 \mu\text{C}/\text{cm}^2$       Potential } to -900 mV vs. S.C.E.  
                                          steps }  
                                          from } -400

[SCN <sup>-</sup> ]	.05 F			0.1 F			0.2 F		
[Cd(II)]	0.5 F			0.75 F			1.0 F		
$E_i =$	-200	-300	-400	-200	-300	-400	-200	-300	-400
0.2	~ 0	~ 0	~ 0	17.3	10.8	6.4	14.7	10.6	6.9
0.5	13.9	11.2	5.8	22.9	17.9	11.8	20.5	14.9	10.1
1.0	21.2	17.1	9.3	22.7	21.8	17.5	21.1	19.2	14.0
0.2	12.1	10.8	4.9	9.4	7.5	5.8	8.3	5.1	3.3
0.5	18.4	14.2	9.8	15.7	12.8	9.8	12.7	10.1	8.0
1.0	24.4	16.1	13.4	18.4	16.9	15.6	15.6	14.1	10.1

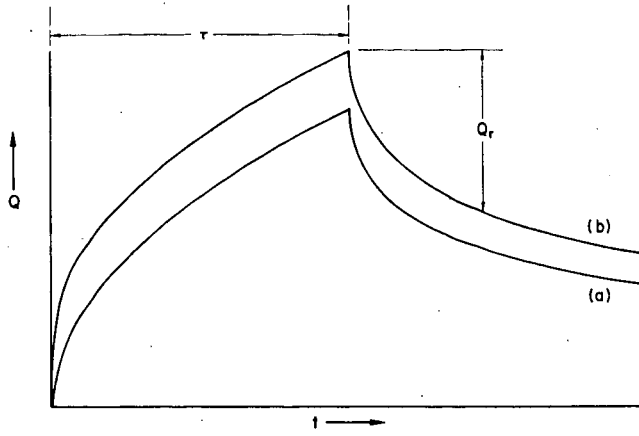


Fig. 1

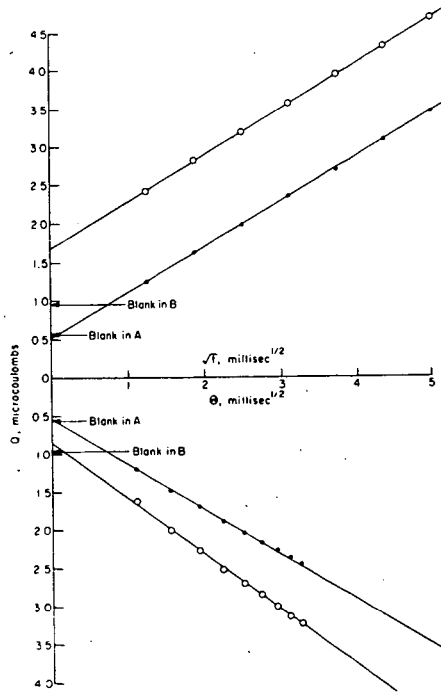


Fig. 2

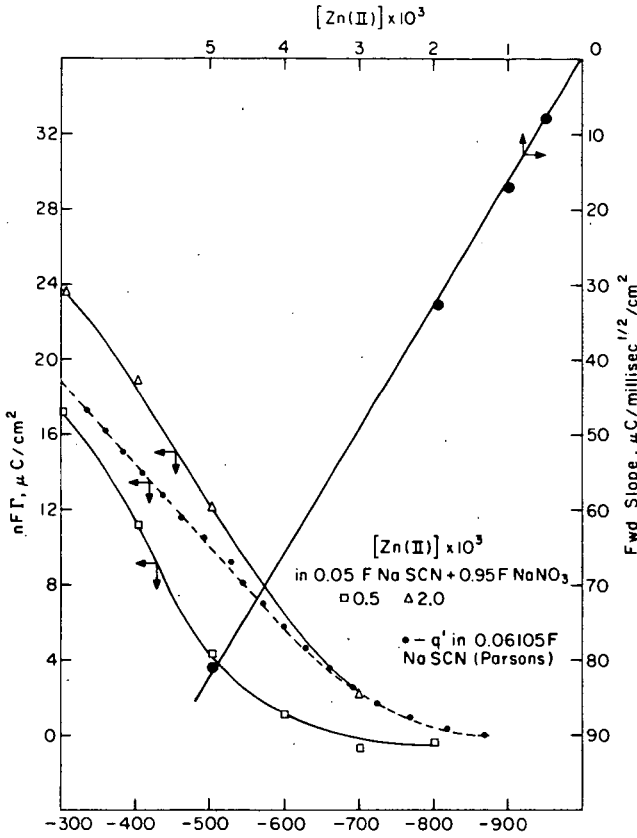


Fig. 3:  $E_i, mV \text{ vs SCE}$

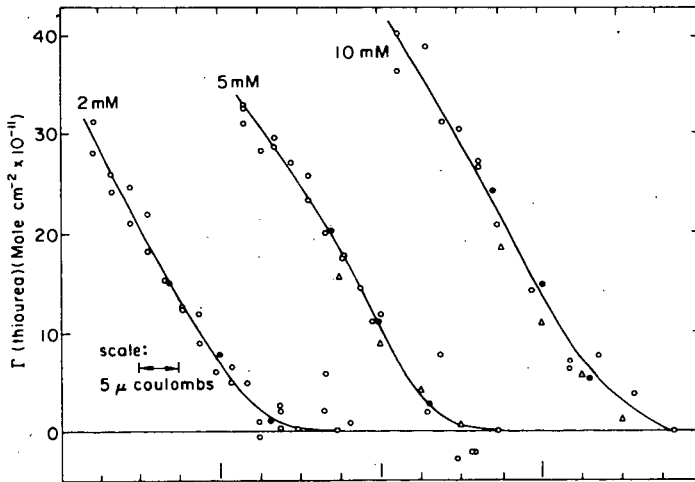


Fig. 4:  $q \text{ (microcoulombs } cm^{-2})$

ROTATING DISC AND RING-DISC TECHNIQUES<sup>+</sup>

Ernest Yeager and Ronald W. Zurilla

Department of Chemistry  
Western Reserve University and Case Institute of Technology  
Cleveland, Ohio

## INTRODUCTION

In kinetic studies of electrode processes, uniformity of the concentration gradients along the electrode surface and quantitative information concerning these gradients are necessary. In many instances the rotating disc electrode technique provides an effective means for realizing these requirements. Furthermore this technique allows the surface concentration of reactants and products to be varied in a controlled manner through changes in the rotation rate and hence can be used to determine the reaction orders through the dependence of the current on the rotation rate without the necessity of varying the bulk concentrations.

An important extension of the rotating disc technique is the ring-disc configuration which consists of a disc surrounded by a closely placed concentric ring with its surface in the same plane and separated from the disc by a thin insulating sleeve. The rotating ring-disc electrode is well suited to the study of electrode reactions involving unstable products or intermediates. Species produced electrochemically on the disc are monitored electrochemically on the ring as the liquid spirals out from the disc across the surface of the ring. The concentration of the species in question, averaged over the surface of the ring, can be determined in most instances by one of the following procedures:

1. Maintain the ring potential at a value such as to reverse the process leading to the formation of the species of interest and measure the ring current.
2. Construct the ring of a metal which is favorable for the completion of the overall electrode process yielding the intermediate in question on the disc or for the further oxidation or reduction of the product. Maintain the ring at a fixed potential favorable for such or scan through an appropriate range of potentials and measure the ring current.

Both the rotating disc and ring-disc techniques have already found substantial use in kinetic studies but also offer promise for analysis when solid electrodes are required.

## THEORY

The problem of mass transport by convective diffusion to a rotating disc electrode has been solved by Levich (1) for the case of a perfectly smooth, horizontal disc of infinite radius rotating at a constant angular velocity in an infinite liquid under conditions of laminar flow. In practice, a disc electrode can effectively meet these requirements if 1) the radius is very large compared to the momentum boundary layer thickness, 2) all other surfaces within or bounding the liquid are at a distance large compared to the radius of the rotating surface, 3) surface irregularities on the disc are small compared to the momentum boundary

\* Some of the experimental aspects of the paper are based on research supported by the Office of Naval Research.

layer thickness, 4) the rotation rate for the particular disc is below the critical Reynolds number for the onset of turbulence [i.e.,  $Re = (r^2 \omega / \nu) < 10^5$  where  $r =$  overall radius of the disc,  $\omega =$  angular rotation rate,  $\nu =$  kinematic viscosity].

According to Levich, the effective thickness of the Nernst transport boundary layer is

$$\delta = 1.80 a D^{1/3} \nu^{1/6} / \omega^{1/2} \quad [1]$$

where  $D$  is the diffusion coefficient of the reacting species in  $\text{cm}^2 \text{sec}^{-1}$ ,  $a$  is a dimensionless constant, and all other quantities are in cgs units. The term  $a$  in eq. [1] was originally designed as  $0.8934$  by Levich using an approximation to the integration. Gregory and Riddiford (2) carried out the graphical integration in a more accurate manner and found for  $D/\nu$  values less than  $4 \times 10^{-3}$  that  $a$  can be calculated to within 1% by the empirical equation

$$a = 0.8934 + 0.316 (D/\nu)^{0.36} \quad [2]$$

The second term is only a few percent at the most for aqueous solutions and hence is really necessary only for rather accurate work--probably more accurate than most rotating disc electrode configurations permit. Newman (3) also has reported a corrected value for  $a$ .

Eq. [1] yields the following expression for the diffusion current density  $i$  in  $\text{A/cm}^2$

$$i = 0.55 a^{-1} z F D^{2/3} \nu^{-1/6} \omega^{1/2} [C(\infty) - C(o)] \quad [3]$$

or

$$i_D = 0.554 a^{-1} z F D^{2/3} \nu^{-1/6} \omega^{1/2} [C(\infty)] \quad [4]$$

where  $i_D$  is the limiting current density,  $zF$  is the number of coulombs of charge transferred per mole of diffusing species, and  $C(\infty)$  and  $C(o)$  are the concentrations of the diffusing reactant in the bulk and at the electrode surface, respectively, in moles  $\text{cm}^{-3}$ .

At the limiting current, the current density is uniform on the rotating disc even if substantial ohmic voltage drop occurs within the electrolyte in the vicinity of the disc. At currents below the limiting value, however, the current distribution may be considerably greater near the periphery of the disc because of the greater accessibility of the edge than the center as a result of the I-R drop in the solution. Figure 1 indicates the current distribution on the disc according to the treatment of Newman (4) when Tafel kinetics are involved and electrolytic transference of species is considered with the transference number  $t = 0.5$ . The parameter  $N$  in this figure is defined by the equation

$$N = - \left( \frac{r_o^2 \omega}{\nu} \right)^{1/2} \left( \frac{0.5102 \nu}{3D} \right)^{1/3} \frac{n z F^2 D [C(\infty)]}{RT(1-t) [\kappa(\infty)]} \quad [5]$$

where  $r_o$  is the radius of the disc electrode,  $n$  is the number of electrons per molecule or ion of reacting species,  $[\kappa(\infty)]$  is the specific conductance in the bulk of the solution, and  $Z = -z_+ z_- / (z_+ - z_-)$  for an electrolyte consisting of a single salt or  $Z = -n$  for solution with a supporting electrolyte. The value of the exchange current density ( $i_o$ ) does not enter into the calculation provided the local current density is high compared to  $i_o$  at all positions on the disc.

In kinetic studies with the rotating disc, it is evident from Figure 1 that substantial errors will be introduced due to non-uniform current distribution unless the parameter  $N$  is a relatively low value. Such can be realized through the use of a supporting electrolyte which increases  $[\kappa(\infty)]$  in the denominator. For example (4) for copper deposition from a  $0.1 \text{ M}$   $\text{CuSO}_4$  solution on a disc with  $r_o = 0.25 \text{ cm}$  at 300 rpm,  $N$  is 79 while with  $0.1 \text{ M}$   $\text{CuSO}_4 + 1.53 \text{ M}$   $\text{H}_2\text{SO}_4$  the corresponding value for  $N$

is 1.6 (although it should be noted that the limiting current density has dropped from 79 mA/cm<sup>2</sup> without the H<sub>2</sub>SO<sub>4</sub> to 50 mA/cm<sup>2</sup> with the addition of the H<sub>2</sub>SO<sub>4</sub> because of the suppression of the transference number from 0.363 to 0). Another approach to reducing the non-uniformity of the current density is to employ a ring-disc electrode assembly with the ring used as a guard by maintaining it at the same potential as the disc with a separate circuit. If the spacing between the disc and ring is very small compared to the radius of the disc and the thickness of the ring, the arrangement is equivalent to examining just that portion of the plot in Figure 1 corresponding to  $(r/r_0) \leq r_1/r_3$  where  $r_1$  and  $r_3$  are the radius of the disc and the outside radius of the ring, respectively.

In kinetic studies with the rotating disc technique the dependence of the disc current on the rotation rate provides a relatively simple means (5-7) for determining the reaction order relative to the diffusing species provided a supporting electrolyte is used at a concentration sufficient to ensure a relatively low value for  $N$  [high  $\kappa(\infty)$ ] and to avoid appreciable double layer corrections. When the back reaction is negligible, the current density can be expressed as a function of the concentration of a reacting species by the equation

$$i = k[C(o)]^n \quad [6]$$

where  $n$  is the reaction order with respect to the diffusing species and  $k$  is a potential-dependent rate-constant. If the rotation rate at a constant potential is increased to a value such that  $C(0)$  approaches closely  $C(\infty)$ , the process will become pure kinetically controlled and the current density then becomes

$$i_L = k [C(\infty)]^n \quad [7]$$

From eq. [3], the actual current density may be expressed as

$$i = B\omega^{1/2} [C(\infty) - C(o)] \quad [8]$$

Let  $\omega_0$  be defined (see Figure 2) such that

$$i_L = B(\omega_0)^{1/2} [C(\infty)] \quad [9]$$

and the observed current density corresponding to  $\omega_0$  for a given potential be  $i_k$ . From eqs. [6-9],

$$i_k = i_L \left[ 1 - \left( \frac{i_k}{i_L} \right)^{1/n} \right] \quad [10]$$

or

$$n = \frac{\log i_L - \log i_k}{\log i_L - \log (i_L - i_k)} \quad [10a]$$

To apply this equation, only one set of values for  $i_L$  and  $i_k$  are required. In practice, a series of values is usually obtained to establish the constancy of  $n$  and hence the validity of the experiment.

Figure 2 indicates the dependence of the observed current density on rotation rate for several reaction orders. For a first order reaction, the limiting value for the current density at infinite rotation rate (corresponding to  $i_L$ ) can be obtained by means of the equation

$$\frac{1}{i} = \frac{1}{i_L} + \frac{1}{B[C(\infty)]\omega^{1/2}} \quad [11]$$

The rotating disc-ring electrode system has been treated by Ivanov and Levich (8) who have obtained the following relationship for the total ring current when the ring is biased to a potential such as to consume electrochemically all of the

intermediate reaching the ring from the disc:

$$i_r = \frac{n_2}{n_1} \cdot \frac{i_D}{1 + \frac{\kappa \delta_x}{D_x}} \cdot M \quad [12]$$

where

$$M = 0.8 \left[ 1 - \frac{3}{4} \left( \frac{r_1}{r_2} \right)^3 \right]^{1/3} \int_1^{r_3/r_2} \frac{(r/r_2)^2 dr}{\left[ \left( \frac{r}{r_2} \right)^3 - 1 \right]^{1/3} \left[ \left( \frac{r}{r_2} \right)^3 - \frac{3}{4} \left( \frac{r_1}{r_2} \right)^3 \right]} \quad [12a]$$

and

$i_D$  = current on the disc to generate only the intermediate

$\kappa$  = rate of conversion of intermediate to final product on the disc (assumed first order in concentration of intermediate)

$n_1$  = number of electrons transferred at disc per molecule of reactant converted to intermediate

$n_2$  = number of electrons transferred at ring per molecule of intermediate

$D_x$  = diffusion coefficient of intermediate

$\delta_x$  = diffusion layer thickness for the intermediate

$r$  = radial distance from center of disc

$r_1$  = radius of disc

$r_2, r_3$  = inner and outer radii of ring, respectively

This equation carries the assumptions that 1)  $(r_2 - r_1) \ll r_1$ , 2) the intermediate does not undergo any homogeneous reaction, and 3) ionic migration can be neglected. The factor  $M$  corresponds to the fraction of the total amount of intermediate diffusing away from the disc, which undergoes electrochemical reaction at the ring. While  $M$  can be evaluated solely from geometric considerations, such requires a numerical evaluation of the integral in eq. [12a]. Bruckenstein and Feldman (9) have carried out this integration analytically.

Ivanov and Levich indicated that several approximations are made in evaluating the constant in eq. [12a] and that it may be 5% too high. Recently Albery and Bruckenstein (10,11), however, carried out an extensive study of the ring-disc electrode and concluded that the Ivanov-Levich expression for  $M$  may be in error by up to 25%, depending on the electrode geometry. Albery and Bruckenstein obtained the following explicit expression for  $M$ :

$$M = 1 - F(\alpha/\beta) + \beta^{2/3} [1 - F(\alpha)] - (1 + \alpha + \beta)^{2/3} \left\{ 1 - F\left[ \frac{\alpha/\beta}{1 + \alpha + \beta} \right] \right\} \quad [13]$$

where

$$\alpha = (r_2/r_1)^3 - 1 \quad [14a]$$

$$\beta = (r_3/r_1)^3 - (r_2/r_1)^3 \quad [14b]$$

and

$$F(\theta) = \frac{3^{1/2}}{4\pi} \ln \frac{(1 + \theta^{1/3})^3}{1 + \theta} + \frac{3}{2\pi} \arctan \left( \frac{2\theta^{1/3} - 1}{3^{1/2}} \right) + \frac{1}{4} \quad [14c]$$

These authors have tabulated values of  $M$  in terms of the parameters  $r_3/r_2$  and  $r_2/r_1$  - a welcome convenience to electrochemists using the ring-disc technique. In an

extensive series of papers, Albery et al. (12-14) have also developed treatments for the current-voltage curves for the ring (11), the effects of first order homogeneous as well as heterogeneous reactions involving the intermediates produced at the disc on the ring current (14), and the shape of the ring current vs. disc current curves during the use of the ring-disc electrode for diffusion layer titrations (13).

## EXPERIMENTAL FEATURES

### A. Electrode design

Riddiford (15) has reviewed the practical aspects of electrode design and the influence of electrode shape on experimental results. Even though it is recommended to use a bell-shaped electrode (Figure 3A), a cylindrical shaped electrode assembly in which the central portion of the lower surface is the electrode (Figure 3B) is often sufficient. This type of electrode is easily made and suitable for convenient interchange of electrodes which maintain the necessary high purity requirement. In an examination (16) of an electrode of this construction with a diameter of 0.48 cm mounted in a Teflon cylinder (0.96 cm diameter), the limiting current density for the reduction of the  $I_3^-$  ion to  $I^-$  in a 0.025 M  $KI_3$  + 0.1 M  $KI$  solution was found to be proportional to  $\omega^{1/2}$  to within 2% for rotation rates from 100 to 18000 rpm. The slope was only 2% higher than the value predicted from eq.[4] using the Gregory-Riddiford value for a or the results of Nelson and Riddiford (17) for this same reduction with an electrode of the bell-shape. In recent years, rotating disc electrodes in cylindrical mounts (Figure 3B) have been used to investigate a number of different electrode reactions in the laboratories at Western Reserve University (e.g., hydrogen oxidation (18), oxygen reduction (16), tin and nickel deposition, various redox couples on semiconductors). In no instance has there been observed any appreciable deviation of the limiting current density from a direct proportional dependence on  $\omega^{1/2}$  at rotation rates in the range 100 to 18000 rpm when the limiting current represented pure mass transport control associated with convective diffusion.

In studies with some types of electrodes (e.g., single crystal NiO) at Western Reserve, it has not been possible to fabricate disc-shaped electrodes without unusual difficulty and hence rotating irregular-shaped, flat electrodes mounted in an insulating cylinder have been used. The limiting mass-transport current has been found to be proportional to  $\omega^{1/2}$  in the same manner as for the disc electrodes, and in fact, the limiting current densities for a square or near square-shaped rotating electrode are almost the same as for the disc. On occasion, difficulty also has been encountered in obtaining electrodes which are extremely flat and void of pits [e.g., certain types of carbon electrodes (16)]. As long as the irregularities are only of the order of microns in dimension, no deviations of more than a few percent from eq. [4] have been observed with disc electrodes in cylindrical mounts with dimensions similar to those described earlier for rotation rates up to 18000 rpm.

Teflon is probably the best material of construction available for mounting disc and disc-ring electrodes from the viewpoint of maintaining purity of solution. In some cases, however, the electrodes are very fragile and can not be machined to a cylindrical shape (e.g., single crystal graphite, semiconducting single crystal metal oxides). Therefore they can not be press-fitted into Teflon mountings with a sufficiently tight seal. In such instances in the authors' laboratory the electrodes are mounted in Kel-F using a high pressure moulding technique at 300°C.

### B. Mechanical system

The basic features of a relatively simple rotating ring-disc system are shown in Figure 4. While both belt drive and direct drive systems have been used, the authors prefer the belt drive because it permits a larger range of rotation rates to be covered with a given motor and the construction of the shaft is simpler and less expensive. For disc and ring-disc electrodes mounted in a cylinder of 1.5-cm diameter or less, a 1/15 HP motor with appropriate pulleys is sufficient for up to

20000 rpm. While a motor control with a feed-back circuit or a variable frequency synchronous motor system is to be preferred for very refined measurements, the authors have found that a simple universal motor with a d.c. field and armature current control provides sufficiently stable rotation rates for most work. Rotation rates in the arrangement shown in Figure 4 are measured by means of a lamp-photocell arrangement connected to a frequency meter with the beam transmitted through a number of equally spaced holes in an aluminum disc attached to the upper part of the shaft. Sealed precision bearings are used to minimize eccentricity in rotation and to prevent any leakage of bearing lubricant. The lead to the disc electrodes extends to the top of the shaft where contact is made by means of a spring-loaded silver-graphite brush. Contact to the ring is made through a slip-ring silver-graphite brush assembly near the top of the shaft. The steel shaft on which the electrode assembly is mounted may be either at ground potential or isolated from ground by supporting the bearing housing on a plastic mounting.

One of the substantial experimental problems in the use of the rotating disc and ring-disc techniques is obtaining a satisfactory seal where the Teflon covered shaft enters the cell. While various types of liquid seals work satisfactorily at rotation rates up to 6000 rpm, at higher speeds they present excessive drag, require cooling, and unless very carefully designed are no longer gas tight. One rather effective technique for preventing gases of the atmosphere from entering the cell around the rotating shaft is to use a relatively long glass or Teflon sleeve around the shaft and then to maintain a slight excess pressure in the gas space above the electrolyte within the cell.

#### APPLICATIONS

The applications of the rotating disc and ring-disc techniques to kinetic studies is well illustrated by recent studies of oxygen reduction on various surfaces with peroxide usually as an unstable intermediate. Some results recently obtained in the authors' laboratory for oxygen reduction using these techniques will be presented as part of the oral presentation of the paper.

#### REFERENCES

1. V. Levich, *Acta Physicochem. URSS* 17, 257 (1942). Physicochemical Hydrodynamics, Prentice Hall, Englewood Cliffs, N.J., 1962.
2. D. Gregory and A. Riddiford, *J. Chem. Soc.* 1956, 3756.
3. J. Newman, *J. Phys. Chem.* 70, 1327 (1966).
4. J. Newman, *J. Electrochem. Soc.* 113, 1235 (1966).
5. A. Frumkin and E. Aikazyan, *Invest. Akad. Nauk SSSR, Otdel. Khim. Nauk* 202 (1959).
6. A. Frumkin and G. Tedoradse, *Z. Elektrochem.* 62, 251 (1958).
7. A. Frumkin in Advances in Electrochemistry and Electrochemical Engineering, Vol. 3, P. Delahay, ed., Interscience Publishers, New York, 1961, pp. 287-391.
8. Y. Ivanov, and V. Levich, *Doklady Akad. Nauk SSSR* 126, 1029 (1959).
9. S. Bruckenstein and G. Feldman, *J. Electroanalyt. Chem.* 2, 395 (1965).
10. W. Albery, *Trans. Faraday Soc.* 62, 1915 (1966).
11. W. Albery and S. Bruckenstein, *ibid.* 62, 1920 (1966).
12. W. Albery, S. Bruckenstein, and D. Napp, *ibid.* 62, 1932 (1966).
13. W. Albery, S. Bruckenstein, and D. Johnson, *ibid.* 62, 1938 (1966).
14. W. Albery and S. Bruckenstein, *ibid.* 62, 1946 (1966).
15. A. Riddiford in Advances in Electrochemistry and Electrochemical Engineering, Vol. 4, P. Delahay, ed., Interscience Publishers, New York, 1966, pp. 47-116.
16. E. Yeager, P. Krouse, and K. Rao, *Electrochim Acta* 9, 1057 (1964).
17. J. Nelson and A. Riddiford, *J. Electrochem. Soc.* 108, 695 (1961).
18. A. Makowski, E. Heitz, and E. Yeager, *J. Electrochem. Soc.* 113, 204 (1966).

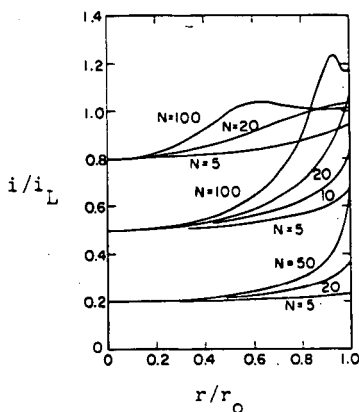


Figure 1. Current distribution on a rotating disc electrode of radius  $r_0$  for Tafel kinetics with transfer coefficients of  $1/2$  and a reaction order of 1, according to Newman (4).

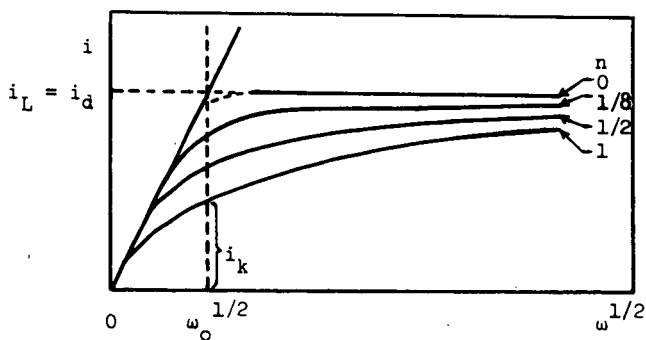


Figure 2. Dependence of current density on rotation rate for various reaction orders [after Frumkin (7)].

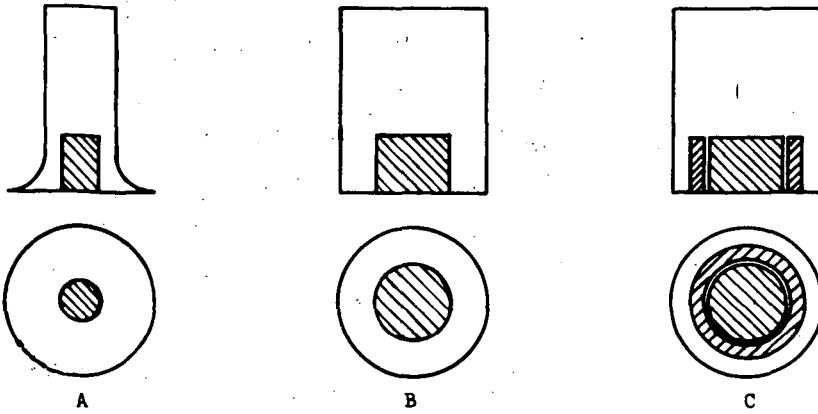


Figure 3. Rotating Disc and Ring-Disc Electrodes.

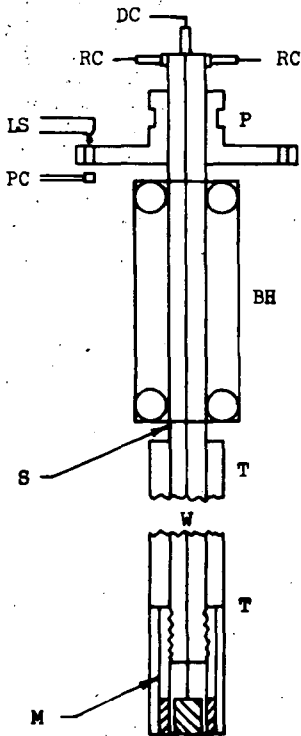


Figure 4. Rotating Ring-Disc Electrode System.

- S steel shaft
- BH bearings and housing
- P pulley
- T Teflon insulation
- M Metal support
- DC disc brush contact
- RC ring brush contact
- W insulated wire for DC
- LS light source
- PC photocell

## EPR AND ELECTROCHEMICAL INVESTIGATION OF TERTIARY AROMATIC AMINES

Robert F. Nelson and Ralph N. Adams

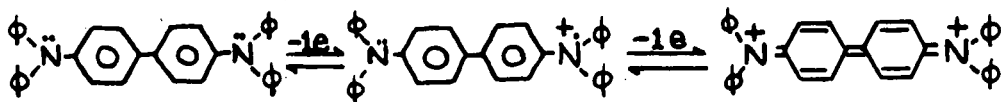
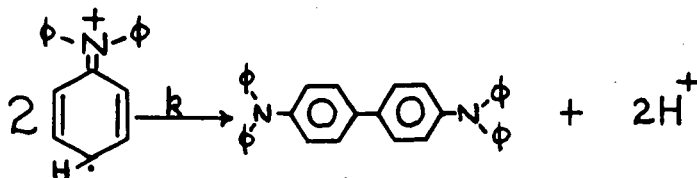
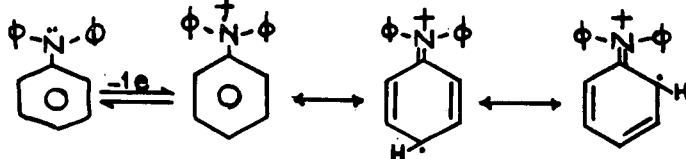
Department of Chemistry  
 Sacramento State College  
 Sacramento, California

and

Department of Chemistry  
 University of Kansas  
 Lawrence, Kansas 66044

Interest in the anodic oxidation reactions of organic compounds led to a study of the electrode processes associated with the electrochemical oxidation of some tertiary aromatic amines in nonaqueous media, primarily acetonitrile. These electrode processes were found to have homogeneous chemical reactions associated with them in many cases, some of which were quite surprising in nature. Substituted triphenylamines were investigated, but generalizations to the electrochemical behavior of other aromatic amines should be possible. Substituent and steric effects were found to have surprisingly great influences over the rates of follow-up reactions associated with the primary electrode processes, but these were found to be entirely predictable from the electron distribution in the amine cation radicals as shown by Hückel molecular orbital (HMO) calculations.

Triphenylamine (TPA), the parent molecule for most of these compounds, was studied in detail, and it was determined by a number of independent methods that the electrode processes and associated chemical reactions are as shown below:



The initial electrode reaction is a one-electron oxidation of TPA to the cation radical,  $\text{TPA}^{\cdot+}$ , which is quite unstable.<sup>1</sup>

---

1. E. T. Seo, et al., J. Am. Chem. Soc., 88, 3498 (1966).

---

The presence of the cation radical was confirmed by rapid-sweep cyclic voltammetry (which showed the initial redox couple to be fairly reversible at 1500 V./min., i.e., cathodic current was observed corresponding to reduction of the cation radical back to the parent species) and visible absorption spectroscopy.<sup>1</sup> Two of the cation radicals (or a cation and a parent molecule - it is difficult to distinguish between the two mechanisms electrochemically) couple rather rapidly ( $k=10^3 \text{ l.mole}^{-1}\text{sec.}^{-1}$ ) at the para ring positions to form N,N,N',N'-tetraphenylbenzidine (TPB), with concomitant liberation of two protons due to coupling. TPB is more easily oxidized than TPA, so reactions (3) also occur at the potential of TPA oxidation, completing the ECE process.

The presence of TPB as the end-product was detected by matching up peak potentials of the cyclic voltammograms of TPA and TPB, by comparing the epr spectra generated by oxidation of the amine and the benzidine (they are identical) and by detection of the visible absorption peak of  $\text{TPB}^{\cdot+}$  upon electrolysis of TPA in situ in a Cary spectrometer<sup>1</sup>.

Substitution at the para positions of the phenyl rings in TPA had a great effect upon this electrode process. If all three para positions were blocked with substituents, a stable cation radical was generated and this species did not undergo the characteristic coupling reaction. These cation radicals were stable enough that the epr spectra could be generated electrolytically and these spectra were then interpreted in terms of the parent molecules, thus confirming the initial one-electron electrochemical behavior. The substituents used were: OMe, Me, F, Cl, Br and COOMe. The cyclic voltammetry of all these molecules was initially a one-electron, completely reversible process, with  $i_{pc}/i_{pa} = 1.0$  at all scan rates. The second oxidation step of all of these is irreversible, and the follow-up reactions are very complex and diverse.

When only one or two of the para positions are blocked, coupling at an open para site takes place readily, the rate of coupling being markedly dependent upon the number and type of substituents. It was not unexpected that if two sites were blocked instead of one (di- as compared to monosubstituted TPA's), the coupling rate was diminished (with the same substituent in both cases), but the effect of various substituents was quite surprising. The methoxy group has a tremendous stabilizing effect upon these cation radicals; 4-methoxy-TPA coupled at a very slow rate (as compared to  $k=10^3$  for TPA). On the other hand, nitro groups in the para positions of TPA appeared to accelerate the coupling reaction to an extraordinary degree. Although the coupling rate of 4-nitro-TPA could not be accurately measured, it was estimated at  $k=10^4$  from chronopotentiometric data. Other substituents appeared to behave normally. Again, when benzidines were formed, they were identified by matching of peak

potentials of cyclic voltammograms, by obtaining identical epr spectra from the benzidine and the amine, and by generating similar visible absorption spectra. In all cases that could be verified, para-benzidines were the only detectable product.

A few ortho-substituted TPA's were also investigated and it was found that substituent effects were somewhat diminished and that twisting of the ring or rings with a substituent considerably altered the electron distribution in these molecules. In the mono-ortho-substituted TPA's (substituents = OMe, Me, Cl), the effect of the substituents was to twist the substituted ring so that interaction with the rest of the molecule was considerably diminished. This increased the unpaired electron density in the unsubstituted rings, thus accelerating the coupling reaction relative to TPA. The substituents do have an effect, though diminished, upon the unsubstituted rings, as evidenced by the fact that each of the substituted TPA's has a different coupling rate, determined qualitatively by chronopotentiometry ( $i\tau^{1/2}/C$  vs.  $i$  plots).

When all three rings are substituted at one ortho position, the molecules are more symmetrical and substituent effects become more of a differentiating factor. Each of these couples at a rate slower than that of TPA, and they are in the order: OMe < Me < Cl. In the case of the methoxy derivative, tri-o-anisylamine, the corresponding benzidine was also available (tri-ortho-substituted TPA's and corresponding benzidines courtesy of Dr. Cecil Frye, Dow Corp., Midland, Michigan) and it was verified as before that the amine couples to form the corresponding para-benzidine. The cyclic voltammograms, epr spectra and visible absorption peaks matched up nicely. It was assumed that the methyl- and chloro-substituted analogs behaved similarly, since the data from these compounds correlated with those from the methoxy derivative.

## ELLIPSO-METRIC METHODS IN ELECTROCHEMISTRY

M. A. Genshaw

The Electrochemistry Laboratory  
The University of Pennsylvania  
Philadelphia, Pa. 19104

Ellipsometry is a useful tool to apply in the study of electrochemical reactions which involve film formation or dissolution. Ellipsometry is useful because it is very sensitive and because it may be applied in situ.

To understand ellipsometry, we must understand polarized light. Light is an electromagnetic wave and so is characterized by an electric and a magnetic vector. Since the electric vector and magnetic vector are always normal to each other, we need only consider the motion of the electric vector in our discussion. In linearly polarized light, the electric vector vibrates in a single plane. The inclination of the light may be described in terms of an angle,  $\alpha$ . To define this ratio, in ellipsometry, it is convenient to take as our reference the directions normal and parallel to the test surface. Then:

$$\tan \alpha = E^P/E^N$$

where  $E^P$  is the amplitude of the parallel electric vector and  $E^N$  the amplitude of the normal vector.

When light is passed through certain materials, polaroid(quinine iodosulfate), for example, or through certain prisms (Nicol prism) only linearly polarized light vibrating in a certain plane is transmitted. When linearly polarized light is reflected or refracted at an interface between dielectrics (e.g., air-water), the plane of polarization is shifted causing a change in  $\alpha$ .

Other materials, anisotropic materials, cause a phase shift in the components of light. Thus when linearly polarized light is passed through calcite, it is resolved into two components along its optical axes. These components travel at different velocities so that a phase shift is introduced between the components. When the light emerges from such a crystal it is no longer linearly polarized but is elliptically polarized. The tip of the electric vector no longer vibrates in a single plane, but rotates with time and traces out an ellipse. This ellipse is characterized by the angle of orientation of its major axis and the ratio of the two components.

An alternate way of characterizing the ellipse is in terms of the amplitude of two components normal to each other and the phase difference between them.

When polarized light is reflected from a conducting surface, both the amplitude ratio,  $\tan \alpha$ , and the phase are changed. Thus, reflection from a metal is similar to a combination of reflection from a dielectric and transmission through anisotropic material. For reflection from a metal, the two basic ellipsometric parameters are defined. The relative amplitude diminution:

$$\tan \psi = \tan \alpha_R / \tan \alpha_I$$

where  $\tan \psi$  is the relative amplitude diminution and R designates the reflected beam and I the incident beam. The difference in phase of the two components is defined as:

$$\Delta = D_R - D_I$$

where  $\Delta$  is the relative phase retardation,  $D_R$  is the phase difference of the normal and parallel components in the reflected beam and  $D_I$  is the same quantity for the incident beam.

When a film is present on the metal surface, the relation between  $\Delta$  and  $\psi$  and film and metal properties becomes quite complex:

$$\tan \psi \exp(i\Delta) = \frac{\frac{r_{12}^p + r_{23}^p \exp(-2i\delta)}{1 + r_{12}^p r_{23}^p \exp(-2i\delta)}}{\frac{r_{12}^n + r_{23}^n \exp(-2i\delta)}{1 + r_{12}^n r_{23}^n \exp(-2i\delta)}}$$

where

$$r_{ab}^p = \frac{n_b \cos \varphi_a - n_a \cos \varphi_b}{n_b \cos \varphi_a + n_a \cos \varphi_b}$$

$$r_{ab}^n = \frac{n_a \cos \varphi_a - n_b \cos \varphi_b}{n_a \cos \varphi_a + n_b \cos \varphi_b}$$

and

$$\delta = \frac{2\pi n_2 \cos \varphi_2 L}{\lambda}$$

where  $n$  is the refractive index of the media (for absorbing media  $n = \bar{n} + i\kappa$  where  $\bar{n}$  is real part of the refractive index and  $\kappa$  an absorption coefficient),  $\varphi$  are the angles of incidence and refraction,  $L$  is the film thickness,  $\lambda$  the wavelength of the light, and the subscripts 1, 2 and 3 represent the medium, film and substrate, respectively. It is apparent that the relation between  $\Delta$  and  $\psi$  and the film thickness and refractive index is complicated. It has only been since the development of modern electronic computers that the complete equations have been used in calculations. Approximate formulas, valid for very thin films ( $< 100 \text{ \AA}$ ), were derived by Drude who also derived the complete expressions but found them too difficult to use.

When plots are made of  $\psi$  versus  $\Delta$  as a function of film thickness, the relation is not complicated. For a transparent film a closed curve is obtained which repeats for each wavelength of thickness ( $\lambda/n$ ). For an adsorbing film this curve is a spiral which ends at the  $\psi$ - $\Delta$  point which corresponds to the reflection from the film alone. This termination of the spiral results when the film is so thick that no light reflected from the substrate reaches the surface. The observed parameters must then be those for the film alone. For such thick films ellipsometry cannot be used to determine the thickness.

An alternative type of representation is the polar coordinate type of plot, in which  $\Delta$  is the angle and  $\tan \psi$  the radial distance.

#### The Application of Ellipsometry to Electrochemistry

To apply ellipsometry to electrochemistry, we must use an electrochemical cell. Thus, the light beam must pass through the cell walls into the solution and then back out again.

The basic criteria is that one must know what effect the cell and solution have on the polarization state of the light. For passage of polarized light through a dielectric-dielectric interface, we have the relation:

$$\frac{\tan \alpha_T}{\tan \alpha_I} = \frac{1}{\cos(\varphi_I - \alpha_T)}$$

where  $\tan \alpha_T$  and  $\tan \alpha_I$  are the amplitude ratio for the transmitted and incident beam and  $\varphi_I$  is the angle of incidence and  $\alpha_T$  is the angle of transmission. To have no change in  $\tan \alpha$  at the interface is desirable. Hence, we must have  $\varphi_I = \alpha_T$ . For media of different refractive indices this can only occur for normal incidence. This arrangement is frequently used. It has the advantage that no corrections need be made for the cell. The major disadvantage of this method is that the angle of incidence is fixed.

The alternate method is to use rectangular cells and correct for the changes at the interfaces. These corrections are not complicated. Another correction which one must apply when working in solution is in the angle of incidence. If one is not working with windows normal to the light path, refraction will occur at the interfaces and thus change the angle of incidence. This is, of course, easily corrected by Snell's law. Neither normal windows or parallel windows offer a clear-cut advantage so that secondary considerations as whether the angle of incidence is to be varied or convenience in cell design will govern the choice.

#### Problems in applying Ellipsometry to Electrochemistry

a. Refractive index of the Metal: To interpret the changes in  $\Delta$  and  $\psi$  upon film growth, one must know  $\Delta^0$  and  $\psi^0$ , the values of  $\Delta$  and  $\psi$  corresponding to the bare metal surface. In many cases it may prove difficult to experimentally obtain a bare metal surface in solution because of metal dissolution and spontaneous film formation. Electrochemistry can aid itself here by controlling the potential of the metal in a region in which the bare surface is stable. When this is not possible, one may use data obtained from high vacuum measurements for the bare surface.

b. The slowness of making measurements: Many electrochemical reactions occur quite rapidly so that it is desirable to make rapid ellipsometric measurements so that competing reactions do not distort the measurements. The manual adjustment of the ellipsometer requires about one minute. This is a very long time compared to electrochemical transients which are often carried out in a few milliseconds. Various types of automated ellipsometers are being made but thus far only give a response on the order of a second. In principle, much faster instruments are possible but require considerable sophistication in the optical and electronic components to give acceptable accuracy.

c. Interpretation of results: The interpretation of results obtained by ellipsometry can be quite difficult. Many electrochemically formed films are electronic conductors and hence absorb light. The films then possess three optical properties: thickness, real part of the refractive index and absorption coefficient. From a single measurement of  $\Delta$  and  $\psi$ , these three quantities cannot be uniquely determined. Several methods of attacking this problem have been suggested. These may be either ellipsometric measurements or involve an independent method. The ellipsometric methods include varying the refractive index of the media, varying the substrate, varying the angle of incidence and varying the wavelength. Non ellipsometric methods are to determine  $n$  or  $k$  from independent measurements on the film material and determining the amount of film by coulometry.

For very thin films ( $100 \text{ \AA}$ ), the method of variation of film thickness with

refractive index assumed constant does not succeed unless very precise (error  $\ll 0.01^\circ$ ) measurements can be made. Since the error is typically greater than this, the method will generally not succeed. Also, for such very thin films, the refractive index is likely to depend on thickness. For films thicker than 100 Å, this method may succeed.

The method of varying the substrate while keeping the same film has been theoretically shown to be successful. In practice, for electrochemical measurements, this method could only be used for adsorbed films. For films formed from the substrate material, the method is not applicable. Also, it may prove experimentally difficult to produce films of the same thickness on different substrates.

Theoretical calculations have shown that the method of variation of the refractive index of the medium should also be a feasible method of obtaining a solution for  $n$ ,  $\kappa$  and  $L$ . However, one must assume that no change occurs in the film as the media is changed - an assumption which may prove difficult to verify.

Calculations have shown that the method of variation of the angle of incidence may succeed in special cases but is not a general method.

The method of variation of wavelength may also be attempted. One complication which would enter is that  $\kappa$  will depend on the wavelength. This will give an additional variable so that a solution would probably not be possible.

The use of values of  $n$  or  $\kappa$  for bulk materials has been used with some success. Here, one must show that the thin film is the same as the bulk material on which the measurements were made. Also, for very thin films, it is probable that  $n$  and  $\kappa$  vary with thickness due to compression of the film.

The use of coulometry with ellipsometry can be used to restrict the range of possible thicknesses. Thus, by combining coulometry with ellipsometry the values of  $n$ ,  $\kappa$  and  $L$  can be restricted.

The overall picture presented on the possibility of uniquely determining  $n$ ,  $\kappa$  and  $L$  for thin films seems rather poor. In reality the situation is not nearly so bad. By restricting the values of  $n$  and  $\kappa$  to ranges which are experimentally found ( $1 < n < 5$ ,  $0 < \kappa < 5$ ), certain restrictions on the film properties may be made. A minimum value of film thickness which is compatible with  $\Delta$  and  $\Psi$  is usually found. Thus one can conclude that the film must be thicker than a minimum value. Also, light absorbing films are readily distinguished from transparent films.

The problem in inhomogeneous film has also received theoretical attention. Here it has been shown that the films are seen by the ellipsometer as a uniform film with an average thickness and refractive index.

### Summary

Ellipsometry is a very sensitive tool which may be applied in situ to study electrochemical reactions involving films. In considering the use of ellipsometry, one should consider the problems in applying the method. These include the difficulty of obtaining the optical parameters of bare metals and the difficulty of analyzing light absorbing films. These problems are not insurmountable so that ellipsometry is becoming increasingly important in research.

## Optically Transparent Electrodes

Theodore Kuwana and George Strojek

Department of Chemistry, Case Institute of Technology, Cleveland, Ohio

Optically transparent electrodes (OTE) made from thin metal layers on glass were first used in electrochemical studies involving photovoltaic effects.<sup>1</sup> More recently, OTE made from "doped" tin oxide coated glasses were applied to electrode reactions where the products formed were followed by optical spectroscopy.<sup>2</sup> The use of these electrodes has now been extended to aid the elucidation of mechanism and kinetics of organic electrode reactions.<sup>3</sup>

The application of internal reflectance spectroscopy (IRS) with OTE for following processes involving absorbing species at a distance from the electrode surface well within the thickness of the diffusion layer has been experimentally demonstrated.<sup>4</sup> The advantages of OTE are quite clear. Normal transmission spectroscopy with the incident light passing normal to the surface of OTE allows spectral monitoring in a minimum of thickness of about  $10^4$  Å, depending on concentration and molar absorptivity of the absorbing species. IRS lowers this minimum thickness by one or two orders of magnitude. IRS using germanium electrodes in the infrared region is also being pursued in various laboratories.<sup>5</sup>

Although some work has been done with thin metal films vapor deposited on glass substrates, most of our studies have employed OTE made from doped tin oxide coatings on glasses obtained from two commercial sources. Although the doping material can be varied, antimony is commonly used and the resulting tin oxide coating is a n type semiconductor with a broad band gap. The carrier density is high, the order of  $10^{20}$  -  $10^{21}$  cm<sup>-3</sup>. The resistance varies considerably, depending on level of doping and thickness of the coating. Surfaces with resistances as low as 5-10 ohm-cm<sup>2</sup> have been prepared.

### EXPERIMENTAL

For electrochemical studies, it is desirable to minimize the ratio of surface area to resistance, so a thin circular ring of conducting surface is used as shown in the cell design of Figure 1. A simple sandwich type cell is employed for spectral studies. A potentiostat utilizing solid state Philbrick operational amplifiers and a Hewlett-Packard Model 467A power amplifier is used. Spectral work is done on either a Cary Model 15 spectrophotometer or a Warner-Swasey Co. Rapid-Scanning millisecond spectrophotometer.

### RESULTS AND DISCUSSION

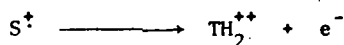
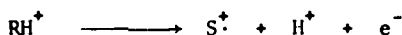
Preliminary measurements of the differential capacitance of these tin oxide electrodes for various pH's and electrolytes have been made by superimposing a small oscillating voltage on a changing dc bias voltage. Since these electrodes behave quite inertly in most electrolytes, the potential range which can be examined is extensive in comparison to most other semiconductor electrodes. It is found that there is a potential region in which the differential capacitance remains fairly independent of electrolytes (e.g. KCl, Na<sub>2</sub>SO<sub>4</sub>, KClO<sub>4</sub>, etc), their concentration and pH, and depends mainly on the particular semiconductor. For

example, a semiconductor with a resistance of  $10 \text{ ohm-cm}^{-2}$  gave a differential capacitance of  $2.4 \text{ uF-cm}^{-2}$  in KCl solutions 0.03 to 1.0 molar (pH = 6.5) over the potential range  $-0.3$  to  $+0.4 \text{ V. vs SCE}$ . Another semiconductor gave a capacitance between  $10$ - $15 \text{ uF-cm}^{-2}$  in a potential range of  $+0.3$  to  $-0.1 \text{ V vs SCE}$  but at more negative potentials,  $C^{-2}$  varied linearly with electrode potential due to depletion of electrons in the space charge layer.

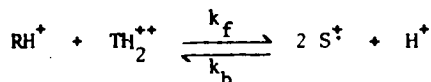
Using these electrodes, it is easy to follow the concentration of absorbing species formed during the course of an electrode reaction. For example absorbancy varies linearly with the reciprocal of the square-root of time during a chronoamperometric experiment as expected if the reaction is diffusion controlled and the product formed absorbs at the wavelength of the monitoring light. Similarly, electrochemical parameters for a variety of experimental techniques, i.e. chronopotentiometry, voltage-scan, etc., can be concurrently evaluated by spectral studies. However, in many cases there are complications due to the electrochemical parameters being affected by pH or by type or concentration of ions.

The oxidation of ferrocyanide has been extensively examined by cyclic voltammetry. Figure 2 gives examples of the changes in the current-potential (i-E) curves when KCl concentration or pH is varied. Since the saturation current for these semiconductors is high, the usual peak-type i-E curves, in which  $i_{\text{max}}$  is diffusion limited are observed. The overvoltage is affected by electrolyte concentration and pH. However, the quantitative aspects of the potential distribution throughout the semiconductor and the Helmholtz layer are complicated. Attempts are being made to further evaluate the electrical properties of these semiconductors and to relate them to the i-E characteristics. The situation appears promising since these electrodes behave quite inertly over a wide potential range.

In the oxidation of o-tolidine at pH 1.0, a one step, two electron i-E wave is observed with both OTE and platinum. Both amino groups are protonated at this pH, and the i-E curves with OTE show large overpotentials. At pH 4.0 with platinum, the wave splits into two peaks; with OTE, these waves are well developed and compare favorably to those obtained at platinum. At this pH, o-tolidine is monoprotonated and apparently, its interaction with the semiconductor surface is responsible for the lower overpotential. From optical studies during various electrochemical experiments, the electrode mechanism and associated reactions were determined to be:



and a disproportionation equilibrium:



where R, S $\cdot$  and T are the reduced, the free radical intermediate and the two-electron, fully oxidized molecule, respectively. The rate constant  $k_f$  has been evaluated under pseudo first order conditions. The rate constant for the slower hydrolysis reaction of  $\text{TH}_2^+$  has been measured.

Rate constants for some chemical coupling and dimerization type reactions which follow the charge transfer step have been also determined using OTE. The spectral examinations and results of these systems will be discussed.

The technique of IRS has been used to monitor surface concentration of species during oxidation at tin oxide coated OTE. The monitoring light was at a wavelength where the species absorbed. Determination of a spectrum is difficult, because simply taking the difference in optical absorbancy with and without absorbing species, does not give the correct spectrum for the species. Recent theoretical analysis<sup>6</sup> of the total IRS phenomenon has made possible the evaluation of changes occurring at the surface. Comments will be made about some results and the possible implications and direction of IRS at OTE.

#### ACKNOWLEDGEMENT

The authors gratefully acknowledge the support of this work by NOL contract N123-(62738)56006A and by NSF Grant No. GP-6479. The hydrolysis rates of oxidized o-tolidine were measured by Jeff Huntington.

#### REFERENCES

1. A. W. Copeland, O. D. Black and A. B. Garrett, *Chem. Revs.*, **31**, 177 (1942).
2. T. Kuwana, R. K. Darlington, and D. W. Leedy, *Anal. Chem.*, **36**, 2023 (1964).
3. T. Kuwana, Abstract No. B213 of papers presented at 17th CITCE meeting, Tokyo, Japan, September 1966.
4. W. N. Hansen, T. Kuwana, and R. A. Osteryoung, *Anal. Chem.*, **38**, 1810 (1966).
5. T. Takamura and H. Yoshida, Abstract No. C301 of papers presented at 17th CITCE meeting, Tokyo, Japan, September 1966; H. B. Mark, Jr. and B. S. Pons, *Anal. Chem.*, **38**, 119 (1966); and E. Yeager, private communication.
6. V. S. Srinivasan and T. Kuwana, Interference Attenuated Total Reflectance on Tin Oxide Glass Substrates, in press.

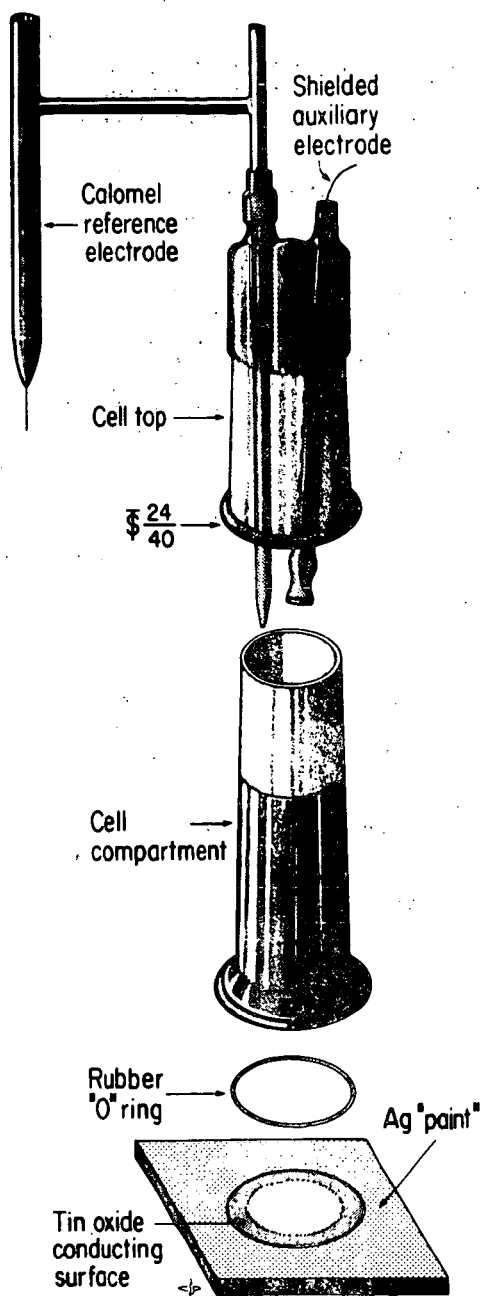


Fig. 1. Cell Design

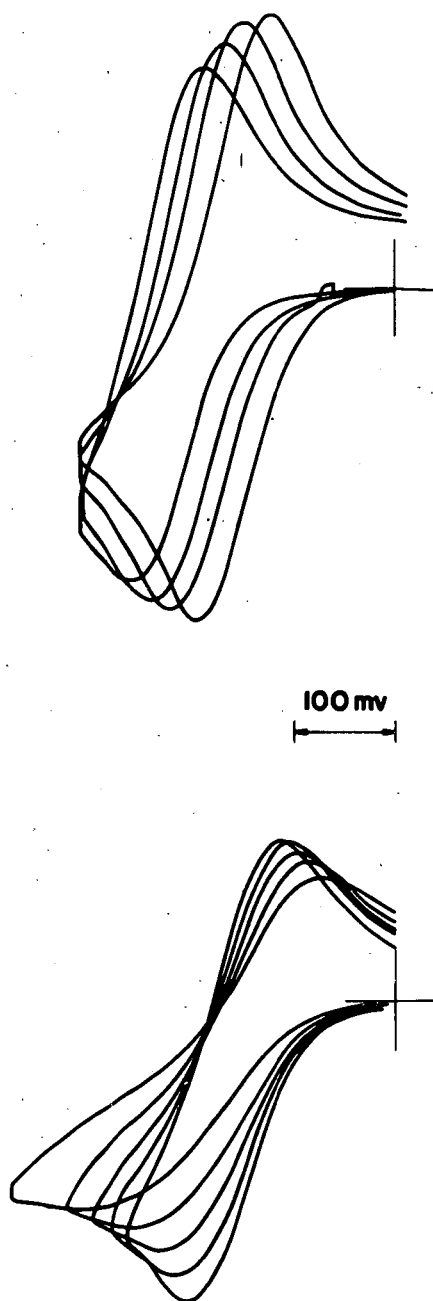


Fig. 2. Examples of  $i$ - $E$  curves for ferrocyanide at OTE using cyclic voltammetry.

Top: (left to right) 0.03, 0.1, 0.3 and 1.0 M KCl.

Bottom: pH 6.8, 7.5, 8.4 and 10 (waves become less reversible with increasing pH).

Constant-Potential Reactions Simultaneously Controlled by  
Charge-transfer and Mass-transfer Polarization at  
Planar, Spherical and Cylindrical Electrodes

Charles A. Johnson and Sidney Barnartt

Edgar C. Bain Laboratory  
For Fundamental Research  
United States Steel Corporation  
Research Center  
Monroeville, Pennsylvania

In general the rate of an electrode reaction will be determined by both charge-transfer and mass-transfer polarization, even in the case of slow reactions if the concentration of one reactant is small. The purpose of this paper is to examine the theoretical time behavior of the reaction rate at constant potential, for electrodes having planar, spherical or cylindrical symmetry. The electrochemical systems considered will be limited to first-order charge-transfer mechanisms. The current-time relation for planar electrodes at constant potential is known. This will be examined in greater detail, particularly from the standpoint of rapid reactions. Then a general solution will be given in closed form for spherical electrodes. Finally an approximate solution will be developed for cylindrical electrodes, and a numerical method for the general solution outlined.

Current-potential relations

The current-potential relation for a reaction of the type:  
 $R(z-n)+ = O^{z+} + ne^-$  was derived by Gerischer:<sup>1</sup>

$$i/i_o = \frac{a_R}{a_o} \exp \left[ (1-\beta)n\varepsilon\eta \right] - \frac{a_o}{a_o} \exp \left[ -\beta n\varepsilon\eta \right] \quad (1)$$

Here  $i$  is the net anodic current density at overpotential  $\eta$ ,  $i_o$  the exchange current density,  $\beta$  the transfer coefficient and  $\varepsilon \equiv F/RT$ . The activities of R and O are designated  $a_R$  and  $a_o$  at the electrode-solution interface at time  $t$ ; these differ from the bulk values  $a_R^o$  and  $a_o^o$  as a result of mass transfer effects. Equation 1 is limited to those charge-transfer mechanisms in which all of the electrical work involved occurs during the rate-determining step, and which are first order (defined at constant potential) with respect to the activities  $a_R$  and  $a_o$ .<sup>2,3</sup>

For rapid reactions the following approximation to eq. 1, also due to Gerischer,<sup>4</sup> is generally used,<sup>5-7</sup>

$$i/i_o = n\varepsilon\eta + \frac{a_R}{a_o} - \frac{a_o}{a_o} = n\varepsilon\eta + \frac{\Delta a_R}{a_R} - \frac{\Delta a_o}{a_o} \quad (2)$$

where  $\Delta a_R = a_R - a_R^0$  and  $\Delta a_O = a_O - a_O^0$ . Equation 2 was derived on the assumption that  $\eta$ ,  $\Delta a_R$  and  $\Delta a_O$  are all small, a set of limitations too confining for rapid reactions where activity changes develop rapidly. We propose, instead, a more basic relation for rapid reactions, valid at all values of  $\Delta a_R$  and  $\Delta a_O$ . This is obtained from eq. 1 by use of  $\exp(k\eta) \approx 1 + k\eta$ :

$$(i/i_0)_{t \rightarrow 0} = n\epsilon\eta \frac{a_R}{a_R^0} + (1 - \beta n\epsilon\eta) \left( \frac{a_R}{a_R^0} - \frac{a_O}{a_O^0} \right) \quad (3)$$

where  $\left( \frac{\Delta a_R}{a_R^0} - \frac{\Delta a_O}{a_O^0} \right)$  may be substituted for the last factor. Equation 3 reduces to

eq. 2 only if the assumption is made that  $\Delta a_R$  and  $\Delta a_O$  are small. This assumption is valid only during a very short interval after a rapid reaction is initiated; at longer times eq. 2 will exhibit greater deviations from the true relation (eq 1) than will eq. 3. An illustration of these deviations will be given below for the case of linear diffusion.

#### Planar electrodes

##### Potentiostatic current-time relations

Gerischer and Vielstich<sup>8</sup> have derived the solution, in closed form, for a first-order reaction described by eq. 1, with semi-infinite linear diffusion as the sole mass-transfer process. The electrolyte is assumed to contain excess neutral salt, so that concentration ratios may replace the activity ratios in eq. 1 with little error. The solution will be reproduced here and applied numerically to a typical fast reaction to illustrate the range of validity for eq. 2 and 3. The solutions for the concentrations and current density at the electrode surface are:

$$c_R = c_R^0 - \left( A/\lambda k^{1/2} \right) \left[ 1 - \exp(\lambda^2 t) \operatorname{erfc}(\lambda t^{1/2}) \right] \quad (4)$$

$$c_O = c_O^0 + (A/\lambda) \left[ 1 - \exp(\lambda^2 t) \operatorname{erfc}(\lambda t^{1/2}) \right] \quad (5)$$

$$i = i_{(t=0)} \cdot \exp(\lambda^2 t) \operatorname{erfc}(\lambda t^{1/2}) \quad (6)$$

where the desired charge-transfer current corresponding to overpotential  $\eta$  is

$$i_{(t=0)} = i_0 \left[ \exp(1-\beta)n\epsilon\eta - \exp(-\beta n\epsilon\eta) \right] \quad (7)$$

Here the quantities  $\lambda$  and  $A$  are defined by

$$\lambda = \frac{i_o \exp[(1-\beta)n\varepsilon\eta]}{nFc_R^o D_R^{\frac{1}{2}}} + \frac{i_o \exp(-\beta n\varepsilon\eta)}{nFc_O^o D_O^{\frac{1}{2}}} \quad (8)$$

$$A = \frac{\kappa^{\frac{1}{2}} i_o \exp[(1-\beta)n\varepsilon\eta]}{nFD_R^{\frac{1}{2}}} - \frac{i_o \exp(-\beta n\varepsilon\eta)}{nFD_O^{\frac{1}{2}}} \quad (9)$$

with  $\kappa \equiv D_R/D_O$ , the ratio of the diffusion coefficients. It should be noted that the equations as given in the Gerischer-Vielstich paper<sup>8</sup> contained two errors (no post-publication correction found): (1) omission of  $\kappa^{\frac{1}{2}}$  from the first term of  $A$ ; (2) the quantity  $(\kappa^{\frac{1}{2}}A/\lambda)$  in eq. 4 was given as  $(\kappa^{\frac{1}{2}}A/\lambda)$ . The quantity  $A$  may be written in terms of the charge-transfer current as

$$A = i_{(t=0)} \left[ nFD_O^{\frac{1}{2}} \right]^{-1} \quad (9a)$$

Substituting for  $A$  in eq. 4 and 5 one obtains the concentrations in terms of the charge-transfer current:

$$c_R = c_R^o - i_{(t=0)} \left[ nFD_R^{\frac{1}{2}} \lambda \right]^{-1} \left[ 1 - \exp(\lambda^2 t) \operatorname{erfc}(\lambda t^{\frac{1}{2}}) \right] \quad (4a)$$

$$c_O = c_O^o + i_{(t=0)} \left[ nFD_O^{\frac{1}{2}} \lambda \right]^{-1} \left[ 1 - \exp(\lambda^2 t) \operatorname{erfc}(\lambda t^{\frac{1}{2}}) \right] \quad (5a)$$

If the electrode reaction is rapid ( $\eta$  small), the current-time relation is still given by eq. 6 but the parameters  $i_{(t=0)}$ ,  $\lambda$  and  $A$  may be simplified to:

$$i_{(t=0)} = i_o n\varepsilon\eta \quad (10)$$

$$\lambda = \frac{i_o}{F} \left[ \frac{\varepsilon\eta}{c_R^o D_R^{\frac{1}{2}}} + \left( \frac{1}{n} - \beta\varepsilon\eta \right) \left( \frac{1}{c_R^o D_R^{\frac{1}{2}}} + \frac{1}{c_O^o D_O^{\frac{1}{2}}} \right) \right] \quad (11)$$

$$A = i_o n / RT D_O^{\frac{1}{2}} \quad (12)$$

The current-time relation (eq. 6) is obtainable from eq. 1 by substitution for  $c_R$  and  $c_O$  from eq. 4 and 5. Similarly, substitution for these concentrations in eq. 2 and 3 yields the corresponding approximate current-time curves. The following numerical case was selected to illustrate the deviations of the approximate curves from the rigorous one:  $i_o = 5 \times 10^{-3}$  A/cm<sup>2</sup> at 25°C,  $\beta = 0.5$ ,  $n = 1$ ,  $c_O^0 = 5 \times 10^{-2}$  and  $c_R^0 = 10^{-2}$  mole/l;  $D_O = 2 \times 10^{-5}$  and  $D_R = 10^{-5}$  cm<sup>2</sup>/s. With these values the reaction rates should be roughly equivalent to those reported<sup>9</sup> for the ferrous-ferric reaction on bright platinum. Figure 1 shows the calculated current-time curves for an applied overpotential of 10 mV. At the longest time shown ( $t = 0.21$  s)  $c_O$  has changed by 2.4% and  $c_R$  17%. These changes are sufficient to cause considerable deviation of eq. 2 from the true curve, but eq. 3 remains extremely close. Thus eq. 3 should be used as the basic rapid-reaction equation, while the former is an approximation useful only for very short reaction times.

It may be noted from eq. 4a, 5a that the maximum change in concentration, which occurs at  $t \rightarrow \infty$  (and  $i \rightarrow 0$ ), is given for each of the diffusing substances, by  $i(t=0) [nFD_0^2 \lambda]^{-1}$ . At any given time  $t$  the same fraction  $[1 - \exp(\lambda^2 t) \operatorname{erfc}(\lambda t^{1/2})]$  of the maximum change has taken place for each substance. In the present example this fraction is 0.572 at the longest time considered (0.21 second).

#### Evaluation of $i(t=0)$ and $\lambda$ .

If the argument  $\lambda t^{1/2}$  is small eq. 6 may be approximated by

$$i = i(t=0) \left[ 1 - (2/\pi^{1/2}) \lambda t^{1/2} + \lambda^2 t \right] \quad (13)$$

For a very short period, up to the time the last term in brackets ceases to be negligible, the initial region of the  $i-t^{1/2}$  curve is linear (e.g.  $t < 10$  ms in Fig. 1). From this line  $i(t=0)$  may be obtained by extrapolation, and the slope of the line yields  $\lambda$ . Experimentally, however, this linear region will often be inaccessible for moderately rapid reactions with present-day potentiostatic circuitry. An appreciable time is required to attain the control potential within a small fraction of a millivolt ( $\eta$  being small), primarily because it is necessary to incorporate automatic compensation for the IR drop between the controlled electrode and the capillary tip of the reference electrode<sup>10</sup>.

To permit analysis of experimental current-time curves which exclude the initial linear region, we present here another simple procedure for evaluating  $i(t=0)$  and  $\lambda$ . In this method one selects an arbitrary time  $t$ , and reads the current from the experimental curve at times  $t$  and  $4t$ . The ratio of these two currents is

$$\frac{i(t)}{i(4t)} = \frac{\exp(\lambda^2 t) \operatorname{erfc}(\lambda t^{1/2})}{\exp(4\lambda^2 t) \operatorname{erfc}(2\lambda t^{1/2})} \quad (14)$$

This ratio is readily calculated for all values of  $\lambda t^{1/2}$  from tables<sup>11</sup> of the function  $\exp(y^2) \operatorname{erfc}(y)$ , and is shown in Fig. 2 for  $\lambda t^{1/2} = 0$  to 1. The experi-

mental value of the current ratio for a specific time  $t_1$  has a corresponding value of  $\lambda t_1^{\frac{1}{2}}$  which is obtained from Fig. 2, and this value yields  $\lambda$ . The procedure may be repeated for times  $t_2, t_3, t_4 \dots$  to obtain a mean value of  $\lambda$ . Utilizing the mean  $\lambda$ , each measured current at  $t_1, t_2, t_3 \dots$  yields  $i(t=0)$  from eq. 6. If the deviations of the individual values of  $\lambda$  or of  $i(t=0)$  about the mean value are found to be small and randomly distributed, one has support for the a priori assumption of a first-order charge-transfer mechanism. As  $\lambda t^{\frac{1}{2}}$  increases, the slope of the curve in Fig. 2 decreases; hence the precision with which  $\lambda$  can be evaluated decreases with increasing time in the intermediate-time range  $(0.85 \lesssim i(t)/i(t=0) \lesssim 0.45)^{10}$ .

#### Evaluation of charge-transfer parameters<sup>6,7</sup>

For slow electrode reactions ( $\eta$  relatively large), it is sufficient to determine  $i(t=0)$  from potentiostatic current-time curves as a function of  $\eta$ , either for anodic ( $\eta$  positive) or cathodic ( $\eta$  negative) polarization. The well-known Tafel plot then yields both  $i_0$  and  $\beta$ . For rapid reactions (small  $\eta$ ), measurement of  $i(t=0)$  in a given solution yields  $i_0$  from eq. 10; since  $i_0$  is given by

$$i_0 = i_{0,s} (a_R^0)^\beta (a_O^0)^{1-\beta} \quad (15)$$

where  $i_{0,s}$  is the standard exchange current density,<sup>12</sup>  $\beta$  is obtained from determinations of  $i_0$  with solutions in which  $a_R^0$  is varied at constant  $a_O^0$ , or  $a_O^0$  varied at constant  $a_R^0$ .

#### Evaluation of $D_R$ or $D_O$

The ratio  $i(t=0)/\lambda$  from eq. 7 and 8 is given by

$$\frac{i(t=0)}{\lambda} = nF [\exp(n\epsilon\eta) - 1] \left[ \frac{\exp(n\epsilon\eta)}{c_R^0 \sqrt{D_R}} + \frac{1}{c_O^0 \sqrt{D_O}} \right]^{-1} \quad (16)$$

and is seen to be independent of  $i_0$  and  $\beta$ . Thus the values of  $i(t=0)$  and  $\lambda$  obtained from a single potentiostatic current-time curve permit estimation of one of the diffusion coefficients if the other is known. This is so even though  $i(t=0)$  and  $\lambda$  are obtained from the current-time curve at short times, where the reaction is partly controlled by the charge-transfer kinetics.

The current at long times ( $\lambda t^{\frac{1}{2}} \gg 1$ ) is under complete mass-transfer control, and a plot of  $i$  vs.  $t^{-\frac{1}{2}}$  is linear with a slope proportional to the ratio  $i(t=0)/\lambda$ , as was shown by Gerischer and Vielstich.<sup>8</sup> Hence the long-time currents permit evaluation of the diffusion coefficient somewhat more directly.

#### Spherical Electrodes

The problem is solved here in closed form for an electrode reaction at constant potential involving a first-order charge-transfer mechanism (eq 1), with diffusion in a system of spherical symmetry as the sole mode of mass transfer. The mathematical formulation of the problem comprises differential equations:

$$D_R \frac{1}{r^2} \frac{\partial}{\partial r} \left( r^2 \frac{\partial c_R}{\partial r} \right) = \frac{\partial c_R}{\partial t}, \quad D_O \frac{1}{r^2} \frac{\partial}{\partial r} \left( r^2 \frac{\partial c_O}{\partial r} \right) = \frac{\partial c_O}{\partial t}$$

with initial conditions ( $t=0, r \geq a$ ):  $c_R = c_R^0, c_O = c_O^0$  and boundary conditions (all  $t$ ):

$$r \rightarrow \infty: \quad c_R \rightarrow c_R^0; \quad c_O \rightarrow c_O^0$$

$$r = a: \quad i = nFD_R \frac{\partial c_R}{\partial r} = -nFD_O \frac{\partial c_O}{\partial r}$$

Here  $a$  is the electrode radius, and  $i$  is the current density given by eq 1 with concentrations substituted for activities.

### General Solution

The general solution of this problem, derived by the Laplace transform method, is presented in the Appendix. Equations A17 and A18 give the concentration changes at the electrode, and eq A19 the current density. Two regions of the current-time curve are of particular interest for extracting the charge-transfer parameters, namely the initial short-time section and the final long-time section.

(a) Short-time solution: This is obtained by use of the approximation,  $\exp x^2 \operatorname{erfc} x = 1 - (2/\pi^{1/2}) x + x^2$ , which is valid for small  $x$ . Equations A17-19 convert to

$$c_R = c_R^0 - \frac{i(t=0)}{nFD_R} \left[ \frac{2}{\pi^{1/2}} t^{1/2} - \left( 1 + \frac{D_R}{a\lambda} \right) \lambda t \right] \quad (17)$$

$$c_O = c_O^0 + \frac{i(t=0)}{nFD_O} \left[ \frac{2}{\pi^{1/2}} t^{1/2} - \left( 1 + \frac{D_O}{a\lambda} \right) \lambda t \right] \quad (18)$$

$$i = i(t=0) \left[ 1 - \frac{2}{\pi^{1/2}} \lambda t^{1/2} + \left( 1 + \frac{\lambda_R D_R + \lambda_O D_O}{a\lambda^2} \right) \lambda^2 t \right] \quad (19)$$

where

$$\lambda_R = \frac{i_0 \exp(1-\beta)n\varepsilon\eta}{nFD_R c_R^0} \quad ; \quad \lambda_O = \frac{i_0 \exp(-\beta)n\varepsilon\eta}{nFD_O c_O^0} \quad (20)$$

and also  $\lambda = \lambda_R D_R^{1/2} + \lambda_O D_O^{1/2}$  and  $i(t=0) = nF(\lambda_R D_R c_R^0 - \lambda_O D_O c_O^0)$  as for planar geometry. A comparison of eq 19 with the corresponding eq 13 for the planar case shows that, over sufficiently short times such that the term in  $t$  is negligible, the sphere and plate electrodes yield the same linear  $i - t^{1/2}$  relation. The linear behavior terminates sooner for the small sphere, however, since the term in  $t$  is larger in eq 19 than in eq 13.

If this linear portion of the curve is experimentally accessible, the values of  $\lambda$  and  $i(t=0)$  obtained from it can be used to determine the charge-transfer parameters and one of the diffusion coefficients, as described above for planar electrodes. For moderately rapid reactions, if the initial portion is inaccessible charge-transfer parameters can be determined from the long-time portion of the curve as shown below.

(b) Long-time solution: Use is made of the approximation,  $\exp x^2 \operatorname{erfc} x = \pi^{-\frac{1}{2}} x^{-1}$ , valid for large values of  $x$ . Equations A17-19 become

$$c_R = c_R^o - \frac{i(t=0)}{nF} \frac{a}{D_R(1 + a\lambda_R + a\lambda_O)} \left[ 1 + \frac{a\lambda_O(x^{\frac{1}{2}} - 1) - 1}{1 + a\lambda_R + a\lambda_O} \frac{a}{(D_R\pi t)^{\frac{1}{2}}} \right] \quad (21)$$

$$c_O = c_O^o + \frac{i(t=0)}{nF} \frac{a}{D_O(1 + a\lambda_R + a\lambda_O)} \left[ 1 + \frac{a\lambda_R(x^{\frac{1}{2}} - 1) - 1}{1 + a\lambda_R + a\lambda_O} \frac{a}{(D_O\pi t)^{\frac{1}{2}}} \right] \quad (22)$$

$$i = \frac{i(t=0)}{1 + a\lambda_R + a\lambda_O} \left[ 1 + \frac{a^2(\lambda_R/D_R^{\frac{1}{2}} + \lambda_O/D_O^{\frac{1}{2}})}{1 + a\lambda_R + a\lambda_O} \frac{1}{(\pi t)^{\frac{1}{2}}} \right] \quad (23)$$

A plot of  $i$  against  $t^{-\frac{1}{2}}$  is a straight line, of form

$$i = i(t \rightarrow \infty) + \sigma t^{-\frac{1}{2}} \quad (23a)$$

with intercept

$$i(t \rightarrow \infty) = \frac{i(t=0)}{1 + a\lambda_R + a\lambda_O} \quad (23b)$$

and slope

$$\sigma = \frac{a^2(\lambda_R/D_R^{\frac{1}{2}} + \lambda_O/D_O^{\frac{1}{2}}) i(t=0)}{\pi^{\frac{1}{2}} (1 + a\lambda_R + a\lambda_O)^2} \quad (23c)$$

It may be recalled<sup>15</sup> that reversible reactions at spherical electrodes also exhibit a linear  $i - t^{-\frac{1}{2}}$  curve at long times, but the intercept and slope are then quite different from the corresponding expressions for irreversible reactions (eq 23b,c).

At long times the current at a spherical electrode goes towards the finite value given by eq 23b, whereas at a plane electrode the corresponding current goes to zero. In the latter case the reaction becomes essentially diffusion controlled<sup>8</sup> at  $\lambda t^{\frac{1}{2}} > 1$  (or at  $i/i(t=0) < 0.43$ ), so that current measurements at long times give no information about the charge-transfer mechanism. With small spherical electrodes, however, the reaction remains under partial charge-transfer control at all times. Provided the diffusion coefficients are known, the charge-transfer parameters may be derived as follows. We define the quantity

$$\rho = \frac{\lambda_R}{\lambda_O} = \frac{c_O^o D_O}{c_R^o D_R} \exp(n\epsilon\eta) \quad (24)$$

The combination of eq 23b, 23c, and 24 yields

$$\frac{1}{\lambda_0} = a \left[ \frac{a i(t \rightarrow \infty)}{\sigma \pi^{\frac{1}{2}}} \left( \frac{\rho}{D_R^{\frac{1}{2}}} + \frac{1}{D_0^{\frac{1}{2}}} \right) - \rho - 1 \right] \quad (25)$$

This permits evaluation of  $\lambda_0$  corresponding to the value of  $\eta$  which establishes the current-time curve. After measuring current-time curves at several values of  $\eta$ , we may plot  $\log \lambda_0$  against  $\eta$ , since from eq 20

$$\log \lambda_0 = \log(i_0/nFD_0c_0^0) - (\beta n e / 2.3) \eta \quad (20a)$$

to obtain  $\beta$  from the slope and  $i_0$  from the intercept at  $\eta = 0$ .

Particular case:  $D_R = D_0$

It is of interest to examine the special case of  $D_R = D_0 = D$  which was treated by Shain, Martin and Ross.<sup>14</sup> The time variations of current density and concentrations at the electrode surface become, from eq A17-19,

$$c_R = c_R^0 - \frac{i(t=0)}{nFD^{\frac{1}{2}}\lambda(1+\delta)} \left[ 1 - \exp((1+\delta)^2\lambda^2 t) \operatorname{erfc}((1+\delta)\lambda t^{\frac{1}{2}}) \right] \quad (26)$$

$$c_0 = c_0^0 + \frac{i(t=0)}{nFD^{\frac{1}{2}}\lambda(1+\delta)} \left[ 1 - \exp((1+\delta)^2\lambda^2 t) \operatorname{erfc}((1+\delta)\lambda t^{\frac{1}{2}}) \right] \quad (27)$$

$$\frac{i}{i(t=0)} = \frac{\delta}{1+\delta} + \frac{1}{1+\delta} \left[ \exp((1+\delta)^2\lambda^2 t) \operatorname{erfc}((1+\delta)\lambda t^{\frac{1}{2}}) \right] \quad (28)$$

where  $\delta = D^{\frac{1}{2}}/\alpha\lambda$ . Equation 28 is equivalent to the solution for the current previously given.<sup>14</sup>

The short-time current at  $\lambda t^{\frac{1}{2}} \ll 1$  now becomes

$$i = i(t=0) \left[ 1 - 2\pi^{-\frac{1}{2}}\lambda t^{\frac{1}{2}} + (1+\delta)\lambda^2 t \right] \quad (29)$$

Thus from a single potentiostatic current-time curve the initial linear  $i - t^{\frac{1}{2}}$  portion yields  $\lambda$  and  $i(t=0)$ , from which the charge-transfer quantities  $\beta$  and  $i_0$  are evaluated, and the ratio  $i(t=0)/\lambda$  gives the diffusion coefficient (eq 16).

If the initial portion of the curve is experimentally inaccessible, it is possible to derive the charge-transfer parameters from the currents at longer times provided the diffusion coefficient is known. Shain et al<sup>14</sup> described a treatment of the longer-time currents involving trial-and-error curve fitting; this treatment is restricted to slow reactions at relatively high  $\eta$ . We note here that the long-time current is given by eq 23, which when simplified for  $D_R = D_0 = D$  yields

$$\frac{i}{i(t=0)} = \frac{\delta}{1+\delta} + \left( \frac{1}{1+\delta} \right)^2 \frac{1}{\pi^{\frac{1}{2}}\lambda t^{\frac{1}{2}}} \quad (30)$$

This provides a more direct method, and one which is applicable to rapid reactions. The slope  $\delta$  and intercept  $i(t \rightarrow \infty)$  of this linear  $i/t^{1/2}$  relation yields  $\lambda$  in the form

$$\lambda = cD\pi^{1/2} (a^2 i(t \rightarrow \infty) - a\sigma\pi^{1/2} D^{1/2})^{-1} \quad (31)$$

From  $\lambda$  the quantity  $\delta = \sqrt{D}/a\lambda$  is calculated, whence  $i(t=0)$  is obtained from the intercept  $i(t \rightarrow \infty) = i(t=0) \delta(1 + \delta)^{-1}$ . We may determine  $i(t=0)$  in this way at several values of  $\eta$ , using a single solution and either anodic or cathodic polarization. Thus for anodic polarization the charge-transfer current is given by eq 7, which may be rearranged to

$$\log \left( \frac{i(t=0)}{\exp(nE\eta) - 1} \right) = \log i_0 - \left( \frac{\beta n E}{2.3} \right) \eta \quad (32)$$

A plot of the left side against  $\eta$  yields  $i_0$  (intercept) and  $\beta$  (slope).

### Cylindrical Electrodes

Here the problem comprises a first-order charge-transfer mechanism (eq 1) combined with diffusion to a cylindrical electrode of radius  $a$  as the sole mass-transfer process. As before, the time variations of current and concentrations at the electrode surface are to be determined for a reaction at constant potential. The mathematical description consists of differential equations:

$$\frac{\partial c_R}{\partial t} = D_R \left[ \frac{\partial^2 c_R}{\partial r^2} + \frac{1}{r} \frac{\partial c_R}{\partial r} \right] ; \quad \frac{\partial c_O}{\partial t} = D_O \left[ \frac{\partial^2 c_O}{\partial r^2} + \frac{1}{r} \frac{\partial c_O}{\partial r} \right]$$

with initial conditions ( $t = 0, r \geq a$ ):  $c_R = c_R^0, c_O = c_O^0$ , and boundary conditions (all  $t$ ):

$$r \rightarrow \infty: \quad c_R \rightarrow c_R^0 \quad ; \quad c_O \rightarrow c_O^0$$

$$r = a: \quad i = nFD_R \frac{\partial c_R}{\partial r} = -nFD_O \frac{\partial c_O}{\partial r}$$

A solution of this problem based on the use of Laplace transforms, is described in the Appendix. The method does not lead to a general solution in closed form, but the entire current-time curve may be determined numerically for any specific case. An approximate solution, valid at sufficiently short times, is derived with the use of asymptotic expansions. The current and the concentrations at the electrode surface are given by eq A33-35 of the Appendix. For the special case  $D_R = D_O = D$ , these equations convert to:

$$i/i(t=0) = 1 - 2\pi^{-1/2} \lambda t^{1/2} + (1 + \delta/2) \lambda^2 t \quad (33)$$

$$c_R = c_R^0 - \frac{i(t=0)}{nFD^{1/2}} (2\pi^{-1/2} t^{1/2} - \lambda t) \quad (34)$$

$$c_O = c_O^0 + \frac{i(t=0)}{nFD^{1/2}} (2\pi^{-1/2} t^{1/2} - \lambda t) \quad (35)$$

where  $\bar{\lambda} = \lambda(1 + \delta/2)$ ; quantities  $\lambda$  and  $\delta$  are the same as defined above for planar and spherical symmetry. The equations reduce to the corresponding ones for planar electrodes if the cylinder is large ( $a \gg D^2/\lambda$ ). It is seen from eq 33 that there will be a short period of time during which a cylindrical electrode of any radius will yield the same linear  $i - t^2$  relation as does the plane electrode. Deviation from this line, represented by the term in  $\lambda^2 t$ , will develop somewhat faster at a small cylindrical electrode than at a plate, but not so fast as at a spherical electrode of the same radius.

#### Comparison of planar, spherical and cylindrical electrodes

A numerical solution was carried out<sup>13</sup> (see Appendix) for the current-time curve at a small cylinder of radius  $a = \sqrt{D/\lambda}$  (hence  $\delta = 1$ ) for the special case of  $D_R = D_O = D$ . This is compared in Fig. 3 with the corresponding curve for a sphere of the same radius, obtained from eq 28. Also shown is the curve for a large sphere or large cylinder ( $a \gg \sqrt{D/\lambda}$ ), which is the same as eq 6 for the plane. At  $\lambda t^2 = 5$  the current ratio for this small sphere is close to the value  $\delta/(1 + \delta) = \frac{1}{2}$  for  $t \rightarrow \infty$  (see eq 28). The current ratio for the planar electrode goes to zero as  $t \rightarrow \infty$ . The curve for the cylinder is positioned about midway between the other two.

Figure 4 presents the short-time approximations to these curves, as given by eqs 13, 20 and 33 for the planar, spherical and cylindrical cases respectively. These approximate curves lie somewhat above the corresponding curves in Fig. 3, but for the range  $\lambda t^2 = 0$  to 0.25 the deviation is small. At  $\lambda t^2 = 0.25$  the currents given in Fig. 4 are 1.4% high for the planar electrode, 2.6% high for the cylindrical and 4.3% high for the spherical electrode.

As the electrode radius is increased above the value  $\sqrt{D/\lambda}$ , the upper two curves in Fig. 3 and 4 will move gradually closer to the planar-electrode curve.

#### Summary

1. A current-potential relation for rapid reactions, applicable to first-order charge-transfer mechanisms, is proposed and illustrated by a numerical example. This equation (eq 3) has a much wider range of validity than the form previously used (eq 2).
2. The analysis of potentiostatic current-time curves for planar electrodes, for reactions controlled simultaneously by charge-transfer and mass-transfer polarization, has been extended. This analysis is based upon measurements of the ratio of current at some time  $t$  to that at  $4t$ , and permits extraction of the charge-transfer parameters  $\beta$  and  $i_0$  from the experimentally more accessible part of the curve following the linear  $i - t^2$  portion.
3. Closed-form solutions to the general boundary-value problem for spherical electrodes are derived.
4. The boundary-value problem for cylindrical electrodes has been treated, and a general method for obtaining numerical solutions outlined. Also approximate analytical solutions valid for short times are derived.
5. Current-time curves for a particular small radius of sphere and cylinder are compared with the corresponding planar-electrode curves. The small sphere yields higher currents at a given time than does the plate. The curve for the cylinder lies between the other two.
6. The current at a small sphere approaches a constant value, different from zero, as  $t \rightarrow \infty$ . The long-time current permits determination of the charge-transfer parameters because the reaction remains under partial charge-transfer control at all times.

## APPENDIX

Solution of the diffusion problem for spherical electrodes.

The diffusion equation for a system having full spherical symmetry is

$$D \frac{1}{r^2} \frac{\partial}{\partial r} \left( r^2 \frac{\partial c}{\partial r} \right) = \frac{\partial c}{\partial t}$$

where  $c = c(r, t)$  is the concentration at time  $t$  and radial distance  $r$ . On making the substitution

$$U(r, t) = r c(r, t)$$

the diffusion equation becomes

$$D \frac{\partial^2 U}{\partial r^2} = \frac{\partial U}{\partial t}$$

and, in terms of the new variable  $U = rc$  can now be treated in much the same fashion as diffusion in a linear system. Thus in the present problem we define

$$U_R(r, t) = r c_R(r, t) ; U_O(r, t) = r c_O(r, t) \quad (A1)$$

which satisfy the differential equations

$$D_R \frac{\partial^2 U_O}{\partial r^2} = \frac{\partial U_O}{\partial t} ; D_O \frac{\partial^2 U_R}{\partial r^2} = \frac{\partial U_R}{\partial t} \quad (A2)$$

with initial conditions, for a spherical electrode of radius  $a$ ,

$$r \geq a : U_R(r, t=0) = c_R^0 r ; U_O(r, t=0) = c_O^0 r \quad (A3)$$

and the boundary conditions:

$$r \rightarrow \infty : U_R(r, t) \rightarrow c_R^0 r, U_O(r, t) \rightarrow c_O^0 r \quad (A4)$$

The remaining condition is that for the electrode current. The current density is given (in terms of the electrode reaction) by eq 1, which in the present notation is

$$\frac{i(t)}{i_0} = \frac{\exp[(1-\beta)n_e\eta]}{c_R^0 a} U_R(r=a, t) - \frac{\exp[-\beta n_e\eta]}{c_O^0 a} U_O(r=a, t) \quad (A5)$$

and (in terms of the diffusion currents) by

$$i(t) = -nFD_R \left( \frac{\partial c_R}{\partial r} \right)_{r=a} = +nFD_R \left[ \frac{1}{a} \left( \frac{\partial U_R}{\partial r} \right)_{r=a} - \frac{1}{a^2} U_R(a, t) \right] \quad (A6)$$

and

$$i(t) = -nFD_O \left( \frac{\partial c_O}{\partial r} \right)_{r=a} = -nFD_O \left[ \frac{1}{a} \left( \frac{\partial U_O}{\partial r} \right)_{r=a} - \frac{1}{a^2} U_O(a, t) \right] \quad (A7)$$

On combining eq A5 - A7 we find the conditions which must be satisfied on the electrode surface  $r = a$ :

$$\left(\frac{\partial U_O}{\partial r}\right)_{r=a} = + U_O(a, t) \left[\lambda_O + \frac{1}{a}\right] - U_R(a, t) \lambda_R \kappa \quad (A8)$$

$$\left(\frac{\partial U_R}{\partial r}\right)_{r=a} = - U_O(a, t) \frac{\lambda_O}{\kappa} + U_R(a, t) \left[\lambda_R + \frac{1}{a}\right]$$

with  $\kappa = D_R/D_O$  and

$$\lambda_R = \frac{i_o \exp[(1 - \beta)n\epsilon\eta]}{nFD_R c_R^o} ; \lambda_O = \frac{i_o \exp[-\beta n\epsilon\eta]}{nFD_O c_O^o} \quad (A9)$$

as in the Gerischer-Vielstich notation<sup>8</sup>. In terms of the Laplace transforms

$$Y_O(r, s) = \int_0^{\infty} e^{-st} U_O(r, t) dt$$

$$Y_R(r, s) = \int_0^{\infty} e^{-st} U_R(r, t) dt$$

the differential equations A2 and initial conditions A3 become

$$D_R \frac{\partial^2 Y_R}{\partial r^2} = sY_R - c_R^o r \quad ; \quad D_O \frac{\partial^2 Y_O}{\partial r^2} = sY_O - c_O^o r \quad (A10)$$

The solution which satisfies the boundary conditions A4 is

$$Y_O(r, s) = \alpha(s) \exp[-\sqrt{s/D_O} r] + c_O^o r/s \quad (A11)$$

$$Y_R(r, s) = \beta(s) \exp[-\sqrt{s/D_R} r] + c_R^o r/s$$

where  $\alpha(s)$  and  $\beta(s)$  are determined by the simultaneous solution of eq A8:

$$\alpha(s) = \frac{[\lambda_R \kappa c_R^o - \lambda_O c_O^o][a\sqrt{sD_O} + \sqrt{D_O D_R}] \cdot \exp[a\sqrt{s/D_O}]}{s[s + \gamma\sqrt{s} + \delta']} \quad (A12)$$

$$\beta(s) = \frac{[\lambda_O c_O^o/\kappa - \lambda_R c_R^o][a\sqrt{sD_R} + \sqrt{D_O D_R}] \cdot \exp[a\sqrt{s/D_R}]}{s[s + \gamma\sqrt{s} + \delta']}$$

with

$$\gamma = \lambda_R \sqrt{D_R} + \lambda_O \sqrt{D_O} + (\sqrt{D_O} + \sqrt{D_R})/a \quad (A13)$$

$$\delta = \sqrt{D_O D_R} [1 + a(\lambda_R + \lambda_O)]/a^2 \quad (A14)$$

Equations A11, with the values of  $\alpha(s)$ ,  $\beta(s)$  from eq A12, determine the Laplace transforms of the variables  $U_0(r,t)$ ,  $U_R(r,t)$  and hence the concentrations  $c_0(r,t)$ ,  $c_R(r,t)$ .

We require the values of the concentrations at the phase boundary  $r = a$  and the current as functions of the time. The current is most easily obtained by taking the Laplace transform of eq A7:

$$J(s) = -nFD_0 \left[ \frac{1}{a} \left( \frac{\partial Y_0}{\partial r} \right)_{r=a} - \frac{1}{a^2} Y_0(a,s) \right] \quad (\text{A15})$$

with  $Y_0(r,s)$  given by eq A11 and

$$J(s) = \int_0^{\infty} i(t) e^{-st} dt$$

The current and concentrations are now readily obtained by inversion of eq A15 and A11. To accomplish this we must first factor the common denominator of  $\alpha(s)$ ,  $\beta(s)$ ,

$$(s + \gamma' \sqrt{s} + \delta') = (\sqrt{s} + \xi)(\sqrt{s} + \mu)$$

$$\xi = \frac{1}{2} \left\{ \lambda + (\sqrt{D_0} + \sqrt{D_R})/a + \left[ \lambda^2 + \left( \frac{\sqrt{D_0} - \sqrt{D_R}}{a} \right)^2 + \frac{2}{a} (\lambda_R \sqrt{D_R} - \lambda_O \sqrt{D_0}) (\sqrt{D_R} - \sqrt{D_0}) \right]^{\frac{1}{2}} \right\} \quad (\text{A16})$$

$$\mu = \frac{1}{2} \left\{ \lambda + (\sqrt{D_0} + \sqrt{D_R})/a - \left[ \lambda^2 + \left( \frac{\sqrt{D_0} - \sqrt{D_R}}{a} \right)^2 + \frac{2}{a} (\lambda_R \sqrt{D_R} - \lambda_O \sqrt{D_0}) (\sqrt{D_R} - \sqrt{D_0}) \right]^{\frac{1}{2}} \right\}$$

with  $\lambda = \lambda_O \sqrt{D_0} + \lambda_R \sqrt{D_R}$ . These relations yield<sup>11</sup>

$$c_R = c_R^0 - \frac{A}{\sqrt{\kappa(\xi - \mu)}} \left[ \frac{\sqrt{D_0}}{a} \left( \frac{1}{\mu} - \frac{1}{\xi} \right) + \left( 1 - \frac{\sqrt{D_0}}{a\mu} \right) \exp \mu^2 t \operatorname{erfc} \mu \sqrt{t} - \left( 1 - \frac{\sqrt{D_0}}{a\xi} \right) \exp \xi^2 t \operatorname{erfc} \xi \sqrt{t} \right] \quad (\text{A17})$$

$$c_0 = c_0^0 + \frac{A}{\xi - \mu} \left[ \frac{\sqrt{D_R}}{a} \left( \frac{1}{\mu} - \frac{1}{\xi} \right) + \left( 1 - \frac{\sqrt{D_R}}{a\mu} \right) \exp \mu^2 t \operatorname{erfc} \mu \sqrt{t} - \left( 1 - \frac{\sqrt{D_R}}{a\xi} \right) \exp \xi^2 t \operatorname{erfc} \xi \sqrt{t} \right] \quad (\text{A18})$$

$$\frac{i(t)}{i(t=0)} = \frac{1}{1 + a\lambda_R + a\lambda_O} + \frac{1}{\xi - \mu} \left[ \frac{(\sqrt{D_R} - a\xi)(\sqrt{D_O} - a\xi)}{a^2\xi} \exp\xi^2 t \operatorname{erfc}\xi\sqrt{t} - \frac{(\sqrt{D_R} - a\mu)(\sqrt{D_O} - a\mu)}{a^2\mu} \exp\mu^2 t \operatorname{erfc}\mu\sqrt{t} \right] \quad (\text{A19})$$

where A is given by eq 9a. These equations reduce to the corresponding results for planar electrodes if a is large, i.e.,  $a \gg (\lambda_R + \lambda_O)^{-1}$ .

Approximate solution of the diffusion problem for cylindrical electrodes.

The diffusion equations for the species O and R in a system having full cylindrical symmetry are

$$D_O \left[ \frac{\partial^2 c_O}{\partial r^2} + \frac{1}{r} \frac{\partial c_O}{\partial r} \right] = \frac{\partial c_O}{\partial t} \quad (\text{A21})$$

$$D_R \left[ \frac{\partial^2 c_R}{\partial r^2} + \frac{1}{r} \frac{\partial c_R}{\partial r} \right] = \frac{\partial c_R}{\partial t}$$

and are to be solved subject to the initial conditions

$$r \geq a : c_R(r, t=0) = c_R^0, c_O(r, t=0) = c_O^0 \quad (\text{A22})$$

and the boundary conditions

$$r \rightarrow \infty : c_R(r, t) \rightarrow c_R^0, c_O(r, t) \rightarrow c_O^0 \quad (\text{A23})$$

$$i(t) = nFD_R \left( \frac{\partial c_R}{\partial r} \right)_{r=a} = -nFD_O \left( \frac{\partial c_O}{\partial r} \right)_{r=a} \quad (\text{A24})$$

The combination of eq 1 and A24 yields the conditions which must be satisfied on the electrode surface  $r = a$ :

$$\left( \frac{\partial c_O}{\partial r} \right)_{r=a} = \lambda_O c_O(a, t) - \lambda_R \kappa c_R(a, t) \quad (\text{A25})$$

$$\left( \frac{\partial c_R}{\partial r} \right)_{r=a} = -\frac{\lambda_O}{\kappa} c_O(a, t) + \lambda_R c_R(a, t)$$

In terms of the Laplace transforms

$$U_O(r, s) = \int_0^\infty c_O(r, t) e^{-st} dt \quad (\text{A26})$$

$$U_R(r, s) = \int_0^\infty c_R(r, t) e^{-st} dt$$

the differential equations A21 and initial conditions A22 become

$$D_O \left[ \frac{\partial^2 U_O}{\partial r^2} + \frac{1}{r} \frac{\partial U_O}{\partial r} \right] = s U_O - c_O^0 \quad (A27)$$

$$D_R \left[ \frac{\partial^2 U_R}{\partial r^2} + \frac{1}{r} \frac{\partial U_R}{\partial r} \right] = s U_R - c_R^0$$

The solution which satisfies the boundary conditions A23 is<sup>11</sup>

$$U_O(r,s) = \frac{c_O^0}{s} + \alpha(s) K_0 \left( \sqrt{\frac{s}{D_O}} r \right) \quad (A28)$$

$$U_R(r,s) = \frac{c_R^0}{s} + \beta(s) K_0 \left( \sqrt{\frac{s}{D_O}} r \right)$$

where  $K_0(x)$  is the modified Bessel function of the second kind of order zero.  $\alpha(s)$  and  $\beta(s)$  are determined by the simultaneous solution of eq A25:

$$\alpha(s) =$$

$$K_1 \left( \sqrt{\frac{s}{D_R}} a \right) \sqrt{D_O} [\lambda_R c_R^0 - \lambda_O c_O^0]$$

---


$$s \left[ \sqrt{s} K_1 \left( \sqrt{\frac{s}{D_O}} a \right) K_1 \left( \sqrt{\frac{s}{D_R}} a \right) + \lambda_O \sqrt{D_O} K_0 \left( \sqrt{\frac{s}{D_O}} a \right) K_1 \left( \sqrt{\frac{s}{D_R}} a \right) + \lambda_R \sqrt{D_R} K_0 \left( \sqrt{\frac{s}{D_R}} a \right) K_1 \left( \sqrt{\frac{s}{D_O}} a \right) \right]$$

$$\beta(s) = \quad (A29)$$

$$K_1 \left( \sqrt{\frac{s}{D_O}} a \right) \sqrt{D_R} [\lambda_O c_O^0 / \kappa - \lambda_R c_R^0]$$

---


$$s \left[ \sqrt{s} K_1 \left( \sqrt{\frac{s}{D_O}} a \right) K_1 \left( \sqrt{\frac{s}{D_R}} a \right) + \lambda_O \sqrt{D_O} K_0 \left( \sqrt{\frac{s}{D_O}} a \right) K_1 \left( \sqrt{\frac{s}{D_R}} a \right) + \lambda_R \sqrt{D_R} K_0 \left( \sqrt{\frac{s}{D_R}} a \right) K_1 \left( \sqrt{\frac{s}{D_O}} a \right) \right]$$

where  $K_1(x) = -dK_0(x)/dx$  is the modified Bessel function of the second kind and of order 1.

Equations A28 together with the values of  $\alpha(s)$  and  $\beta(s)$  from eq A29, determine  $U_O(r,s)$  and  $U_R(r,s)$ , the Laplace transforms of the concentrations  $c_O(r,t)$ ,  $c_R(r,t)$ . From either of these expressions, together with eq A24, we obtain the Laplace transform,  $J(s)$ , of the current  $i(t)$ :

$$J(s) = \frac{i(t=0)}{\sqrt{s} \left[ \sqrt{s} + \lambda_O \sqrt{D_O} \left[ K_0 \left( \sqrt{\frac{s}{D_O}} a \right) / K_1 \left( \sqrt{\frac{s}{D_O}} a \right) \right] + \lambda_R \sqrt{D_R} \left[ K_0 \left( \sqrt{\frac{s}{D_R}} a \right) / K_1 \left( \sqrt{\frac{s}{D_R}} a \right) \right] \right]} \quad (A30)$$

Unfortunately the expressions for  $U_0, U_R$  and  $J$  cannot be inverted analytically to give  $c_0, c_R$  and  $i$ . A complete solution may be obtained, however, by numerical inversion of the Laplace transforms, following the method described by Papoulis<sup>13</sup>. We used this procedure for the specific cases discussed in the text. In addition, an approximate analytic solution has been derived. This is valid for times much shorter than the smallest of  $a^2/D_0, a^2/D_R, a/\lambda\sqrt{D_R}, a/\lambda\sqrt{D_0}$  (i.e., times sufficiently short that the diffusion distance is small in comparison with the radius of the electrode). The approximate short-time solution for the current,  $i(t)$ , will be sketched; short-time approximate solutions for the concentrations are found in much the same way, and only the final expressions will be given.

The approximate solution for  $i(t)$  is based on the fact that the behavior of  $i(t)$  for small  $t$  is determined by the behavior of  $J(s)$  for large  $s$ . For large  $s$  we have<sup>11</sup>

$$\frac{K_0(\sqrt{\frac{s}{D_0}} a)}{K_1(\sqrt{\frac{s}{D_0}} a)} \rightarrow 1 - \frac{\sqrt{D_0}}{2a\sqrt{s}} + \frac{3D_0}{8a^2s} + O(s^{-\frac{3}{2}})$$

so that, as  $s \rightarrow \infty$ ,

$$J(s) \sim \frac{i(t:0)}{s + \lambda\sqrt{s} - (\lambda_0 D_0 + \lambda_R D_R)/2a} \quad (A31)$$

On factoring the denominator of this equation, as in the above treatment of the spherical electrode, we obtain

$$\frac{i(t)}{i(t:0)} = \frac{1+\delta}{2\delta} \exp\left[\left(\frac{1+\delta}{2}\right)^2 \lambda^2 t\right] \operatorname{erfc}\left[\frac{1+\delta}{2} \lambda \sqrt{t}\right] - \frac{1-\delta}{2\delta} \exp\left[\left(\frac{1-\delta}{2}\right)^2 \lambda^2 t\right] \operatorname{erfc}\left[\frac{1-\delta}{2} \lambda \sqrt{t}\right] \quad (A32)$$

where

$$\delta = \left[1 + \frac{2(\lambda_R D_R + \lambda_0 D_0)}{a\lambda^2}\right]^{\frac{1}{2}}$$

This result may be simplified by introducing the approximation  $\exp x^2 \operatorname{erfc} x \approx 1 - 2\pi^{-\frac{1}{2}} x + x^2$ , valid for  $x \ll 1$ , to obtain

$$\frac{i(t)}{i(t=0)} \approx 1 - \frac{2}{\sqrt{\pi}} \lambda \sqrt{t} + \left( 1 + \frac{\lambda_R D_R + \lambda_O D_O}{2a\lambda^2} \right) \lambda^2 t \quad (\text{A33})$$

Similarly the concentrations at the electrode surface, for small  $t$ , are given by

$$c_R(a,t) \approx c_R^o - \frac{i(t=0)}{nF\sqrt{D_R}} \left[ \frac{2}{\sqrt{\pi}} \sqrt{t} - \left( 1 + \frac{\sqrt{D_R}}{2a\lambda} \right) \lambda t \right] \quad (\text{A34})$$

$$c_O(a,t) \approx c_O^o + \frac{i(t=0)}{nF\sqrt{D_O}} \left[ \frac{2}{\sqrt{\pi}} \sqrt{t} - \left( 1 + \frac{\sqrt{D_O}}{2a\lambda} \right) \lambda t \right] \quad (\text{A35})$$

For large cylindrical electrodes, such that  $a \gg (\lambda_R + \lambda_O)^{-1}$ , these equations reduce to the corresponding results for planar electrodes.

References

1. H. Gerischer, Z. Elektrochem. 54, 362 (1950).
2. R. Parsons, Trans. Faraday Soc. 47, 1332 (1951).
3. S. Barnartt, Electrochimica Acta 11, 1531 (1966).
4. H. Gerischer, Z. Elektrochem. 55, 98 (1951).
5. W. Vielstich and P. Delahay, J. Amer. Chem. Soc. 79, 1874 (1957).
6. P. Delahay, Advances Electrochemistry Electrochemical Eng. 1, 233 (1961).
7. P. Delahay, "Double layer and electrode kinetics", Interscience Publishers, New York (1965).
8. H. Gerischer and W. Vielstich, Z. physik. Chem. (N.F.) 3, 16 (1955).
9. H. Gerischer, Z. Elektrochem. 54, 366 (1950).
10. S. Barnartt, to be published.
11. H. S. Carslaw and J. C. Jaeger, "Conduction of heat in solids", 2nd ed. Clarendon Press, Oxford (1959).
12. S. Barnartt, J. Phy. Chem. 70, 412 (1966).
13. A. Papoulis, Quarterly Appl. Math. 14, 405 (1957).
14. I. Shain, K. J. Martin and J. W. Ross, J. Phys. Chem. 65, 259 (1961).
15. P. Delahay, "New Instrumental Methods in Electrochemistry", Interscience Publishers, New York, New York (1954).
16. A quantitative treatment of this decrease in precision with time was given recently by K. B. Oldham and R. A. Osteryoung, J. Electroanal. Chem. 11, 397 (1966). These authors also present a novel method of evaluating  $\lambda$  and  $i_{(t=0)}$  from current measurements in the intermediate-time range. Their method differs significantly from ours in that it involves current measurements from tangents drawn to the experimental current-time curve.

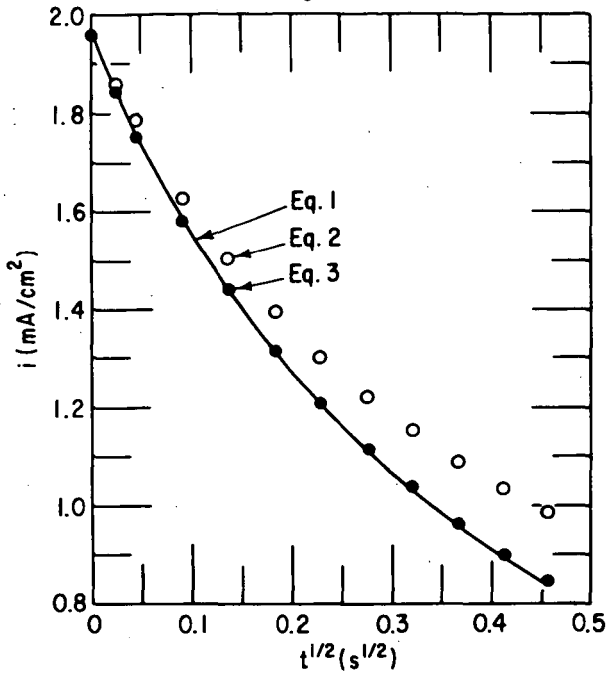


FIG. 1-- CALCULATED CURRENT-TIME RELATIONS, PLANE ELECTRODES:  
 — Eq. 1, ○ Eq. 2, ● Eq. 3.

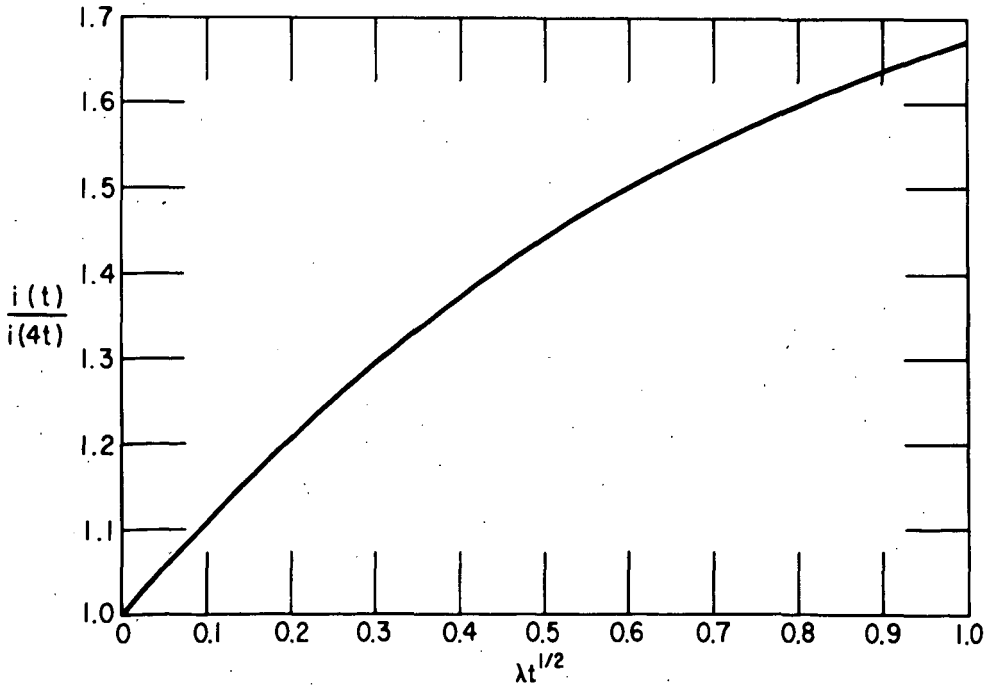


FIG. 2-- VARIATION OF CURRENT RATIO  $i(t)/i(4t)$  WITH  $\lambda t^{1/2}$ , PLANAR ELECTRODES.

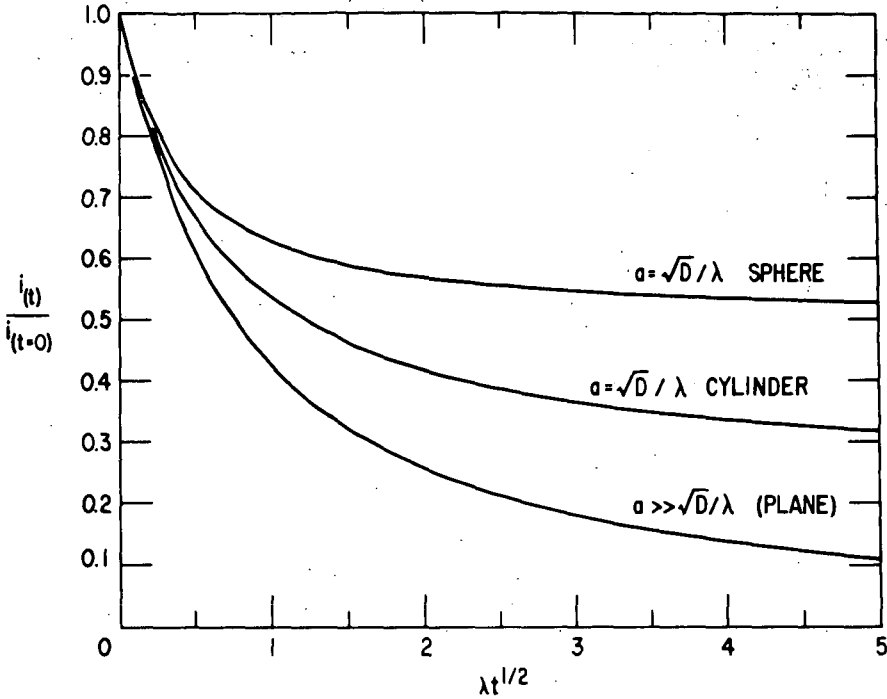


FIG. 3--CONSTANT-POTENTIAL CURRENT-TIME RELATIONS FOR SPHERICAL AND CYLINDRICAL ELECTRODES.

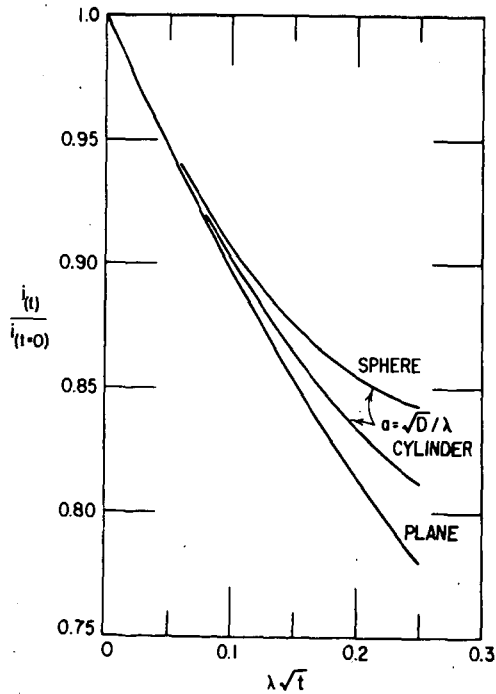


FIG. 4--CURRENT-TIME RELATIONS AT SHORT TIMES.

Generalized Theory of Electrode Kinetics at Constant Potential

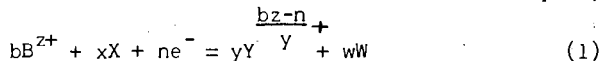
Charles A. Johnson and Sidney Barnartt

Fundamental Research Laboratory, U. S. Steel Corp., Monroeville, Pa.

The theory of irreversible electrode reactions at constant potential treats reactions under simultaneous control by charge-transfer and mass-transfer polarization.(1-5) It predicts the current-time curve following an abrupt change in electrode potential from the reversible potential to a new value which is maintained by use of a potentiostat. The treatment assumes that mass transfer occurs by diffusion only; experimentally this condition is closely approached by use of short electrolysis time, of unstirred solutions to minimize convection, and of large excess of supporting electrolyte in the solution to minimize migration of reacting ions in the applied field. Electrodes of planar geometry have been of greatest interest, (1-4) although cylindrical and spherical electrodes have also been treated.(4,5)

All of the previous theory has been limited to first-order charge-transfer mechanisms with the further restriction that the electrical work involved in the reaction occur only during the rate-determining step. The purpose of this paper is to extend the theory to higher-order mechanisms, with removal of the restriction on the electrical work involved. The treatment is for conditions of planar electrode geometry, mass transfer only by semi-infinite linear diffusion, and excess supporting electrolyte. Approximate solutions valid for small concentration changes are derived in closed form.

The general electrode reaction is formulated conventionally (6,7) as



The important reaction steps in the anodic direction are



where P and Q are intermediate states defining the rate-determining step, and v is the stoichiometric number. The total number of electrons (n/v) involved in the decomposition of one mole of the anodic activated complex ( $\ddagger A_a$ ) is placed in braces to indicate that the number of electrons used up in forming the intermediates P,  $\ddagger A_a$  or Q is not fixed. Electrical work done during formation of P from the cathodic reactants will be represented by p, and that done in formation of Q from the anodic reactants by q. The net anodic reaction rate at potential  $\epsilon$  (overpotential  $\eta$  positive) is expressed as current density by (8)

$$i = i_0 \left( \frac{\ddagger f}{f} \right) \cdot \exp \left[ \frac{(1-\beta)(p_r - p) + \beta(q_r - q)}{RT} \right] \cdot \left\{ \left( \frac{a_Y}{a_O} \right)^{y/v} \left( \frac{a_W}{a_O} \right)^{w/v} \cdot \exp(1-\beta) \frac{n}{v} \epsilon \eta - \left( \frac{a_B}{a_O} \right)^{b/v} \left( \frac{a_X}{a_O} \right)^{x/v} \cdot \exp(-\beta) \frac{n}{v} \epsilon \eta \right\} \quad (2)$$

Here  $i_0$  is the exchange current density,  $f^\ddagger$  the activity coefficient of the activated complex,  $\beta$  the transfer coefficient and  $\epsilon \equiv F/RT$ . The activity of a reactant, e.g. B, is designated  $a_B$  in the solution at the electrode surface and  $a_B^0$  in the bulk. Quantities  $f^\ddagger$ ,  $p$  and  $q$  refer to the reaction at the applied potential  $\mathcal{E}$  and may be time dependent, while the same quantities with subscript  $r$  refer to the reaction at the reversible electrode potential  $\mathcal{E}_r$ . At the reversible potential the exchange current density is given by

$$i_0 = i_{0,s} \cdot \left[ \frac{(a_B^0)^b (a_X^0)^x}{(a_Y^0)^y (a_W^0)^w} \right]^{(1-\beta)/\nu} \cdot \exp \left[ \frac{(1-\beta)(p_s - p_r) + \beta(q_s - q_r)}{RT} \right] \quad (3)$$

where  $i_{0,s}$  is the exchange current density at the standard electrode; (7) quantities  $p_s$  and  $q_s$  also refer to the standard electrode. Equations (2) and (3) have general applicability with one limitation, namely that the activated complex  $\ddagger A$  must contain the reactants B and X in the ratio  $b/x$ , but this limitation is easily eliminated when desired without introduction of any new principle. (6,7)

It is evident from Eq. (3) that the reaction order, as conventionally determined from  $i_0$ , is not a simple quantity. (7) Thus for substance B:

$$\left( \frac{\partial \ln i_0}{\partial \ln a_B^0} \right)_{T, a_X, a_Y, a_W} = \frac{b(1-\beta)}{\nu} - \frac{1}{RT} \left( \frac{\partial (p_r - \beta p_r + \beta q_r)}{\partial \ln a_B} \right)_{T, a_X, a_Y, a_W} \quad (4)$$

As a general rule, therefore, complex electrode reactions may not be described as being of first order, second order, etc., in the usual manner of chemical kinetics. It is expedient for the theory of combined charge- and mass-transfer polarization to describe the reaction by a pseudoorder, which we define here as simply the exponent of the activity ratio in the general rate equation (Eq. 2). Thus the pseudoorder of the reaction is  $y/\nu$  with respect to Y,  $w/\nu$  with respect to W, etc., if each of the reacting substances undergoes changes in concentration during the reaction. If one of the substances involved, e.g. W, exhibits minute fractional changes in concentration during the entire reaction period, the term  $(a_W/a_W^0)^{w/\nu}$  becomes unity in Eq. 2 and then the reaction becomes effectively zero pseudoorder in W.

For simplicity we will formulate the electrolyte to contain one of the cathodic reactants, X, and one of the anodic reactants, W, in sufficiently high concentration that the ratios  $a_X/a_X^0$  and  $a_W/a_W^0$  remain essentially unity. In addition, we will consider only short reaction times such that all concentration changes at the electrode surface remain small. From the latter condition plus the use of excess supporting electrolyte, it may be assumed that  $f^\ddagger/f^\ddagger$  is replaceable by unity and that concentration ratios may be substituted for the corresponding activity ratios with negligible effect. Then Eq. 2 converts to

$$i = i_0 \exp \left[ \frac{(1-\beta)(p_r - p) + \beta(q_r - q)}{RT} \right] \cdot \left\{ \left( \frac{c_Y}{c_Y^0} \right)^{y/\nu} \exp(1-\beta) \frac{n}{\nu} \epsilon \eta - \left( \frac{c_B}{c_B^0} \right)^{b/\nu} \exp(-\beta) \frac{n}{\nu} \epsilon \eta \right\} \quad (5)$$

It would be desirable to obtain analytical solutions of the diffusion problem for a current of the form given in Eq. 5 but one cannot apply the method of Laplace transforms. An alternative approach is to obtain an approximate solution by linearizing Eq. 5 with respect to concentrations, so that the Laplace transform

method may be utilized. The latter approach will be developed in this paper. For the sake of brevity we restrict our discussion to cases for which the electrical work occurs only in the rate-determining step, so that  $p_1 = p = q_1 = q = 0$ . (In general, provided only that  $p$  and  $q$  are continuous functions of the concentrations, Eq. 5 can always be linearized with respect to concentrations. The form of the approximate solution does not change; however, the coefficients involved become somewhat more complicated.)

It is convenient to introduce the fractional changes in concentration at the electrode surface:

$$u_Y \equiv (c_Y - c_Y^0)/c_Y^0 \quad u_B = (c_B - c_B^0)/c_B^0 \quad (6)$$

Then, for small concentration changes,

$$\left(\frac{c_Y}{c_Y^0}\right)^{y/v} = 1 + \left(\frac{y}{v}\right)u_Y \quad \left(\frac{c_B}{c_B^0}\right)^{b/v} = 1 + \left(\frac{b}{v}\right)u_B$$

and, in the present case ( $p=q=0$ ), Eq. 5 becomes

$$i = i_{(t=0)} + U_Y u_Y - U_B u_B \quad (7)$$

with

$$i_{(t=0)} = i_0 \left[ \exp(1-\beta) \frac{n}{v} \epsilon \eta - \exp(-\beta \frac{n}{v} \epsilon \eta) \right] \quad (8)$$

$$i_0 = i_{0,s} \left[ (a_B^0)^b (a_X^0)^x \right]^{(1-\beta)/v} \cdot \left[ (a_Y^0)^y (a_W^0)^w \right]^{\beta/v}$$

and

$$U_B = \frac{b}{v} i_0 \exp(-\beta \frac{n}{v} \epsilon \eta) \quad ; \quad U_Y = \frac{y}{v} i_0 \exp(1-\beta) \frac{n}{v} \epsilon \eta \quad (9)$$

The diffusion problem: We consider the semi-infinite linear diffusion of two species, B and Y, with concentrations  $c_B(x,t)$ ,  $c_Y(x,t)$  coupled together at the electrode surface  $x=0$  by a general current-concentration relationship like that of Eq. 5.

$$i(t) = f(c_B(0,t), c_Y(0,t)) \quad (10)$$

The diffusion equations for  $c_B$  and  $c_Y$  are

$$D_B \frac{\partial^2 c_B}{\partial x^2} = \frac{\partial c_B}{\partial t} \quad ; \quad D_Y \frac{\partial^2 c_Y}{\partial x^2} = \frac{\partial c_Y}{\partial t} \quad (11)$$

where  $D_B$  and  $D_Y$  are the diffusion coefficients of substances B and Y. The initial conditions are  $c_B = c_B^0$  and  $c_Y = c_Y^0$  at  $t=0$  for all  $x$ . The boundary conditions are

$$(1) \quad c_B \rightarrow c_B^0 \quad \text{and} \quad c_Y \rightarrow c_Y^0 \quad \text{as} \quad x \rightarrow \infty \quad \text{for all } t \quad (12)$$

$$(2) \quad i(t) = \frac{nF}{v} D_Y \left( \frac{\partial c_Y}{\partial x} \right)_{x=0} = - \frac{nF}{b} D_B \left( \frac{\partial c_B}{\partial x} \right)_{x=0} = f[c_B(0,t), c_Y(0,t)] \quad (13)$$

When the current,  $i(t)$ , contains non-linear terms in the concentrations the complete solution to the problem of Eq. 11-13 cannot be obtained by standard analytic techniques. However, a useful relationship, valid for any functional

dependence of  $i(t)$  upon the concentrations, can be found by applying the Laplace transform technique to Eq. 11-13 as they stand.

To obtain this relationship we require only that  $i(t)$  be some arbitrary (and, indeed, at this point unknown) function of the time whose Laplace transform exists. Then a straightforward application of the Laplace transform technique yields the relation

$$\frac{c_B(x=0,t) - c_B^0}{c_Y(x=0,t) - c_Y^0} = \frac{b}{y} \sqrt{\frac{D_Y}{D_B}} \quad (14)$$

The principal utility of Eq. 14 is that it permits the diffusion problem to be solved in terms of just one of the components B and Y. In the actual expression for the current in terms of concentrations at the electrode surface (see Eq. 10), we eliminate  $c_B(x=0,t)$  by using Eq. 14 and are left with a diffusion problem for component Y in which component B plays no part whatsoever.

However, although Eq. 14 simplifies the diffusion problem to one involving the diffusion of only one component (Y, say), it does not remove the generally non-linear dependence of current on concentration, and recourse must be had either to numerical solutions or to an approximate solution based on the linearized form of Eq. 7.

In this linearized form, and with component B eliminated via Eq. 14, the diffusion problem is expressed in terms of the fractional change in concentration  $u_Y(x,t)$  (Eq. 6) as

$$D_Y \frac{\partial^2 u_Y}{\partial x^2} = \frac{\partial u_Y}{\partial t} \quad (15)$$

with

$$u_Y(x,t=0) = 0, \quad u_Y(x \rightarrow \infty, t) \rightarrow 0 \quad (16)$$

and the conditions on the current:

$$i(t) = \frac{n}{y} F c_Y^0 D_Y \left( \frac{\partial u_Y}{\partial x} \right)_{x=0} \quad (17)$$

$$i(t) = i_{(t=0)} + u_Y(x=0,t) \left[ U_Y + \left( \frac{b c_Y^0 \sqrt{D_Y}}{y c_B^0 \sqrt{D_B}} \right) U_B \right]$$

The solution of Eq. 15-17 is found by Laplace transform techniques to be

$$i = i_{(t=0)} \exp(\lambda^2 t) \operatorname{erfc}(\lambda \sqrt{t}) \quad (18)$$

$$c_Y = c_Y^0 - i_{(t=0)} \left[ \frac{n}{y} F \lambda \sqrt{D_Y} \right]^{-1} \cdot [1 - \exp(\lambda^2 t) \operatorname{erfc}(\lambda \sqrt{t})] \quad (19)$$

$$c_B = c_B^0 + i_{(t=0)} \left[ \frac{n}{b} F \lambda \sqrt{D_B} \right]^{-1} \cdot [1 - \exp(\lambda^2 t) \operatorname{erfc}(\lambda \sqrt{t})] \quad (20)$$

where

$$\lambda = \frac{U_Y}{(n/y) F c_Y^0 \sqrt{D_Y}} + \frac{U_B}{(n/b) F c_B^0 \sqrt{D_B}} \quad (21)$$

which, on substituting for  $U_Y$  and  $U_B$  from Eq. 9, becomes

$$\lambda = \left(\frac{y}{v_n}\right)^2 \frac{i_0 \exp(1-\beta) \frac{n}{v} \epsilon \eta}{F c_Y^0 \sqrt{D_Y}} + \left(\frac{b}{v_n}\right)^2 \frac{i_0 \exp(-\beta) \frac{n}{v} \epsilon \eta}{F c_B^0 \sqrt{D_B}} \quad (22)$$

This equation and Eq. 18-20 reduce to the corresponding equations for first-order reactions (2,4) when  $b=y=v=1$ .

Thus the approximate solution for charge-transfer reactions of higher order has the same form as the exact solution for simple first-order reactions.(2,4) The major difference lies in the quantity  $\lambda$ . According to Eq. 18 the larger the value of  $\lambda$  the more rapidly the relative current  $i/i(t=0)$  decreases with time. The evaluation of the quantities  $\lambda$  and  $i(t=0)$  from an experimental current-time curve can be carried out using methods previously developed for simple first-order reactions.(2,4,9) The charge-transfer parameters  $i_0$ ,  $\beta$  and  $v$  can then be found either from measurement of the anodic or cathodic Tafel line in the case of slow reactions or from measurements of  $i(t=0)$  for varying activity of B or Y in the case of faster reactions.

Validity of approximate solution: The approximate solution given by Eq. 18-21 is valid only for small changes in concentration; its utility is chiefly determined by the range over which it gives the true current to within an acceptable accuracy. In order to test this we have developed exact numerical solutions using the Schmidt method,(10) Some of these exact current-time curves for net anodic reactions are presented in Fig. 1: curve I refers to a simple first-order reaction for which  $b/v = y/v = n/v = 1$ ; curve II refers to a reaction second pseudoorder in the anodic reactant Y with  $y/v = n/v = 2$  and  $b/v = 1$ ; curve III refers to a reaction third pseudoorder in Y, with  $y/v = n/v = 3$ . The set of numerical data used here is the same as in the previous paper:(4)  $i_0 = 5 \times 10^{-3}$  A/cm<sup>2</sup> at 25°C,  $\beta = 0.5$ ,  $\eta = 0.0100V$ ;  $c_Y^0 = 10^{-5}$  and  $c_B^0 = 5 \times 10^{-5}$  mole/cm<sup>3</sup>;  $D_Y = 10^{-5}$  and  $D_B = 2 \times 10^{-5}$  cm<sup>2</sup>/s. Fig. 1 shows that, as the reaction pseudoorder in Y is increased, the current falls more rapidly with time.

The approximate and exact solutions for reactions of second pseudoorder in Y are shown in Fig. 2 for various values of the transfer coefficient  $\beta$ ; except for  $\beta$  the set of numerical data employed is the basic set used for Fig. 1. It is seen that in every case the approximate solution for the current decreases more rapidly with time than does the true current.

We have chosen to designate the range in  $i/i(t=0)$  over which Eq. 18 gives satisfactory agreement with the true current by the point at which the approximate solution deviates by 5% from the true current. These points are indicated by vertical bars in Fig. 2; the approximate solution is acceptably accurate down to  $i/i(t=0) \approx 0.45$ , independent of the value of  $\beta$ . As Oldham and Osteryoung (9) have emphasized, the reaction kinetics are primarily diffusion controlled below  $i/i(t=0) \approx 0.5$ . Thus, in this case, the approximate solution (eq. 18) is acceptably accurate over the entire range in  $i/i(t=0)$  from which information about the charge-transfer parameters can be obtained.

For a reaction third pseudoorder in the anodic reactant Y the approximate and exact solutions are compared in Fig. 3. The numerical data are the basic set used for Fig. 1, with  $\beta = 0.5$  and  $y = 3$ . The range in  $i/i(t=0)$  over which acceptable agreement is found is shorter than that for the similar second pseudoorder reaction: the point of 5% deviation occurs at  $i/i(t=0) \approx 0.6$ .

The agreement to be expected for somewhat slower reactions is shown in Fig. 4. Here the basic data set was varied by increasing the anodic overpotential to  $\eta = 0.1$  V and decreasing the exchange current density to  $i_0 = 10^{-5}$  A/cm<sup>2</sup>. The limits of acceptable agreement are indicated by vertical bars. In this case the point of 5% deviation occurs at  $i/i_0(t=0) \approx 0.61$  and is again essentially independent of the value of the transfer coefficient  $\beta$ .

Thus far we have examined only net anodic reactions in which the higher pseudoorder component was the anodic reactant (Y). In these cases, because of the disparity of the exponential factors in Eq. 5, the current is predominantly controlled by the higher pseudoorder component, this predominance becoming greater the greater the overpotential. This is the reason for the poorer agreement shown in Fig. 4 ( $\eta = 0.1$ V) than in Fig. 2 ( $\eta = 0.01$ V).

The agreement between the approximate and exact numerical solutions improves dramatically when the controlling reactant is the first order reactant (for example, a net anodic reaction in which the higher pseudoorder component is the cathodic reactant (B)). This is illustrated in the anodic current-time curves of Fig. 5, for which the values of temperature, diffusivities and initial concentrations are those of the basic data set. Curve II, for which the cathodic reactant (B) is second pseudoorder while the anodic reactant (Y) is first order, shows no measurable deviation between the approximate and exact solutions down to  $i/i_0(t=0) < 0.2$ .

These examples suggest some general rules about the range of validity of the approximate solution:

- (1) The range of validity decreases when the pseudoorder of either component is increased.
- (2) The range of validity is extended greatly by ensuring that the current is predominantly controlled by the component of lower pseudoorder. If, for example, the higher order component is the cathodic component then a net anodic reaction is desirable.
- (3) If rule (2) has been complied with there is an advantage in working at the highest feasible overpotentials. If not, the advantage is obtained by working at the lowest feasible overpotentials.
- (4) The range of validity is insensitive to the value of the transfer coefficient  $\beta$ .

#### References:

1. P. Delahay, "New Instrumental Methods in Electrochemistry", Interscience Publishers, New York, N.Y. (1954).
2. H. Gerischer and W. Vielstich, Z. physik. Chem., N.F. 3, 16 (1955).
3. P. Delahay, Advances Electrochem. Electrochemical Eng. 1, 233 (1961).
4. C. A. Johnson and S. Barnartt, to be published.
5. I. Shain, K. J. Martin and J. W. Ross, J. Phys. Chem. 65, 259 (1961).
6. R. Parsons, Trans. Faraday Soc. 47, 1332 (1951).
7. S. Barnartt, J. Phys. Chem. 70, 412 (1966).
9. K. B. Oldham and R. A. Osteryoung, J. Electroanal. Chem. 11, 397 (1966).
10. J. C. Jaeger, Proc. Cambridge Phil. Soc. 46, 634 (1950).
8. S. Barnartt, Electrochimica Acta 11, 1531 (1966).

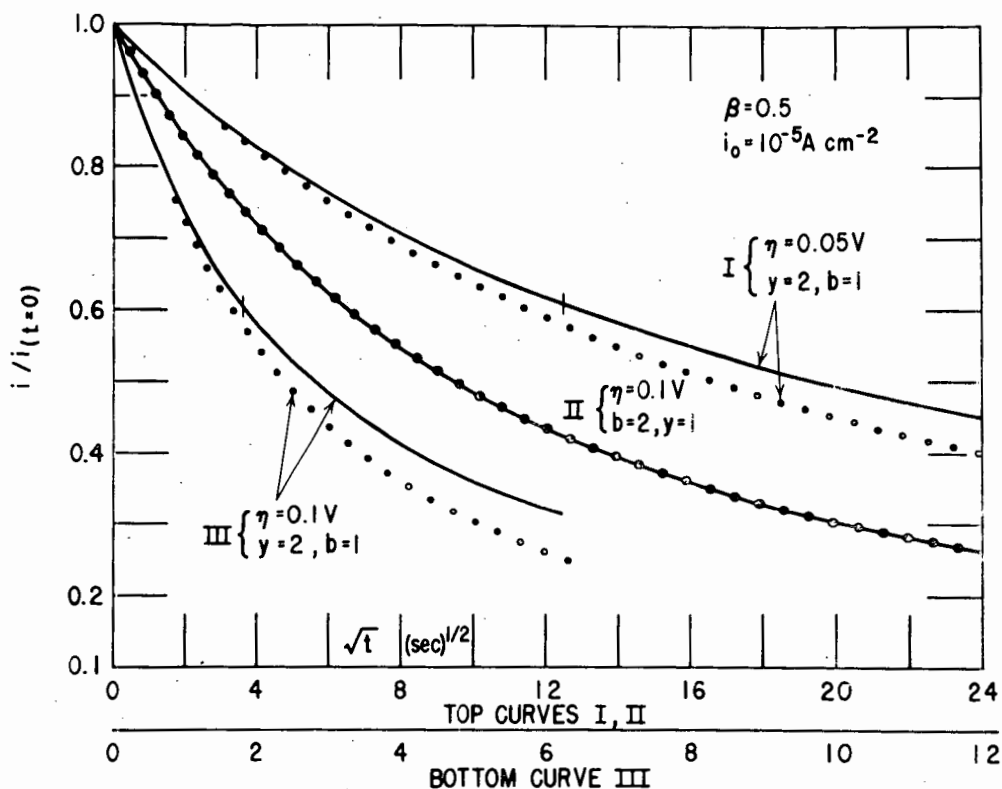


FIG. 5--ANODIC CURRENT-TIME CURVES FOR REACTIONS OF PSEUDOORDER TWO WITH RESPECT TO ANODIC REACTANT Y (CURVES I, III) OR CATHODIC REACTANT B (CURVE II). SOLID CURVE--EXACT NUMERICAL SOLUTION. DOTTED CURVE--SOLUTION OF LINEARIZED PROBLEM.

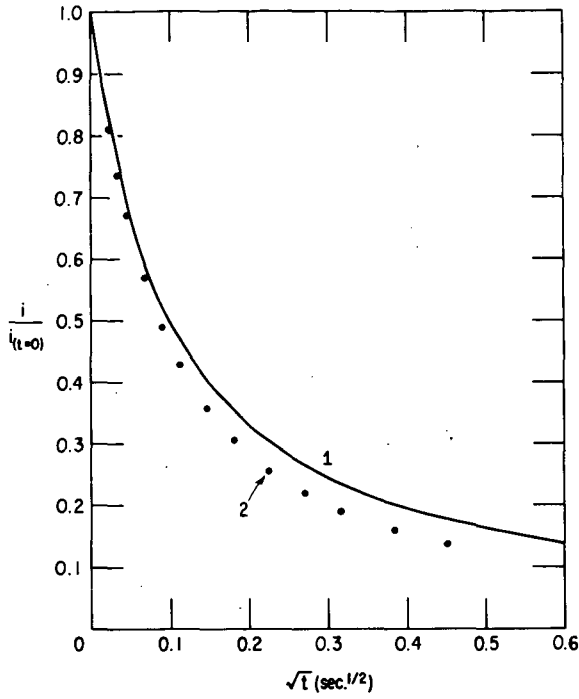


FIG. 3 CURRENT-TIME BEHAVIOR FOR REACTION OF PSEUDOORDER THREE WITH RESPECT TO Y. CURVE 1-EXACT NUMERICAL SOLUTION; 2-SOLUTION OF LINEARIZED PROBLEM.

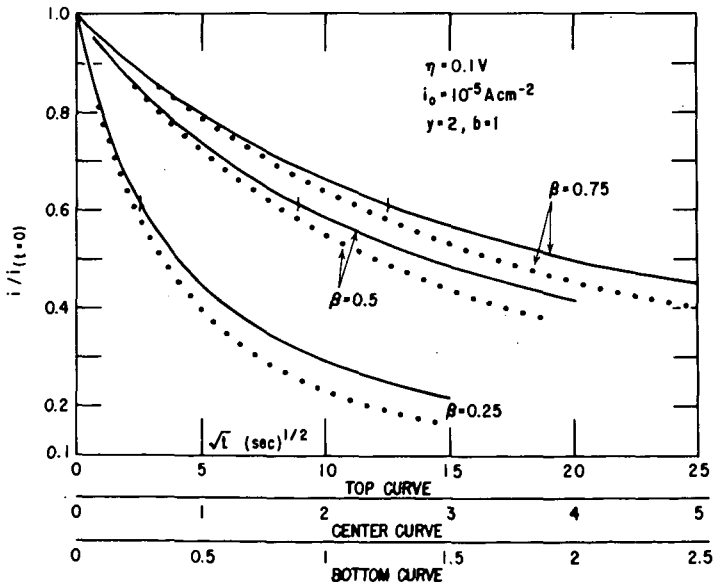


FIG. 4--EFFECT OF  $\beta$  ON ANODIC CURRENT-TIME CURVES FOR REACTION OF PSEUDOORDER TWO WITH RESPECT TO ANODIC REACTANT Y. SOLID CURVES--EXACT NUMERICAL SOLUTION. DOTTED CURVES--SOLUTION OF LINEARIZED PROBLEM.

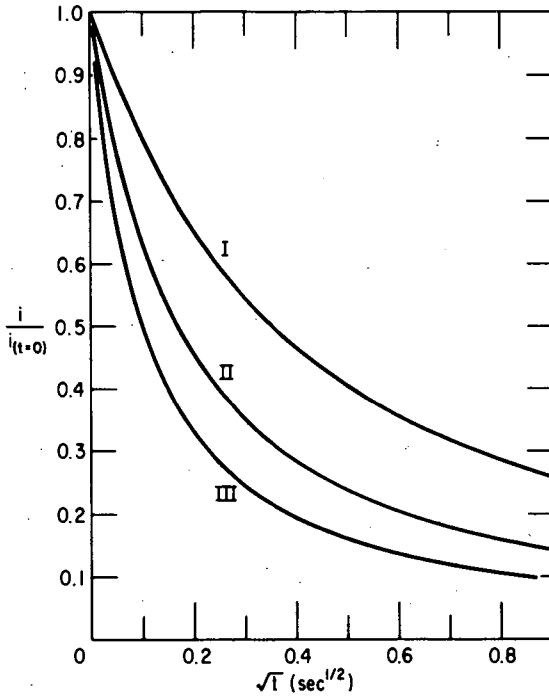


FIG. 1 EXACT CURRENT-TIME BEHAVIOR FOR SELECTED ELECTRODE REACTIONS OF PSEUDOORDER ONE (CURVE I), TWO (II) OR THREE (III) WITH RESPECT TO SUBSTANCE Y.

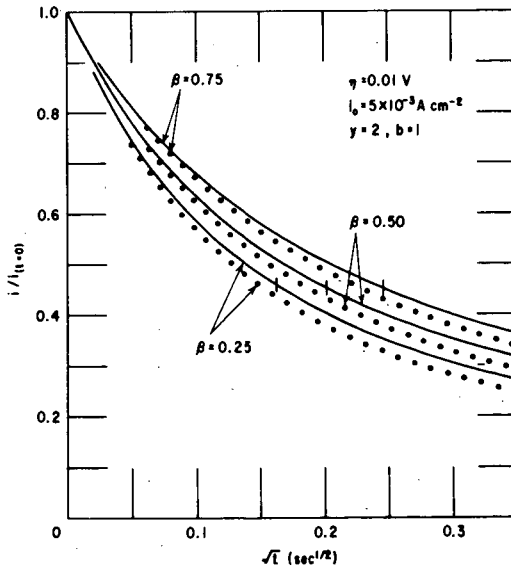


FIG. 2--EFFECT OF  $\beta$  ON ANODIC CURRENT-TIME CURVES FOR REACTION OF PSEUDOORDER TWO WITH RESPECT TO ANODIC REACTANT Y. SOLID CURVES--EXACT NUMERICAL SOLUTION. DOTTED CURVES--SOLUTION OF LINEARIZED PROBLEM.

## Derivative Chronopotentiometry of Multicomponent Systems

(Abstract)

Robert H. Gibson, University of North Carolina at Charlotte,  
and Peter E. Sturrock, Georgia Institute of Technology

In a previous paper<sup>1</sup>, derivative chronopotentiometry was applied to systems of only one electroactive species. In this paper the method is extended to systems with several electroactive species.

Using the Response Function Additivity Principle of Murray and Reilley<sup>2</sup>, the bulk concentration of the  $j$ -th component is given by equation (1).

$$C_{o,j}^* = \frac{2i_o}{n_j F (\pi D_{o,j})^{1/2}} \left[ \left( \sum_{m=1}^j \tau_m \right)^{1/2} - \left( \sum_{m=1}^{j-1} \tau_m \right)^{1/2} \right] \quad (1)$$

During the  $j$ -th step of the chronopotentiogram  $\left( \sum_{m=1}^j \tau_m > t > \sum_{m=1}^{j-1} \tau_m \right)$

$$D_{o,j}^{1/2} [C_{o,j}^* - C_{o,j}(o,t)] = D_{r,j}^{1/2} C_{r,j}(o,t) = \frac{2i_o}{n_j F \pi^{1/2}} \left[ t^{1/2} - \left( \sum_{m=1}^{j-1} \tau_m \right)^{1/2} \right] \quad (2)$$

Solving equations (1) and (2) for  $C_{o,j}(o,t)$  and  $C_{r,j}(o,t)$

$$C_{o,j}(o,t) = \frac{2i_o}{n_j F (\pi D_{o,j})^{1/2}} \left[ \left( \sum_{m=1}^j \tau_m \right)^{1/2} - t^{1/2} \right] \quad (3)$$

$$C_{r,j}(o,t) = \frac{2i_o}{n_j F (\pi D_{r,j})^{1/2}} \left[ t^{1/2} - \left( \sum_{m=1}^{j-1} \tau_m \right)^{1/2} \right] \quad (4)$$

If the  $j$ -th component is reversible, the potential time relationship is obtained by substituting equations (3) and (4) into the Nernst equation.

$$E = E_{1/2} + \frac{RT}{n_j F} \ln \frac{\left( \sum_{m=1}^j \tau_m \right)^{1/2} - t^{1/2}}{\left[ t^{1/2} - \left( \sum_{m=1}^{j-1} \tau_m \right)^{1/2} \right]} \quad (5)$$

Differentiating equation (5)

$$\frac{dE}{dt} = \frac{-RT}{2n_j F t^{1/2}} \left[ \frac{1}{\left( \sum_{m=1}^j \tau_m \right)^{1/2} - t^{1/2}} + \frac{1}{t^{1/2} - \left( \sum_{m=1}^{j-1} \tau_m \right)^{1/2}} \right] \quad (6)$$

For the case,  $j=1$ , equations (5) and (6) reduce to those for a single component system<sup>3</sup>. The minimum of the derivative function is evaluated by taking the second derivative and equating it to zero.

$$n_j \left( \sum_{m=1}^{j-1} \tau_m \right) \left( \frac{dE}{dt} \right)_{\min} = \frac{-4.5 RT/F}{a+1 + (a^2-a+1)^{1/2}} \left[ \frac{1}{2a-1-(a^2-a+1)^{1/2}} + \frac{1}{a+(a^2-a+1)^{1/2}-2} \right] \quad (7)$$

where

$$a = \frac{\left( \sum_{m=1}^j \tau_m \right)^{1/2}}{\left( \sum_{m=1}^{j-1} \tau_m \right)^{1/2}} = \frac{\sum_{m=1}^j n_m C_{o,m}^* D_{o,m}^{1/2}}{\sum_{m=1}^{j-1} n_m C_{o,m}^* D_{o,m}^{1/2}} \approx \frac{\sum_{m=1}^j n_m C_{o,m}^*}{\sum_{m=1}^{j-1} n_m C_{o,m}^*} \quad (8)$$

A digital computer was programmed to solve the right side of equation (7) for specified values of "a" and to print out the results in tabular form. All of the terms on the left side of equation (7) are known or obtainable by experiment. Then the corresponding value of "a" can be read from the table.

Combining equations (1) and (8),

$$C_{o,j}^* = \frac{2i_o (a-1)}{n_j F (\pi D_{o,j})^{1/2}} \left( \sum_{m=1}^{j-1} \tau_m \right)^{1/2} \quad (9)$$

Equation (9) may be used to obtain  $C_{o,j}^*$  directly, provided the current density and diffusion coefficient are known with sufficient accuracy. If such is not the case, graphical, standard-addition techniques can be employed.

These standard-addition techniques are based on the fact that a plot of

$$C_{o,j}^{*} \text{ versus } (a-1) \left( \sum_{m=1}^{j-1} \tau_m \right)^{1/2}$$

is a straight line through the origin. Thus such a plot can be constructed with  $C_{o,j}^{*}$  added, and then the plot can be shifted along the concentration  $C_{o,j}^{*}$  axis until the extrapolated line intersects the origin. The concentration, of the point for zero addition, then can be read off of the plot.

This procedure may be simplified if the addition is carried out without dilution of the species more reducible than the  $j$ -th species. For example, the sample may be split into two equal portions, the addition made to one portion and then both solutions diluted to the same total volume. Derivative chronopotentiograms are then performed on various mixtures of the two solutions. In this way  $\sum_{m=1}^{j-1} \tau_m$  is kept constant and a plot of  $C_{o,j}^{*}$  versus  $(a-1)$  is linear.

The preceding derivations do not consider the effect of the double-layer charging current. For single component systems, derivative chronopotentiometry is relatively insensitive to double-layer charging<sup>3</sup> and semiempirical correction techniques have proved effective<sup>1</sup>. However, the situation appears to be more serious for multicomponent systems. Work is continuing in these laboratories in an attempt to devise a correction technique similar to that devised for single component systems. An alternative approach is available, however, since an instrumental method for charging current correction has recently been reported<sup>4</sup>.

#### References

1. Peter E. Sturrock, Gregg Privett, and Anderson R. Tarpley, J. Electroanal. Chem., in press (1967).
2. Royce W. Murray and Charles N. Reilley, J. Electroanal. Chem., 3, 182 (1962).
3. Dennis G. Peters and Stanley L. Burden, Anal. Chem., 38, 530 (1966).
4. W. D. Shults, F. E. Haga, T. R. Mueller, and H. C. Jones, Anal. Chem., 37, 1415 (1965).

Applications of Charge-Step Chronocoulometry

Fred C. Anson

Gates and Crellin Laboratories of Chemistry, California  
Institute of Technology, Pasadena, California 91109

A preliminary description of the technique of charge-step chronocoulometry has appeared (1). The technique consists of very rapid (0.1 to

(1) F. C. Anson, *Anal. Chem.*, **38**, 1924 (1966).

10  $\mu$  seconds) injection of rather large amounts of charge (5-50  $\mu$ coulombs/cm<sup>2</sup>) into an electrode and observing oscilloscopically the resulting open circuit potential-time transient. The potential-time transient are then converted into the corresponding charge-time transient by means of the appropriate charge-potential data so that the time variation of the charge on the electrode is obtained.

If the experiment is performed in the presence of one half of a redox couple, e.g. cadmium ion in a sodium nitrate supporting electrolyte with a mercury electrode, and the charge injected is chosen so that the electrode potential is well out on the diffusion plateau of the corresponding polarogram the rate at which charge is removed from the electrode at open circuit by the resulting faradaic reaction, e.g.  $\text{Cd} + 2\text{e}^- = \text{Cd}(\text{Hg})$ , will be the diffusion limited rate of transfer of cadmium ion to the electrode surface. Thus the open circuit rate of loss of charge on the electrode will be entirely analogous to the rate of charge accumulation observed in the usual potential-step chronocoulometric experiments (2-5) which are, of course, closed circuit

(2) J. H. Christie, G. Lauer, R. A. Osteryoung and F. C. Anson, *Anal. Chem.*, **36**, 975 (1963).

(3) J. H. Christie, G. Lauer and R. A. Osteryoung, *J. Electroanal. Chem.*, **7**, 60 (1964).

(4) F. C. Anson, *Anal. Chem.*, **36**, 932 (1964).

(5) *Ibid*, **38**, 54 (1966).

experiments with the electrolysis cell under the control of a potentiostat. Thus, the equation for the charge-time behavior in charge-step chronocoulometry is

$$Q = Q^0 + Q_{inj.} - 2nFAC\left(\frac{Dt}{\pi}\right)^{\frac{1}{2}} \quad (1)$$

where  $Q^0$  is the initial charge on the electrode,  $Q_{inj.}$  is the charge injected,  $F$  is the Faraday,  $n$  is the number of electrons involved in the electrode reaction,  $A$  is the electrode area,  $C$  is the bulk concentration of the reactant,  $D$  is its diffusion coefficient, and  $t$  is the time since charge injection. A plot of  $Q - Q^0$  versus the square root of time is linear with an intercept at  $t = 0$  corresponding to the injected charge.

The advantages of the open circuit, charge-step method over the closed circuit, potential-step method are these: 1. All problems associated with the resistance in the cell for which the potentiostat is unable to compensate are avoided. In non-aqueous solvents or aqueous solutions having concentrations of supporting electrolyte less than about 0.2 M, where these problems are the most severe, the charge-step method or some other open circuit technique would appear to be the method of choice. 2. Because it is possible to inject charge into an electrode very much faster than its potential can be stepped and held with presently available potentiostats the charge-step method permits experiments to be conducted on much shorter time scales than is true with potential-step techniques so that information about faster electrode processes can be obtained.

Applications of the charge-step technique have been made to the study of reactant adsorption (1, 6) the kinetics of electrode reactions (7), and

---

(6) F. C. Anson and R. A. Osteryoung, unpublished experiments.

(7) F. C. Anson, unpublished experiments.

---

the rate of establishment of concentration equilibrium just outside the diffuse double layer when it is abruptly enlarged or diminished (7). In the case of reactant adsorption the equation for the charge time behavior becomes

$$Q - Q^0 = Q_{inj} - 2nFAC \left(\frac{Dt}{\pi}\right)^{\frac{1}{2}} - nFT \quad (2)$$

where  $\Gamma$  is the amount of adsorbed reactant in moles/cm<sup>2</sup> and the other symbols are the same as in equation 1. In this case the difference between the intercept of a  $Q - Q^0$  versus  $t^{\frac{1}{2}}$  and the amount of injected charge,  $Q_{inj}$ , gives the amount of reactant adsorbed. An attractive feature of this method is the ability to allow the ionic strength of the solution to become quite low. In a previous study of cadmium adsorption from sodium thiocyanate solutions by potential-step chronocoulometry (8) sodium nitrate was also present "to keep the ionic

---

(8) F. C. Anson, J. H. Christie, and R. A. Osteryoung, *J. Electroanal. Chem.*, **13**, 000 (1967).

---

strength constant at 1.0", but also because potential-step chronocoulometry may not be safely applied to solutions having ionic strengths below about 0.2. Charge-step chronocoulometry can easily be employed down to ionic strengths of slightly below 0.01 and it would be of considerable interest to compare the values obtained for cadmium adsorption in the presence and absence of nitrate.

When relatively large quantities of charge are injected into an electrode in dilute solutions of electrolytes significant changes in the ionic concentrations just outside the diffuse double layer can occur which alter the resulting potential-time (and charge-time) transients. Due allowance for such perturbations can be made (9) and are essential in applications of charge-

---

(9) F. C. Anson, experiments to be published.

---

step chronocoulometry to dilute solutions.

ELECTROCHEMICAL STUDIES OF THE RATE OF CHEMICAL REACTIONS  
COUPLED TO CHARGE TRANSFER REACTIONS

John R. Kuempel and Ward B. Schaap

Department of Chemistry  
Indiana University, Bloomington, Indiana

The rates of the reactions of cadmium ion with EDTA species in solutions containing excess calcium ion are being studied using the electrochemical method known as "cyclic voltammetry" or "cyclic stationary electrode polarography" (1). Cadmium ions are introduced into calcium-EDTA solutions by oxidizing a cadmium amalgam by application of a linear voltage scan in the anodic direction. The generated cadmium ions then react with the EDTA species at a rate dependent upon the concentrations of the reactants to form a difficultly and irreversibly reduced complex. Before this complexation reaction is complete, the unreacted cadmium ions may be quickly reduced back into the amalgam by reversing the direction of the voltage scan. The amount of cadmium ion that reacts with the EDTA species is determined by comparing the cathodic faradaic current with the anodic current. The rate of the repetitive anodic and cathodic scans (cycles/sec) establishes a time base for the experiment and makes it possible to calculate pseudo first-order rate constants from the electrochemical data. The rate processes being studied have half-lives in the range of 10 to 1000 milliseconds.

In order to calculate second-order rate constants from the electrochemically determined pseudo first-order rate constants, it is necessary to consider the equilibrium process in solution. Procedures were devised to determine the formation constants and to calculate the activities of all the EDTA species present in solution under the conditions of the experiment. These methods are similar to the methods originally developed by Schwarzenbach (2) in basic approach, but are more precise due to computerized methods of data processing now available. Equations are derived for the acid-base titration curves of the parent acid EDTA in the presence of excess calcium ion and potassium nitrate. Simultaneous equations are then solved by the computer using the data from the pH titration curve to calculate the various equilibrium constants. Previously unreported species were detected and their formation constants determined.

The overall problem can be divided into two parts: (1) The electrochemical measurement of the pseudo first-order rate constants. (This involves development of the technique and methodology and the design and construction of the electronic equipment and electrochemical cells.) (2) The potentiometric measurement of the equilibrium constants needed to compute the appropriate second-order rate constants from the electrochemically measured pseudo first-order rate constants. These two parts of the problem will be discussed separately.

The Electrochemical Experiment

The diffusion equations applicable to a reversible electrochemical reaction in which the product of that reaction is deactivated by a further irreversible reaction with a substance in solution have been derived for many of the electrochemical techniques. The theoretical treatment of this type of system for the cyclic stationary-electrode polarographic method has been published by Shain and co-workers. (1)

In the present work, the experiment does not correspond exactly to the model Shain used in his theoretical treatment. The electroactive species is

present initially in its reduced form so that the first scan is anodic and performs an oxidation rather than a reduction as described by Shain. During the initial anodic scan, the cadmium amalgam is oxidized into a calcium-EDTA solution and the cadmium ion so produced undergoes a spontaneous reaction with the EDTA species to form a species which is not electroactive at the potential of reduction of hydrated cadmium ion. During the reverse cathodic scan the uncomplexed cadmium ion is reduced back into the amalgam. Thus, the ratio of cathodic to anodic peak currents rather than the ratio of anodic to cathodic peak currents is related to the rate constant.

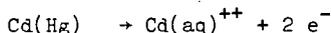
The electrochemical cell used in this work incorporates a strictly planar mercury electrode (4) with a Luggin capillary probe as shown in Figure 1.

Cadmium amalgam is prepared by reducing cadmium nitrate solution at constant potential into mercury. The transfer of the amalgam to the cell must be performed in a closed system under a nitrogen atmosphere to avoid rapid air oxidation of the cadmium from the amalgam.

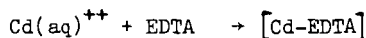
The three-electrode, potentiostatic circuit used to apply the cyclic potential program to the working electrode is a conventional operational amplifier circuit. The complete electronic configuration is shown in Figure 2.

The cyclic scan generator (3) is also an operational amplifier instrument which is capable of supplying continuously variable cycling rates ranging from 100 sec/cycle to 100 cycle/sec.

If  $1 \times 10^{-4} M$  cadmium amalgam is oxidized and then reduced as described above in contact with a solution buffered at pH 8 and containing 0.01 M EDTA and 1.0 M  $KNO_3$ , with no calcium ion present, an anodic current is observed that corresponds to the reaction:



No cathodic current is observed under these conditions on the subsequent reduction cycle, even though the cycling rate is increased to as much as 100 cycles/sec. This means that, even during the very short time corresponding to the experiment carried out at 100 cycles/sec, the reaction



has gone essentially to completion. Since 100 cycles/sec is the upper limit of the cycling rate allowed by the electronics and also by the reversibility of the  $Cd^{++}/Cd(Hg)$  couple, it is necessary to slow down the coupled chemical reaction in some way in order to apply the cyclic voltammetric method to its study. The reaction can be slowed down by reducing the concentration of the reactant EDTA species to a lower level. A convenient way to achieve this is to add an excess of some metal ion to the solution which forms labile complexes with the EDTA and yet is inactive at the potential of the  $Cd/Cd^{++}$  couple. For example, addition of excess calcium ion to the solution buffers the solution with respect to the free EDTA species at a very low concentration determined by the equilibrium constants of the system. As long as the rates of the dissociation and recombination reactions of the  $Ca^{++}$ -EDTA system are much faster than the rates of the reactions between the free EDTA species and cadmium ion and, as long as the free calcium ions and the calcium-EDTA complex ions are in large excess of the reacting cadmium ions at all times, the concentrations of the free EDTA species will remain essentially constant and will not be affected by their reaction with cadmium ion.

The following table shows some data obtained with this system.

Table I

Electrochemical Data for Determination of Pseudo First-order Rate Constants.  
 Solution Conditions:  $\Sigma_{Ca^{++}} = 0.0159$  M;  $\Sigma_{EDTA} = 0.0120$  M; pH = 9.210 (0.05 M Boric acid - NaOH Buffer);  $\mu = 1.0M$  ( $KNO_3$ );  $T = 25.0^\circ C$ .

Current Ratio	$\tau$ (sec.)	$k\tau$	$k$ ( $sec^{-1}$ )	$k\tau$ "calculated"
0.473	0.3585	1.125	3.14	1.133
0.711	0.1215	0.375	3.09	0.384
0.772	0.0879	0.272	3.09	0.278
0.806	0.0699	0.224	3.20	0.221
0.729	0.1062	0.343	3.23	0.336
0.650	0.1639	0.505	3.08	0.518
0.523	0.2750	0.900	3.27	0.869

AVE = 3.16

Because of the rather fast cycling rates, it was necessary to display the current-voltage curves on an oscilloscope and to photograph the oscilloscope screen. The resulting photographs were analyzed using methods described by Nicholson (3). The experimental results are shown in the first two columns of Table I. The values of  $k\tau$  entered in the third column of the table were obtained by extrapolation from the theoretical curve of  $(i_{cp}/i_{ap})$  vs.  $k\tau$  as described by Shain (1). The values of  $k$  were obtained by dividing the appropriate values of  $k\tau$  by the experimental values of  $\tau$ . The "calculated" values of  $k\tau$  were obtained by multiplying the average value of  $k$  by each experimental value of  $\tau$ . When these "calculated" values of  $k\tau$  are plotted vs. the experimental current ratios, the solid points in Figure 3 are obtained. The solid curve in this figure is the theoretical line calculated by Shain. The diagram demonstrates that the experimental data do indeed correspond to the coupled reaction model used to solve the diffusion equations. Meaningful pseudo first-order rate constants can therefore be obtained and, if the concentrations of various EDTA and EDTA-complex species are calculated, the dependence of the rate of the reaction on these species can be determined.

#### Measurement of Equilibrium Constants

If a solution containing tetraprotic EDTA,  $H_4Y$ , and an excess of inert supporting electrolyte added to control the ionic strength is titrated with strong base, the titration curve can be used to evaluate the successive acid dissociation constants of the free acid. If  $H_4Y$  is also titrated in the presence of a slight excess of calcium ion, the data from this titration curve can be combined with the  $K$ 's for the free acid to allow calculation of the formation constants of all the calcium-EDTA species formed. In order to make the calculations as general as possible, provision was made for the possible existence of two protonated Ca-EDTA complexes.

All calculations were computerized in order to minimize the time spent in calculation, to make it possible to use more data points and to obtain increased precision by averaging the results. The computer programs are written in Fortran and were used with a Control Data Corporation 3600 Computer at the Research Computing Center of Indiana University. The programs utilize the basic data from the experiment (initial M moles of  $H_4Y$ , ml of base corresponding to an equivalent of acid, initial volume, pH, ml of base added, and mmoles of  $Ca^{++}$  present) and solve the appropriate simultaneous equations using the method of determinants. Some typical experiments and results are shown in Table II.

Table II

Potentiometric Determinations of Formation Constants for Ca-EDTA System.

Experiment	Number of Simultaneous Eq'ns Solved	Average Value of K
Titration of $1 \times 10^{-3}M$ $H_4Y$ - $1.0 M KNO_3$ From $a = 0$ To $a = 2$ With $KOH$ - $1.0 M KNO_3$ ; $T = 25.0^\circ C$	13 Equations Solved From 26 Data Points	$K_1 = 6.15 \times 10^{-3}$ $K_2 = 2.41 \times 10^{-3}$
Titration of $1 \times 10^{-3}M$ $H_4Y$ - $1.0 M KNO_3$ From $a = 3$ to $a = 4$ with $KOH$ - $1.0 M KNO_3$ ; $T = 25.0^\circ C$	24 Equations Solved From 48 Data Points	$K_4 = 1.36 \times 10^{-10}$ $K_{KY} = 0.37$
Titration of $1 \times 10^{-3}M$ $H_4Y$ - $3 \times 10^{-3}M Ca^{++}$ - $1.0M KNO_3$ From $a = 0$ to $a = 4$ with $KOH$ - $1.0M KNO_3$ ; $T = 25.0^\circ C$	12 Equations Solved From 36 Data Points	$K_{CaY} = 4.33 \times 10^{+9}$ $K_{CaHY} = 1.94 \times 10^{+3}$ $K_{CaH_2Y} = 27.4$

Equilibrium constants obtained in this manner can be used to calculate the concentrations of EDTA species present at any pH in potassium nitrate solutions of ionic strength 1.0. Two plots giving the fraction of each EDTA species present in solution as a function of pH in the absence and in the presence of excess calcium ion are shown in Figures 4 and 5. The species  $KY^{-3}$ ,  $CaHY^{-}$  and  $CaH_2Y$ , whose formation constants have not been previously reported, were found to be present at appreciable concentrations.

#### References

- (1) Nicholson and Shain, Anal. Chem., **36**, 706 (1964).
- (2) Schwarzenbach and Ackerman, Helv. Chim. Acta, **30**, 1798 (1947).
- (3) DiSalvo and Schaap, to be published.
- (4) Kuempel and Schaap, Anal. Chem., **38**, 664 (1966).
- (5) Nicholson, Anal. Chem., **38**, 1406 (1966).
- (6) Bates, "Determination of pH", New York, Wiley (1964), p. 123-30.

#### Acknowledgement

This work was supported in part by a U. S. Public Health Service Predoctoral Fellowship (1-F1-GM-28, 705-01) and in part by the U. S. Atomic Energy Commission through Contract AT(11-1)-256. (A.E.C. Document No. COO-256-69.)

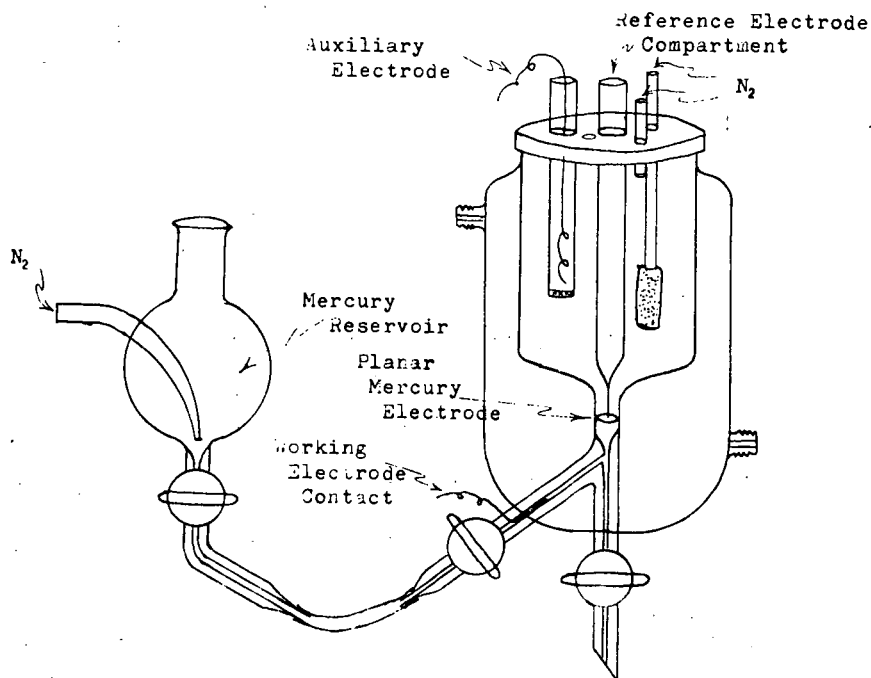


Figure 1: Electrochemical Cell

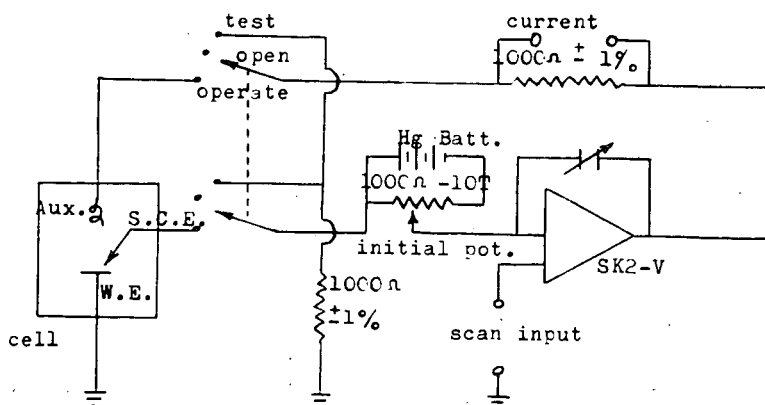


Figure 2: Potentiostatic Circuit

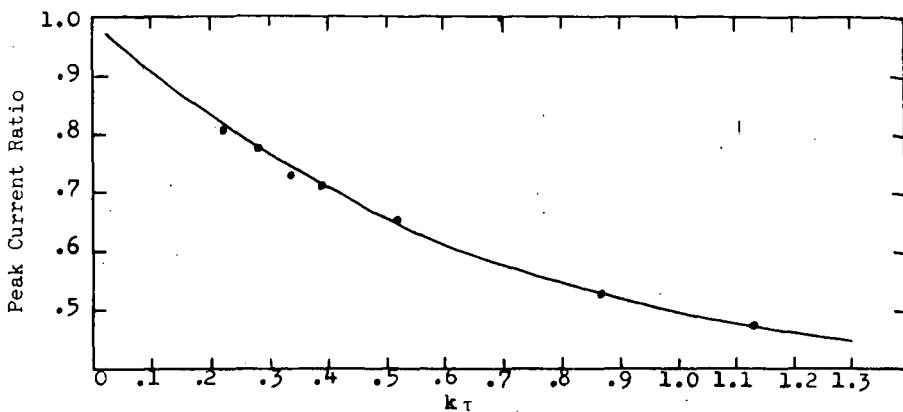


Figure 3: Experimental and Theoretical Plot of  $k\tau$  vs Peak Current Ratio

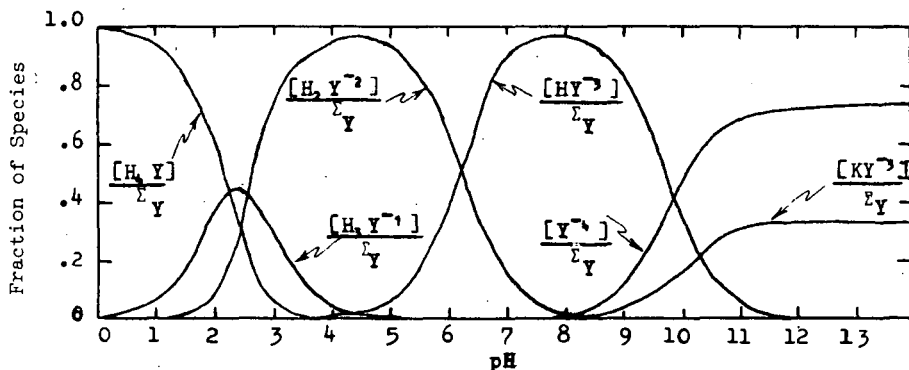


Figure 4: pH vs Fraction of Species plot for EDTA  
 $\mu = 1.0$  ( $\text{KNO}_3$ );  $T = 25.0^\circ\text{C}$

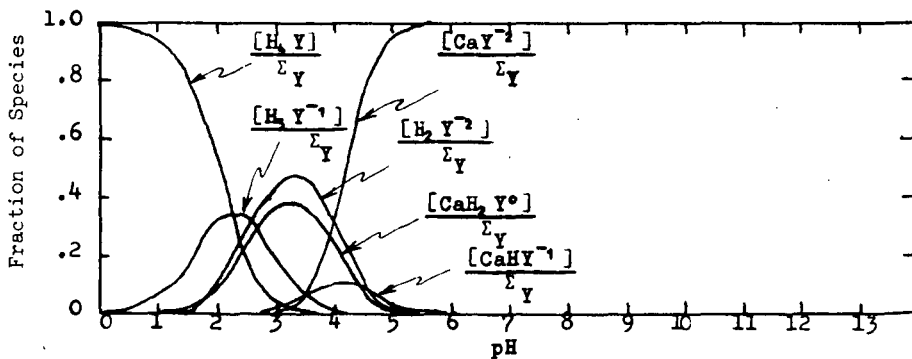


Figure 5: pH vs Fraction of Species Plot for Ca-EDTA  
 $\mu = 1.0$  ( $\text{KNO}_3$ );  $T = 25.0^\circ\text{C}$ ;  $\Sigma_{\text{Ca}^{++}}/\Sigma_{\text{EDTA}} = 2.0$

Ligand Bridging in the Oxidation of Chromium(II)  
at Mercury Electrodes

JANET JONES AND FRED C. ANSON

Gates and Crellin Laboratories of Chemistry, California  
Institute of Technology, Pasadena, California 91109

It has been shown that many ligands dramatically affect the electrochemical oxidation of Cr(II). Pecsok and Lingane (1) have investigated the polarographic behavior of Cr(II) in the presence of KCl, KSCN, CaCl<sub>2</sub>, Me<sub>4</sub>NBr, and several carboxylic acids. Large changes in apparent half-wave potential and in the degree of irreversibility of the oxidation were found by changing the nature of the supporting electrolyte solution.

Kemulá and Rakowska (2), who studied the reduction of various Cr(III) species using cyclic voltammetry, showed that CrCl<sup>2+</sup> is formed when Cr(II) is oxidized at a hanging mercury drop electrode in chloride solution.

Aikens and Ross (3) have studied the rates of oxidation of Cr(II) at mercury electrodes in the presence of fluoride, chloride, and iodide. They found that the rate of Cr(II) oxidation is proportional to the concentration of chloride over a fifty-fold change in chloride concentration, and that at a fixed potential, the accelerating effect of the halides decreases in the order (I<sup>-</sup>) > (Cl<sup>-</sup>) > (F<sup>-</sup>), the effect of fluoride being very small. They point out that the tendency for specific adsorption of halides also decreases in this order, while the stability of the Cr(II) complexes probably increases markedly in the same order.

Cr(III) is sufficiently inert to chloride substitution that the reaction  $\text{Cr}^{3+} + \text{Cl}^- \rightarrow \text{CrCl}^{2+}$  may be ignored as a source of the complex CrCl<sup>2+</sup>. Therefore if the product of electro-oxidation of Cr(II) in chloride solutions is CrCl<sup>2+</sup> the transition state must contain chloride. This in turn implies that the reaction mechanism is halide-bridged electron transfer (or halide atom transfer). Jones and Anson (4) have carried out exhaustive controlled potential electrolyses of Cr(II) solutions at a stirred mercury pool electrode in the presence of chloride. They found that when the initial chloride to Cr(II) ratio is less than or equal to one, no free chloride is found in the product solution, and when the initial chloride to Cr(II) ratio is greater than one the amount of chloride found is equal to the initial excess of chloride over Cr(II). This proves that the ligand-bridge mechanism obtains in that case.

We have studied this reaction further using chronopotentiometry to show that the formation of CrCl<sup>2+</sup> in the oxidation of Cr(II) is quantitative when microcoulomb quantities of Cr(II) are oxidized as well as in mass electrolysis, to see if there is reactant adsorption, and to see if the reacting species is CrCl<sup>+</sup>.

The ratio of forward to reverse transition times was found to be three for oxidation of Cr(II) in solution containing excess chloride followed by reduction of generated CrCl<sup>2+</sup>. This demonstrates that CrCl<sup>2+</sup> is the sole product of the oxidation.

Constancy of the chronopotentiometric constant with change in current density placed an upper limit of  $1 \mu\text{C}/\text{cm}^2$  on the amount of reactant adsorbed on the electrode.

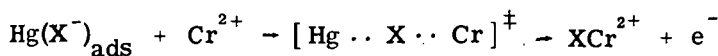
A lower limit of  $500 \text{ sec}^{-\frac{1}{2}}$  was found for the quantity  $k_f(k_f+k_b)^{\frac{1}{2}}/k_b$ , where these constants are the forward and back pseudo-first-order rate constants for the reaction  $\text{Cr}^{2+} + \text{Cl}^- = \text{CrCl}^+$  in 0.5 F chloride solution. The spectroscopic measurements of Pecsok and Bjerrum (5) place an upper limit of  $5 \times 10^{-4}$  l/mole on the equilibrium constant for this reaction. Combination of these two quantities places a lower limit of  $10^{12} \text{ sec}^{-1}$  on the quantity  $k_f + k_b$ . This limit is sufficiently high that it rules out prior complex formation as an important feature of the mechanism.

The effect of bromide on the oxidation of Cr(II) is qualitatively similar to that of chloride. Polarographic measurements of the rate of reduction of  $\text{CrBr}^{2+}$  and the rate of oxidation of Cr(II) in the presence of bromide show that the standard potential for the reaction  $\text{Cr}^{2+} + \text{Br}^- = \text{CrBr}^{2+} + e^-$  is -0.500 v. vs. SCE and the pseudo-first-order standard rate constant is  $1.85 \times 10^{-3} \text{ cm/sec}$ . The apparent transfer coefficient obtained from the anodic reaction in the region -0.500 to -0.300 v. vs. SCE is 0.21 and that obtained from the cathodic reaction in the region -0.500 to -0.600 v. vs. SCE is 0.48. These values are uncorrected for double layer. The corresponding values for the reaction  $\text{Cr}^{2+} = \text{Cr}^{3+} + e^-$  obtained from both the anodic and cathodic reactions are  $0.74 \times 10^{-5} \text{ cm/sec}$  and 0.63. The standard potential is -0.650 v. vs. SCE.

Using these rate parameters one can show that the bromide-independent and bromide-dependent oxidations should proceed at roughly comparable rates over a wide range of potential and bromide concentration. Because of the potential dependence of the relative current efficiencies for the two reactions, a controlled potential technique, double potential step chronocoulometry (6), was chosen to study the reaction. An equation was derived which gives the coulombic yields for the two reaction pathways as a function of the kinetic parameters and experimental conditions (7). Calculations showed that under conditions where the oxidation of Cr(II) is diffusion controlled the product should be almost entirely  $\text{CrBr}^{2+}$ . This result was confirmed by double potential step chronocoulometric data.

The oxidation of Cr(II) in the presence of iodide is more difficult to study because the reaction occurs at potentials near that for depolarization of mercury. Cyclic voltammetry at slow sweep rates in solutions with constant iodide concentration and varying amounts of Cr(II) demonstrated that the product of Cr(II) oxidation is  $\text{CrI}^{2+}$ . Exhaustive electrolysis at -0.192 v. vs. SCE of Cr(II) solutions containing chloride and iodide were carried out to determine the product distribution between  $\text{CrCl}^{2+}$  and  $\text{CrI}^{2+}$ . The results obtained were in good agreement with values calculated from the rates of the competing reactions.

We conclude from these investigations that the oxidation of Cr(II) at mercury electrodes in the presence of chloride, bromide, or iodide proceeds via the mechanism



This mechanism undoubtedly also obtains for many other ligands which are adsorbed on mercury and for many other transition metal ions.

1. R. L. Pecsok and J. J. Lingane, *J. Am. Chem. Soc.*, **72**, 189 (1950).
2. W. Kemula and E. Rakowska, *Roczniki Chemii, Ann. Soc. chim. Polonorum*, **36**, 203 (1962).
3. D. A. Aikens and J. W. Ross, Jr., *J. Phys. Chem.*, **65**, 1213 (1961).
4. Janet Jones and Fred C. Anson, *Anal. Chem.*, **36**, 1137 (1964).
5. R. L. Pecsok and J. Bjerrum, *Acta Chem. Scand.*, **11**, 1418 (1957).
6. Joseph H. Christie, R. A. Osteryoung, and Fred C. Anson, *J. Electroanal. Chem.*, **13**, 236 (1967).
7. Janet Jones, Joseph H. Christie, and Fred C. Anson, to be published.

THE ELECTROCHEMICAL REDUCTION OF PENTAMMINECOBALT (III)  
COMPLEXES. THE QUESTION OF LIGAND  
BRIDGING AT ELECTRODES

William M. Schwarz

National Bureau of Standards  
Washington, D. C. 20234

The electrochemical reduction of a number of pentamminecobalt complexes was investigated using linear scan voltammetry at a slowly dropping mercury electrode. An attempt was made to obtain direct evidence for the existence of an electron conducting ligand bridge intermediate in an electrochemical reduction, chiefly by comparing the electrochemical reduction--the electrochemical rate parameters (particularly  $\alpha$ ) and activation effects--with the corresponding homogeneous reductions. The electron transfer coefficient,  $\alpha$ , was found to range from 0.64 to 0.84 for complexes containing succinic, fumaric, maleic and various isomeric pyridinium carboxylic acids as ligands. The values showed little correlation with the ability of the ligand to form electron conducting bridges in the homogeneous sense; they did correlate with the degree of saturation of the ligand. One type of activation effect was investigated--the isomerization of maleic to fumaric acid when maleic acid is functioning as an electron conducting bridging ligand. No isomerization was found to occur for the electrochemical reduction of the maleatopentamminecobalt complex. Similarly no isomerization was observed in the case of homogeneous reduction by vanadium (II) in acidic solutions. The latter results are in disagreement with previous reports of this "activation effect." These results show no evidence for a ligand bridging electroreduction mechanism in these systems.

## Polarographic Irreversibility of the Copper(II) Pyrophosphate System

Peter E. Sturrock and Gibson W. Higgins

Georgia Institute of Technology, Atlanta, Georgia

The polarographic waves of a number of complex ion systems are known to be irreversible in alkaline solution. One such system is the copper(II)-pyrophosphate complex, formally represented as  $\text{Cu(Py)}_2$ . Below pH 6 a reversible polarographic wave is obtained for the system. As the pH approaches 9 the wave becomes split into two parts, and the normal diffusion current is not attained until the electrode potential is at least -1.3 volts versus S.C.E. In addition to the varying behavior of the reduction wave, the appearance of the polarogram of an alkaline solution of the complex is affected by the concentration of the supporting electrolyte, through the influence of the latter upon the electrical double layer. In this work potassium nitrate was used as the supporting electrolyte. As its concentration is decreased a maximum appears on the rising portion of the wave, and is followed by a pronounced minimum before the current finally rises to its diffusion-limited value.

Both relaxation and steady-state techniques were used to study the combined effects of pH and supporting electrolyte concentration. Techniques employed included the potential step method, chronocoulometry, triangular sweep voltammetry, drop-time electrocapillary measurements, and regular and A.C. polarography. Hanging drop and dropping mercury electrodes were used exclusively.

Since it was initially hypothesized that perhaps adsorption was the cause of the irreversibility, double-layer capacity data were obtained from triangular sweep voltammetry of the sodium nitrate-sodium pyrophosphate system. No adsorption of pyrophosphate was detected by this method, or by searching for the Esin-Markov effect for pyrophosphate. The value of the potential of a streaming mercury electrode in 0.1 and 0.2 F solutions of sodium pyrophosphate was a constant -0.428 volts versus S.C.E., actually less than the -0.435 volts expected in the absence of anionic adsorption, and this discrepancy was attributed to a slight cationic adsorption.

Near the end of the investigation, evidence supporting the existence of the specific adsorption of nitrate ion on mercury was published, and subsequent correlation with data taken in the present study confirmed that fact. The value of the ECM in 1 F  $\text{KNO}_3$  solution was confirmed to be -0.519 volts versus S.C.E.

Chronocoulometry and double-step chronocoulometry, selective for the detection of adsorption of electroactive species, were employed to determine whether any of the copper pyrophosphate complex is adsorbed. The greatest possible amount of adsorption was found to be only about  $0.5 \times 10^{-10}$  moles  $\text{cm}^{-2}$ . Thus it may be said that no detectable adsorption of the copper pyrophosphate complex occurs. Inspection of drop time electrocapillary curves for alkaline solutions of potassium nitrate, some with copper pyrophosphate and some without, showed no noticeable differences at any potential among the various curves. This is additional evidence against the existence of specific adsorption of the complex.

A previous report, plus evidence found in the present study, indicate that in alkaline solution the rate of the electrochemical reaction is controlled by the rate of dissociation of the 2:1 complex to form the reducible species, the latter being  $\text{Cu(Py)}_2^{2-}$  in the absence of substances which form complexes with copper pyrophosphate ions. By employing the potential step method it was possible to measure the parameters of the electrochemical reduction step in both acid and alkaline solutions. The values found for the parameters for 1 F  $\text{KNO}_3$  of pH = 9.34 are the following:  $i_a^0 = 0.596 \times 10^{-3}$  amp.  $\text{cm}^{-2}$ ,  $k_a^0 = 0.38 \times 10^{-3}$  cm.  $\text{sec}^{-1}$ ,  $\alpha = 0.4$ . At pH = 3.0 the values are  $i_a^0 = 6.92 \times 10^{-3}$  amp.

$\text{cm.}^{-2}$ ,  $k_s^0 = 3.90 \times 10^{-2} \text{ cm. sec.}^{-1}$ ,  $\alpha = 0.3$ . These apparent values tended generally to increase with decreasing  $\text{KNO}_3$  concentration and pH.

Double layer corrections were applied to the above results. These calculations yielded so-called true values of the parameters, as follows. At pH = 9.34,  $i_t^0 = 1.21 \times 10^{-6} \text{ amp. cm.}^{-2}$ ,  $k_t^0 = 6.7 \times 10^{-6} \text{ cm. sec.}^{-1}$ ,  $\alpha = 0.5$ . At pH = 3.0,  $i_t^0 = 1.07 \times 10^{-2} \text{ amp. cm.}^{-2}$ ,  $k_t^0 = 5.94 \times 10^{-2} \text{ cm. sec.}^{-1}$ ,  $\alpha = 0.5$ .

The apparent values of the kinetic parameters at pH 3 are only 20 per cent less than values, also uncorrected for double layer effects, reported in the literature for reduction of copper(II) from 1 F  $\text{KNO}_3$  solution. Thus it is thought that the complex is weak in acidic solution, particularly in the presence of 1 F sodium ion. This conclusion is strengthened by the results obtained for the ionic charge  $z$  on the reducible species in the bulk of the solution. These values were obtained as a by-product of the application of double layer corrections. At pH 9,  $z = 2$ , while at pH 3,  $z = +1$ .

A series of polarograms of the copper pyrophosphate complex was taken for varying concentrations of potassium nitrate. From the polarograms, values for an apparent rate constant  $v^*$  were computed from the formula of Koutecky for a kinetic polarographic current. Values for  $\psi_0 = f(C, E)$  were obtained from electrocapillary measurements and the Gouy-Chapman theory. In each case the value for  $\phi = 0$  was taken as the experimental point of zero charge for that solution. The values of  $v^*$  and  $\psi_0$  were then plotted as functions of  $\phi$  and the concentration, in the manner of Gierst (4). The results obtained from a graphical determination of  $\alpha$ ,  $z$ , and  $v^0$  from this plot are as follows. From the potential region of positive electrode charge,  $\alpha = 0.4$ ,  $z = -1.2$ ,  $v^0 = 8.0 \times 10^{-4} \text{ cm. sec.}^{-1}$ . From the potential region of negative electrode charge,  $\alpha = 0.1$ ,  $z = -0.32$ ,  $v^0 = 8.7 \times 10^{-4} \text{ cm. sec.}^{-1}$ .

In the region of positive electrode charge, observation of the  $v^*$  versus  $\phi$  curve for 1 F  $\text{KNO}_3$  indicates that the rate is nearly independent of  $\phi$ , and it is thought that in this potential region only the 1:1 complex is reduced. At more negative values of  $\phi$  both the mono- and di-ligand complexes are thought to undergo reduction, and the observed rate slowly increases until finally, at very negative potentials, the rate becomes diffusion controlled. In the region of positive electrode charge the value obtained for  $z$  is approximately equal that obtained from the relaxation experiments. The value for  $\alpha$  is moderately less. In the potential region of negative electrode charge, both  $\alpha$  and  $z$  are surprisingly small. This is attributed to the simultaneous reduction of more than one complex species, in addition to double layer effects.

The evidence indicates, therefore, that the effects are different on the two sides of the point of zero charge. The low value of  $\alpha$  at negative  $\phi$  indicates via the Frumkin equation that the effect of  $\phi$  on  $v^*$  is considerably lessened in this potential range. This is to be expected if both the 1:1 and 2:1 complexes are reduced in this region, since the 2:1 complex has an even larger negative charge than does the 1:1, and then the reactant, the adsorbed nitrate ions, and the electrode are all negative, and the  $\psi$  effect should then be at its maximum.

## POLAROGRAPHY OF DIPHENYLTHALLIUM(III) CATION IN AQUEOUS SOLUTION

Joseph S. Di Gregorio, Michael D. Morris

Department of Chemistry, The Pennsylvania State University  
University Park, Pennsylvania 16802

Thallium forms ionic organocompounds of the type  $R_2TlX$  where R is an alkyl or aryl group and X is a halide, sulphate, cyanide, nitrate or other anion (1). These compounds are stable and many are water soluble. Dialkyl- and diarylthallium(III) cations are electroreducible at the dropping mercury electrode.

Costa (2) studied the polarographic reduction of dialkylthallium bromides,  $R_2TlBr$ , in aqueous propanol solution where R is an ethyl, propyl or butyl group. He reported that these species are reducible to lower oxidation states of thallium and ultimately to thallium amalgam. He proposed a mechanism involving the formation of a Tl-Tl bond but did not attempt to identify the reaction products. We have examined in detail the mechanism of the polarographic reduction of the diphenylthallium(III) cation and have established the decay schemes for the subvalent organothallium radicals formed at the dropping mercury electrode.

**Experimental.** Diphenylthallium bromide was prepared by the Grignard synthesis (3). Diphenylthallium fluoride was prepared by reaction of commercial diphenylthallium iodide (Metallomer Laboratories, Fitchburg, Mass.) and silver fluoride (4). The electrochemical behavior of diphenylthallium bromide and diphenylthallium fluoride is identical. Triton X-100 (Rohm and Haas) was used as received. The supporting electrolyte (pH = 6.20) was prepared from reagent grade potassium dihydrogen phosphate and sodium hydroxide. All solutions were prepared using distilled water and contained 0.001% Triton X-100 as a maximum suppressor.

Polarograms were made on solutions in a water-jacketed cell maintained at  $25.0 \pm 0.1^\circ C$ . Potentials are reported versus the saturated calomel electrode.

**Results.** The mechanism of the polarographic reduction of aqueous solutions of diphenylthallium(III) cation,  $(C_6H_5)_2Tl^+$ , at the dropping mercury electrode is concentration dependent. At low concentrations,  $0.1 \times 10^{-3}M$  to  $0.5 \times 10^{-3}M$ , three irreversible, diffusion-controlled, one-electron waves are observed. At high concentrations, above  $0.5 \times 10^{-3}M$ , two irreversible, diffusion-controlled, one-electron waves are observed.

A typical low concentration polarogram ( $0.1 \times 10^{-3}M (C_6H_5)_2Tl^+$ ) is shown in Figure 1. On the ascending portion of the first wave, the current, as a function of time, does not increase monotonically, but instead reaches a maximum value during the lifetime of the drop and then decreases as the drop continues to grow. The current on the ascending portion of the second wave is also non-monotonic. The shape of the current-time curve as a function of potential is currently under investigation, and apparently is related to the adsorption of intermediate species at the electrode surface. Controlled potential electrolysis ( $0.1 \times 10^{-3}M (C_6H_5)_2Tl^+$ ) at a mercury pool cathode at a potential corresponding to the first diffusion-current plateau yields diphenylmercury. That the compound formed (M.P.  $125^\circ C$ ) is diphenylmercury was verified by comparison of its infrared spectrum with that of an authentic sample of diphenylmercury. Electrolysis at a potential corresponding to the second diffusion-current plateau was not attempted because of the ill-defined

nature of the wave. No diphenylmercury is formed during electrolysis at a potential on the third diffusion-current plateau.

A typical high concentration polarogram ( $1.0 \times 10^{-3}M (C_6H_5)_2Tl^+$ ) is shown in Figure 2. The first wave is preceded by an adsorption wave. As in the low concentration case, the current, as a function of time, does not increase monotonically. A non diffusion-controlled third wave is observed at potentials more cathodic than  $\sim 1.3$  V. An electrocapillary curve of a solution ( $1.0 \times 10^{-3}M (C_6H_5)_2Tl^+$ ) is shown in Figure 3. Depressions corresponding to adsorption of the parent cation and of both intermediate species at the electrode surface are observed. The more pronounced depressions in the regions of stability of the intermediate species are indicative of the stronger adsorption of these species than of the parent cation. Controlled potential electrolysis at potentials corresponding to both the first and second diffusion-current plateaus yields diphenylmercury.

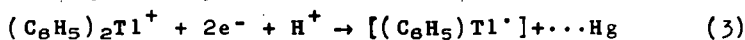
Conclusions. The following reaction scheme is proposed to account for the concentration dependence of the polarographic reduction of diphenylthallium(III) cation. At low concentrations the first electron transfer yields an adsorbed diphenylthallium(II) radical as given by Equation 1.



Transmetalation with the mercury electrode yields diphenylmercury as in Equation 2.



The second electron transfer yields an adsorbed phenylthallium(I) radical as shown in Equation 3.



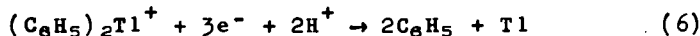
Transmetalation with the mercury electrode yields a phenylmercury radical as in Equation 4.



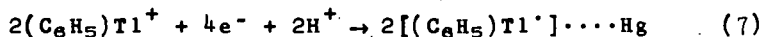
Rapid disproportionation of the mercury radical yields diphenylmercury as in Equation 5.



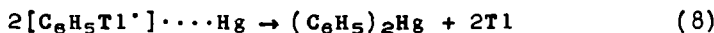
The third electron transfer corresponds to Equation 6.



At high concentrations the first electron transfer proceeds as in Equations 1 and 2. The second electron transfer is given by Equation 7.



Although the stoichiometry is the same in both the low and high concentration cases, the structures of the intermediates are different as shown below. Transmetalation of the phenylthallium radical with the mercury electrode leads directly to diphenylmercury as in Equation 8.



At both low and high concentrations the first reduction proceeds via formation of a radical adsorbed onto the mercury surface followed by transmetalation of the radical. Structure I represents a likely intermediate.



At low concentrations the adsorbed monophenylthallium(I) radicals formed during the second electron transfer are so far apart that each radical reacts with a different mercury atom as shown schematically in structure II.



At high concentrations the adsorbed monophenylthallium(I) radicals are so close together that two radicals can react with the same mercury atom as in structure III.



The third electron transfer at low concentrations (Equation 6) corresponds to reduction of an adsorbed monophenylthallium(I) or phenylmercuric radical to thallium and benzene or mercury and benzene. At high concentrations the direct reaction between two monophenylthallium(I) radicals and a single mercury atom (Equation 8, structure III) removes monophenylthallium(I) radicals so rapidly that further reduction does not occur. If the electroactive species is a phenylmercuric radical, a similar argument applies. Decay of intermediate structure III proceeds directly to diphenylmercury leaving no phenylmercuric radicals available for further reduction.

The transmetalation of diphenylthallium(III) bromide with mercury has been observed in a non-electrochemical system by Gilman and Jones (5). They reported an excellent yield (90%) of diphenylmercury after refluxing eight hours. There have been several reports in the literature of systems involving transmetalations of organometallic compounds with mercury during electrochemical reductions. Morris, McKinney and Woodbury (6) reported arylation of the mercury electrode with aqueous solutions of tetraphenylantimony(V) cation to yield diphenylmercury. Recently Dessy and coworkers (7) studied the electrochemical behavior of triphenyllead acetate and diphenyllead diacetate in dimethoxyethane and reported arylation of the mercury electrode by products of the electroreductions to yield diphenylmercury in both cases.

REFERENCES

1. G. E. Coates, *Organometallic Compounds*, 2nd edition, John Wiley and Sons, Inc., New York, 1960.
2. G. Costa, *Ann. Chim. (Rome)*, 40, 559 (1950).
3. D. Goddard and A. E. Goddard, *J. Chem. Soc.*, 256 (1922).
4. E. Krause and A. V. Grosse, *Ber.*, 58B, 272 (1925).
5. H. Gilman and R. G. Jones, *J. Am. Chem. Soc.*, 61, 1513 (1939).
6. M. D. Morris, P. S. McKinney and E. C. Woodbury, *J. Electroanal. Chem.*, 10, 85 (1965).
7. R. E. Dessy, W. Kitching and T. Chivers, *J. Am. Chem. Soc.*, 88, 453 (1966).

CAPTIONS FOR FIGURES

- Figure 1. Polarogram of  $0.10 \times 10^{-3}$  F  $(C_6H_5)_2Tl^+$  in 0.05F  $(H_2PO_4^- + HPO_4^{2-})$ . 0.001% Triton X-100 present as maximum suppressor.
- Figure 2. Polarogram of  $1.00 \times 10^{-3}$  F  $(C_6Y_5)_2Tl^+$  in 0.05F  $(H_2PO_4^- + HPO_4^{2-})$ . 0.001% Triton X-100 present as maximum suppressor.
- Figure 3. Drop time dependence on potential; capillary flow rate = 2.70 mg/sec.
- A. 0.05 F  $(H_2PO_4^- + HPO_4^{2-})$
  - B. 0.05 F  $(H_2PO_4^- + HPO_4^{2-})$  containing 0.001% Triton X-100.
  - C.  $1.00 \times 10^{-3}$  F  $(C_6H_5)_2Tl^+$  in 0.05 F  $(H_2PO_4^- + HPO_4^{2-})$ .
  - D.  $1.00 \times 10^{-3}$  F  $(C_6H_5)_2Tl^+$  in 0.05 F  $(H_2PO_4^- + HPO_4^{2-})$  containing 0.001% Triton X-100.

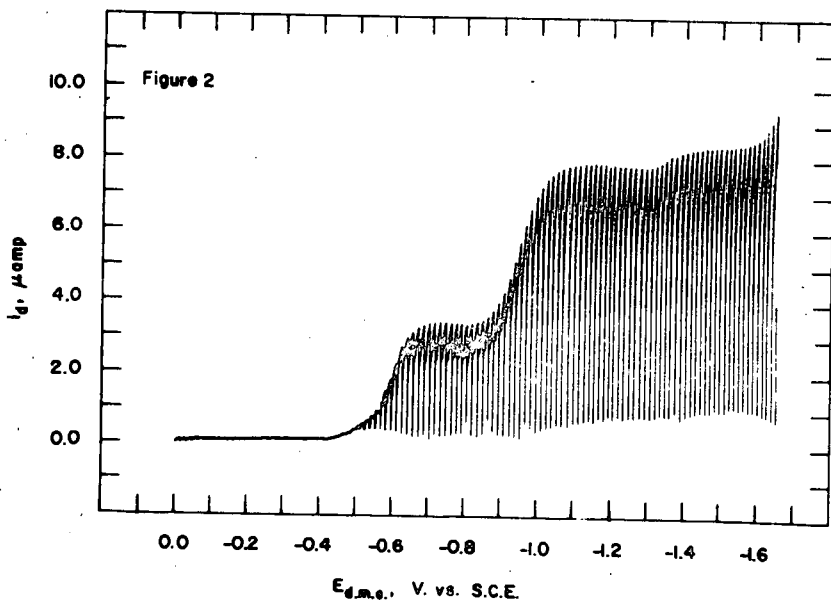
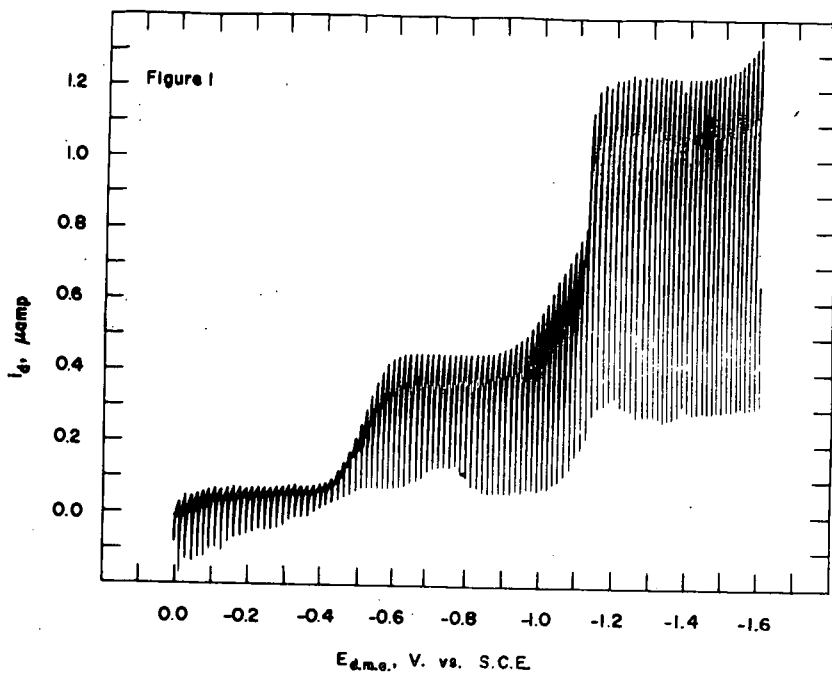
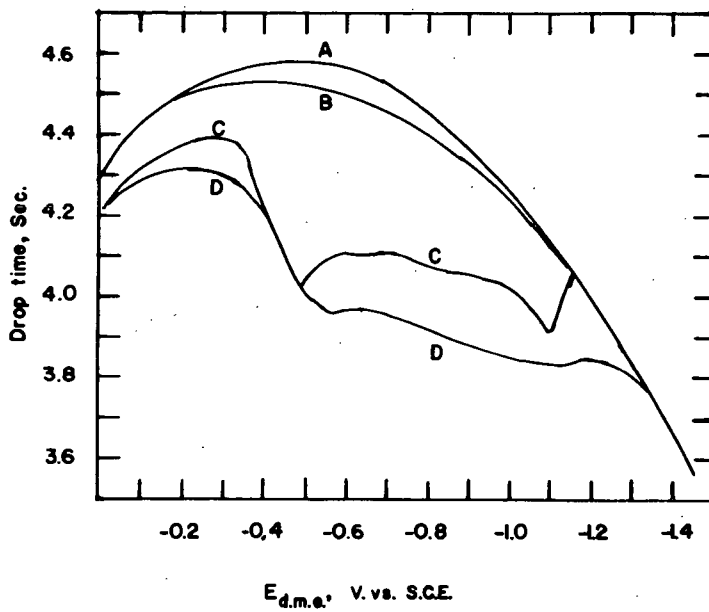


Figure 3



POLAROGRAPHIC BEHAVIOR OF A SERIES  
OF SUBSTITUTED HYDRAZINES

A. F. Krivis\* and G. R. Supp

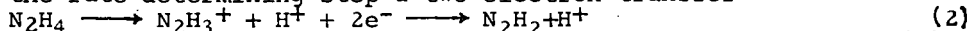
Olin Mathieson Chem. Corp., New Haven, Conn.

\*Present Address: Department of Chemistry,  
The University of Akron, Akron, Ohio

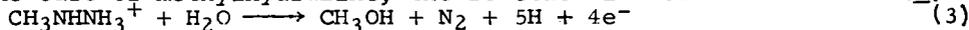
The oxidation of hydrazine and its organic derivatives is of importance in a number of areas. One may cite the use of hydrazines as propellents, as oxygen scavengers, in fuel cells, or as electrode depolarizers, to name just a few applications. In almost all cases, the oxidation path of the hydrazine controls its utility. Chemically, hydrazine oxidation proceeds through a diimide or hydrazyl radical to form nitrogen, or nitrogen and ammonia, or ammonia and hydrazoic acid, depending on the conditions of reaction (1). Electrochemical studies of hydrazine (4, 2) and of methylhydrazine (5) have shown that an overall four-electron reaction of the following sort takes place:



with the rate-determining step a two-electron transfer



In the case of methylhydrazine, the reaction in acid solution is (5)



The work presently reported was undertaken to elucidate some of the reasons for the apparent differences in stability of organic hydrazines. In particular, the electrochemical behavior of a series of monosubstituted hydrazines was studied. In order to minimize ambiguities due to the catalytic effects of noble metals (1), such as those found with platinum electrodes (2, 5), a normal dropping mercury electrode was utilized in strongly basic solution. This experimental arrangement produces well defined, reversible anodic waves easily interpreted (4).

EXPERIMENTAL

Chemicals - Monomethylhydrazine (MMH), 1,1-dimethylhydrazine (UDMH), 1,2-dimethyl hydrazine (SDMH), 1,2-diisobutylhydrazine (DiBH), *n*-hexylhydrazine (nHH) and acetic hydrazide (AcX) (Olin Mathieson Chemical Corp.) were distilled under reduced pressure and assayed by an iodometric titration (7). Hydrazine sulfate and diacetyl hydrazine (DACX) (Olin Mathieson Chemical Corp.) were recrystallized from water. Ethyl hydrazine acetate hydrochloride (EtH) and *n*-propyl hydrazine oxalate (PrH) (K and K Laboratories) were used without further purification, but assay indicated the purity to be 84%. Phenyl hydrazine hydrochloride (Eastman White Label) also was used without further purification. All other chemicals were reagent grade.

APPARATUS - A Sargent Model XXI polarograph was used in conjunction with a thermostated H-cell (25.0 ± 0.1°C.) containing a saturated mercurous sulfate reference electrode (6). The mercurous sulfate reference was used to permit the application of more positive voltages. The capillary used had a constant of 1.98 mg<sup>2/3</sup> second<sup>1/6</sup> at 25 cm. of Hg.

PROCEDURE - Stock solutions of the hydrazines were prepared immediately before use and degassed with nitrogen pre-saturated with a portion of the stock solution. Background electrolyte solutions (0.1M sodium hydroxide-0.005% gelatin) were deoxygenated for 10

minutes in the H-cell and the requisite volume of hydrazine stock solution added. The mixture was mixed thoroughly and the polarogram run immediately. All polarograms were run using a span of 0.5 volts with the initial and final voltages measured accurately with a Rubicon Portable Precision potentiometer.  $E_{1/2}$  and  $i_d$  values were obtained graphically using the average of the recorder traces.

#### RESULTS AND DISCUSSION

In order to maintain conditions as constant as possible, all the hydrazine samples were run at ca. 0.5 mM concentration. The effect of any concentration dependency of the half-wave potentials thus would be minimized. Table I lists the polarographic values obtained for a variety of substituted hydrazines in 0.1M NaOH, vs. a mercurous sulfate electrode.

The results for the monosubstituted alkyl hydrazines is of particular interest. In general, as the carbon skeleton is lengthened, the half-wave potential is shifted to more negative voltages. A plot of  $E_{1/2}$  vs. molecular weight is shown in Fig. 1. An even more instructive plot is that of  $E_{1/2}$  vs. the number of carbon atoms in the substituent chain (Fig. 2). The latter graph demonstrates that the half-wave potential is shifted linearly to negative voltages as a function of the number of carbon atoms in the substituent. The linearity held over the wide range of  $C_1$  to  $C_6$ .

Hydrazine, itself, however, did not fit the curve; extrapolation of the linear portion of the curve to zero carbon atoms gave a value of -0.600 v. which was 52 mv more negative than the experimentally determined value. The data shown in Figs. 1 and 2 may be interpreted in terms of the electron donating properties of alkyl chains. As the chain was increased in length, the half-wave potential for the anodic reaction was shifted negatively, or the oxidation occurred more readily. This increase in ease of oxidation might be explained on the basis of the electron donating effect of increasing alkyl chain length (3). The slope of the line in Fig. 2 corresponded to -31 mv./ carbon atom.

A low value for the diffusion current of  $nHH$  was noted. This may be due to a combination of factors including a higher degree of instability in solution, difference in diffusion coefficient, or lessened water solubility. Disubstituted hydrazines, either symmetrical or unsymmetrical, did not appear to fit the same pattern as the monosubstituted compounds (Table I). UDMH and SDMH produced essentially identical half-wave potentials ( $\Delta E_{1/2} = 3.4$  mv.) which were shifted negatively from the expected value for a  $C_2$  compound. In addition, based on the diffusion current constant for the monosubstituted hydrazines, the currents for UDMH and SDMH indicated a two-electron reaction rather than a four-electron step. This behavior is similar to that encountered with a platinum electrode in acid medium (5). Di-BH also appeared to undergo only a two-electron oxidation; the half-wave potential was significantly more negative than the methyl substituted compounds, however.

In comparison with the alkyl hydrazines, phenyl hydrazine gave an anodic wave which was shifted positively from that expected for a mono-substituted six carbon hydrazine; the shift was 39.1 mv. In this case, the electron withdrawing character of the benzene ring contributed to produce the positive shift. The lower diffusion current for phenyl hydrazine appears to be due to a difference in diffusion coefficient.

Acetic hydrazide gave an anodic wave which was shifted positively from ethyl hydrazine by 38.8 mv. The disubstituted hydrazide, diacetyl hydrazine, however, was not electroactive over the entire range studied.

LITERATURE CITED

- (1) Audrieth, L. F., Ogg, B. A., "The Chemistry of Hydrazine", John Wiley and Sons, Inc., New York, 1951.
- (2) Bard, A. J., Anal. Chem., 35, 1602 (1963).
- (3) Ingold, C. K., "Structure and Mechanism in Organic Chemistry", Cornell Univ. Press, Ithaca, New York, 1953.
- (4) Karp, S., Meites, L., J. Am. Chem. Soc., 84, 906 (1962).
- (5) King, D. M., Bard, A. J. ibid, 87, 419 (1965).
- (6) Komyathy, J. C., Malloy, F., Elving, P. J., Anal. Chem., 24, 431 (1952).
- (7) Pennman, R. A., Audrieth, L. F., ibid, 20, 1058 (1948).

Table I  
POLAROGRAPHIC VALUES FOR SUBSTITUTED HYDRAZINES IN 0.1M NaOH.

Compound	$-E_{1/2}$ , v. <sup>a</sup>	$i_d$ , $\mu$ a
Hydrazine	0.5475	7.4
Monomethylhydrazine	0.6344	8.0
<u>n</u> -Propyl hydrazine	0.6891	6.0
<u>n</u> -Hexyl hydrazine	0.7907	1.7
1,1-Dimethyl hydrazine	0.6944	4.4
1,2-Dimethyl hydrazine	0.6978	2.7
1,2-Diisobutyl hydrazine	0.7566	4.5
Phenyl hydrazine	0.7516	4.9
Acetic hydrazide	0.6185	7.1
Diacetyl hydrazine	-	-

<sup>a</sup> vs. a saturated mercurous sulfate electrode.

Figure 1

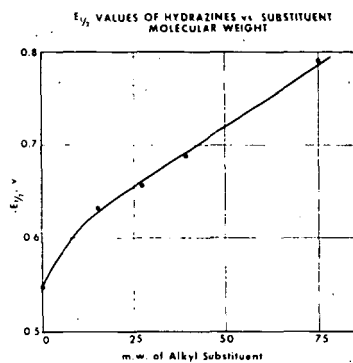
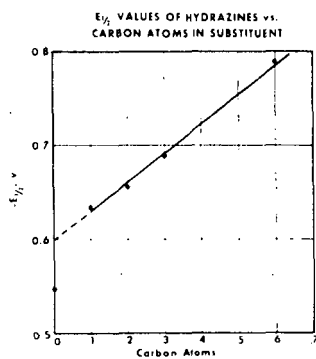


Figure 2



Voltammetric and Emf Measurements on the Nickel-Nickel(II)  
Couple in Molten Fluorides\*

D. L. Manning, Gleb Mamantov,\*\* H. W. Jenkins\*\*

Analytical Chemistry Division  
Oak Ridge National Laboratory  
Oak Ridge, Tennessee and

\*\*Chemistry Department, University of Tennessee,  
Knoxville, Tennessee

Extensive electrochemical investigations have been reported for molten salt systems in recent years.<sup>(1-3)</sup> From such work, valuable insight has been gained into the behavior of electroactive constituents in molten chloride and nitrate systems, and to a lesser degree, sulfate and phosphate melts. It appears that the electrochemistry of molten fluorides has been investigated least of all. The most probable reason for this lack of interest is the inability to use (on a long term basis) glass or quartz as insulators and container materials.

Interest in molten fluorides has increased immensely at the Oak Ridge National Laboratory due to their application as reactor fuels. As a result, considerable research is being conducted to characterize to a greater extent this class of molten salt systems. We are engaged in electroanalytical measurements in molten fluorides with the hope of adapting such techniques to in-line methods of analysis; this paper is concerned with the application of controlled-potential voltammetry and Emf measurements to the study of the Ni/Ni<sup>2+</sup> couple in molten LiF-NaF-KF (46.5-11.5-42 mole %) and LiF-BeF<sub>2</sub>-ZrF<sub>4</sub> (65.6-29.4-5.0 mole %). Nickel is usually encountered in molten fluorides as a corrosion product.

For the controlled-potential voltammetric studies, the molten fluoride, ~40 ml volume, is contained in a graphite cell (~2" dia x 4" long) which is then enclosed in a quartz jacket to maintain a vacuum or controlled atmosphere. The stationary dip type electrodes are inserted into the melt through the Swagelok compression fittings which are located on the cap of the quartz enclosure. To isolate the counter electrode, it is inserted into a porous graphite or thin walled boron nitride inner compartment of the cell. Usually the melt is maintained in an inert atmosphere. Provisions are made, however, to evacuate the cell whenever necessary. Disassembly of the cell, salt additions, etc. are always performed in a dry box.

A controlled-potential voltammeter, ORNL Model Q-1988, modified to measure cell currents to 5 milliamperes and to produce rates of voltage scan from 0.05 to 10 volts per minute was used for the voltammetric measurements. The potential of the pyrolytic graphite indicator electrode is measured versus a platinum quasi-reference electrode because at the time of the voltammetric work we did not have a practical reference electrode for molten fluoride systems.

In high-temperature melts, the transport process to the electrode is governed by both diffusion and convection. Convection is predominant at relatively slow scan rates (~50 m.v. per min.) with the result that the current-voltage curves at stationary electrodes are s-shaped. Such curves are analytically useful, however, because the limiting current is usually proportional to the concentration of electroactive species, but they are difficult or impossible to interpret theoretically.

To minimize convection and achieve conditions where diffusion is predominant, the current-voltage curves were recorded at scan rates of 1 to 10 volts per minute. Such curves are shown in Figure 1; in general, peak-shaped curves were obtained.

The equation for the peak current,  $i_p$ , for the reversible deposition of an insoluble substance at 500°C is  $i_p = 2.28 \times 10^5 n^{3/2} A D^{1/2} C v^{1/2}$  where  $i_p$  is peak current,  $\mu a$ ,  $n$  - electron change,  $A$  - electrode area,  $cm^2$ ,  $D$  - diffusion coefficient,  $C$  - concentration of diffusion species,  $mM$  and  $v$  is voltage scan, volts per sec. Plots of  $i_p$  versus  $v^{1/2}$  for nickel were linear at temperatures of 500, 570 and 600°C. The diffusion coefficient as calculated from the slope of the line at 500°C is approximately  $1 \times 10^{-8} cm^2/sec$ . From plots of  $\log D$  vs  $1/T$ , and the equation

$\log D = -E/2.3 RT + \log A$ , an activation energy ( $E$ ) of about 18 k cal/mole was calculated for the reduction of nickel in molten LiF-NaF-KF.

The analytical utility of the voltammetric approach to the determination of nickel in the molten state was demonstrated from the linear dependence of  $i_p$  on nickel concentration over the range studied, i.e. approximately 10 to 80 ppm.

Electromotive force measurements were carried out on the Ni/Ni<sup>+2</sup> couple in concentration type cells in molten fluorides to check for Nernstian reversibility and to ascertain the feasibility of utilizing the Ni/Ni<sup>+2</sup> couple as a high-temperature reference electrode for fluoride systems. The approach is similar in principle to utilization by Laitinen and Liu<sup>(4)</sup> of the Pt/Pt<sup>+2</sup> couple as a reference electrode in molten chlorides.

The apparatus used to contain the melt is shown in Figure 2. Essentially it is a small vacuum dry box (24" long, 20" deep and 15" high) which is outfitted with a furnace, vacuum and controlled atmosphere facilities and a moisture monitor. Utmost care is exercised to protect the molten fluorides from moisture contamination because of the affinity of the molten fluorides to moisture and the resultant precipitation of oxides. A schematic diagram of the cell and furnace assembly is shown in Figure 3. The melt (~400 ml) is contained in a graphite cell. A spiral nickel electrode, platinum stirrer, Pt-10% Rh thermocouple and the inner electrode compartment are positioned in the melt. The inner compartment of the cell is shown in Figure 4. It consists of a thin-walled boron nitride compartment which contains the same fluoride melt and a fixed concentration of dissolved NiF<sub>2</sub>. A nickel electrode is inserted into this compartment. Hot pressed boron nitride is an insulator in molten fluorides but is slowly penetrated by them. As a result of this effect, BN can be utilized to separate the two half-cells and yet achieve electrical contact because such contact is made when the BN becomes wetted by the melt. For molten LiF-NaF-KF, penetration of the BN (1/32" wall thickness) occurs within a day or so; however, it is much slower for LiF-BeF<sub>2</sub>-ZrF<sub>4</sub> melts. Approximately a week is required for the resistance through the BN to drop to ~1000 ohms or less.

With stirring, weighed portions of NiF<sub>2</sub> were added to the melt. After each addition, measurements were made and a sample withdrawn for nickel analysis. From the equation  $\Delta E = RT/2.3 nF \log X_1/X_2$  and plots of  $\Delta E$  versus  $\log X_{Ni}$ , as shown in Figure 5, it was demonstrated that the nickel system exhibits reasonable Nernstian behavior at 500°C. The concentration of nickel varied from approximately 10<sup>-5</sup> to 10<sup>-3</sup> mole fraction. From the standpoint of Nernstian reversibility, the nickel couple appears to be a good choice for a reference electrode in molten fluorides.

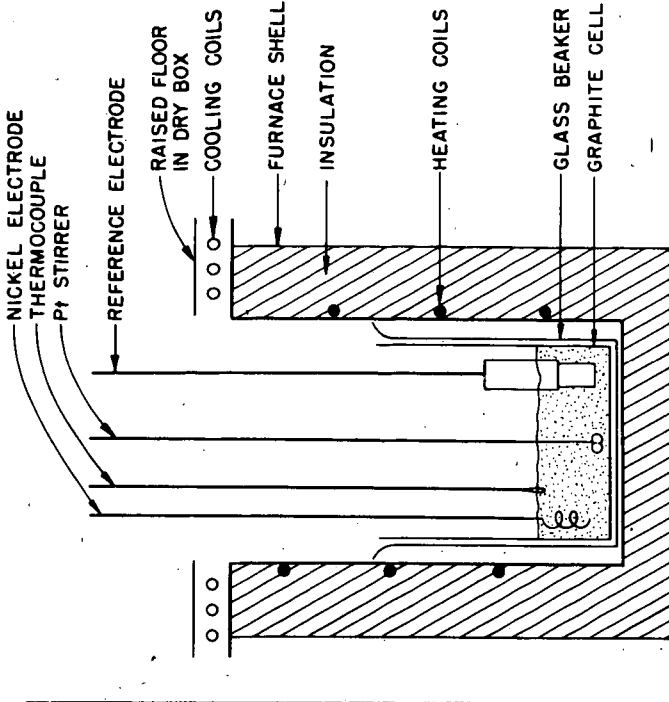
Stability studies conducted so far are encouraging. For a run in molten LiF-NaF-KF, the Emf remained constant to within  $\pm 2$  mv over a two-week period. These studies are continuing and longer stability tests are planned.

#### References

1. Delimarskii, Iu. K., Markov, B. F., "Electrochemistry of Fused Salts," Sigma Press, Washington, D. C., 1961.
2. Laitinen, H. A., Osteryoung, R. A., "Fused Salts," B. R. Sundheim, ed., McGraw-Hill, New York, 1964.
3. Liu, C. H., Johnson, K. E., Laitinen, H. A., "Molten Salt Chemistry," M. Blander, ed., Interscience, New York, 1964.
4. Laitinen, H. A., Liu, C. H., J. Am. Chem. Soc. 80, 1015 (1958).

\*Research sponsored by the U. S. Atomic Energy Commission under contract with the Union Carbide Corporation.

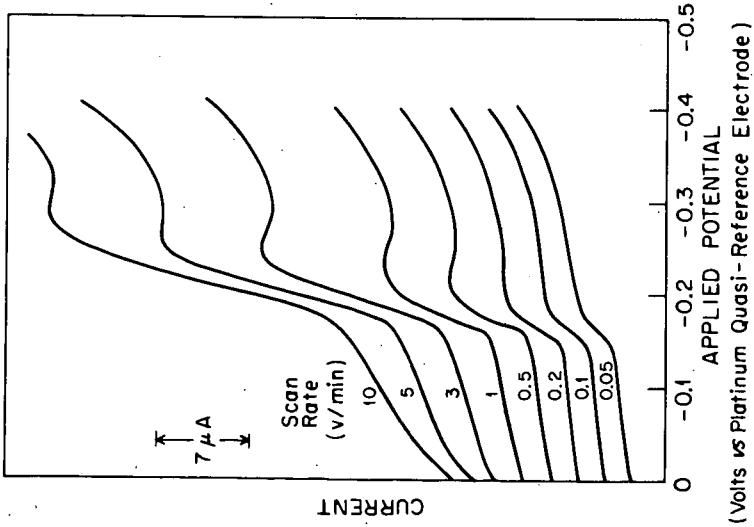
ORNL - DWG. 66 - 11928



Furnace and Cell Assembly.

Fig. 3

ORNL - DWG. 63 - 8003



Effect of Scan Rate on the Current-Voltage Curves for Nickel

LiF-NaF-KF, 500°C  
Nickel, 23 ppm

Fig. 1

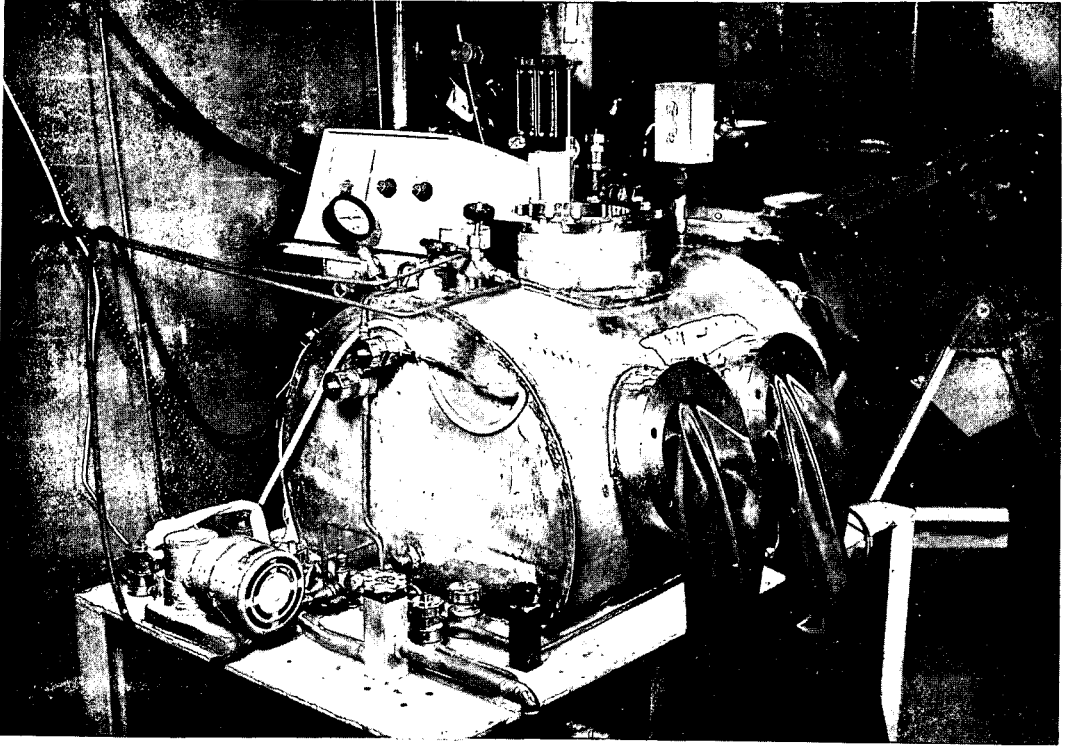
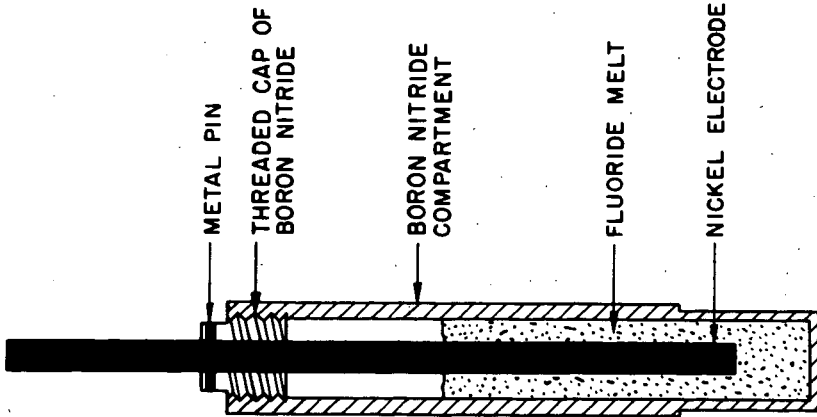
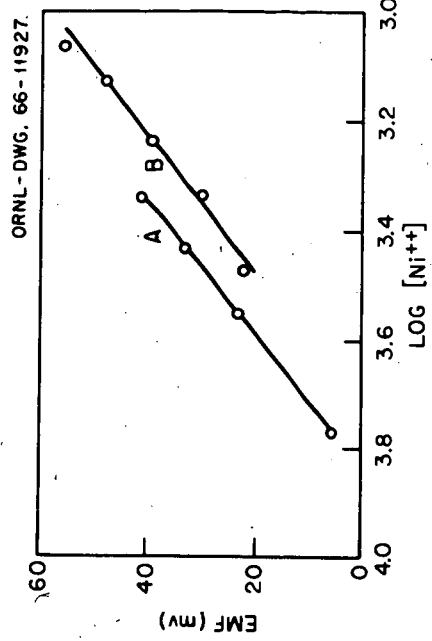


Fig. 2. Dry Box-Furnace Combination for Containing Fluoride Melts.



Nickel Electrode in Boron Nitride.



Nernstian Log Plots for Ni/Ni<sup>2+</sup> Couple in Molten Fluorides.  
 (A) LiF-NaF-KF (517°C) Slope 0.080; Theo. 0.078.  
 (B) LiF-BeF<sub>2</sub>-ZrF<sub>4</sub> (507°C) Slope 0.081; Theo. 0.077.

FIG. 5

Exchange Current Measurements on the Nickel-Nickel(II)  
Couple in Molten Fluorides\*

Gleb Mamantov, <sup>\*\*</sup> H. W. Jenkins, <sup>\*\*</sup> D. L. Manning

<sup>\*\*</sup>Chemistry Department, University of Tennessee,  
Knoxville, Tennessee

and  
Analytical Chemistry Division  
Oak Ridge National Laboratory  
Oak Ridge, Tennessee

We have been concerned with the development of a practical reference electrode for molten fluoride compositions of importance in nuclear technology.<sup>(1)</sup> In the course of this work it became desirable to obtain an additional quantitative measure of the reversibility of the electrode process  $\text{Ni(II)} + 2e \rightleftharpoons \text{Ni}$ . It was decided to use one of the relaxation methods,<sup>(2)</sup> since a fast charge-transfer was expected on the basis of available data on electrode kinetics in other molten salt solvents.<sup>(3)</sup> The voltage-step method of Vielstich and Delahay<sup>(4)</sup> was selected primarily due to the simplicity of instrumentation. This method has been employed previously for the determination of kinetic parameters in molten salts,<sup>(5)</sup> although the results obtained in that work have been questioned recently.<sup>(6)</sup> Molten fluorides are of great technological importance (Hall process, uses in nuclear technology as in the molten salt reactor<sup>(7)</sup> and the fluoride volatility process,<sup>(8)</sup> the plating of refractory metals<sup>(9)</sup>) however, relatively few electrode processes have been studied in these melts (for a partial summary see<sup>(10)</sup>). To our knowledge, the present work is the first attempt to apply a relaxation method to the study of a charge transfer process in molten fluorides.

### Experimental

To date the kinetics of the  $\text{Ni}^{+2} + 2e \rightleftharpoons \text{Ni}$  process have been studied in molten  $\text{LiF-BaF}_2\text{-ZrF}_4$  (65.6-29.4-5.0 mole %) at 497°C. Measurements in  $\text{LiF-NaF-KF}$  (46.5-11.5-42 mole %) are in progress. The melt is contained in a graphite crucible enclosed in a dry box equipped with a furnace. The experimental arrangement has been described.<sup>(1)</sup> The working electrode in this work was a nickel rod ( $A = 7.5 \times 10^{-3} \text{ cm}^2$ ) sheathed in hot-pressed boron nitride. The walls of the BN sheath were sufficiently thick ( $> 1/8''$ ), so that no penetration by the melt was observed during the duration of the experiment. The counter electrode was a large nickel spiral. The Ni(II) concentration in the melt was determined by chemical analysis.

The circuit for the voltage step method is essentially that of Laitinen, Tischer and Roe.<sup>(5)</sup> Two mercury relays (Clare HG 1002) were used to make sure that the short circuit between the electrodes is broken before applying the voltage step (usually 4 mv.). The oscilloscope (Tektronix 535A) is triggered by the signal obtained across the coil of one of the mercury relays. The signal across the precision measuring resistor (1, 5, or 10 ohms) was fed directly into the plug-in amplifier (Type D or Type CA) of the oscilloscope.

### Results and Discussion

The experimental current-time curve (total current,  $I_T$ ) and other calculated or extrapolated current functions described below, for the Ni(II) concentration of  $9.8 \times 10^{-3}$  moles/liter are shown in Fig. 1. We have followed the procedure used by Laitinen, Tischer and Roe,<sup>(5)</sup> except that the charging current,  $I_{CH}$ , curve was obtained by the extrapolation of the initial current values according to the equation,

$$I_{CH} = \frac{V}{R_T} \exp\left(-\frac{t}{R_T C d.l.}\right),$$

where  $R_T$  is the total resistance in the circuit and  $C_{d,1}$  is the differential double layer capacity. This conventional equation for the charging of a capacitor in series with a resistor was used previously<sup>(5)</sup> in molten salts. We have found that the initial current values when plotted against time on semilog paper result in a good linear plot;  $R_T$  values, calculated from the intercept, are of expected magnitude. Values of  $C_{d,1}$ , calculated from the slope and the estimated geometrical area of the working electrode, ranged from  $186 \mu\text{F}/\text{cm}^2$  to  $314 \mu\text{F}/\text{cm}^2$ . The double layer capacity increased with time. This is believed to have been caused by adsorption of impurities, diffusing from the boron nitride sheath as well as the melt. It was found that the presence of boron nitride definitely increases the double layer capacity. Additional experiments with unsheathed thin wire nickel electrodes are in progress. The method described above for the calculation of  $I_{CH}$  took into account the variation of  $C_{d,1}$  with time. Also shown in Fig. 1 is the difference of  $I_T$  and  $I_{CH}$ , which is the current due to the faradaic process (net faradaic current). The plot of the net faradaic current vs.  $t^{1/2}$  is shown in the bottom half of Fig. 1. Similarly to Laitinen et. al., we have extrapolated the linear portion to zero time and then transferred the extrapolation to the top graph. The procedure for the selection of the "effective zero time" was the same as used by Laitinen et. al.<sup>(5)</sup> The exchange current density was calculated from the value of current at the "effective zero time" using equation (2) in reference (5). Attempts to apply the corrections suggested by Oldham and Osteryoung,<sup>(6)</sup> resulted in continuously increasing values of the exchange current density, although our data obeyed the criteria (equations (17) and (19) reference (6)) proposed by Oldham and Osteryoung<sup>(6)</sup> for the presence of kinetic information. It is felt, therefore, that the values of  $i_0$  shown in Table 1, represent the lower limits of  $i_0$  at respective concentrations.

Table I

Exchange Current for Ni/Ni(II) in  $\text{LiF}-\text{BeF}_2-\text{ZrF}_4$   
(65.6-29.4-5.0 mole %) at  $497^\circ\text{C}$

Concentration of Ni(II), moles/liter	$i_0$ amp./cm <sup>2</sup>
$0.982 \times 10^{-2}$	$7.30 \times 10^{-2}$
$1.18 \times 10^{-2}$	$8.32 \times 10^{-2}$
$1.42 \times 10^{-2}$	$8.73 \times 10^{-2}$
$1.75 \times 10^{-2}$	$11.5 \times 10^{-2}$
$2.07 \times 10^{-2}$	$12.8 \times 10^{-2}$

From the plot of  $\log i_0$  vs.  $\log \text{Ni(II)}$  (Fig. 2), the transfer coefficient  $\alpha$  was calculated as 0.23 (the slope is  $1 - \alpha$ ). The standard rate constant,  $k^0$ , was found to be approximately  $3.2 \times 10^{-3}$  cm/sec, using the relationship  $i_0 = nFk^0 C_{\text{Ni(II)}}^{1-\alpha}$ .

#### References

1. Manning, D. L., Mamantov, G., and Jenkins, H. W., "Voltammetric and Emf Measurements on the Nickel-Nickel-Nickel(II) Couple in Molten Fluorides", submitted for presentation at the Symposium on Electrochemical Reactions in Solution, American Chemical Society Meeting, April 1967.
2. Delahay, P., in P. Delahay, ed., "Advances in Electrochemistry and Electrochemical Engineering", Vol. I, Interscience, New York, 1961.
3. Graves, A. D., Hills, G. J., and Inman, D., in "Advances in Electrochemistry and Electrochemical Engineering", Vol. IV, Interscience, New York, 1966.
4. Vielstich, W., and Delahay, P., J. Am. Chem. Soc., 79, 1874 (1957).

5. Laitinen, H. A., Tischer, R. P., and Roe, D. K., J. Electrochem. Soc., 107, 546 (1960).
6. Oldham, K. B., and Osteryoung, R. A., J. Electroanal. Chem., 11, 397 (1966).
7. Shaffer, J. H., et. al., U.S. At. Energy Comm. Rept. ORNL-3789, 99 (1965).
8. Milford, R. P., et. al., Ind. and Eng. Chem., 53, 357 (1961).
9. Senderoff, S. and Mellors, G. W., J. Electrochem. Soc., 113, 66 (1966).
10. Mamantov, G., and Manning, D. L., Anal. Chem., 38, 1494 (1966).

---

\*Research sponsored by the U.S. Atomic Energy Commission under contract with the Union Carbide Corporation.

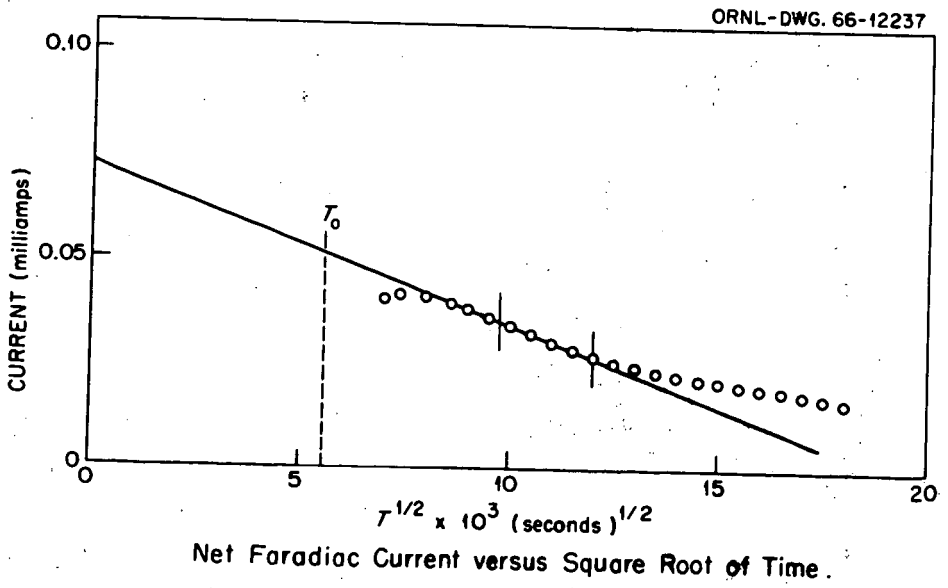
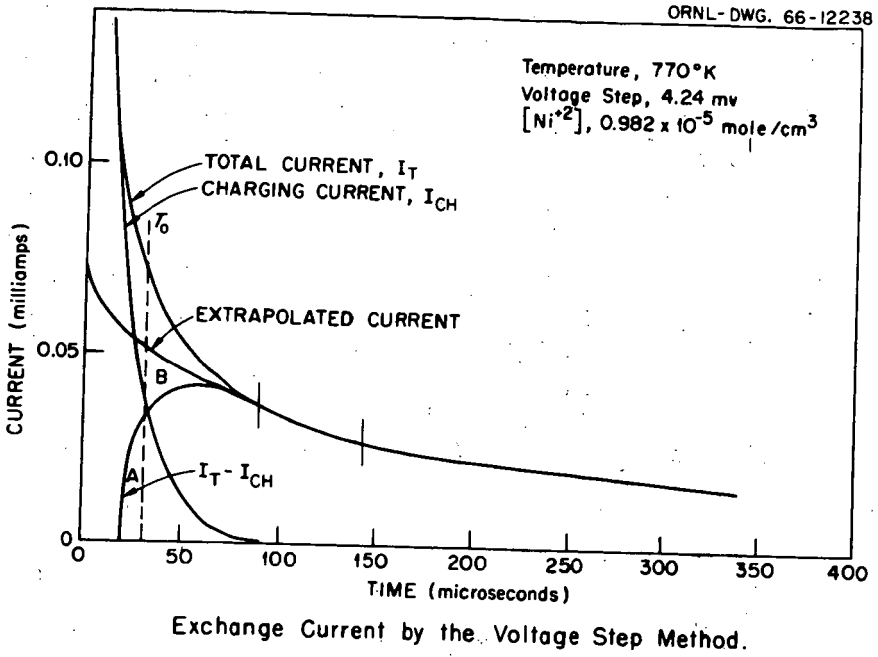
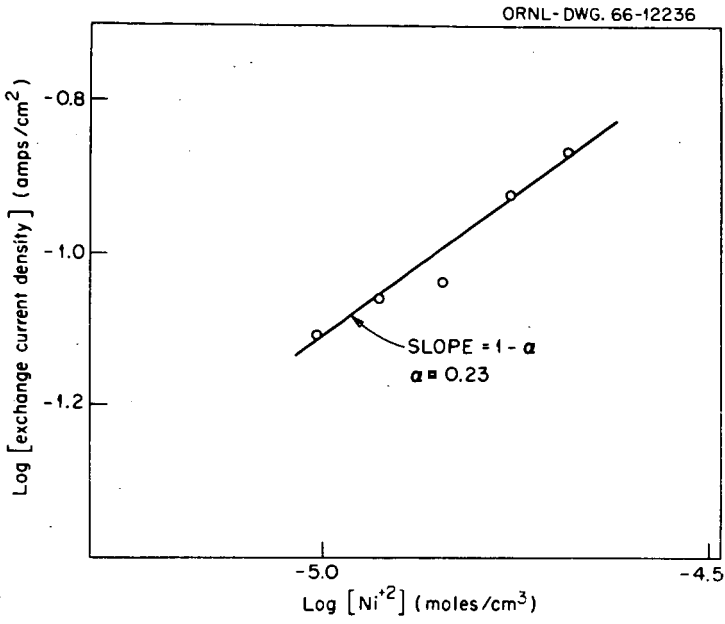


Figure 1



Determination of  $\alpha$  for the Ni/Ni<sup>2+</sup> Couple in Molten LiF-BeF<sub>2</sub>-ZrF<sub>4</sub>.

Figure 2

A Quantitative Study of Desorption in the Zinc(II)-Thiocyanate System  
 R. A. Osteryoung and J. H. Christie  
 North American Aviation Science Center, Thousand Oaks, California, 91360

Chronocoulometric studies had indicated that Zn(II), adsorbed at the Hg-solution interface in thiocyanate solutions, desorbs as the potential from which the experiment is initiated is made progressively more cathodic. As it was recognized that this "desorption effect" could have an appreciable effect on adsorption studies as carried out, for instance, by chronopotentiometric means, an effort was made to study this desorption quantitatively.

The amount of Zn(II) adsorbed in thiocyanate solutions decreases rather linearly as the initial potential in a chronocoulometric experiment is made more cathodic, until, at about -850 mV vs. SCE, there is no adsorbed Zn(II).<sup>1</sup> Biased chronopotentiometric measurements yield qualitatively similar results.<sup>2</sup> An initial potential can therefore be chosen at which a large amount of Zn(II) is adsorbed and complete desorption can be obtained just prior to the Zn(II) reduction wave (at about -1.0 V).

**Chronocoulometry.** An electrode, at an initial potential,  $E_0$ , at which an oxidant O is adsorbed to the extent of  $\Gamma$  moles/cm<sup>2</sup> or  $nF\Gamma$  coulombs/cm<sup>2</sup>, is stepped to a potential  $E_1$ , at which the species O desorbs. Only O is initially present in the solution and E is such that no faradaic current flows. We assume that the desorption is instantaneous and is complete. After a time,  $a$ , the potential is stepped to  $E_2$ , at which the reaction



takes place at its diffusion limited rate.<sup>3</sup> The charge-time behavior for  $t > a$  is given by

$$Q(t > a) = \frac{2nF\sqrt{D_0} C_0}{\sqrt{\pi}} \sqrt{t-a} + \frac{2}{\pi} nF\Gamma \tan^{-1} \sqrt{\frac{t-a}{a}} + \Delta q_{O_2} \quad (2)$$

where  $C_0$  is the bulk concentration of O and  $\Delta q_{O_2}$  is the charge consumed in charging the double layer from  $E_0$  to  $E_2$ . The other symbols have their usual electrochemical significance. The E-t function and a Q-t response are shown in Figure 1a. If  $a = 0$ , Equation 2 reduces to the familiar chronocoulometric equation for the presence of adsorption.<sup>3,4</sup>

$$Q(t) = \frac{2nF\sqrt{D_0} C_0}{\sqrt{\pi}} \sqrt{t} + nF\Gamma - \Delta q_{O_2} \quad (3)$$

Qualitatively, the longer the time,  $a$ , that the electrode potential is at  $E_1$ , the greater the curvature in a plot of Q vs.  $(t-a)^{1/2}$ .

**Chronopotentiometry.** An electrode, biased at  $E_0$ , at which the species O is adsorbed, has impressed on it a constant current density,  $i_0$ . It is assumed that desorption takes place linearly with time in the double layer charging region, that desorption is complete prior to any faradaic reaction occurring, and that the faradaic reaction starts immediately upon completion of the desorption. (Only one chronopotentiometric wave is observed.) The resulting  $i_0$ - $\tau$  behavior is given by

$$i_0 \sqrt{\tau-a} = \frac{nF\sqrt{D_0} C_0}{2} + \frac{nF\Gamma}{a} [\sqrt{\tau} - \sqrt{\tau-a}] \quad (4)$$

where  $a$  is the length of time taken for desorption and  $\tau$  is the time from the start of the experiment to the transition time. If we identify  $a$  with the time spent in the double layer charging region, then  $a \ll \tau$  and Equation 4 becomes

$$i_0 \tau = \frac{1}{2} nF\sqrt{D_0} C_0 \sqrt{\tau} + \frac{1}{2} nF\Gamma \quad (5)$$

This equation is the same, except for the factor of  $1/2$  in the second term on the right, as that derived by Lorenz<sup>5</sup> for the case in which a constant fraction of the applied current is consumed by reaction of the adsorbed species, the "constant current efficiency" model.

**Sweep-Step Chronocoulometry.** A potential sweep is applied from potential  $E_0$  to  $E_1$ , followed by a step from  $E_1$  to  $E_2$ . This routine was previously used to demonstrate the existence of the desorption effect.<sup>2</sup> We assume that the desorption takes place linearly with potential (or time) in the region  $E_0-E_1$  and that the desorption is just complete at  $E_1$  when the step to  $E_2$  is applied. The  $Q-t$  behavior is then given by

$$Q(t > a) = \frac{2nF\sqrt{D_0} C_0}{\sqrt{\pi}} \sqrt{t-a} + nF\Gamma \left\{ 1 + \frac{2}{\pi} \left[ \sqrt{\frac{t-a}{a}} - \frac{t}{a} \sin^{-1} \sqrt{\frac{a}{t}} \right] \right\} + \Delta q_{O2} \quad (6)$$

where  $a$  is the sweep time from  $E_0$  to  $E_1$ . The  $E-t$  function and a  $Q-t$  response are shown in Figure 1b. If  $a$  is zero, Equation 6 becomes the chronocoulometric Equation 3.

### Experimental

Potential step chronocoulometric measurements were carried out with the multi-channel analyzer data acquisition system previously described.<sup>6</sup>  $E_0$  for these experiments was chosen as -300 mV,  $E_1$  as -900 mV, and  $E_2$  as -1400 mV vs. SCE.

The chronopotentiometric data were analyzed according to the "reacts first," the "constant current efficiency," the "reacts last" (Lorenz), and the "equilibrium-linear isotherm" models using the weighted least-squares procedure described by Lingane.<sup>7</sup> For the purpose of this analysis, we estimated the relative error in the transition time determination to be  $\pm 5\%$ . The analysis according to the "reacts last" model failed to converge.

The potential sweep-step experiments were carried out using an updated version of a multi-purpose electrochemical instrument. The initial potential,  $E_0$ , was again chosen to be -300 mV. The instrument was adjusted so that the sweep was halted when a preset potential (-900 mV) was reached and a step to -1400 mV was then applied to the electrode. Sweep rates of 10 to 100 volts/second were used. The data were recorded on the multi-channel analyzer.

All solutions were prepared from reagent grade materials using triply distilled water.

A commercially available (Brinkman Instruments, Inc.) hanging mercury drop electrode was used. The electrode area was 0.032 cm<sup>2</sup>. All potentials were measured, and are reported, with respect to the saturated calomel electrode (SCE).

### Results

The values of  $nF\Gamma$ ,  $D_0$ , and  $\Delta q_{O2}$ , estimated by fitting the experimental chronocoulometric data to Equation 2, are shown in Table 1. The results seem to be little affected by variation in the delay time,  $a$ . The values of the diffusion coefficient are smaller than the infinite dilution value of  $7.2 \times 10^{-6}$  cm<sup>2</sup>/sec, but they are the same as the diffusion coefficient of Cd(II) in one formal supporting electrolyte. The infinite dilution value for the diffusion coefficient of Cd(II) is also  $7.2 \times 10^{-6}$  cm<sup>2</sup>/sec.

The values of  $nF\Gamma$  shown in Table 1 are in good agreement with the value of 31  $\mu\text{C}/\text{cm}^2$  determined in the same solution by double potential step chronocoulometry.

The values of  $\Delta q_{O2}$  shown in Table 1 are in good agreement with the "blank" value of 33  $\mu\text{C}/\text{cm}^2$  measured in the absence of Zn(II) and with the value of 31  $\mu\text{C}/\text{cm}^2$  determined by double potential step chronocoulometry.<sup>1</sup> A further check on  $\Delta q_{O2}$  may be made by using the relationship

$$\Delta q_{O2} = \Delta q_{O1} + \Delta q_{12} \quad (7)$$

Since no faradaic current flows at  $E_1$ ,  $\Delta q_{O1}$  will be the step change in charge when the potential is stepped from  $E_1$  to  $E_2$ ; since Zn(II) is not adsorbed at  $E_1$ , a chronocoulometric plot ( $Q$  vs.  $t^{1/2}$ ) for a potential step from  $E_1$  to  $E_2$  will have an intercept  $\Delta q_{12}$ . The sum of these two values (25.3 and 9.3  $\mu\text{C}/\text{cm}^2$ , respectively) is in good agreement with the values of  $\Delta q_{O2}$  shown in Table 1.

Figure 2 shows plots of  $Q$  vs.  $(t-a)^{1/2}$  for various delay times at -900 mV. (The double layer charging contribution has been removed by subtracting the appropriate value of  $\Delta q_0$  from the data for all experiments. Since, for a given value of  $(t-a)$ , less of the desorbed material is recovered the longer it had to diffuse away from the electrode, there is a downward trend as the delay time,  $a$ , is increased.

A similar comparison of the experimental sweep-step chronocoulometric data with the predictions of Equation 6 was made. In order to show the comparison as clearly as possible, the quantity plotted was the value of the term in Equation 6 due to the desorbed material,  $nF\Gamma\left\{1 + \frac{2}{\pi}\left[\frac{\sqrt{(t-a)}\sqrt{a}}{\sqrt{t}}\right] - \frac{t}{a}\sin^{-1}\sqrt{\frac{a}{t}}\right\}$ . The curves were calculated using  $nF\Gamma = 33 \mu\text{C/cm}^2$  and the various values of  $a$ . The points were calculated from the experimental data by subtracting  $\Delta q_{01}$  and the value of  $Q(t)$  (at  $t = t-a$ ) for a direct step from -900 to -1400 mV from the corresponding value of  $Q(t > a)$  for the sweep-step combination.

$$nF\Gamma \left\{ 1 + \frac{2}{\pi} \left[ \sqrt{\frac{t-a}{a}} - \frac{t}{a} \sin^{-1} \sqrt{\frac{a}{t}} \right] \right\} = Q(t > a)_{\text{sweep-step}} - Q(t-t-a)_{\text{step: -900 - -1400 - } \Delta q_{01}}$$

Less of the desorbed material is recovered, for a given value of  $(t-a)$ , the larger the value of  $a$ . Agreement between theory and experiment was good.

The chronopotentiometric results are given in Table 2 which presents the results of the analysis of the data according to the various chronopotentiometric models.

### Discussion

The good fit of the chronocoulometric data to Equation 2 (cf. Table 1) indicates that the desorption is rapid and is complete when the potential is stepped to -900 mV. This was expected since adsorption equilibrium is generally attained at the diffusion limited rate and no Zn(II) is adsorbed at equilibrium at -900 mV.

The assumption of a linear desorption between -300 and -900 mV in the sweep-step experiments was less well obeyed. Nevertheless, the fact that the experimental data is predicted semi-quantitatively by Equation 6 indicates that the desorption is approximately linear in time.

The chronopotentiometric results in Table 2 show that the "constant current efficiency" model gives one-half of the chronocoulometric value for  $nF\Gamma$ , but the data are not sufficiently precise to allow us to say that the data fits this model better than any of the others.

This work is further evidence for the unreliability of chronopotentiometry for the quantitative study of adsorption, since it both illustrates the need for large amounts of precise data, as pointed out by Lingane, and it demonstrates that there is yet another possible bias, i.e., desorption, which needs to be considered.

Even though the Zn(II)-thiocyanate system is unusual, in that complete desorption is obtained before the faradaic reaction starts, any desorption, or adsorption, in the double layer charging region must affect, to a greater or lesser extent, the value of  $nF\Gamma$  determined by fitting the data to any chronopotentiometric model and must invalidate any conclusion about the mechanism of the reaction of the adsorbed material. We are in accord with Lingane's conclusion that chronopotentiometry is of very limited value for the quantitative study of adsorption.

\* Symbols on Fig. 2 and the delay times are:  $\Delta$ , 0 (a single step from -300 to -1400 mV); o, 0.4125 msec;  $\circ$ , 6.600 msec;  $\bullet$ , 52.8 msec;  $\cdot$ ,  $\cdot$ , i.e., a single step from -900 to -1400 mV.

## References

1. R. L. Myers and R. A. Osteryoung, unpublished experiments, 1966.
2. J. H. Christie and R. A. Osteryoung, *Anal. Chem.*, **38**, 1620 (1966).
3. J. H. Christie, G. Lauer, and R. A. Osteryoung, *J. Electroanal. Chem.*, **7**, 60 (1964).
4. J. H. Christie, G. Lauer, R. A. Osteryoung, and F. C. Anson, *Anal. Chem.*, **35**, 1979 (1963).
5. W. Lorenz, *Z. Elektrochem.*, **59**, 730 (1955).
6. G. Lauer and R. A. Osteryoung, *Anal. Chem.*, **38**, 1137 (1966).
7. P. J. Lingane, *Anal. Chem.*, in press.
8. G. Lauer, H. Schlein, and R. A. Osteryoung, *Anal. Chem.*, **35**, 1789 (1963).

Table 1: Results of Analysis of Chronocoulometric Data According to Equation 2.

1.0 mF  $Zn(NO_3)_2$  in 0.5 F NaSCN + 0.5 F  $NaNO_3$

Delay Time m sec	$D \times 10^6$ $cm^2/sec$	$nF\Gamma$ $\mu C/cm^2$	$\Delta q_{0.02}$ $\mu C/cm^2$
0.4125	6.2	32.3	37.5
	6.2	33.4	37.5
1.6500	6.4	34.3	37.1
	6.6	35.5	37.2
3.3000	6.1	32.6	35.3
	6.4	36.2	35.1
6.6000	6.2	34.2	35.9
	6.1	33.0	35.2
13.2000	6.3	33.6	35.9
	6.0	33.3	35.0
26.4000	6.5	30.9	36.0
	6.5	31.9	35.5
52.8000	6.4	27.7	34.9
	6.3	27.1	34.2

Table 2: Results of Analysis of Chronopotentiometric Data According to Various Models

1.0 mF  $Zn(NO_3)_2$  in 0.5 F NaSCN + 0.5 F  $NaNO_3$

Model	$nF\Gamma$ $\mu C/cm^2$	$D \times 10^6$ $cm^2/sec$	$\chi^2/N-3$
"reacts first"	28.8	7.6	0.86
"reacts last"	failed to converge		
"constant current efficiency" <sup>(a)</sup>	17.0	7.4	0.76
"reacts last" (Lorenz)	8.2	5.6	0.63
"equilibrium-linear isotherm"	19.8	7.4	0.80

- (a) Equation 5 predicts fit to "constant current efficiency" model with  $nF\Gamma$  equal to one-half the true value.

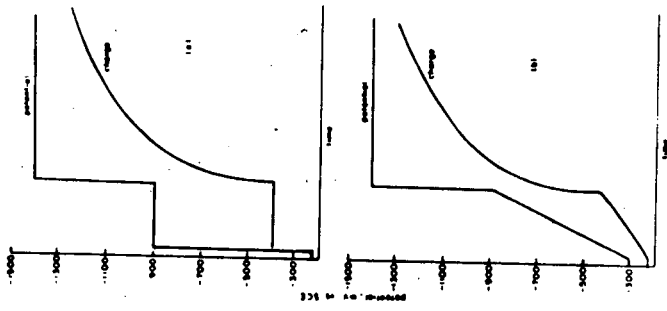


Fig 1

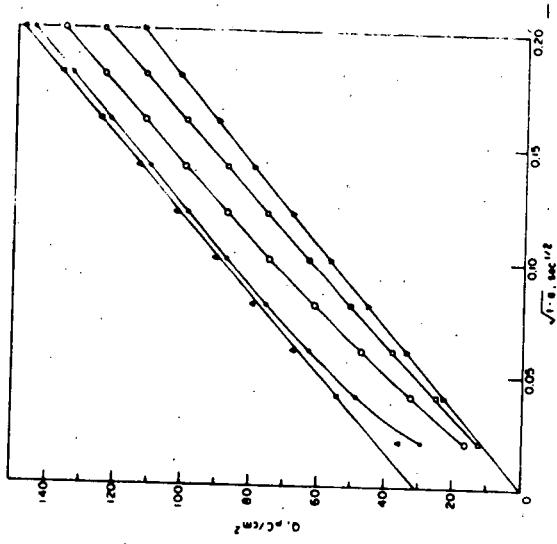


Fig 2

## Adsorption of Halides at the Mercury-Water Interface

John Lawrence, Roger Parsons (1)

Department of Physical Chemistry, The University, Bristol, 8. England

and Richard Payne

Air Force Cambridge Research Laboratories, L. G. Hanscom Field  
Bedford, MassachusettsIntroduction

Recent discussions (2, 3, 4) of the measurement of adsorption of ions at the mercury-water interface have suggested that discrepancies exist between the two principal methods of obtaining these results: electrocapillary measurements and capacity measurements. It has been suggested that some of the discrepancies are due to inevitable inaccuracies in the computation of data by the different routes and that some arise from essential differences in the quantities measured.

In order to assess the situation, existing capacity data on KCl (5) and KI (6), together with new data on KBr, are compared with electrocapillary data (7, 8, 9, 10) with particular attention to the accuracy with which the required data can be obtained.

Experimental

Measurements of the double layer capacity of mercury in aqueous KBr solution were made using the bridge previously described (11). The balance point was usually taken just after the eighth second on a drop whose total life was 10 - 12 seconds, but the capacity was checked over the range between the 4th and 10th second to ensure independence of the drop age. Similar checks were made in the frequency range from 600 c/s to 3 kc/s. No frequency dependence was observed and measurements were made at 1 kc/s. Reproducibility of capacities within a given run was 0.05% while that from one run to another was 0.15%. The flow rate of Hg (normally about  $0.2 \text{ mg s}^{-1}$ ) was determined by collecting mercury over an accurately timed (1 kc/s tuning fork + dekatron scaler) interval, drying and weighing. It remained constant within 0.2%. Thin-walled, tapering capillaries were drawn from 1 mm bore capillary tubing, selected by trial and siliconed by brief exposure to dichlorodimethyl silane vapor followed by wet nitrogen. The tip was then recut to ensure that the solution should wet the horizontal surface of the tip. The potential of the electrocapillary maximum was determined by the streaming electrode method (12) and was reproducible to 0.5 mV. All potentials were measured using a Croydon type P3 potentiometer and a Pye "Scalamp" 1400  $\Omega$  galvanometer. The reference electrode was a 0.1 M KCl calomel electrode joined to a reservoir containing 0.1 M KBr. This solution was then put in contact with the working solution of KBr, forming the junction in a tap. Both these liquid junctions were stable and potentials were reproducible to 0.1 mV. All measurements were made with the cell immersed in a water thermostat at 25°C. Mercury was purified by a wet process followed by three distillations in a Hulett still (13). Laboratory distilled water was redistilled from dilute alkaline permanganate in a still with special splash traps. BDH Analar KBr was dissolved in this water.

Results and Analysis

Measurements were made of the capacity and potential of the electro-

(1) At present Visiting Professor, Division of Chemistry and Chemical Engineering, California Institute of Technology, Pasadena, California 91109.

capillary maximum at ten concentrations of KBr from 0.005 M to 5 M. The interfacial tension at the electrocapillary maximum was obtained by plotting the experimental values found by Gouy (7) and by Devanathan and Peries (9) as a function of log activity and interpolating. Small differences exist between the two sets of electrocapillary data but it is unlikely that errors exceed  $0.2 \text{ dyn cm}^{-1}$  at concentrations below 1 M; at higher concentrations they may rise to  $0.5 \text{ dyn cm}^{-1}$ . The capacity-potential curves were integrated with the aid of a computer (Elliott 503) using a program written in Algol but similar to that described previously (14) in the first routine where values of the function  $\xi_{\pm} = \gamma + qE_{\pm}$  are calculated. Here  $\gamma$  is the interfacial tension,  $q$  the charge on the metal and  $E_{\pm}$  the potential of the mercury electrode with respect to an electrode reversible to the cation (+ subscripts) or anion (- subscripts). The new program further fits the pairs of values of  $\xi_{\pm}$  and log activity at a given value of  $q$  to a power series by the method of least squares. The ionic surface excesses are then calculated according to the appropriate form of the electrocapillary equation (15)

$$\left( \partial \xi_{\pm} / RT \partial \ln a_{\pm}^{\pm} \right)_q = -\Gamma_{\mp} = -q_{\mp} / z_{\mp} e$$

From the charge due to the cation, the program then uses Gouy-Chapman theory (16) to calculate outer Helmholtz potential ( $\phi_o$ ) and the charge in the diffuse layer due to the anion. Finally, the charge ( $q^+$ ) due to specifically adsorbed anions and the potential drop ( $\phi^{M-s}$ ) across the inner layer are computed. Some typical results are shown in Tables 1, 2, and 3.

#### Discussion

Direct comparison of the integrated capacity curves with the electrocapillary curves measured by Devanathan and Peries (9) is possible at 0.01, 0.1, and 1 M. Deviations between the two curves are never greater than  $1 \text{ dyn cm}^{-1}$  in the range  $+24$  to  $-18 \mu\text{C cm}^{-2}$  and more often of the order of  $0.1 \text{ dyn cm}^{-1}$ . Thus in this system there appears to be little doubt that the two methods of measurement are in agreement within experimental error. Similar conclusions may be drawn from a comparison of the integral of Grahame's data (5, 6) for 0.1 M and 1 M KCl, 0.015 M, 0.1 M and 1 M KI with electrocapillary results (7, 8, 9, 10). The integral of Grahame's capacity data for 0.1 M NaF agrees well with electrocapillary data on 0.1 M  $\text{NH}_4\text{F}$  obtained in Bristol by Dr. E. Dutkiewicz; small divergencies occur

on the anodic branch amounting to  $1.6 \text{ dyn cm}^{-1}$  at  $+10 \mu\text{C cm}^{-2}$ .

Agreement in dilute solutions of weakly adsorbed electrolytes is poorer, as already mentioned (14, 4) with  $\text{H}_2\text{PO}_4^-$  and  $\text{Cl}^-$ . The appearance of the diffuse layer minimum in the capacity curve is an indication of conditions under which such disagreement may be expected. In the case of  $\text{H}_2\text{PO}_4^-$ , where the disagreement is large, evidence was presented (14) supporting the proposal that the electrocapillary data is in error under these conditions.

Comparison of charge-potential curves derived from the two types of measurement confirms that they are usually in good agreement within the errors to be expected from graphical differentiation of electrocapillary curves. This accuracy will depend on the spacing of experimental points; 50 mV intervals have been usual in recent studies (9, 14, 17). Comparison of the present results with those of Devanathan and Peries (9) suggests that the general trend is in good agreement though a scatter of  $1 \mu\text{C cm}^{-2}$  in individual points is fairly frequent. At the far anodic end when the charge is greater than  $20 \mu\text{C cm}^{-2}$  and both the electrocapillary curve and the capacity curve are very steep, the errors may be much larger. Electrocapillary curves were also differentiated using a computer following a procedure based on an unpublished suggestion by D. C. Grahame. From the set of  $\gamma$ -E points a new set of points  $y$ -E was computed where  $y = \gamma + q^*E$ ,  $q^*$  being a constant. The curve  $y$ -E now has a maximum at the value of  $E$  for which  $q^*$  is the slope of the original  $\gamma$ -E curve. Thus, by repeating this procedure a set of values of  $E$  corresponding to given values of  $q^*$  may be found. The value of  $y$  at the maximum of the  $y$ -E curve is, of course,

the value of  $\xi$  corresponding to  $q^*$  and the fact that the  $\gamma$ -E curve has a flat maximum shows that  $\xi$  may be obtained with accuracy comparable to the original values of  $\gamma$ . In fact, the calculation of  $\xi$  does not depend upon an accurate differentiation of the electrocapillary curve in contrast to the remark of Devanathan and Tilak (3). This procedure is thus excellent for converting from  $\gamma$  to  $\xi$  but does not produce charge-potential curves of any greater accuracy than those from graphical differentiation.

Direct comparison of twice differentiated electrocapillary curves with capacity curves again confirms qualitatively the agreement between the two types of measurement, but the inaccuracies introduced by differentiation are too great to allow more quantitative conclusions.

The most important information obtained from capacity and electrocapillary measurements concerns the ionic composition of the double layer. This is obtained by the application of Gibbs adsorption equation in one form or another and necessarily involves a differentiation step, although this may be carried out by fitting integrated theoretical isotherms to the experimental data (15) and then differentiating analytically. Such a procedure has particular advantages if the isotherm constants are independent of charge, but there is a risk of imposing this condition on a set of data since the surface-pressure curve is not very sensitive to variations in isotherm constants. A more direct procedure might therefore have advantages. The computer program described above is an attempt to solve this problem in a simple way. In fitting a polynomial to the  $\xi_{\pm} - \ln a_{\pm}$  points different degrees of polynomial were examined. High-order polynomials produce results that are too sensitive to experimental error and are consequently meaningless. The criterion adopted was that of comparing the results of an  $n$ -th order fits with that of an  $(n + 1)$ th order fit. Best agreement was obtained when  $n = 3$ . Even so, the end points produced large variations, the results being less plausible for the 4th than for the 3rd order fit. It is, therefore, recommended that a 3rd order polynomial provides the most satisfactory simple route to the differentiation of  $\xi_{\pm} - \ln a_{\pm}$  curves. Agreement with graphical differentiation for the KBr system was found to be within  $0.3 \mu\text{C cm}^{-2}$  except at extreme concentrations or charges. The curves of  $q^{\pm}$  against  $q$  can be compared directly with the results of Grahame and Söderberg (18) at 0.1 M and of Devanathan and Peries (9) at 0.01 M, 0.1 M, and 1 M. With the former no deviation is greater than  $0.7 \mu\text{C cm}^{-2}$  while with the latter discrepancies of greater than  $1 \mu\text{C cm}^{-2}$  are found undoubtedly as a result of errors introduced by graphical differentiation to obtain both  $q^{\pm}$  and  $q$ .

As a further check the data of Grahame (6) for aqueous KI was put through the computer program using integration constants based on electrocapillary data (7, 8, 9, 10). In this case the agreement between the 3rd and 4th order fits was much better and at the lower concentrations good agreement with the published data (6) was obtained. The results obtained from this system are undoubtedly better primarily because the concentration points are more closely spaced. Grahame (6) measured capacities at 17 concentrations between 0.015 M and 1.2 M; that is, over 8 points per decade. The present KBr results are based on 3 points per decade and must be correspondingly less accurate. This must be considered as the main weakness of much recent work on the electrical double layer (14, 19) especially that based on 2 points per decade (9, 17).

At concentrations of the order of 1 M and higher the computed KI results differ from the published data (6) owing to the effect of the thickness of the inner layer previously discussed (5). In spite of contrary assertions (2) there seems good reason to suppose that the correction for this effect is charge dependent (14). Since no way of measuring this effect in the presence of specific adsorption has been devised, values of  $q^{\pm}$  for solutions of higher concentrations are subject to error from this cause as well as from defects in diffuse layer theory.

Data from the dilute solutions calculated from capacity measurements with the aid of electrocapillary integration constants also appear to deviate by a micro-coulomb or two from the expected values at negative charge, as

commented upon recently (19). It is possible that this may be the result of the slow transport of ions to the double layer (20, 21) but a clear proof that this is the cause is at present lacking.

We should like to thank Dr. W. R. Fawcett for assistance with the differentiation program, the University of Bristol Computer Unit for computing facilities, and the Somerset L. E. A. for a grant to J. L. during the course of this work.

#### References

- (2) M. A. V. Devanathan and S. G. Canagaratna, Electrochim. Acta, 8, 77 (1963).
- (3) M. A. V. Dēvanathan and B. V. K. S. R. A. Tilak, Chem. Rev., 65, 635, (1965).
- (4) J. O'M. Bockris, K. Müller, H. Wroblowa, and Z. Kovac, J. Electroanal. Chem., 10, 416 (1965).
- (5) D. C. Grahame and R. Parsons, J. Am. Chem. Soc., 83, 1291 (1961).
- (6) D. C. Grahame, J. Am. Chem. Soc., 80, 4201 (1958).
- (7) G. Gouy, Ann. Chim. Physique, (7) 29, 145 (1903).
- (8) O. A. Esin and B. Markov, Acta Physiochim. U. R. S. S., 10, 373 (1939).
- (9) M. A. V. Devanathan and P. Peries, Trans. Faraday Soc., 50, 1236 (1954).
- (10) W. Anderson and R. Parsons, Proc. II and Internatl. Congress Surface Activity, Butterwatts, London, 1957.
- (11) G. J. Hills and R. Payne, Trans. Faraday Soc., 61, 316 (1965).
- (12) D. C. Grahame, R. P. Larsen, and M. A. Poth, J. Am. Chem. Soc., 71, 2978 (1949).
- (13) G. A. Hulett and H. D. Minchin, Phys. Rev., 31, 388 (1905).
- (14) R. Parsons and F. G. R. Zobel, J. Electroanal. Chem., 9, 333 (1965).
- (15) R. Parsons, Trans. Faraday Soc., 51, 1518 (1955).
- (16) D. C. Grahame, Chem. Rev., 41, 441 (1947).
- (17) H. Wroblowa, Z. Kovac, and J. O'M. Bockris, Trans. Faraday Soc., 61, 1523 (1965).
- (18) D. C. Grahame and B. Soderberg, J. Chem. Phys., 22, 449 (1954).
- (19) R. Payne, J. Electrochim. Soc., 113, 999 (1966).
- (20) D. C. Grahame, J. Am. Chem. Soc., 68, 301 (1946).
- (21) G. C. Barker, J. Electroanal. Chem., 12, 495 (1966).

Table 1

0.01 M KBr in water at 25°C

q	-E	C	q <sub>+</sub>	q <sub>-</sub> <sup>1</sup>	φ <sub>2</sub>	φ <sup>M-2</sup>	γ
μC cm <sup>-2</sup>	V	μF cm <sup>-2</sup>	μC cm <sup>-2</sup>	μC cm <sup>-2</sup>	mV	mV	dyn cm <sup>-1</sup>
-18	1.592	17.59	16.0	1.4	-172	-958	329.8
-16	1.475	16.65	14.0	1.5	-165	-848	349.7
-14	1.353	16.04	12.1	1.4	-158	-733	368.0
-12	1.227	15.90	10.2	1.3	-150	-616	384.3
-10	1.102	16.16	8.3	1.1	-140	-500	398.1
-8	0.982	17.04	6.5	1.0	-128	-392	408.9
-6	0.868	18.24	4.5	1.0	-111	-295	416.9
-4	0.761	18.88	2.5	1.0	-86	-213	422.3
-2	0.656	19.76	+ 0.8	+ 0.8	- 46	-149	425.4
0	0.572	29.08	0.0	0.0	0	-105	426.3
+ 2	0.512	37.75	- 0.1	- 1.8	+ 8	- 58	425.7
4	0.463	42.74	+ 0.1	- 4.1	- 5	+ 4	424.3
6	0.417	43.75	0.3	- 6.6	- 23	69	422.0
8	0.371	45.09	0.7	- 9.0	- 41	131	418.8
10	0.328	46.40	1.2	-11.5	- 56	190	414.9
12	0.286	51.51	1.7	-14.1	- 69	245	410.32
14	0.250	60.00	2.2	-16.7	- 81	293	405.6
16	0.220	72.20	2.9	-19.4	- 92	334	401.1
18	0.191	95.88	3.5	-22.0	-100	371	396.3
20	0.173	130.9	4.0	-24.5	-106	395	392.9
22	0.160	165.1	4.6	-27.2	-112	415	390.0
24	0.144	231.0	5.2	-29.7	-118	436	386.7

Table 2

1 M KBr in water at 25 °C							
q	-E	C	q <sub>+</sub>	q <sub>1</sub> <sup>-</sup>	φ <sub>2</sub>	φ <sup>M-2</sup>	γ
μC cm <sup>-2</sup>	V	μF cm <sup>-2</sup>	μC cm <sup>-2</sup>	μC cm <sup>-2</sup>	mV	mV	dyn cm <sup>-1</sup>
-18	1.488	18.09	13.0	0.9	-60	-969	334.0
-16	1.373	17.09	11.3	0.9	-55	-859	353.4
-14	1.254	16.71	9.7	0.6	-50	-746	371.2
-12	1.136	17.13	8.4	0.2	-46	-632	386.7
-10	1.025	19.28	7.4	-0.7	-42	-524	398.9
-8	0.931	24.10	7.0	-2.2	-40	-432	407.4
-6	0.858	30.94	7.1	-4.3	-41	-359	412.5
-4	0.799	37.50	7.6	-6.9	-43	-298	415.45
-2	0.750	43.16	8.4	-9.8	-46	-246	417.0
0	0.705	45.87	9.3	-12.8	-49	-198	417.4
+2	0.663	48.05	10.1	-15.8	-52	-153	417.0
+4	0.621	48.80	10.9	-18.7	-54	-109	415.7
+6	0.581	49.56	11.7	-21.6	-56	-66	413.7
+8	0.540	48.48	12.5	-24.5	-59	-23	410.9
+10	0.499	49.63	13.3	-27.4	-61	+20	407.2
+12	0.460	53.67	14.1	-30.2	-63	61	402.9
+14	0.425	60.42	14.9	-33.1	-65	98	398.3
16	0.394	69.34	15.6	-35.8	-67	131	393.6
18	0.367	80.57	16.3	-38.6	-68	160	389.1
20	0.343	94.77	17.0	-41.4	-70	186	384.5
22	0.323	113.1	17.7	-44.1	-71	206	380.5
24	0.307	132.2	18.3	-46.7	-73	224	376.7

Table 3

0.1 M KBr in water at 25 °C							
q	-E	C	q <sub>+</sub>	q <sub>1</sub> <sup>-</sup>	φ <sub>2</sub>	φ <sup>M-2</sup>	γ
μC cm <sup>-2</sup>	V	μF cm <sup>-2</sup>	μC cm <sup>-2</sup>	μC cm <sup>-2</sup>	mV	mV	dyn cm <sup>-1</sup>
-18	1.543	17.79	17.6	-1.3	-121	-962	331.7
-16	1.428	16.87	15.5	-1.1	-115	-853	351.4
-14	1.307	16.24	13.3	-0.9	-108	-739	369.5
-12	1.182	16.03	11.0	-0.6	-100	-623	385.6
-10	1.059	16.40	8.9	-0.4	-90	-508	399.3
-8	0.940	17.57	6.9	-0.3	-80	-400	409.9
-6	0.833	20.17	5.3	-0.7	-69	-304	417.4
-4	0.745	25.87	4.2	-1.5	-61	-223	421.9
-2	0.678	33.90	3.8	-3.0	-57	-160	424.0
0	0.624	41.56	3.8	-5.1	-58	-107	424.5
+2	0.578	45.58	4.1	-7.4	-60	-59	424.1
+4	0.536	47.56	4.5	-9.8	-63	-13	422.8
+6	0.494	47.87	4.9	-12.2	-66	+33	420.7
+8	0.452	48.20	5.4	-14.8	-70	78	417.8
+10	0.411	50.29	5.9	-17.3	-74	122	414.1
+12	0.373	56.50	6.5	-14.9	-77	164	404.9
14	0.341	65.56	7.0	-22.5	-81	200	405.7
16	0.312	73.86	7.6	-25.1	-84	232	401.4
18	0.285	87.43	8.2	-27.7	-87	262	396.9
20	0.265	105.7	8.8	-30.3	-90	285	392.9
22	0.242	144.4	9.3	-32.9	-92	310	388.5
24	0.230	189.5	9.8	-35.4	-95	324	385.7

## THE SPECIFIC ADSORPTION OF ALKALI METAL IONS AT THE MERCURY-FORMAMIDE INTERFACE

George H. Nancollas and David S. Reid.

State University of New York at Buffalo, Buffalo, N.Y. 14214.

### Introduction

The possibility of specific adsorption of the alkali metal ions at a mercury-solution interface has been investigated by a number of workers, but as yet no firm conclusions have been reached. Most of the work has been done in aqueous solutions, for which there are now abundant data. In a recent paper we reported results of measurements of the surface excesses of potassium and chloride ions at the interface between a mercury electrode and a solution of potassium chloride in formamide which indicated that specific adsorption of the potassium ion was occurring. In an attempt to clarify the situation, the surface excesses of anion and cation have been determined from electrocapillary and double layer capacity measurements for a mercury electrode in contact with a cesium chloride solution in formamide. The results for both the potassium chloride and cesium chloride solutions have been subjected to a components of charge analysis.

### Experimental

The procedures used for the purification of reagents and preparation of solutions have been described previously. Interfacial tensions were measured as a function of applied potential, using a capillary electrometer<sup>1</sup> in 0.050, 0.0889, 0.100 and 0.179 molal solutions of cesium chloride in formamide. The reference of potential was a silver-silver chloride electrode in the same solutions, and interfacial tensions were reproducible to  $\pm 0.2$  erg cm<sup>-2</sup> except at the most cathodic potentials, where the agreement was  $\pm 0.5$  erg cm<sup>-2</sup>.

### Results

Figure 1 shows the variation of interfacial tension,  $\gamma$ , with applied potential for the concentrations of cesium chloride studied. From the variation of interfacial tension with chemical potential,  $\mu$ , at constant potential  $E_0$ , the surface excesses of cesium and chloride ions can be evaluated. This has been done for 0.100 m cesium chloride, following the procedure outlined by Bockris et al.<sup>2</sup> The magnitude of the electrode charge at a given potential was obtained from previously reported capacitance data<sup>1</sup>. Figure 2 shows a plot of the surface excesses  $z \pm F \Gamma \pm$  as a function of potential for 0.100 m cesium chloride and for comparison the surface excesses in 0.071 m potassium chloride<sup>1</sup>.

## Discussion

The form of the surface excess plots in figure 2 indicates that specific adsorption of cations is occurring in the far cathodic region in both potassium and cesium chloride solutions. The surface excess of anions reaches a minimum value and then increases as the potential becomes more cathodic.

Payne<sup>3</sup> has shown that iodide ions are not specifically adsorbed at electrode charges more cathodic than  $-10 \mu\text{coul.cm}^{-2}$ . Since the chloride ion would be expected to be specifically adsorbed to a smaller extent than iodide, it is reasonable to assume that beyond  $-1.2 \text{ v}$ , at which the electrode charge is approximately  $-13 \mu\text{coul.cm}^{-2}$ , there is no specific adsorption of chloride ions. In this region, therefore, the charge due to specifically adsorbed cations,  $q_+^1$ , can be calculated from the relationships

$$z_- F \Gamma_- = -q_-^{2-s} \quad (\text{a})$$

$$q_-^{2-s} = -A(e^{19.46 \phi_2} - 1) \quad (\text{b})$$

$$q_+^{2-s} = A(e^{-19.46 \phi_1} - 1) \quad (\text{c})$$

$$q_+^1 = z_+ F \Gamma_+ - q_+^{2-s} \quad (\text{d})$$

where the symbols have their usual meanings. In both potassium chloride and cesium chloride, a plot of  $q_+^1$  vs  $E_-$  was linear, and similar linear relationships involving  $q_-^1$  have been obtained in aqueous solutions for specifically adsorbed anions<sup>4,5</sup>. It is reasonable to assume that this linear relationship in formamide solution will hold so long as there is no anionic specific adsorption. Extrapolation to lower potentials gives values of  $q_+^1$ , from which  $q_-^1$  can be calculated by means of the following relationships.

$$q_+^{2-s} = z_+ F \Gamma_+ - q_+^1 \quad (\text{e})$$

$$q_-^1 = z_- F \Gamma_- - q_-^{2-s} \quad (\text{f})$$

together with (b) and (c) above.

The results of this calculation, figure 3, show that  $q_-^1$ , the anionic specific adsorption, is zero at potentials more cathodic than  $-0.9 \text{ v}$ . When  $q_-^1$  has a negative value, corresponding to specifically adsorbed anion, it is not possible to assign any more than qualitative importance to the results. At the present time there is no way of analysing for simultaneous specific adsorption of both anions and cations.

In the region where the anion specific adsorption is zero, the amount of specific adsorption appears essentially equal for both potassium and cesium ion. The extent of specific adsorption occurring at the cathodic extreme is worthy of note, and it is interesting to compare this with previous results. Payne<sup>3</sup> found no specific adsorption of cation to occur in solutions of potassium iodide in formamide. Recent surface excess results, however, in sodium and cesium chloride solutions in formamide, obtained by Damaskin<sup>6</sup>, while slightly lower than the present data, lead to similarly large values of the cation specific adsorption.

The amount of cation specific adsorption occurring at a given cathodic potential appears to be constant for the potassium, cesium and sodium ions, and probably also for the rubidium ion. At first sight this is difficult to understand, but by considering the behaviour of these ions in water and in formamide we can rationalise the observation. Somsen and Coops<sup>7</sup> have measured the heats of solution of the alkali halides in formamide, and calculated  $\Delta H^{\circ}_{sol}$ , the heat of solution at infinite dilution, in each case. Comparison of these  $\Delta H^{\circ}_{sol}$  values with similar values obtained for the solution of the alkali halides in water shows that  $[\Delta H^{\circ}_{sol}(H_2O) - \Delta H^{\circ}_{sol}(HCONH_2)]$  is a constant for each series of salts of the four alkali metals K, Na, Rb, Cs with a given halide ion. Using Van Eck's approach to the solvation of ions<sup>8</sup>, this has been explained as being due to the constancy of the term  $(\Delta H_s + \Delta H_c)$  for all four cations in each solvent where symbols have the same meaning as in (7). If we accept Grahame's<sup>9</sup> suggestion that specific adsorption can be considered as solvation of the ion by mercury, a solvent of infinite dielectric constant, then if all four cations are desolvated to the same extent the enthalpy change on specific adsorption would be constant and given by

$$\begin{aligned} -\Delta H &= k (\Delta H_s^f - \Delta H_s^m) \\ &= k (\Delta H_c^f + \Delta H_{nc}^f + \Delta H_h^f - \Delta H_{nc}^m - \Delta H_h^m - \Delta H_c^m) \\ &= k (\Delta H_c^f - \Delta H_c^m + \text{constant}) \end{aligned}$$

In this equation  $\Delta H_s$  is the ionic enthalpy<sub>c</sub> of solvation, f and m refer to formamide and mercury respectively, and the value of k is a measure of the extent of desolvation, k = 1 indicating complete desolvation.  $-\Delta H_c$  for inert gas-type cations has been shown to be equal to the sum of the ionisation potential and the electron affinity of the corresponding metal ions in both water and formamide. The same is probably also true for mercury, and so  $-\Delta H = \text{constant}$ , since  $\Delta H_c^f - \Delta H_c^m = 0$ . It is reasonable to assume a small or constant entropy of specific adsorption, since we have considered all the cations to be desolvated to the same extent. This would mean that the free energy of specific adsorption would be constant, resulting in an equivalent amount of specific adsorption in each case.

Extending this approach to the halide salts of a given cation,  $[\Delta H^{\circ}_{sol}(H_2O) - \Delta H^{\circ}_{sol}(HCONH_2)]$  increases in the order  $Cl^- < Br^- < I^-$ .

Since the anions are of similar size,  $\Delta H_{nc} + \Delta H_p$  will again be constant in each solvent, and the increase reflects an increase in  $(\Delta H_C^w - \Delta H_C^f)$  along the series. It is reasonable to assume that  $(\Delta H_C^f - \Delta H_C^m)$  will show a similar increase since in each case we are going from the solvent of lower dielectric constant to the solvent of higher dielectric constant.  $-\Delta H (= \Delta H_C^f - \Delta H_C^m + \text{constant})$  will increase in going from chloride to iodide and the free energy of specific adsorption can be expected to follow the same trend, resulting in the observed increase in specific adsorption.

Similar arguments can be advanced for the mercury electrode in aqueous systems, so that we would expect  
 1) equality of cation specific adsorption.  
 2) an increase in specific adsorption along the series  $\text{Cl}^-$ ,  $\text{Br}^-$ ,  $\text{I}^-$ .  
 The latter is in accordance with the known behaviour of these anions at the mercury-water interface.

#### References.

1. Nancollas, G.H., Reid, D.S., and Vincent C.A., *J. Phys. Chem.*, **70**, 3300, (1966).
2. Bockris, J.O'M., Muller, K., Wroblowa, H., and Kovac, Z., *J. Electroanal. Chem.* **10**, 416, (1965).
3. Payne, R., *J. Chem. Phys.* **42**, 3371, (1965).
4. Mott, J.F., and Watts-Tobin, R.J., *Electrochim. Acta*, **4**, 79, (1961).
5. Devanathan, M.A.V. and Peries, P., *Trans. Faraday Soc.*, **50**, 236, (1954).
6. Damaskin, B.B., Ivanova R.V., and Survila, A.A., *Elektrokhimiya*, **1**, 767, (1965).
7. Somsen, G., and Coops, J., *Rec. Trav. Chim.*, **84**, 985, (1965).
8. van Panthaleon van Eck, C.L., Thesis, Leiden 1958.
9. Grahame, D.C., *J. Electrochem. Soc.* **98**, 343, (1951).

**Fig.1.**  $\gamma$  as a function of  $E_-$  for cesium chloride, (1) 0.050 m; (2) 0.0889 and 0.100 m; (3) 0.179 m.

**Fig.2.** Surface excesses. (1)  $K^+$  and  $Cs^+$ ; (2)  $Cl^-$

**Fig.3.**  $q_+^1$  as a function of  $E_-$  for cesium chloride. (1)  $q_+^1$ ; (2)  $q_-^1$

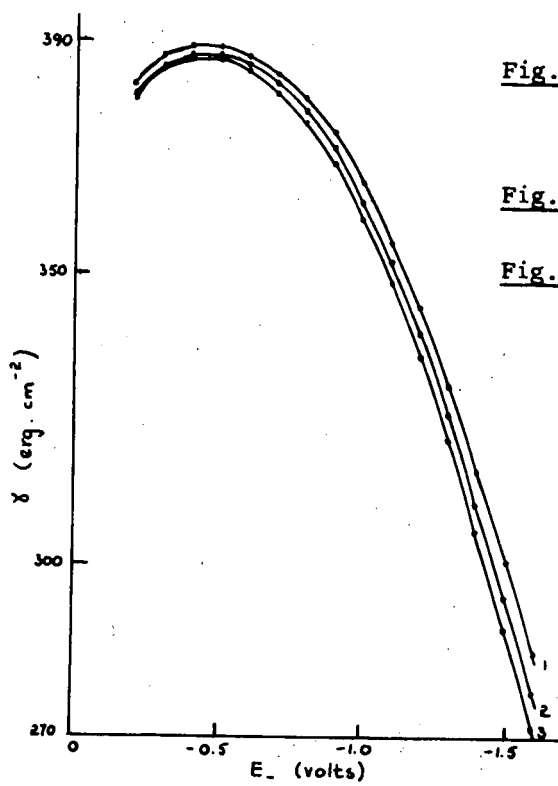


**Fig.1.**

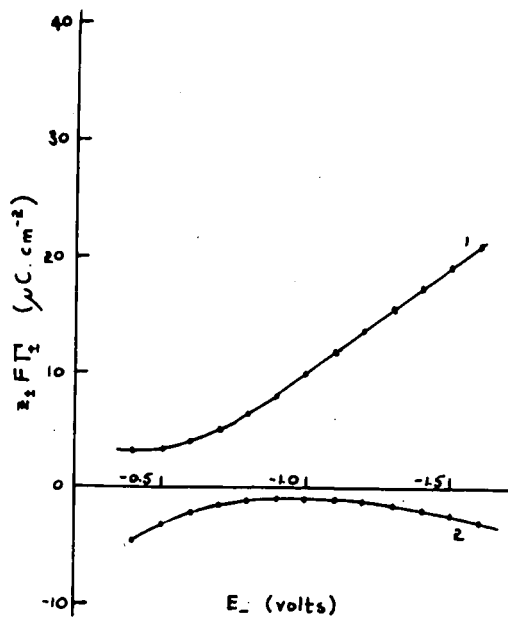


**Fig.2.**

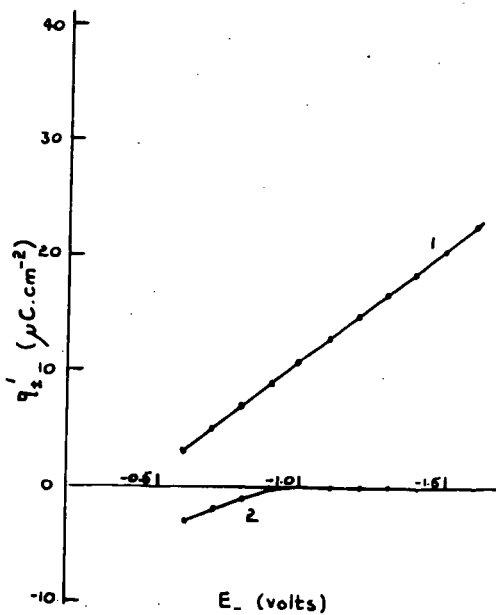


**Fig.3.**

# Interference Attenuated Total Reflectance On Tin-Oxide Glass Substrates

V. S. Srinivasan and T. Kuwana

Case Institute of Technology, Cleveland, Ohio 44106

The application of Attenuated Total Reflectance spectroscopy has been used for the study of interfacial phenomena.<sup>1</sup> The specific application of this technique to identify and to study species formed during an electrochemical process has been successfully demonstrated by Hansen, Kuwana, and Osteryoung.<sup>2</sup> The conducting surface for the electrochemical process may be either a thin metallic film or a thin layer of "doped" tin oxide on glass substrate. To obtain the spectrum of the species under study, the difference in the values of the reflectance absorbance with and without the generated species at the surface, was plotted against wavelength. As noticed by these authors, the shape of the spectra depended on the thickness of the films. It was assumed that the film (tin oxide) acted merely as a neutral filter. However this approach is not valid as will be shown. The approach presented in this paper is based on Murmann-Forsterling formula for reflection of light from thin films.<sup>3</sup>

## Experimental:

Reagent grade chemicals were used and the solutions were made with doubly distilled water. Tin oxide coated glass plates were obtained from Corning Glass Co. Spectra were obtained on a Cary Model 15 spectrophotometer. Thin films of gold were deposited on glass plates by vacuum evaporation method. The design of the cell was similar to the one previously described.<sup>2</sup>

The Univac 1107 computer using algol system was used for computations.

## Theory:

The problem is divided into two sections. First the Fresnel reflective coefficients are calculated for reflections at the interface of two absorbing media. Then these values are used in the general formula for reflection from thin films, first derived by Forsterling for normal reflection, but modified to include any angle of incidence.

## Fresnel Reflective Coefficients:

The equation for Fresnel reflective coefficient,  $r_1$ , for perpendicularly polarized light at the interface of two absorbing media is

$$r_1 = \frac{\hat{n}_1 \cos \phi_1 - \hat{n}_2 \cos \phi_2}{\hat{n}_1 \cos \phi_1 + \hat{n}_2 \cos \phi_2} \quad (1)$$

where  $\hat{n}_1$  and  $\hat{n}_2$  are the complex refractive indices, with  $\hat{n}_1$  equal to  $n_1 - i\kappa_1$  and  $\hat{n}_2$  equal to  $n_2 - i\kappa_2$  where  $n_1$  and  $n_2$  are the refractive indices and  $\kappa_1$  and  $\kappa_2$  are the attenuation indices of tin oxide film and solution respectively.  $\phi_1$  and  $\phi_2$

are the angle of incidence and the angle of refraction for the light beam entering from the glass substrate. In the above equation, the angles are also complex, but they can be replaced in terms of the real experimental quantities,  $\phi_0$  the angle of incidence of the light beam on the transparent glass substrate and its refractive index  $n_0$ , using Snell's law.

$$n_0 \sin \phi_0 = \hat{n}_1 \sin \phi_1 = \hat{n}_2 \sin \phi_2 \quad (2)$$

Simplification of equation (1) leads to the Fresnel reflective coefficient

$$r_1 = \frac{\left[ \xi - \eta \right]^{1/2}}{\left[ \xi + \eta \right]} \quad (3)$$

where

$$\xi = x^2 + y^2 + p^2 + q^2 \quad \text{and}$$

$$\eta = 2(px + qy)$$

with

$$x = 1/\sqrt{2} \sqrt{\sqrt{(N_1^2 - N_1^2 \kappa_1^2 - \sin^2 \phi_0)^2 + (2N_1 \kappa_1)^2} + \sqrt{(N_1^2 - N_1^2 \kappa_1^2 - \sin^2 \phi_0)^2 + (2N_1 \kappa_1)^2}}$$

$$y = -1/\sqrt{2} \sqrt{-\sqrt{(N_1^2 - N_1^2 \kappa_1^2 - \sin^2 \phi_0)^2 + (2N_1 \kappa_1)^2} + \sqrt{(N_1^2 - N_1^2 \kappa_1^2 - \sin^2 \phi_0)^2 + (2N_1 \kappa_1)^2}}$$

$$p = 1/\sqrt{2} \sqrt{\sqrt{(N_2^2 - N_2^2 \kappa_2^2 - \sin^2 \phi_0)^2 + (2N_2^e \kappa_2)^2} + \sqrt{(N_2^2 - N_2^2 \kappa_2^2 - \sin^2 \phi_0)^2 + (2N_2^e \kappa_2)^2}}$$

$$q = -1/\sqrt{2} \sqrt{-\sqrt{(N_2^2 - N_2^2 \kappa_2^2 - \sin^2 \phi_0)^2 + (2N_2^e \kappa_2)^2} + \sqrt{(N_2^2 - N_2^2 \kappa_2^2 - \sin^2 \phi_0)^2 + (2N_2^e \kappa_2)^2}}$$

The signs for the square roots are dictated by the condition that the reflectivity always be equal or less than unity. Further  $N_1 = n_1/n_0$  and  $N_2 = n_2/n_0$ .

The phase angle  $\beta$  associated with the above electric vector is calculated to be

$$\sin \beta = 2(py - qx) / (\xi^2 - \eta^2) \quad (4)$$

Table I

## Comparison Between Experimental and Simulated Spectra

	Experimental	Simulated
Maxima	390 m $\mu$	390 m $\mu$ <sup>+</sup>
	458 "	460 "
	748 "	760 "
Minima	415 "	420 "
	508 "	510 "
	635 "	655 "

The thickness of the film is taken to be 960 m $\mu$ .

For individual cases of reflection, the amplitude and the phase angle can be evaluated from equations (3) and (4).

**Murmann-Forsterling Formula:**

The reflections from thin films give rise to maxima and minima, the distance between the peaks being dependent upon the thickness of the film. The ray of light entering the glass substrate is partially reflected with a Fresnel coefficient  $r_1$  and phase angle  $\gamma$ , at the film-glass interface. The transmitted part travels through the film with thickness  $d$  being attenuated by a factor  $\alpha$  and undergoes a phase lag of  $\delta$ . This ray is further reflected with a Fresnel coefficient  $r_2$  and a phase angle  $\beta$  at the film-solution interface. Thus the progressively attenuated rays undergo multiple reflections in the thin film. These partially emergent electric vectors may constructively or destructively interfere with the first reflected ray. The net addition of these vectors and subsequent manipulation with the complex conjugate gives

$$\text{Reflectivity} = I/I_0 = \frac{r_1^2 + (\alpha r_2)^2 + 2\alpha r_1 r_2 \cos(\gamma - (\beta - \delta))}{1 + (\alpha r_1 r_2)^2 + 2\alpha r_1 r_2 \cos(\gamma + (\beta - \delta))} \quad (5)$$

where

$$\alpha = \exp \frac{4\pi d n_o y}{2 \lambda}$$

and

$$\delta = \frac{4\pi d n_o x}{2 \lambda}$$

$\lambda$  being the wavelength.

**Experimental Results and Discussion:**

In figure 1. experimental reflectance spectra for the tin oxide-air and tin oxide-water interfaces with perpendicularly polarized light are shown. Absorbance is defined as  $-\log$  Reflectivity.

The validity of equation (5) was checked by the computer by simulating the spectrum with substituted values. The value of  $\kappa_1$ , the attenuation index for tin oxide, was evaluated as 0.0035. The value for the thickness of the film was chosen to be 960 m $\mu$ , as this number gave simulated spectra similar to experimental ones as may be seen in Table I. This value is near the value of 1 micron quoted by the manufactures. Further agreement at all wavelengths is not expected because of the assumed constant value for the refractive index.

The refractive index for tin oxide and glass were taken as 1.88 and 1.49 respectively. The angle incidence  $\phi_0$  was  $72^\circ$ .

An important conclusion drawn from the results is that the change in refractive index affects the position as well as the heights of the absorbance peaks.

The second interesting aspect of these spectra is the following. In A.T.R. if the absorbance of the species is independent of wavelength, the spectrum would be a straight line parallel to the wavelength axis. In the interference A.T.R. non-linear effect of  $\kappa_2$ , the attenuation index of species in solution is seen on the spectrum. For a constant  $\kappa_2$ , the maximum of absorbance for species coincides with the maximum due to the interference A.T.R. In figure 2 the relative change of absorbance is plotted as a function of wavelength with  $\kappa_2 = 0.005$ . It is clear that the shape of the spectrum for the species at the solution-film interface is greatly dependent on the optical properties of the film.

Figure 3A is the A.T.R. spectrum of Eosin-Y with the tin oxide coated plate replaced by a plastic one. There is no evidence for adsorption of Eosin-Y on this surface. The peak occurs at 521 m $\mu$ . Using formulas (1) and (3), the  $\kappa_2$  values are calculated for different wavelengths and then substituted into equation (5). The computer calculations give the resultant absorbance which is shown in Figure 3B. Figure 3C is the experimentally determined absorbance curve for Eosin-Y with the tin oxide coated cell. It is clear that the A.T.R. thin film simulated spectrum is in agreement with the experimental spectrum but shifted to longer wavelengths with respect to the experimental A.T.R. spectrum without the thin film.

The preliminary calculations for parallel polarized light showed that the Reflectivity was relatively lower than that for perpendicular polarization. The electric vector experiences a field effect as it penetrates the medium and is reflected at the interface. Optical rotation may therefore be expected in an applied electric field. In the absence of any absorbing species (only the supporting electrolyte) the peak height changes with applied potential. It is very important that the future workers report similar observations in addition to giving the effect of potential in the presence of absorbing species. Further, our observation that the Absorbance-time relationship for potentiostatic jump is much longer than the one expected on the basis of diffusion and penetration depth agrees with those reported previously.<sup>2</sup> This time dependence is very difficult to understand by only considering the surface concentration unless there is a time dependent adsorption of the material occurring. Similar time dependence is noticed with only supporting electrolyte (pH 1, HCl buffer) and this may be from the orientation of molecules in the tin oxide film, which leads to the time dependent anisotropic behavior. Figure 4 gives the potentiostatic jump to 0.6 v with respect to s.c.e. with gold and tin oxide films. One might notice the rapid response with the gold film, compared to that of the tin oxide film. Though one cannot discount the effect of film formation totally, it should be borne in mind that the new film will definitely alter the shape of the spectrum, both in the height and the position of the peaks. In Figure 5

the reflectance spectrum of tin oxide plate coated with a thin layer of gold is shown. This spectrum is predicted by Forsterling relationship for reflections from multiple films.

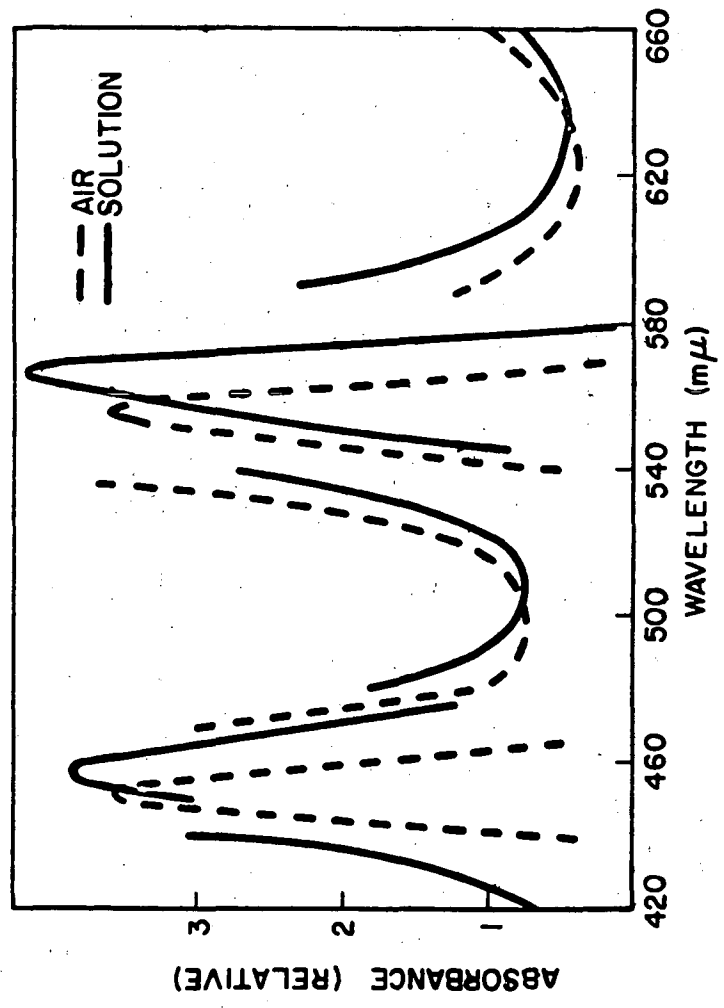
To summarize, extreme care should be exercised in interpreting the chemical phenomenon on surface purely from optical measurements, when thin films are used. The calculation penetration depth is in error because of multiple reflections in the thin film.

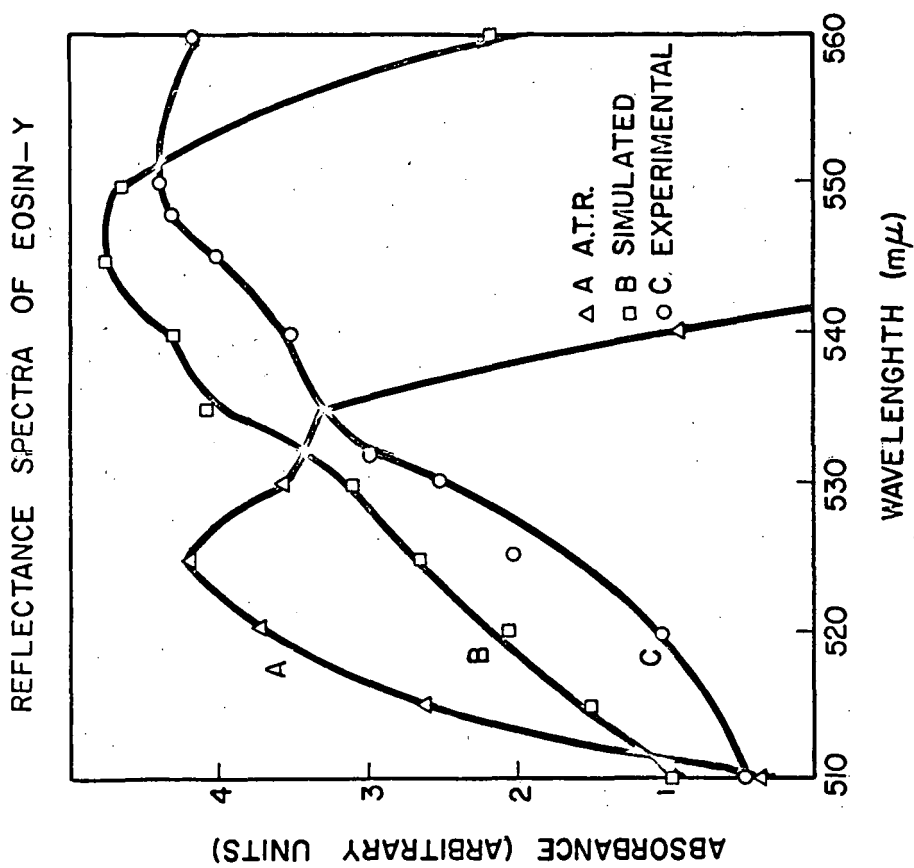
The authors gratefully acknowledge the support of this work by Grant GM 14036 from the Research Grant Branch of National Institutes of General Medical Sciences, NIH and by NOL contract N123-(62738)56006A. The assistance of Richard Chang during the early part of this work is hereby acknowledged.

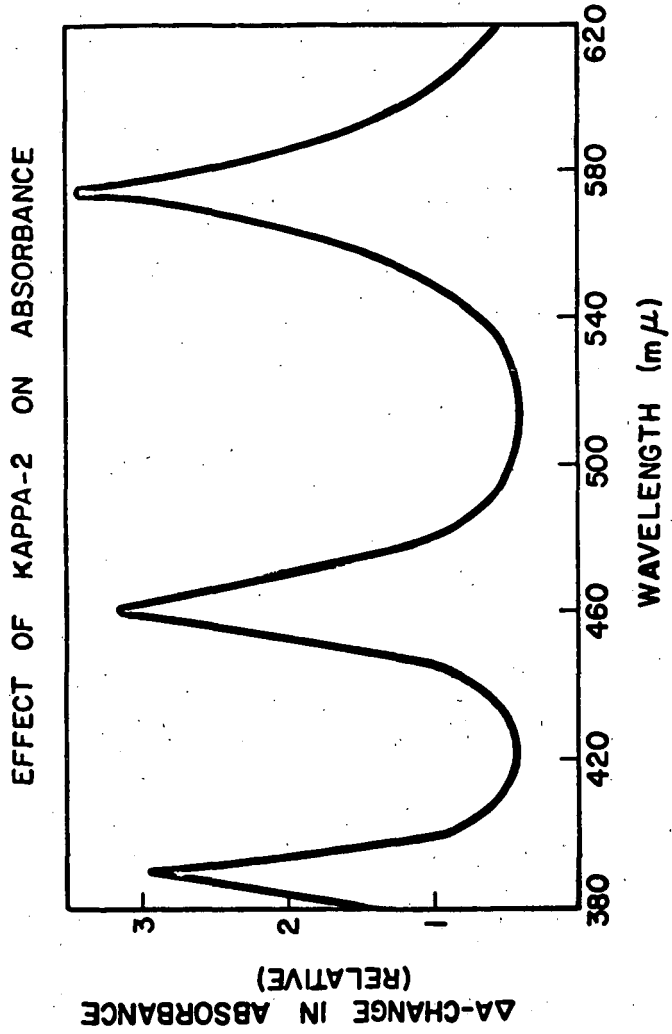
#### References:

1. Wendlandt, W. W. and Hecht, H. G., "Reflectance Spectroscopy", Interscience Publishers, New York, N.Y. (1966).
2. Hansen, W. W., Kywana, T. and Osteryoung, R. A., "Observation of Electrode-Solution Interface by Means of Internal Reflection Spectrometry", *Anal. Chem.*, 38, 1809 (1966).
3. Vasicek, A., "Optics of Thin Films", pp. 323-327, North-Holland Publishing Co., Amsterdam (1960).

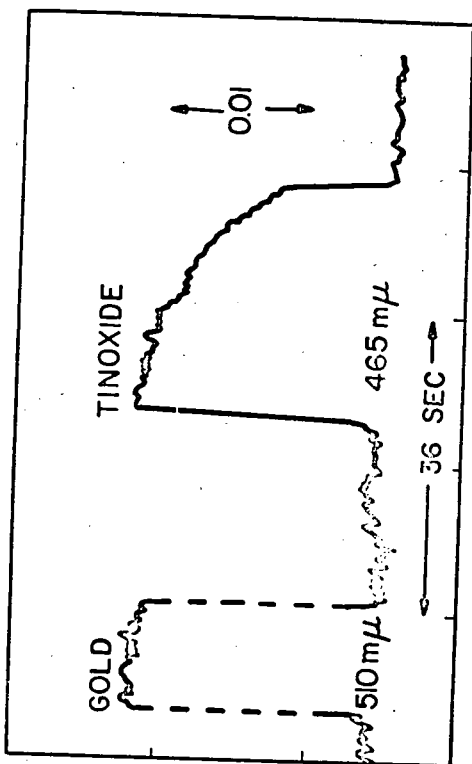
REFLECTANCE SPECTRA OF SnO<sub>2</sub>-GLASS





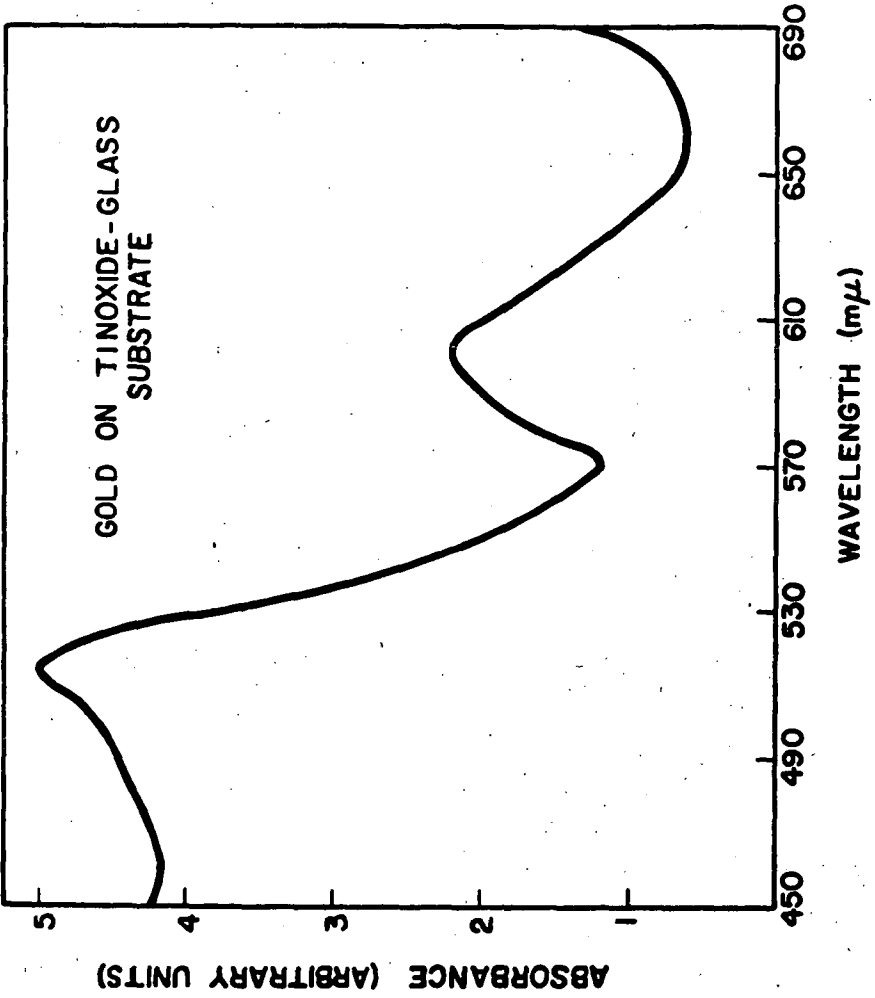


CHANGE IN ABSORBANCE FOR SUPPORTING ELECTROLYTE



TIME

ABSORBANCE CHANGE



APPLICATION OF DEPOSITED THIN METAL FILMS AS OPTICALLY TRANSPARENT ELECTRODES FOR THE INTERNAL REFLECTION SPECTROSCOPIC OBSERVATION OF ELECTRODE SOLUTION INTERFACES

B. Stanley Pons  
Leon O. Winstrom  
James S. Mattson  
Harry B. Mark, Jr.

Department of Chemistry  
The University of Michigan  
Ann Arbor, Michigan 48104

The feasibility of using Internal Reflectance Spectroscopy (IRS) as a method for monitoring electrochemical reactions spectrophotometrically at the electrode surface has been demonstrated previously (3,7). Since that time, it has been found that it would be highly advantageous to produce IRS crystal-electrodes which have surfaces with better electrochemical characteristics than those used previously [i.e., those which employed doped tin oxide in the visible range of the electromagnetic spectrum (3) and germanium in the infrared region (7)]. The semiconductor properties of tin oxide and germanium make these materials quite unsuitable for many experiments as their electrode properties are quite complex (5,10). This, therefore, makes the characterization of this combination electrolysis-spectrophotometric technique extremely difficult. Experimentally, it has been observed that the absorption baseline of tin oxide coated glass electrodes does not remain constant from one electrolysis to the next (5,10). Other investigators have also observed the same changes in the optical properties on electrolysis (6,9) which indicates that the surface is changing in some way.

For these reasons, the possibility of using thin platinum and palladium metal films on optically transparent substrates which can then be employed as IRS electrodes has been investigated.

We would like to report a relatively rapid and inexpensive method of producing such films and present some preliminary electrode-optical characteristics of these electrodes.

#### EXPERIMENTAL

##### Platinum-Glass IRS-Electrode

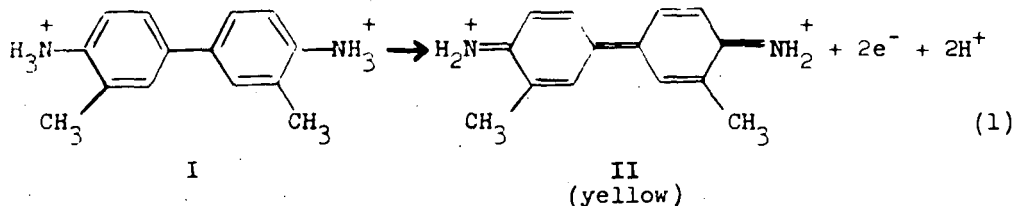
The method of producing the platinum-glass IRS-electrode employs the use of a solution of an organic ligand complex of platinum, (Liquid Platinum No. 1, Engelhard Industries Inc., Hanovia Liquid Gold Division, East Neward, N. J.) which is readily reduced to platinum metal on an inert substrate, such as glass, at sufficiently high temperatures.

To lessen the viscosity of the available Liquid Platinum (which enables a thin platinum film to be produced), a small amount (0.1 to 0.2 ml, depending on the thickness of film desired) is dissolved in 3 ml of dichloromethane, and the resulting solution is painted on to the IRS plate using brush strokes parallel to the light path. Several

coatings may be applied, again depending on the thickness of film desired. The plate is then allowed to cure in air for about one hour at room temperature. It is then fired in an open oven for about four hours. The firing temperature for Pyrex plates is between 650°C and 680°C (approximately the fusion point of the glass).

The cell was essentially the same as employed by Hansen *et al.* (3,9).

Constant current chronopotentiometry was carried out on the previously characterized (3) *o*-toluidine system. The apparatus is similar to those described earlier (2,3). A 5 millimolar solution of *o*-toluidine in a pH 2.00 KCl-HCl buffer was placed in the reaction cell, and on electrolysis the following reaction occurs:



Species I is colorless in the visible range, but II absorbs at 4,380 Å ( $\lambda_{\text{max}}$ ). The Cary Model 14 was set at this wavelength and simultaneous absorbance-time and potential-time plots of the oxidation reaction were carried out. The results are shown in Figure 1.

Christie (1) and Hansen *et al.* (3) have shown for forward current chronopotentiometry that the absorbance observed is proportional to the  $\sqrt{t}$  provided that the penetration depth of the electric field vector is small compared to the diffusion layer. Figure 2 shows a typical absorbance  $-t^{1/2}$  plot. These plots are linear over a wide range of current densities and reactant concentrations. They have also been found to be reproducible for successive runs with no shift appearing in the baseline which is what was originally desired. This is an absolutely necessary condition for scanning wavelength during an electrolysis to obtain a spectrum of the electrolysis product or intermediate.

Typical IRS spectrum scan results during the electrooxidation of *o*-toluidine are shown in Figure 3. A  $5.0 \times 10^{-3}$  M *o*-toluidine and 0.22 M chloride (pH = 2.0) solution was potentiostated at +0.60 V vs SCE. Curve 1 represents the spectrum (baseline) of the solution at zero applied voltage and Curve 2 represents the spectrum obtained during actual electrolysis. A very pronounced absorbance peak is observed which has a maximum at 4375 Å. This corresponds almost exactly to the normal transmission peak ( $\lambda_{\text{max}} = 4380$  Å) observed for the oxidation product (species II of equation 1) of *o*-toluidine (Curve 3 of Figure 3 actually shows the transmission spectra of this compound prepared during electrolysis). It should be noted at this point that the IRS-spectra obtained during electrolysis at platinum film electrodes as several orders of magnitude better, with respect to both  $\Delta\lambda$  and resolution, than any obtained with tin-oxide conducting glass electrodes (1, 6, 9, 10). A replicate IRS cell containing supporting electrolyte was placed in the reference beam of the Cary 14 during all runs.

Experiments were also carried out varying the applied potential with cells containing only supporting electrolyte solution to see if the IRS absorption baseline was effected or varied in any way (a possible change in refractive index in the solution at the electrode surface might occur as the concentrations of the anions and cations of the supporting electrolyte in the compact and diffuse double layer vary with potential). As expected, however, no significant change in the baseline with potential was observed. The penetration or effective path length into a solution of the electric field vector is approximately  $1000 \text{ \AA}$  in the visible range and the slight change in concentration of the various ions in the double layer (approx.  $100 \text{ \AA}$ ) predicted by Guoy-Chapman theory does not appreciably alter the integrated or average environment seen by the electric vector in the  $1000 \text{ \AA}$  thick solution volume. However, whenever the potentials were sufficient to reach solvent or electrolyte breakdown large shifts in absorption are observed, especially with the halide solutions where corrosion of the film was found at anodic breakdown.

In designing an IRS-Electrode, such as the metal film type described above, it is desired to have the film as thin as possible yet thick enough to have good electrical conductivity. Transmission measurements on the above IRS cells have shown that the film is not completely uniform in thickness in some small areas but appeared to be covered to the eye. The average optical absorbance of the films was about 0.40 absorbance units which would indicate an average thickness of about  $75 \text{ \AA}$  (11). The electrical resistance of such a thin film would be exceedingly high, however. Actual measurements of the contact resistance of the actual films was about  $25 \text{ } \Omega\text{-cm}$ . To resolve this discrepancy, electronphoto micrographs were made of the surface of the films. Two distinct characteristics were observed that offer a possible explanation as to the operation of these plates. Figure 4a is a portion of the enlarged (45,000 diameters) surface which shows that there are a large number of small holes (estimated to be about  $1.5 \times 10^{-5} \text{ cm}$  in diameter on the average). These holes appear to penetrate to the glass surface which explains why the film has such good optical transparency. They are made up essentially of bare areas and thick opaque interconnected areas of metal. The size of the holes is small compared to the diffusion layer thickness, of course, so all IRS measurements appear diffusion controlled to a plane electrode.

The second anomaly in the optical behavior of these films is the experimental fact that absorbances obtained using these electrodes are an order of magnitude larger than those observed at conducting glass IRS Electrodes [compare Figure 3 to Figure 16 of Reference (2)] even though the cell geometries were essentially the same number of internal reflections. Figure 4b shows a second type of structure of the films. These are long parallel tunnels [rather than grooves as can be distinguished by the shadowing and other features of the picture] (11) in the film which are also parallel to the brush strokes. It is postulated that these tunnels, perhaps formed in some way by the initial entrapment of solvent, act as tiny "wave channels" (8). The light beam entering one of these "wave channels" will undergo an extremely high number of reflections because of the small dimension in traveling down the tunnel. Thus, the overall effective number of "reflections" is very large compared to those calculated from the gross geometry of the crystal. The average width of these "tunnels" was about  $1 \times 10^{-5} \text{ cm}$ . This concept is further substantiated by the fact that IRS-Electrode made in the exact manner except

that the film was applied with brush strokes perpendicular to the light path were essentially opaque with respect to the solution phase. At present this theory is only speculation; however, detailed investigations of the film construction and the optical theory of these "wave channels" is being investigated and will be reported in the near future.

#### CONCLUSIONS

It is felt that these results show that it is possible to produce suitable thin metal surfaces on glass that are optically transparent as far as IRS is concerned and that enable one to study the IRS-electrochemical technique and electrode reaction mechanisms without serious changes of the electrode itself or the absorbance background during electrolysis. This conclusion is supported by the fact that the data in the visible region of the spectrum was reproducible and fitted theory well. Further investigation of other metal surfaces, methods of film deposition, characteristics of the deposited layer, and optical characteristics of the film are in progress and will be reported at an early date. Also, metal film deposits on quartz plates are being studied in the ultraviolet region and on AgCl and KRS-5 are being studied in the IR region (preliminary experiments have shown that Palladium films on KRS-5 crystals have a much broader IR window (5 to 16 microns) than conducting Germanium crystals (2 to 10 microns) used in previous in situ IRS-electrolysis studies (7).

REFERENCES

1. Christie, J. H., North American Aviation Co., Inc., Thousand Oaks, California, Unpublished Work, 1966.
2. Hansen, W. N., Kuwana, T., and Osteryoung, R. A., Anal. Chem., 38, 1811-1821 (1966).
3. Hansen, W. N., Osteryoung, R. A., and Kuwana, T., J. Amer. Chem. Soc., 88, 1062 (1966).
4. Heavens, O. S., Optical Properties of Thin Solid Films, Academic Press, New York, 1955, p. 162.
5. Holmes, P. J., editor, The Electrochemistry of Semiconductors, Academic Press, New York, 1962.
6. Kuwana, T., Chemistry Dept., Case Institute of Technology, Unpublished Work, 1966.
7. Mark, H. B., Jr., and Pons, B. S., Anal. Chem., 38, 119 (1966).
8. Meyer, D. I., Physics Department, University of Michigan, Private Communication, 1966.
9. Osteryoung, R. A., North American Aviation Co., Inc., Thousand Oaks, California, Private Communication, 1966.
10. Pons, B. S., Winstrom, L. O., Mattson, J., Mark, H. B., Jr., Unpublished Work, 1966.
11. Rosen, J., Department of Metallurgical Engineering, University of Michigan, Private Communication, 1966.

Research supported by a grant from the U.S. Army Research Office, Durham, Contract No. DA-31-124-ARO-D-284.

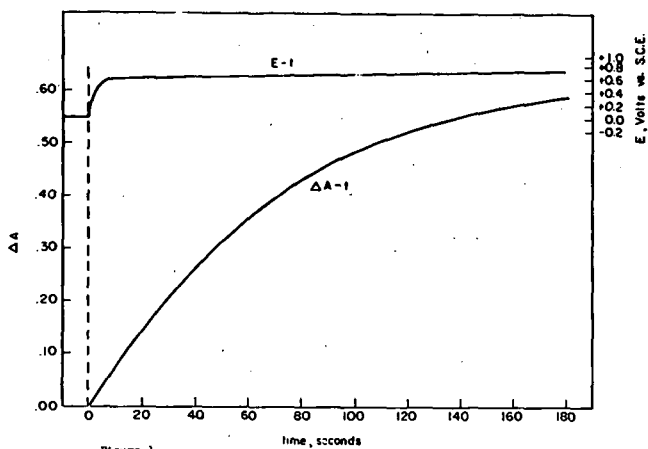


Figure 1.

Absorbance-time and potential-time curves for the chronopotentiometric electrolysis of 5 millimolar *o*-tolidine in a pH 2.00 HCl-KCl solution. The current was 1.00 milliamperes. The electrode area is approximately  $6 \text{ cm}^2$ .

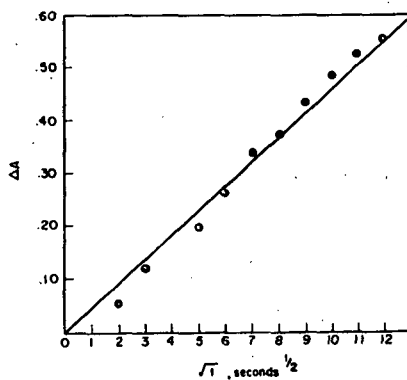


Figure 2.

Absorbance  $-t^{1/2}$  plot of a typical chronopotentiometric electrolysis of the *o*-tolidine system at pH 2.00.

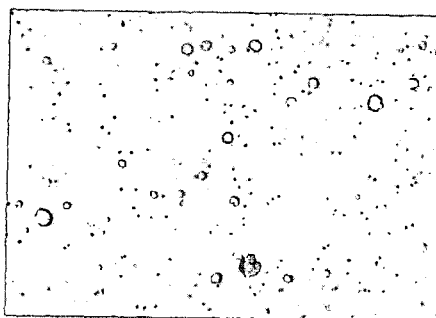
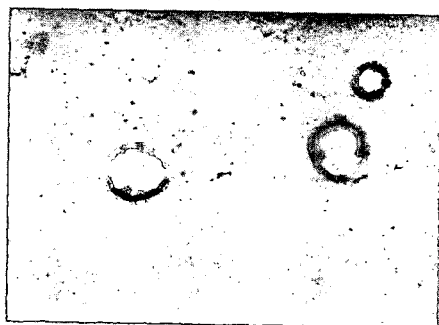
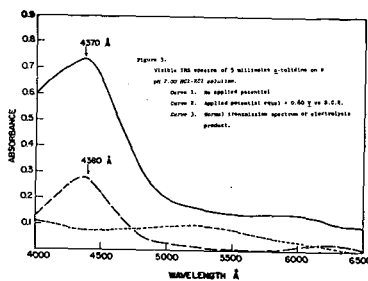


Figure 4.  
Electron photomicrographs of the  
platinum coated IRS electrode

- a) 45,000 Diameters, showing  
hole penetration of  
surface
- b) 7,000 Diameters, showing  
one of the "wave channels"

## PHOTO-ELECTROCHEMICAL REACTIONS IN SOLUTION

S. P. Perone, J. R. Birk, H. E. Drew and H. E. Stapelfeldt

Department of Chemistry  
Purdue University  
Lafayette, Indiana 47907

The apparent similarity between photolytic and electrolytic processes in solution has prompted recent work combining photochemical and electrochemical techniques (1,2). Two objectives can be discerned: First, chemical transients present in photolytic processes can be generated electrolytically under accurately controlled conditions, and their subsequent chemistry studied. The results of these studies can be used to interpret photochemical data.

A second objective in this work is to use electrochemical techniques as a means of monitoring transient photolytic species during a photochemical process. Several analytical advantages are obtained in this way: sensitivity is available for dilute concentrations of a wide range of compounds; nearly the same detection limit exists for all electroactive compounds; and time resolution in the microsecond range is available.

The flash photolysis technique was used in this work to initiate the photochemical processes. A Xenon flash lamp (XFX47A, Edgerton, Germeshausen & Grier, Inc., Boston, Mass.) was employed, and flash times of the order of 5 to 20 microseconds were obtained with about 100 joules of U.V.-visible radiant energy. Potentiostatic measurements of transient photolytic products were made using a simple fast-rise potentiostat employing Philbrick SK2-V and SK2-B operational amplifiers (Philbrick Researches, Inc., Dedham, Mass.). A hanging mercury drop electrode was used as the working electrode, and was placed in solution in the region of greatest photolytic activity. (The flash lamp itself was partially immersed in solution.)

### Results and Discussion

The specific objectives of the work reported here were, one, to follow very rapid photolytic reactions; two, to study photochemical processes where the electrochemical characteristics had not been well-evaluated previously; and, three, to evaluate the electrochemical characteristics of electronically excited species.

In order to accomplish the first objective, two instrumental problems had to be solved. The electronic instability in the potentiostat generated by the flash lamp discharge had to be eliminated; and the time resolution (rise-time) of the potentiostat had to be optimized. In addition, the time-delayed potentiostatic method developed previously (2) had to be modified in order to obtain kinetic data for photolytic processes with half-lives less than 1 msec.

The initial potentiostat instability was traced to the flash lamp triggering technique which had improperly resulted in an extraneous arc discharge in the trigger circuit. This arc discharge, when coupled to the overall potentiostatic circuit, resulted in a loss of potential

control lasting from 50 to 2000 microseconds. This problem was solved by imposing directly to the flash lamp a voltage sufficient to cause its self-discharge. With this approach, negligible initial potentiostat instability was obtained.

Fast time resolution was obtained by employing a single-amplifier potentiostat with greater than 1 MHz band pass, coupled with an electrolysis cell design minimizing uncompensated and total cell resistance (3).

One chemical system chosen for study was benzophenone in 80% ethanol, at pH's from 7 to 13, where the dimerization of the photo-produced free radical occurs very rapidly. This system provided a real test of the time-resolving capabilities of the instrumentation.

The second objective mentioned above, to demonstrate the applicability of the overall photo-electrochemical technique for processes where the electrochemistry was not well-defined, was accomplished by selecting two other systems for study: the photoreduction of Fe(III) in oxalate medium, and the photoreduction of methylene blue. Although the general polarographic characteristics of these systems were well known, the nature of transient intermediates in the overall electrode process had not been characterized. Thus, rapid cyclic electrochemical investigations were carried out with these systems. Cyclic voltammetry and cyclic potential-step electrolysis were used with frequencies up to 50 kHz. The semiquinone radical ion intermediate in the methylene blue reduction process was observed in both the photolytic and electrolytic experiments. The kinetics of its chemical decomposition were measured from both electrochemical and photochemical studies.

Elucidation of the Fe(III)-oxalate system involved similar electrochemical studies. However, a separate study of the electrochemistry of oxalate was necessary in order to interpret photo-electrochemical data.

The electrochemical detection of excited species has not been conclusively verified in our work as of this writing. However, experimental studies are continuing along these lines. The triplet state of methylene blue, for example, has a life-time of the order of 100 microseconds; and, with the present time resolution of the photo-electrochemical technique, its electrochemical characteristics ought to be discernible.

#### Literature Cited

1. Berg, H., Z. Anal. Chem., 216, 165 (1966).
2. Perone, S. P., and Birk, J. R., Anal. Chem., 38, 1589 (1966).
3. Perone, S. P., Ibid., 1158.

ELECTROLYTIC GENERATION OF SOLVATED ELECTRONS IN A SOLVENT OF HIGH PROTON DONOR CAPABILITY; ELECTROLYTIC REDUCTION OF THE BENZENE RING

Heinz W. Sternberg, Raymond E. Markby, Irving Wender, and David M. Mohilner\*

U. S. Bureau of Mines, 4800 Forbes Avenue, Pittsburgh, Pa. 15213

\*Department of Chemistry, Colorado State University, Fort Collins, Colorado 80521

Until now, electrolytic generation of solvated electrons could be achieved only in solvents of low donor capability such as liquid ammonia<sup>1,2/</sup> or certain amines,<sup>3-5/</sup> a fact which imposed severe restrictions on the choice of solvent and reaction conditions. Attempts, described below, to generate solvated electrons electrolytically in a solvent of relatively high proton donor capability such as ethanol were doomed to failure due to hydrogen evolution at a potential far below that required for release of electrons into the solvent. The recently published discovery<sup>6/</sup> that hexamethylphosphoramide (HMPA),  $[(CH_3)_2N]_3PO$ , is capable of dissolving alkali metals prompted us to investigate whether electrolytic generation of solvated electrons in a solution of ethanol containing HMPA was possible.

#### EXPERIMENTAL

**Reagents.** Lithium chloride, tetralin, 1-octene and HMPA were of the highest purity available commercially. HMPA was purified by vacuum distillation and the fraction boiling between 89° and 92° at 4-5 mm was used.

**Apparatus.** The electrolysis vessel, described previously,<sup>4/</sup> consisted of an H-cell of 150 ml total capacity. The two compartments were separated by a coarse, 25 mm glass frit. A carbon rod (spectroscopic grade), 3.5 cm long and 0.5 cm in diameter served as the anode. A rectangular piece of sheet aluminum of 4.5 cm<sup>2</sup> total immersed surface served as the cathode. Reproducible cathode potentials during current flow were obtained by inserting the Luggin capillary into a sleeve formed by folding over one edge of the aluminum electrode.<sup>4/</sup>

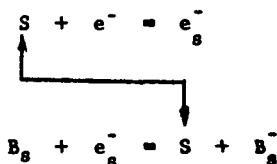
**Electrolytic Reduction.** The electrolytic reduction of tetralin (1 ml, 7.35 mmole) and 1-octene (1 ml, 6.37 mmole) was carried out at a constant current of 500 ma in 60 ml of ethanol-HMPA solution containing 33 mole pct HMPA, 0.3 M in LiCl. At the start of the electrolysis, the cathode potential was -2.5 volts (vs. Ag wire) and slowly changed to -2.4 volts in the course of 25 minutes at which point the electrolysis was interrupted. The solution in the cathode compartment was diluted with water and the aqueous solution was extracted with pentane. The pentane extract was warmed in a current of nitrogen to remove the solvent and the residue was analyzed by mass spectrometric and GLC methods.

#### RESULTS AND DISCUSSION

When a solution of HMPA, 0.3 M in LiCl, is electrolyzed, dark blue globules, characteristic of solvated lithium, form at the cathode surface at a potential of -2.3 volts (vs. Ag wire) and the solution in the cathode compartment becomes deep blue, visual evidence that the reaction  $Li_s^+ + e^- \rightarrow Li_s^+ \dots e_s^-$  is taking place. The half-life of the solvated electron at room temperature was determined by dissolving lithium in HMPA and measuring the decrease in ESR signal peak height with time. The half-life was 38 minutes,<sup>7/</sup> a value which compares well with that of 15 hours found for the half-life in liquid ammonia as reported by J. Corset and G. Lepoutre.<sup>8/</sup> In the presence of ethanol, the intensity of the color is lower and the cathode potential is different, depending on the amount of alcohol present. In ethanol containing 33 mole pct. HMPA, for example, the blue color appears at a cathode potential of -2.5 volts (vs. Ag wire). However, in the presence of both alcohol and benzene the solution remains colorless during electrolysis, with only

a small amount of blue color visible at the cathode surface. Proof that electrolytic reduction of the benzene ring in ethanol-HMPA solution is possible was obtained by electrolysis of tetralin in a solution composed of 67 mole pct. ethanol and 33 mole pct. HMPA, 0.3 M in LiCl. The electrolysis was carried out at a cathode potential of -2.5 to -2.4 volts (vs. Ag wire). After completion of the electrolysis, analysis of the recovered product by mass spectrometric and GLC methods showed that it consisted of (vol. pct): tetralin (80), hexalin (2), octalin (1) and decalin (17), and that tetralin had been hydrogenated at a current efficiency of 54 pct. Under the same conditions, 1-octene was reduced to octane at a current efficiency of 26 pct. When the electrolysis of tetralin is carried out under the same conditions but in the absence of HMPA, copious hydrogen evolution takes place and the cathode potential during electrolysis is now -1.5 volts (vs. Ag wire), i.e., 0.8 to 1.0 volt more anodic than that at which release of electrons was observed into HMPA or ethanol-HMPA solution. Under these conditions not even traces of reduced tetralin could be detected in the recovered material. It is remarkable that the strong hydrogen evolution that occurs during electrolysis of ethanol at -1.5 volts is drastically reduced in the presence of as little as 33 mole pct. HMPA. This suggests adsorption of the aprotic but highly polar<sup>9/</sup> HMPA at the electrode surface to the near exclusion of ethanol. In the presence of HMPA, the charge transfer process is release of electrons into the solvent and not hydrogen evolution. The high percentage of decalin in the reaction product is probably due to the high proton availability in the solution containing 67 mole pct. ethanol, since electrolytic reduction of tetralin in ethanol-HMPA containing only 25 mole pct. ethanol gave hexalin as the main product. Tetralin is not reduced when the electrolysis is carried out in HMPA in the absence of ethanol. Under these conditions, the catholyte becomes dark green colored during electrolysis. Mass spectrometric analysis of the recovered reaction product indicates the presence of considerable amounts of mono- and dimethyltetralin and small amounts of dimers of these methyltetralins in addition to unchanged starting material, tetralin.

On the basis of these results and previous work on the reduction of the benzene ring in ethylenediamine,<sup>4/</sup> we believe that electrochemical reduction of the benzene ring in ethanol-HMPA involves addition of the solvated electron,  $e_s^-$ , to the solvated benzene ring,  $B_s$ .



where S indicates the solvent molecules required to solvate an electron. Subsequent protonation of the benzene anion,  $B_s^-$ , and further addition of electron and proton completes the hydrogenation of a double bond as has been pointed out previously.<sup>10/</sup> Apparently, the cathode in ethanol-HMPA solution containing alkali halide functions in the same way as in liquid ammonia<sup>2/</sup> and amines,<sup>4/</sup> i.e., as an electron electrode.

The present results demonstrate for the first time that electrolytic generation of solvated electrons in a solvent of relatively high proton donor capability is feasible and that these electrons are available for addition to organic compounds.

100  
REFERENCES

1. A. J. Birch. *Nature*, 158, 60 (1946).
2. H. A. Laitinen and C. J. Nyman. *J. Am. Chem. Soc.*, 70, 3002 (1948).
3. H. W. Sternberg, R. E. Markby, and I. Wender. *J. Electrochem. Soc.*, 110, 425 (1963).
4. H. W. Sternberg, R. E. Markby, I. Wender, and D. M. Mohilner. *J. Electrochem. Soc.*, 113, No. 10, 1960 (1966).
5. R. A. Benkeser, E. M. Kaiser, and R. F. Lambert. *J. Am. Chem. Soc.*, 86, 5272 (1964).
6. G. Fraenkel, S. H. Ellis, and D. T. Dix. *J. Am. Chem. Soc.*, 87, 1406 (1965).
7. Herbert L. Retcofsky. Unpublished work.
8. J. Corset and G. Lepoutre in "Metal-Ammonia Solutions," G. Lepoutre and M. J. Sienko, Editors, W. A. Benjamin, Inc., New York, p. 190.
- 9: The dielectric constant of HMPA at 25° is 30 according to J. E. Hofmann, A Schriesheim and D. D. Rosenfeld. *J. Am. Chem. Soc.*, 87, 2523 (1965).
10. A. P. Krapcho and A. A. Bothner-By. *J. Am. Chem. Soc.*, 81, 3658 (1959).

MECHANISM OF CATHODIC PROCESSES ON  
THE SEMICONDUCTOR ZINC OXIDE\*

T. Freund and S. Roy Morrison

Stanford Research Institute  
Menlo Park, California

## ABSTRACT

The cathodic reduction of the aqueous ferricyanide ion was investigated on a single crystal zinc oxide electrode. The experimental results substantiate that this chemical reduction process obeys the model used in semiconductor physics for electron capture by surface states. It is concluded that the rate determining step of the reduction process is the capture of electrons from the conduction band of the ZnO by the sorbed ferricyanide ions. This process was shown to be irreversible, i.e., electrons are not transferred from sorbed ferrocyanide (reduced ferricyanide) to the semiconductor electrode. The capacitance, voltage and current were measured as a function of the concentration. The rate of ferricyanide reduction was measured by the current and was found to be first order in sorbed ferricyanide ion and first order in the electron concentration at the surface. The electron concentration at the surface of the electrode was determined from the capacitance-voltage measurement. The sorption isotherm for ferricyanide was found to be linear in concentration over the range from  $7 \times 10^{-5}$  to 0.7 molar.

## INTRODUCTION

The understanding of the role of the solid in charge transfer process on the surface is an important objective in electrochemistry and heterogeneous catalysis. With this objective, we have measured the current-voltage characteristics of the cathodic reduction of aqueous ferricyanide ion using a single crystal of the n-type semiconductor, zinc oxide. Primarily by measuring the voltage-capacity characteristics, we have concluded that the rate of the cathodic process (the measured current) is determined by charge transfer from the solid to the sorbed species. Evidence will be presented that the charge transfer process is an irreversible bimolecular reaction governed by the concentration of the conduction-band electrons at the surface and the concentration of sorbed oxidizing agent. Thus, the role of the solid is twofold: to provide electrons at the surface and to form electronic surface states with the sorbed oxidizing agent.

While Dewald has reported<sup>1</sup> in detail data for the voltage-capacitance behavior of the ZnO/electrolyte system in the absence of reducing or oxidizing agents, his reported<sup>2</sup> data for the current-voltage behavior with hexacyanoferrate ions was very incomplete. This lack of experimental data for voltage, capacitance, current, and concentration relations prompted us to investigate in detail this chemically simple ferrous-ferric redox couple on a single face of single crystal zinc oxide. We believed this to be important because our previous studies,<sup>3</sup> carried out in connection with the ZnO photocatalyzed reaction of oxygen and formate ions indicated that

---

\* Part of this work was supported by a group of industrial companies sponsoring a program in heterogeneous catalysis and part of this work was performed for Jet Propulsion Laboratory, California Institute of Technology, sponsored by National Aeronautics and Space Administration under Contract NAS7-100.

electrode processes on ZnO can be irreversible. Our conclusion concerning reversibility was in disagreement with Dewald's interpretation for  $\text{Fe}(\text{CN})_6^{-3}$ , which was in terms of a reversible redox reaction characterized by a Helmholtz potential. In a review paper<sup>4</sup> Gerisher came to the same conclusion as Dewald. In this communication, we will present detailed evidence for the irreversibility of cathodic processes on ZnO as illustrated by the reduction of  $\text{Fe}(\text{CN})_6^{-3}$ .

### EXPERIMENTAL

The borosilicate glass electrochemical cell used contained a zinc oxide single crystal as one electrode, a platinum wire as the working electrode, and a saturated KCl calomel reference electrode. The (0001) face of the crystal was used after lapping and then etching with 85 percent  $\text{H}_3\text{PO}_4$  for a minimum of ten minutes. The area of zinc oxide exposed to the electrolyte was the order of  $6\text{mm}^2$ .

The electrolyte contained 1M KCl and was buffered with  $\text{BO}_2^-/\text{HBO}_2$  (0.2M in total boron) to a pH of  $8.8 \pm 0.1$ . The ferri- and ferrocyanide were added as the potassium salts and the pH of the buffer was adjusted if necessary. The chemicals employed were Reagent grade and were used without purification. All electrical measurements were made with solutions deoxygenated in situ by bubbling with unpurified tank nitrogen. In no case could more than 5 percent of the current be attributed to any substance other than  $\text{Fe}(\text{CN})_6^{-3}$ . That is, the current at any given voltage was increased by at least a factor of 20 with the addition of  $\text{Fe}(\text{CN})_6^{-3}$  to the KCl buffered solution.

Three types of measurements were made: (1) the current through the ZnO, (2) the capacitance between the ZnO and the platinum electrodes, and (3) the voltage of the ZnO with respect to a saturated KCl calomel electrode (SCE). The values of the capacitance, voltage, and current reported are steady-state measurements and were shown to be independent of stirring. All measurements were made in the dark. The capacitance was measured at a frequency of 1 kc.

Two types of measurements, the current as function of the applied voltage and the capacitance as a function of voltage, were made at various ferricyanide concentrations from 0.7M to  $7 \times 10^{-5}\text{M}$  with and without added ferrocyanide. Figures 1 and 2 show typical results for the two types of measurements.

Figure 1 shows data for the cathodic current,  $J$ , vs the applied voltage,  $V$ , for two solutions both containing  $7 \times 10^{-3}$  ferricyanide. The solutions differ only in that one contains no ferrocyanide and the other was  $7 \times 10^{-2}\text{M}$  in ferrocyanide. The data for both solutions are identical within experimental error. The linearity of the dependence of  $\log J$  vs  $V$  shown in Figure 1 is typical for all solutions examined. In the range of current investigated, from 1 to 1000 na, plots of the  $\log J$  vs  $V$  for all solutions showed slopes corresponding to  $60 \pm 5$  mv per decade change in cathodic current. Typically all solutions including those containing ferrocyanide gave anodic currents below 5 na up to anodic voltages as high as 10 V vs SCE.

Figure 2 shows the voltage dependence of the capacitance plotted as  $1/C^2$  vs  $V$ . The linearity of the experimental data is typical of all solutions investigated including those free of iron salts. The value of the ZnO voltage vs SCE at  $1/C^2 = 0$  is called the flat band voltage,  $V_0$ . In practice, the linear portion of  $1/C^2$  vs  $V$  is extrapolated to  $1/C^2 = 0$ , since deviations from simple theory are known<sup>1</sup> to occur near  $V_0$ . The surface barrier,  $V_s$ , is related to the ZnO voltage vs SCE,  $V$ , by Eq. 1; in our experiments  $V_s$  always has a positive value.

$$V_s = V - V_0 \quad (1)$$

The significance of the parameters, the surface barrier and the flat band voltage will be presented in the "Discussion" in terms of semiconductor concepts. For the present, they will be taken simply as convenient variables.

The values of  $V_0$  for the various solutions reported in this paper ranged from  $-0.370$  to  $-0.410$  V vs SCE. The variations in  $V_0$  were not systematic and hence their origin is not known.

Figure 3 is plot of the log of the  $[\text{Fe}(\text{CN})_6^{-3}]$  vs the surface barrier,  $V_S$ , at constant current of 10 na. The plot is linear and the slope corresponds to a surface barrier change of 0.06 V per tenfold change in concentration.

The above experimental data can be summarized empirically by Eq. (2), where  $k$  is a proportionality constant independent of voltage and concentration.

$$J = k [\text{Fe}(\text{CN})_6^{-3}] \exp \left\{ (V_0 - V) / 0.025 \right\} \quad (2)$$

Preliminary investigations with several other oxidizing agents, including Cu(II), I(O), Mn(VII), O(-I), indicate similar behavior, at least qualitatively.

#### THEORETICAL MODEL

We will present arguments supported by the above results to show: (1) the changes in the applied voltage all occur within the semiconductor and that the cathodic current is dominated in its voltage dependence by the properties of the semiconductor; (2) the electrochemical reduction reaction is a one-electron process and is irreversible since the reverse reaction, the oxidation of Fe(II), does not proceed at an appreciable rate. The lack of the oxidation reaction is attributed to the difficulty of injecting electrons from sorbed oxidizing agent into the conduction band of the ZnO; (3) the reaction rate is first order in the concentration of reducible species on the surface.

The arguments are most easily presented in terms of an electronic energy band diagram. Figure 4 shows a band diagram of the n-type semiconductor ZnO with acceptor surface states. The abscissa is distance from the zinc oxide surface which is in contact with the electrolyte solution; the ordinate is the potential energy of an electron. Within the solid there are three energy regions: two have allowed electronic levels, the valence and conduction bands; separating them is a forbidden region, the energy gap which is about 3 eV. Within the gap, there is a donor level located slightly below the bottom of the conduction band. The donors associated with this level result from the stoichiometric excess of zinc in zinc oxide and are presumably either interstitial zinc atoms or oxide ion vacancies. Since they are ionized at room temperatures, they are shown as "+." The conduction band electrons are indicated by "-" at the bottom of the conduction band. It should be noted that the ionized donors are immobile charges at room temperature in contrast to conduction band electrons.

An allowed electronic energy level on the surface is indicated by X; such a surface state can be created by sorption of a chemical species from the electrolyte solution. It is shown at an energy,  $E$ , below the top of the conduction band. We will restrict this symbol to the surface state created by sorption of  $\text{Fe}(\text{CN})_6^{-3}$ . When this state is electronically occupied (X) by the addition of an electron it is equivalent to sorbed  $\text{Fe}(\text{CN})_6^{-4}$ .

A potential gradient, in the region  $0 < x < x_0$ , is indicated by the bending of bands. The extent of the bending is indicated by the energy of the surface barrier,  $qV_S$ , where  $q$  is the electronic charge. The surface barrier is associated with the

double layer formed by the ionized donors in the electron depletion layer ( $0 < x < x_0$ ) and the compensating negative charge arising from charged surface states and ions in the electrolyte. Because of the electrical compensation of the ionized donors in the electron depletion region by ions in solution, the surface barrier can be controlled by the externally applied voltage in the electrochemical cell. It should be noted that in the interior of the crystal ( $x > x_0$ ) the charge of ionized donors are compensated by the negatively charged conduction band electrons.

The surface barrier can be measured experimentally by the capacitance. A rigorous development of the interpretation of the experimentally measured capacitance and voltage is given in the appendix.\* The surface barrier,  $V_s$ , is related to the depth of the depletion region  $x_0$  (shown in Fig. 4) by the Schottky relation,<sup>5</sup> Eq. (3), where  $q$  is the electronic charge,  $N_D$  the density of the ionized donors,  $\epsilon$  the dielectric constant for zinc oxide, and  $\epsilon_0$  the permittivity of vacuum.

$$V_s = qN_D x_0^2 / 2\epsilon\epsilon_0 \quad (3)$$

The value of  $V_s$  can be obtained experimentally when the Schottky relation is valid through the capacitance measurement. The differential capacitance,  $C$ , can be used to determine the thickness of the depletion layer by the parallel plate capacitor relationship, Eq. (4), where  $A$  is the area.

$$x_0 = \frac{A\epsilon\epsilon_0}{C} \quad (4)$$

Substitution of Eq. (4) in Eq. (3) gives Eq. (5), a relationship between the surface barrier and a measurable quantity, the capacitance.

$$V_s = \frac{1}{2} qN_D A^2 \epsilon\epsilon_0 (1/C^2) \quad (5)$$

Since we found experimentally for each solution that  $V$  is linearly dependent on  $1/C^2$  (e.g., Fig. 1) and from the above semiconductor theory  $V_s$  has the same dependence on  $1/C^2$ , it follows that  $V_s$  differs from  $V$  by a constant given in Eq. (1). This constant,  $V_0$ , is the sum of: the voltage difference between the Fermi levels at the surface and in the interior of the crystal at flat band condition, the Helmholtz and Gouy potentials at the solution side of the ZnO electrode and the calomel electrode, and any possible voltage drop between the ZnO and its metallic contact. Following Dewald,<sup>1</sup> we adopt the simplest explanation for the linearity of  $1/C^2$  with  $V$  for a given solution and crystal. The explanation is that the component voltages of  $V_0$ , including the Helmholtz potential at the ZnO/electrolyte interface, remain invariant as a function of  $V$ . It should be noted that the Helmholtz voltage must be presumed to be independent of the hexacyanoferrate species, either in the oxidizing or reducing form, since we found that  $V_0$  was essentially constant for all solutions at pH = 8.8.

This agreement of theory and experiment shows that variations in applied potential appear only as variations of potential within the electrode and that the potentials on solution side of the electrode, i.e., Helmholtz (and Gouy) are invariant. With the demonstration that the voltage variation is in the surface barrier, we will proceed to show that electron transfer is the rate-limiting step in the reduction reaction.

The model to which we shall compare our results involves two parts. First, the electron transfer process is governed by semiconductor theory for irreversible electron capture by unoccupied surface states. Second, the formation of surface states is governed by a linear isotherm for sorption from solution.

\* Appendix is not included in this preprint.

The electron current density,  $J$ , passing from the conduction band of a semiconductor to a single type of surface state for an irreversible reaction should have the magnitude given<sup>5</sup> by Eq. (6).

$$J = q \bar{c} \sigma [X] n \quad (6)$$

The current is proportional to the average thermal velocity of electrons,  $\bar{c}$ ; the concentration of the unfilled surface states,  $[X]$ ; the cross section of this state for electron capture,  $\sigma$ ; and the electron density at the surface,  $n$ . The electron concentration in the conduction band at the surface,  $n$ , is given<sup>6</sup> by the ionized donor density of the ZnO multiplied by the Boltzmann factor associated with  $V_S$ , i.e.,  $N_D \exp(-qV_S/kT)$ ; therefore, Eq. (6) can be expressed as Eq. (7).

$$J = q \bar{c} \sigma [X] N_D \exp(-qV_S/kT) \quad (7)$$

Therefore, Eq. (7) contains the assumptions that the conduction band electrons at the surface are in thermal equilibrium with the interior and that their concentration at the surface is not appreciably disturbed by the cathodic currents. Implicit in this formulation is the absence of any tunneling effects; we believe these should be negligible.

The theoretical relationship, Eq. (7), between the current and the surface barrier can be compared to our experimental finding, Eq. (2), in order to find the relationship between the  $[X]$ , the density of unfilled surface states and the  $[\text{Fe}(\text{CN})_6^{-3}]$ , the concentration of oxidizing agent in solution. Since  $(q/kT)$  at room temperature has a value of  $1/0.025$  a comparison of Eq. (7) and Eq. (2) gives Eq. (8).

$$k [\text{Fe}(\text{CN})_6^{-3}] = q \bar{c} \sigma [X] N_D \quad (8)$$

The simplest explanation for the linearity of the concentration of sorbed ferricyanide with the concentration in solution is to assume the linear isotherm expressed by Eq. (9) with the equilibrium constant  $K$ .

$$K = [X]/[\text{Fe}(\text{CN})_6^{-3}] \quad (9)$$

This assumption implies that the rate of the electron capture process is slow compared to the rate of desorption of  $\text{Fe}(\text{CN})_6^{-3}$  so that the  $[X]$  is not appreciably lowered by the current of the cathodic reaction. This simple assumption was borne out experimentally in the ranges of current and concentrations investigated since the current,  $J$ , was linearly proportional to the concentration in solution,  $[\text{Fe}(\text{CN})_6^{-3}]$  at constant  $V_S$ . Equation (7), the current as a function of the density of unfilled surface states, may be written in terms of the experimental variable, the concentration ferricyanide ion in solution, by the use of Eq. (9) to give Eq. (10).

$$J = q \bar{c} \sigma K [\text{Fe}(\text{CN})_6^{-3}] N_D \exp(-qV_S/kT) \quad (10)$$

The substantial agreement of the theoretical model with the experimental results (the 0.06V change in the surface barrier per decade change in iron concentration and the linear proportionality between the current and the iron concentration) leads to the following conclusions:

1. The rate limiting step in this reduction process is the transfer of electrons from the solid to the surface state. The rate is first order in the density of electrons at the surface of the solid,  $N_D \exp(-qV_S/kT)$ , and first order in the density of unfilled surface states,  $[X]$ .

2. In the current and concentration ranges investigated the density of unfilled states is determined by the equilibrium linear adsorption isotherm for  $\text{Fe}(\text{CN})_6^{-3}$ ; moreover the desorption of filled surface states as  $\text{Fe}(\text{CN})_6^{-4}$  is rapid compared to the electronic process.
3. The unidirectional nature of the electron transfer assumed in our model is confirmed by the lack of dependence of the current on the  $\text{Fe}(\text{CN})_6^{-4}$  concentration.

#### DISCUSSION

Before analyzing in detail the implications of the semiconductor surface-state model and our results, it may be helpful to describe some reasons accounting for observing the simple behavior of surface states in the zinc oxide/ferricyanide system. The first reason is connected with the electrode material being a semiconductor and the second is connected with the chemical simplicity of the behavior of the hexacyanoferrate ion.

For a semiconductor, in contrast to a metal, it is possible to vary the electron concentration at the surface by the applied voltage and to measure this concentration by the capacitance. However, starting with the classical semiconductor/electrolyte investigations of Brattain and Garrett<sup>7</sup> it has become evident that not all semiconductor/electrolyte systems are simple, e.g., Ge.<sup>8</sup> We feel that the simplicity of our results adds to the many advantages that Body<sup>9</sup> has recently pointed out for ZnO Dewals'd<sup>1</sup> pioneering work with ZnO/electrolyte showed that this system obeyed simple solid-state theory for a semiconductor. In the course of preliminary studies we did not find any common laboratory reducing agents which would inject electrons into ZnO.

The second reason for predicting a simple behavior of the  $\text{ZnO}/\text{Fe}(\text{CN})_6^{-3}$  system is concerned with the chemical nature of the six coordinate iron. Ferricyanide ion on sorption would be expected to form a single type of surface state and the chemical reduction of this surface state would be expected to be simple electron capture without any chemical rearrangements. Our expectation was based on the known aqueous chemistry of hexacyanoferrate ions, i.e., one-equivalent reduction of  $\text{Fe}(\text{III})$  normally occurs by single electron transfer without atom transfer (both oxidation states are relatively inert to chemical substitution).

It should not be anticipated that all solutions containing oxidizing agents will exhibit the simple behavior described by Eq. (10). First, a multiplicity of types of unfilled states may be present; these could arise from factors such as multi-equivalence of the oxidizing agent, inhomogeneous surfaces, and the presence of more than one oxidizing agent in the solution. For such cases Eq. (6) must be replaced with Eq. (11) where the summation is carried out over the concentration of the various surface states,  $X_1$ , with the appropriate electron capture cross-sections,  $\sigma_1$ .

$$J = q n \bar{c} \sum_1 \sigma_1 [X_1] \quad (11)$$

While Eq. (11), involving surface concentrations, is always valid for irreversible electron capture processes, a second class of complication can arise. This class arises when the current is expressed as a function of solution concentrations of the oxidizing agents and may involve factors such as: multi-equivalence of the oxidizing agents, slow sorption or desorption, or non-linearity of isotherms. For such kinetic features, the current can become non-linear in electron concentration at the surface as well as solution concentrations.

It has normally been the custom to treat theoretically semiconductor electrodes by an approach equivalent to metal electrodes and to discuss reduction or oxidation electrochemistry in terms of deviation from the reversible potential. This approach is theoretically valid, but the model may be of little value in interpreting experimental results. The invariance of the Helmholtz potential and the irreversibility of the current are two indications that the reversible potential model is not applicable here.

First we will discuss the invariance of the Helmholtz voltage for the ZnO/Fe(CN)<sub>6</sub><sup>-3</sup> system as a function of concentration and measured current. Such behavior contrasts with a metal electrode in which the net current is normally controlled through deviations from the reversible redox potential. Basically the reason such a situation can arise is that the current due to the reduction of Fe(CN)<sub>6</sub><sup>-3</sup> is only a small fraction of the reversible currents passing through the Helmholtz layer, and these reversible currents determine the Helmholtz voltage. By the argument presented by Dewald,<sup>1</sup> changes in Helmholtz potential at the ZnO electrode should be manifested by changes in the values of the flat band voltage,  $V_0$ . Conversely, changes in the flat band voltage with changes in the chemical composition of the solution, in principle, can be attributed to variations in the Helmholtz and/or surface voltage of the ZnO electrode.

Experimentally, we found only small random variations in the flat band voltage as a function of Fe(CN)<sub>6</sub><sup>-3</sup> concentration and the ratio of the concentrations of Fe(CN)<sub>6</sub><sup>-3</sup> to Fe(CN)<sub>6</sub><sup>-4</sup>. Since it seems unlikely that changes in the surface voltage (determined by the Fermi level at the surface vs the interior when the bands are flat) should exactly compensate changes in the Helmholtz voltage, we conclude that both the Helmholtz and surface voltage at the flat band condition are independent of the concentrations of hexacyanoferrate species. Experimentally for any single solution composition, the value of  $V_0$  remains constant as a function of the applied voltage as observed by the straight line behavior typified by Fig. 2. From this observation, we conclude that the Helmholtz voltage is independent of the dominant reduction process on the ZnO, the reduction of ferricyanide. In preliminary experiments, we have found that the flat band voltage is sensitive to the pH of the solution but insensitive to the several reducing and oxidizing agents investigated.

It is, therefore, our belief that the Helmholtz voltage of the electrode is not associated with any electron transfer redox reaction occurring on the surface, but should be ascribed to proton transfer, or to some equivalent chemical process which does not involve electrons or holes.

Next we shall consider the currents passing between the surface and the interior of the semiconductor. In our semiconductor surface-state model, as previously discussed, the flow of negative current from the interior to the surface is associated with an activation energy of  $qV_s$  which arises from the endothermicity of moving an electron in the conduction band from the interior to the surface. The reverse process is the oxidation and could occur by transfer of an electron from the reduced sorbed species to the bottom of the conduction band in the interior of the semiconductor. The latter process would be expected to have an activation energy equal to  $E$ , the energy difference between the surface state and the bottom of the conduction band at the surface (Fig. 4). For the surface state on ZnO due to the hexacyanoferrate, the value of  $E$  could be as high as 3 eV. If the value of  $E$  is high, the rate of the oxidation process can be extremely low.

Thus deviations from a "reversible potential" on the solution side (Helmholtz) or within the semiconductor can not be used to describe the net current flowing through the electrochemical cell. Furthermore, the experimental condition of zero

net current does not correspond to some "reversible potential" analogous to a metal electrode since the rate of the anodic process in the semiconductor model is always essentially zero.

Experimentally, however, we do observe small residual net anodic currents. The residual anodic current observed with ZnO can sometimes be attributed to stray ultraviolet illumination (energies greater than the band gap), which produces holes. In other cases, thermal generation of hole-electron pairs in the bulk will provide a higher anodic current than electron injection having an activation energy E. In either case, the potential at zero current is not the reversible potential of a chemical redox reaction but is the result of opposing currents, both of which are determined by physical processes not occurring in the solution.

We believe the major sources of the low anodic currents in the dark may be imperfections and impurities on the surface of the sample. The results with our crystals are consistent with this notion, i.e., the saturation dark anodic current varied randomly from 0.1 to 10 na cm<sup>2</sup> with repeated etchings in phosphoric acid under presumably identical conditions. On the other hand, the addition to the solution of the reducing agent, Fe(CN)<sub>6</sub><sup>-4</sup>, had a negligible effect on the anodic current.

This behavior is probably quite typical of electrochemical reactions on wide band gap semiconductors and theoretical analysis based on reversible reactions may often be very misleading.

The last point of our discussion concerns the surface-state capacitance, C<sub>ss</sub>, which is defined<sup>5</sup> as dQ<sub>ss</sub>/dV where Q<sub>ss</sub> is the charge in the surface states. We will present arguments to show that there is no inconsistency between our experimental results which indicate the absence of a surface-state capacitance and our theoretical model which depends on the existence of surface states. It should be emphasized that the experimental absence of a surface state capacitance in a semiconductor electrolyte system should not be taken to imply the absence of surface states. This point is important because the absence of a surface-state capacitance has often<sup>1,3</sup> been taken to indicate the absence of surface states.

Experimentally, the absence of a surface-state capacitance in parallel with the space charge is shown by the linearity of (C)<sup>-2</sup> with V. The reasoning is based on the expectation that, in general, (C<sub>ss</sub>)<sup>-2</sup> will not be linear with V. The details of the formulation of the various capacitances and voltages in a semiconductor/electrolyte system are contained in the appendix. It should be recalled that all the solutions studied in our investigation showed a linear relationship between (C)<sup>-2</sup> and V.

There are two possible reasons why a capacity C<sub>ss</sub> is not observed: one, the implicit assumptions of the derivation are not met; and second, there are no surface states over the region spanned by the surface Fermi level as V is varied. We will present arguments that both of these causes are present with most semiconductor electrolyte systems.

Implicit in the derivation of the surface-state capacity is the assumption that the charge dQ<sub>ss</sub> is stored from the semiconductor side and is returned to the semiconductor when the voltage increment dV is removed. This assumption is not met for two types of surface states: those that are electronically irreversible (i.e., charge cannot transfer in both directions) and those that are reversibly adsorbed from solution. If the states are irreversibly charged within the period of the a.c. signal, then the charge will not be returned to the semiconductor and the states will not act as charge storage centers. If the states are desorbable, so that they maintain equilibrium with the solution, they will simply lower the real part of the impedance rather than the capacitive part.

The second reason for the inability to observe a capacitance for surface states is connected with a pinned surface Fermi level. A pinned surface level, independent of known parameters, can arise from the presence of second surface state which can not store charge from the semiconductor. This second surface state may be of two types: (a) present at a high density on the surface, either formed by irreversible or reversible sorption, or (b) present at low density and formed by reversible sorption. The effectiveness of type (a) in pinning the Fermi level is self evident. Type (b) is effective since any attempt at changing the surface Fermi level by changing the applied voltage is prevented by sorption or desorption of type (b) surface states in the appropriate state of oxidation. Thus, the existence of a low density of sorbable-desorbable surface states can prevent observance of a capacitance for another surface state that meets the normal requirements for observation.

In summary, in order to observe a surface-state capacitance the surface states must be: (1) electronically reversible within the period of the a.c. signal; (2) nondesorbable from the semiconductor; and (3) in contact with an electrolyte free of chemicals that can rapidly exchange charge with the surface state or with the semiconductor in order to prevent pinning the surface Fermi level.

In the case of our ZnO studies, none of these criteria were met, according to the evidence. There have been no reversible surface states identified in our studies, most of the chemical species examined were appreciably soluble in both the oxidized and reduced forms and species normally were available that could be adsorbed and could pin the Fermi level. However, it is possible that common contaminants present in our solutions were sufficient to pin the Fermi level.

#### SUMMARY

We have shown, by analysis of the one-equivalent reduction of the ferric iron, that for semiconductors the electronic activation energy can dominate the rate of electrochemical reactions and a simple surface-state trapping law describes the process. We have also shown that the reaction is irreversible and an unknown oxidation reaction (not oxidation of ferrous) is important in defining the "zero current" potential. In addition, we found that adsorption of ferricyanide ion on zinc oxide follows a linear isotherm.

#### REFERENCES

1. J. F. Dewald, *J. Phys. Chem. Solids* **14**, 155 (1960); *Bell Systems Tech. J.* **39**, 615 (1960).
2. J. F. Dewald in *Surface Chemistry of Metals and Semiconductors*, Ed. John Wiley, New York, 1960.
3. S. Roy Morrison and T. Freund, submitted for publication.
4. H. Gerisher in *Surface Chemistry of Metals and Semiconductors*, Ed. H. C. Gatos, John Wiley, New York, 1960.
5. A. Many, Y. Goldstein, and N. B. Gover, *Semiconductor Surfaces*, John Wiley, 1965.
6. W. H. Brattan and Bartein, *Bell Systems Tech. J.* **32**, 1 (1953).
7. W. H. Brattan and C. G. B. Garrett, *Bell Systems Tech. J.* **34**, 129 (1955).
8. H. Gerischer, *Ann. Rev. Phys. Chem.* **12**, 227 (1961).
9. P. J. Body, *J. Electroanalytical Chem.* **10**, 199 (1965).

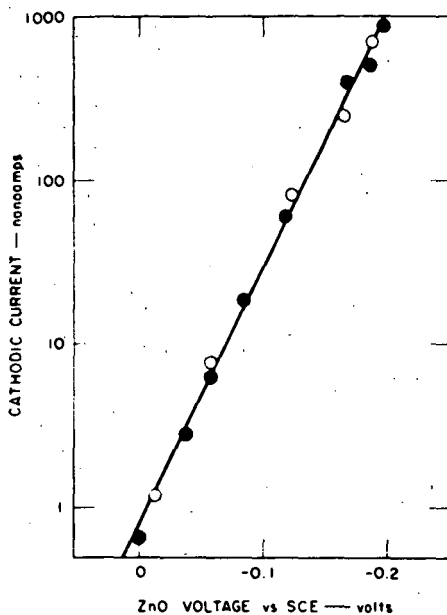


FIG. 1 CURRENT DEPENDENCE ON VOLTAGE AT pH = 8.8 AND  $7 \cdot 10^{-3} \text{M}$   $\text{Fe}(\text{CN})_6^{3-}$ : ●, NO ADDED  $\text{Fe}(\text{CN})_6^{4-}$ ; ○,  $7 \times 10^{-2} \text{M}$   $\text{Fe}(\text{CN})_6^{4-}$  ADDED

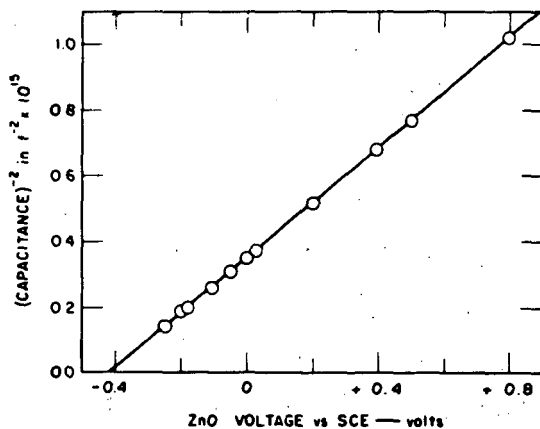


FIG. 2 VOLTAGE DEPENDENCE OF CAPACITANCE FOR  $7 \times 10^{-4} \text{M}$   $\text{Fe}(\text{CN})_6^{3-}$

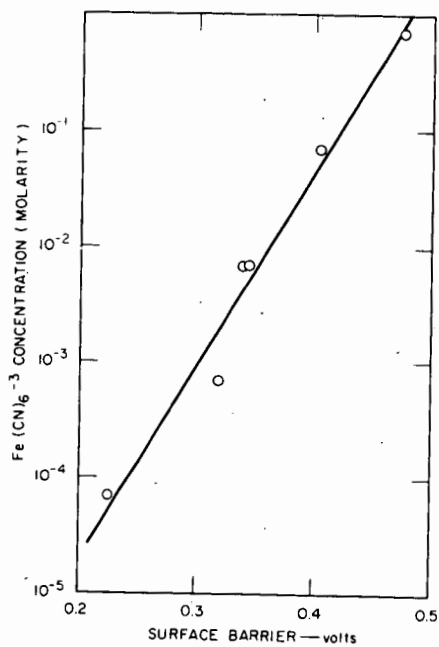


FIG. 3 SURFACE BARRIER AS A FUNCTION OF CONCENTRATION AT  $10^{-10}$  AMP CURRENT

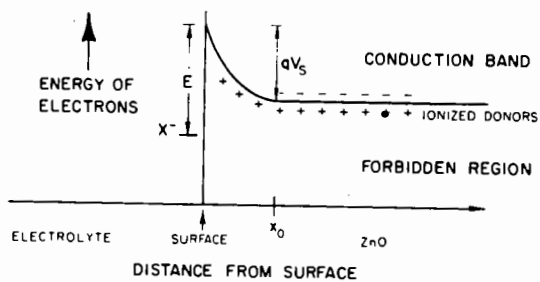


FIG. 4 ENERGY BAND DIAGRAM

THE ROLE OF HYDROGEN PEROXIDE IN OXYGEN REDUCTION  
AT Pt, Rh AND Au ELECTRODES

M. A. Genshaw, A. Damjanovic and J. O'M. Bockris

The Electrochemistry Laboratory  
The University of Pennsylvania  
Philadelphia, Pa. 19104

For oxygen reduction at electrodes in acid solutions, some workers have reported<sup>1,2</sup> that oxygen reduces only to water, others that hydrogen peroxide is either an intermediate in the reduction to water or a product in the reduction.<sup>3-8</sup> A similar situation exists for alkaline solution where hydrogen peroxide appears to be a reaction intermediate which reduces further.

Little or no attention was paid to the possibility that parallel reactions may be present. In one reaction, oxygen could be reduced to water without hydrogen peroxide as a stable intermediate. In the other, hydrogen peroxide could form as a reaction intermediate which then reduces at least partially to water. These parallel reactions may be represented by



Hydrogen peroxide, which is an intermediate in path (2), is partially reduced to water and partially diffuses away from the electrode.  $I_1$ ,  $I_2$  and  $I_3$  are the corresponding currents, and  $I_4$  represents the rate by which  $\text{H}_2\text{O}_2$  diffuses away.

Recently, it was demonstrated that it is possible to analyze these parallel reaction paths, and to determine whether hydrogen peroxide is a reaction intermediate in a single reaction path, or a product in a reaction path parallel to that in which oxygen is reduced to water without hydrogen peroxide intermediate.<sup>9</sup> For this analysis, a rotating disk electrode with a concentric ring is used.

In this communication, the application of the rotating disk electrode with the concentric ring in the study of oxygen reduction at Pt, Rh and Au disk electrodes in acid and alkaline solutions is described, and some data are presented and discussed.

If hydrogen peroxide is formed at the test, the disk electrode, kept at a required potential, it may diffuse away from the disk to the ring electrode. The potential of the ring electrode is kept at 1.4 V\* so that all hydrogen peroxide which diffuses to the ring electrode is oxidized and detected. For the current at the disk electrode at a given potential,  $I_d$ , and the current at the ring electrode,  $I_r$ , the following relationship holds

$$\frac{I_d}{I_r} = \frac{x+1}{N} + \frac{x+2}{N} \cdot \frac{\nu^{1/6} k_3}{D^{2/3} \omega^{1/2}} \quad (3)$$

Here,  $N$  is a geometrical factor which depends on the dimensions of the disk and

\*All potentials are with respect to the hydrogen electrode in the same solution.

ring electrodes,  $D$  is the diffusion coefficient for the reaction intermediates,  $\nu$  is kinematic viscosity,  $k_3$  is the rate constant for the reduction of  $H_2O_2$  intermediate at the disk electrode and  $\omega$  is the rate of disk rotation. In this equation,  $x$  is defined as

$$x = I_1/I_2 \quad (4)$$

with  $I_1$  being the partial current due to the reduction of oxygen to water in the path without hydrogen peroxide intermediate, and  $I_2$  the partial current due to the reduction to hydrogen peroxide.

From the plots of  $I_d/I_r$  against  $\omega^{-1/2}$  the intercept with the  $I_d/I_r$  axis,

$$\text{Intercept} = (x + 1)/N, \quad (5)$$

can be read. With  $N$  known,  $x$  can be calculated and hence the ratio  $I_1/I_2$  obtained.

Pt, Rh and Au disk electrodes are examined in acid (0.1 N  $H_2SO_4$ ) and alkaline (0.1 N KOH) solutions saturated at room temperature by  $O_2$  under 1 atm. pressure. Currents at the disk and ring electrodes have been measured as functions of the disk potential and for various rates of disk rotation.

For Pt electrode in acid solution the plots of  $I_d/I_r$  against  $\omega^{-1/2}$  consists of a series of lines parallel to the  $\omega^{-1/2}$  axis (Fig. 1). Each line corresponds to a given potential of the disk electrode and has an intercept with  $I_d/I_r$  axis greater than  $1/N$ . Hence, oxygen reduction proceeds along two parallel reaction paths. Hydrogen peroxide is produced in a path parallel to the reaction path which does not involve  $H_2O_2$  as an intermediate. At potentials anodic to, say, 0.60 V, the intercepts are all greater than 20, and  $x \gg 7.6$  ( $N = 0.38$ ). Hence, the major reaction is that in which  $O_2$  is reduced to  $H_2O$  without  $H_2O_2$  intermediate (90% or more of the total current). Since the slopes of the lines are zero,  $k_3$  in equation (3) is small. It implies that  $H_2O_2$  formed in the parallel reaction path is not reduced further to water with any rate comparable to that by which it is produced.

The solution in which the above experimental data are obtained was prepared from "Baker Analyzed Reagent"  $H_2SO_4$  and conductivity water. However, if this solution was further purified electrochemically, no hydrogen peroxide is detected to form at potentials anodic to 0.150 V. Such a different behavior of the electrode in "pure" and "insufficiently" purified solutions is believed to be due to the adsorption at the electrode surface of residual, mostly organic, impurities from the solution.

At Pt electrode in alkaline solution,  $I_d/I_r$  plots reveal that oxygen reduction proceeds with comparable rates along two reaction paths (Fig. 2). In one of these paths, hydrogen peroxide is an intermediate which partially reduces further. In contrast to Pt electrode in acid solution, Pt electrode in alkaline solution appeared to be not affected by the presence of residual impurities in the solution.

Similar experiments with Rh in acid solution showed that the behavior of the electrode is also affected by purification of the solution. In "insufficiently" purified solutions,  $H_2O_2$  is formed in a path parallel to that in which  $O_2$  is reduced to water without hydrogen peroxide as an intermediate. The major reaction is the reduction to  $H_2O$  without hydrogen peroxide intermediate. In contrast to a Pt electrode, at potentials cathodic to 0.60 V hydrogen peroxide formed at Rh electrode reduces, at least partially, further to water. In "pure" acid solutions oxygen reduction at Rh electrode proceeds along a single reaction path which does not involve hydrogen peroxide intermediate. In alkaline solution, the major reaction path is that in which  $O_2$  is reduced to hydrogen peroxide. Hydrogen peroxide reduces further to water.

For a gold electrode in acid solution, the current-potential relationship for oxygen reduction has a characteristic "S" shape. This is illustrated in Figure 3. Two linear regions in  $V$ - $\log i$  plots are evident, each with a slope close to  $-2RT/F$ . Similar results have previously been reported.<sup>7</sup> Reaction path for oxygen reduction in these two regions can now be examined by the disk electrode with a concentric ring.

The plots of  $I_d/I_r$  against  $\omega^{-1/2}$  are shown in Figures 4 and 5. In the potential range 0.55 - 0.65 V, the  $I_d/I_r$  lines have negative slopes at smaller values of  $\omega^{-1/2}$ . The lines are essentially parallel to the  $\omega^{-1/2}$  axis from 0.50 to 0.25 V but show positive slopes at 0.20 V and more cathodic potentials. The intercepts of the lines with the  $I_d/I_r$  axis in the potential range 0.00 to 0.35 V are clustered between 2.7 and 3. At higher potentials, the intercepts increase with increasing potential. In contrast to Pt and Rh, oxygen reduction at Au electrodes is not affected by the presence of residual impurities in solution.

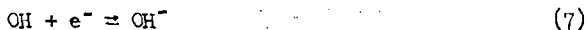
From the intercept given by (5), and with  $N$  equal to 0.39, it appears that at and below 0.30 V  $x$  is small. With  $x \approx 0$ , oxygen reduction at Au in acid solution proceeds along a single reaction path with hydrogen peroxide as an intermediate. At and below 0.20 V, hydrogen peroxide intermediate reduces further to water with a rate which increases with decreasing electrode potential. In the potential region 0.35 - 0.55 V,  $x \neq 0$  and hence oxygen reduction proceeds with nearly equal rates along two parallel reaction paths. At still higher electrode potentials, the major reaction is the reduction of oxygen to water without hydrogen peroxide intermediate. Hydrogen peroxide which at these high potentials forms in a parallel path does not reduce to water with any significant rate. A representation of this discussion is shown also in Figure 3. Just at the potential at which there is the change from one Tafel region in the  $V$ - $\log i$  curve to the other, the change in the importance of the reaction paths occurs. Thus, at potentials anodic to 0.60 V, oxygen is reduced mainly to water while at potentials cathodic to 0.5 V, the main path is that in which oxygen is reduced to hydrogen peroxide.

The characteristic change in the  $V$ - $\log i$  curve at a current of about  $5 \cdot 10^{-6} A$  resembles the attainment of a limiting current for the reaction which predominates in the low current density region, until another reaction, which predominates in the high current density region, takes over. It is difficult to see any reason for this change in the reaction other than the surface heterogeneities. If heterogeneity of the electrode surface is assumed, about 1% of some active "sites" will be enough to sustain the major reaction in the region of low currents. Negative slopes of  $I_d/I_r$  lines in Figure 5, suggest also that this major reaction, which is reduction of oxygen to water, occurs at some active "sites." These slopes are observed in the current region in which the reduction to water becomes apparently diffusion controlled. With increasing rate of disk rotation, diffusion of oxygen to these "sites" increases and so does the current for the reduction of oxygen to water. Consequently, the disk current increases while the ring current remains unchanged, and, for the same electrode potential,  $I_d/I_r$  decreases with increasing  $\omega^{-1/2}$ .

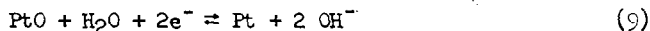
In alkaline solution at gold electrode it appears that oxygen reduction proceeds along a single reaction path with hydrogen peroxide as an intermediate which reduces further to water.

From the slopes of the lines of  $I_d/I_r$  against  $\omega^{-1/2}$ ,  $k_3$  in equation (3) can be calculated for a given potential. In Figure 6,  $\log k_3$  is plotted against potential for the reduction at Pt electrodes in alkaline solution. If a straight line were drawn through the points, the slope would be about 0.6 V. This unusually high slope for the change of the log rate with potential probably indicates that the reduction of hydrogen peroxide is controlled by a chemical rather than a charge transfer step. Accordingly, two possible mechanisms for the reduction of hydrogen

peroxide at Pt in alkaline solution may be suggested:



or



These mechanisms are indistinguishable by usual electrochemical means. Similar situation exist for Rh and Au electrodes in alkaline solution.

The above examples clearly demonstrate the complexity of oxygen reduction at electrodes. More often than not, parallel reaction paths are present, particularly at lower potentials and insufficiently pure solutions. If hydrogen peroxide formed in a parallel reaction or as a reaction intermediate in a single reaction path, it may reduce further with the rate lower than that by which it is formed. The same examples also illustrate the suitability of the rotating disk electrode with the concentric ring in the study of parallel reaction paths.

#### REFERENCES

1. J. J. Lingane, *J. Electroanal. Chem.*, **2**, 296 (1961).
2. K. I. Rozenthal and V. I. Veselovskii, *Zh. Fiz. Khim.*, **35**, 2481 (1961).
3. L. Muller and L. N. Nekrasov, *Electrochim. Acta*, **9**, 1015 (1964).
4. A. Kozava, *J. Electroanal. Chem.*, **8**, 20 (1964).
5. G. Bianchi and T. Mussini, *Electrochim. Acta*, **10**, 445 (1965).
6. A. I. Krasilshchikov, *Zh. Fiz. Khim.*, **26**, 216 (1952).
7. G. Bianchi, F. Mazza and T. Mussini, *Electrochim. Acta*, **11**, 1509 (1966).
8. J. P. Hoare, *Electrochim. Acta*, **11**, 311 (1966).
9. A. Damjanovic, M. A. Genshaw and J. O'M. Bockris, submitted for publication.

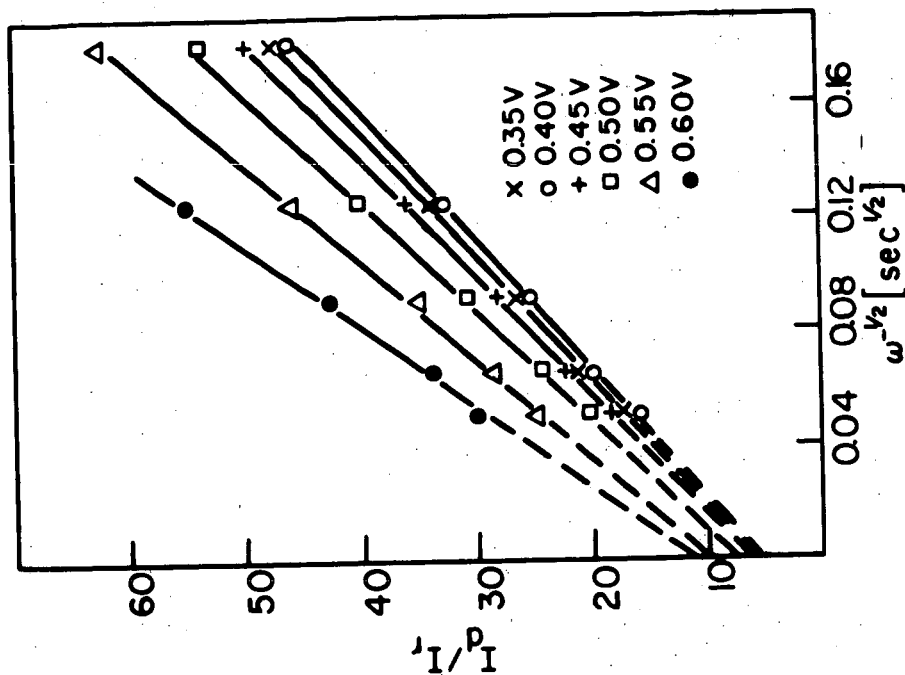


FIG.2  $I_d/I_r$  against rate of disk rotation.  
Pt in 0.1N KOH.

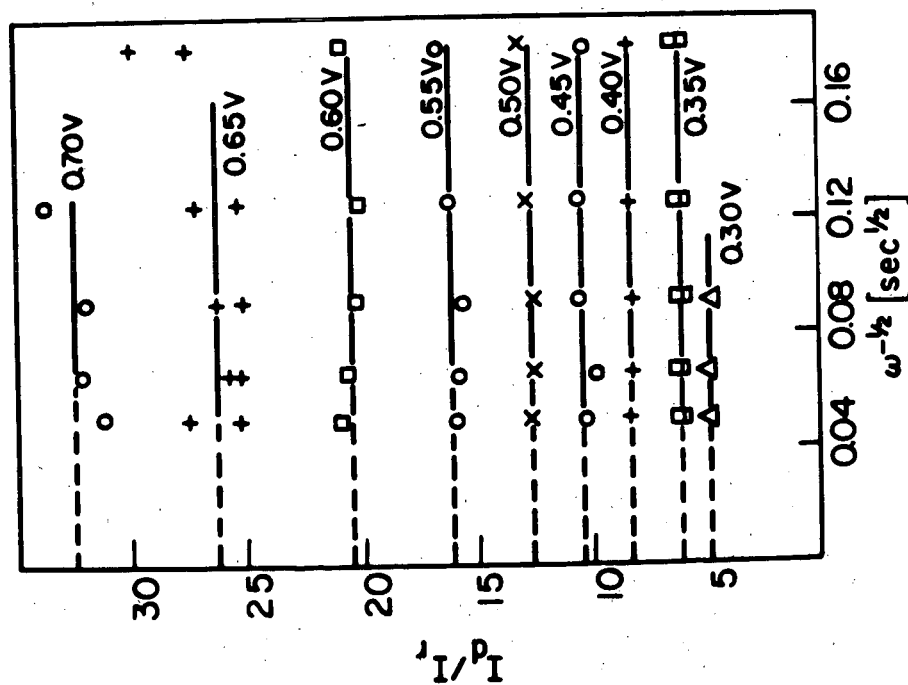


FIG.1  $I_d/I_r$  against rate of disk rotation.  
Pt in 0.1N H<sub>2</sub>SO<sub>4</sub>.

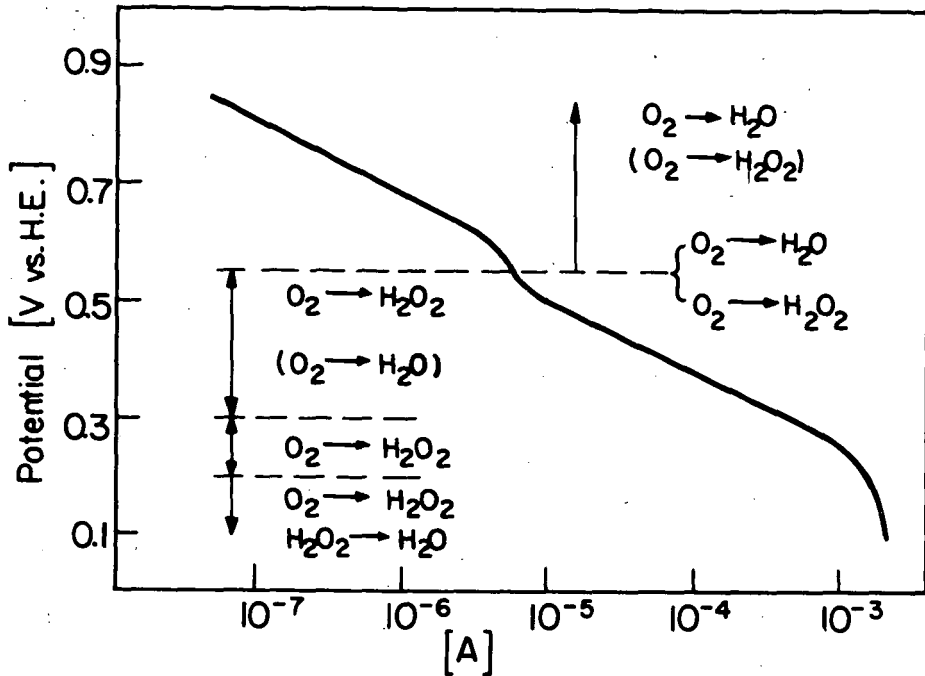


FIG.3 Disk current. Au in 0.1N H<sub>2</sub>SO<sub>4</sub>. Minor reaction given in brackets.

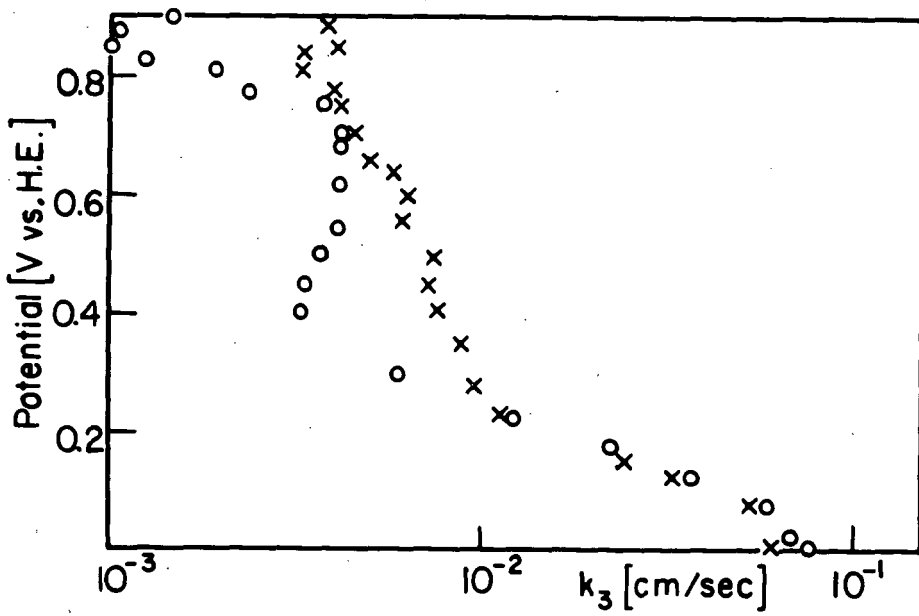


FIG.6  $k_3$  vs. potential plot. Pt electrode in alkaline solution. Two measurements.

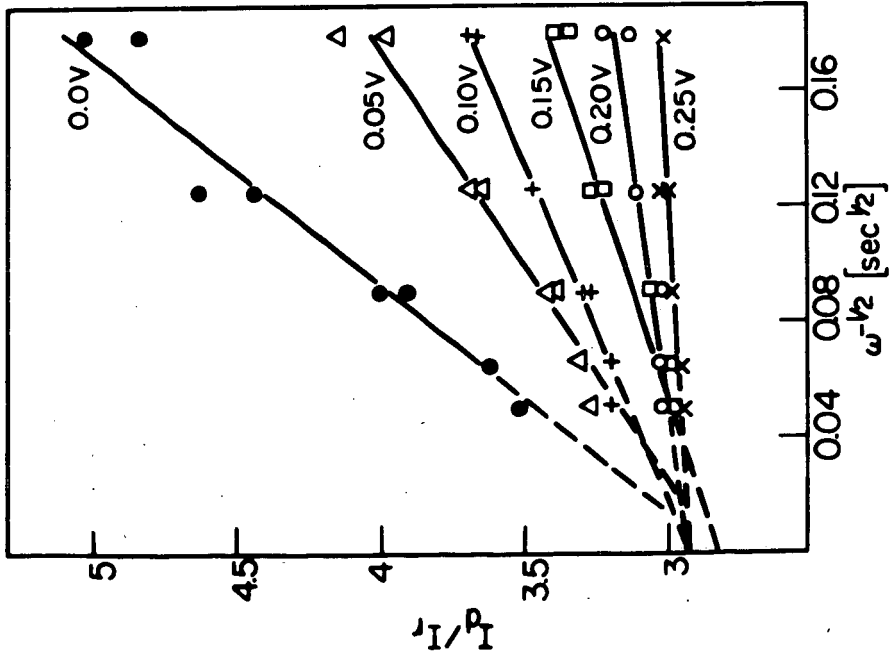


FIG.4  $I_L/I_p$ , against rate of disk rotation.  
Au in 0.1N H<sub>2</sub>SO<sub>4</sub>.

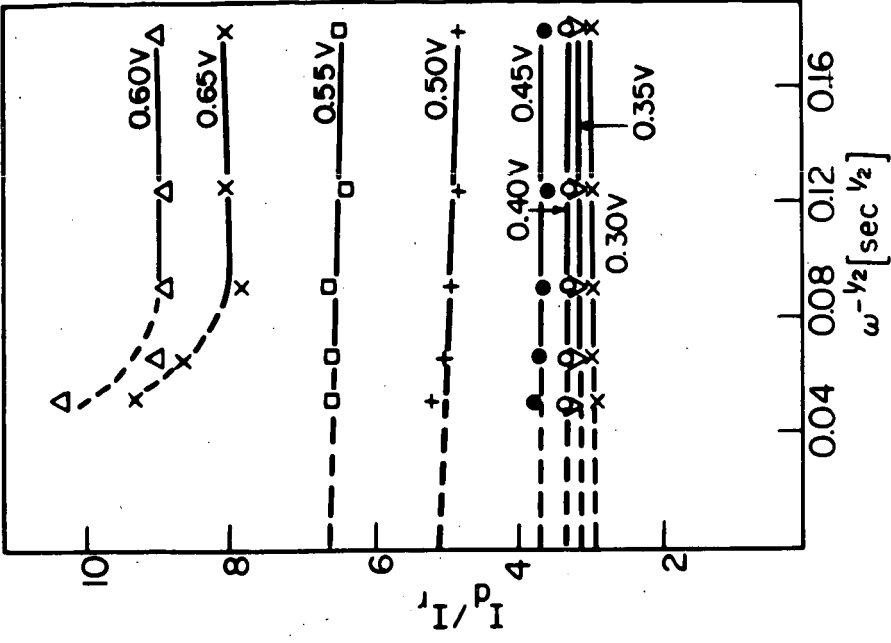


FIG.5  $I_L/I_p$ , against rate of disk rotation.  
Au in 0.1N H<sub>2</sub>SO<sub>4</sub>.

KINETIC ISOTOPE EFFECTS IN OXYGEN ELECTRODE REACTIONS  
 I. General Theory of Primary and Solvent H/D Isotope  
 Effects in the Electrochemical Reduction of Oxygen

J. D. E. McIntyre and M. Salomon\*

Bell Telephone Laboratories, Incorporated  
 Murray Hill, New Jersey

INTRODUCTION

The effects of isotopic substitution on chemical reaction rates have been employed extensively to elucidate reaction mechanisms and to provide criteria for the identification of rate-determining steps.<sup>1,2</sup> Although isotopic effects in chemical kinetics were first demonstrated experimentally<sup>3</sup> by the electrolysis of water in 1932, it is only recently that this method has been applied successfully to detailed kinetic studies of electrochemical reactions.<sup>4</sup> In the present communication, we discuss the kinetic theory of the effects of H/D isotopic substitution on the electrochemical reduction of oxygen in aqueous electrolytes. As a result of the calculations presented below, various mechanisms proposed for the reduction process can be distinguished on the basis of the magnitude of the H/D isotope effect. It is interesting to note that the ratio of standard rate constants for the electrolysis reaction may be very large, near unity, or inverse, depending upon the mechanism operative.

It has been well established<sup>5</sup> that hydrogen peroxide may be formed as a stable intermediate species during the electrochemical reduction of oxygen to water. On electrode materials of high catalytic activity, however, hydrogen peroxide decomposes rapidly via a surface-catalyzed chemical reaction to regenerate oxygen. The effects of this coupled heterogeneous catalytic reaction on the kinetics of oxygen reduction have been discussed previously.<sup>6,7</sup> To provide further criteria for establishment of the decomposition reaction mechanism, we have calculated the magnitude of H/D effects for several proposed schemes.

In the treatment which follows, we consider only the effects of complex isotopic substitution of the electrolyte. Species of mixed isotopic composition need not be considered therefore. The ratio of exchange current densities for an electrochemical reaction in light and heavy water electrolytes is given by

$$R_1 = \frac{i_o(H)}{i_o(D)}$$

where the subscript 1 denotes the step in the reaction sequence which is rate-controlling. In calculating this ratio from absolute rate theory we make the following simplifying assumptions:

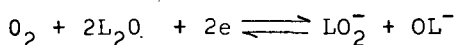
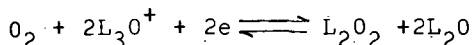
\*On leave of absence from Rutgers, The State University,  
 Department of Chemistry, New Brunswick, New Jersey

- i) All pre-rate-determining steps are in quasi-equilibrium.
- ii)  $\Psi_1$ -effects ( $\Psi_1$  is the potential at the outer Helmholtz plane) can be neglected since they are small and we are only interested in their ratios (cf. reference (8)).
- iii) Limiting Langmuir adsorption conditions are applicable.
- iv) Secondary isotope effects are negligible.

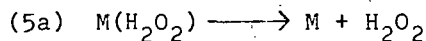
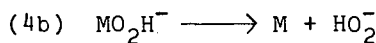
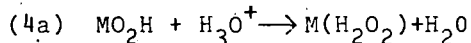
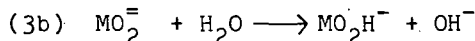
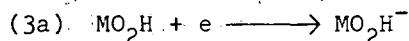
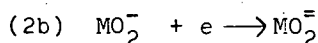
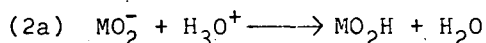
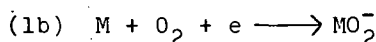
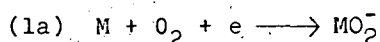
## THEORY

I. Oxygen-Peroxide Electrode

This couple may be represented in acid and alkaline solutions, respectively, as



where L is either H or D. In light water electrolytes, the electrochemical production of  $H_2O_2$  is believed to occur via the following schemes:<sup>5</sup>

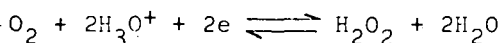
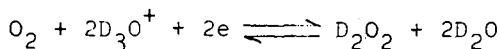


Other schemes are of course conceivable and will be considered in the full paper.<sup>10</sup>

If, in acid solutions, reaction step (1a) is rate-controlling, the ratio of exchange current densities is given by

$$R_{1a} = \frac{[O_2]_{H_2O}}{[O_2]_{D_2O}} \cdot \frac{q_{O_2(D_2O)}}{q_{O_2(H_2O)}} \cdot \frac{q_{O_2^{\ddagger}(H_2O)}}{q_{O_2^{\ddagger}(D_2O)}} \cdot \exp(\beta \Delta \phi F/RT)$$

where the bracketed terms denote the concentrations of molecular oxygen in  $H_2O$  and  $D_2O$  solutions,  $q$  is the molecular partition function of the species indicated (superscript  $\ddagger$  refers to the activated complex) and  $\Delta \phi$  is the potential difference ( $\phi_{D_2O_2} - \phi_{H_2O_2}$ ) for the two overall half-cell reactions



The contribution of the zero-point energy to the vibrational partition function is included in each  $q$ . It will be recalled that this term is principally responsible for the primary kinetic isotope effect of H/D substitution.<sup>1,2</sup> The expression for the exchange current ratio with step (1a) rate-controlling reduces to

$$R_{1a} = \exp(\beta\Delta\phi F/RT)$$

By an analogous method we obtain the following expressions

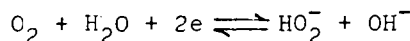
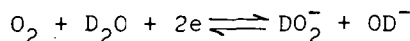
$$R_{2a} = \frac{q_{\text{D}_3\text{O}^+}}{q_{\text{H}_3\text{O}^+}} \cdot \frac{q_{\text{O}_2^{\ddagger}}(\text{H}_2\text{O})}{q_{\text{O}_2^{\ddagger}}(\text{D}_2\text{O})} \exp(\Delta\phi F/RT)$$

$$R_{3a} = \frac{q_{\text{D}_3\text{O}^+}}{q_{\text{H}_3\text{O}^+}} \cdot \frac{q_{\text{H}_2\text{O}}}{q_{\text{D}_2\text{O}}} \cdot \frac{q_{\text{O}_2^{\ddagger}}(\text{H}_2\text{O})}{q_{\text{O}_2^{\ddagger}}(\text{D}_2\text{O})} \exp[(1 + \beta)\Delta\phi F/RT]$$

$$R_{4a} = \left( \frac{q_{\text{D}_3\text{O}^+}}{q_{\text{H}_3\text{O}^+}} \right)^2 \cdot \frac{q_{\text{H}_2\text{O}}}{q_{\text{D}_2\text{O}}} \cdot \frac{q_{\text{O}_2^{\ddagger}}(\text{H}_2\text{O})}{q_{\text{O}_2^{\ddagger}}(\text{D}_2\text{O})} \exp(2\Delta\phi F/RT)$$

$$R_{5a} = \left( \frac{q_{\text{D}_3\text{O}^+}}{q_{\text{H}_3\text{O}^+}} \cdot \frac{q_{\text{D}_2\text{O}}}{q_{\text{H}_2\text{O}}} \right)^2 \cdot \frac{q_{\text{O}_2^{\ddagger}}(\text{H}_2\text{O})}{q_{\text{O}_2^{\ddagger}}(\text{D}_2\text{O})} \exp(2\Delta\phi F/RT)$$

Similarly, in alkaline solutions, we obtain for the reactions



where  $\Delta\phi = \phi_{\text{DO}_2^-} - \phi_{\text{HO}_2^-}$ , the following exchange current ratios.

$$R_{1b} = \exp(\beta\Delta\phi F/RT)$$

$$R_{2b} = \exp[(1 + \beta)\Delta\phi F/RT]$$

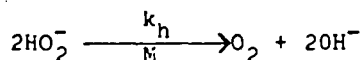
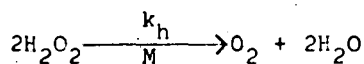
$$R_{3b} = \frac{q_{\text{D}_2\text{O}}}{q_{\text{H}_2\text{O}}} \cdot \frac{q_{\text{O}_2^{\ddagger}}(\text{OH}^-)}{q_{\text{O}_2^{\ddagger}}(\text{OD}^-)} \exp(2\Delta\phi F/RT)$$

$$R_{4b} = \frac{q_{D_2O}}{q_{H_2O}} \cdot \frac{q_{OH^-}}{q_{OD^-}} \cdot \frac{q_{O_2(OH^-)}}{q_{O_2(OD^-)}} \exp(2\Delta F/RT)$$

The evaluation of partition function ratios for the isotopic species  $L_2O$ ,  $L_3O^+$  and  $OL^-$  were carried out as before<sup>8,9</sup> (cf. Appendix); those for the species  $L_2O_2$ ,  $LO_2$  and  $LO_2^-$  were evaluated from spectroscopic and acid-base equilibrium data. The partition function ratios for the activated complexes were evaluated by assuming that the vibrational frequencies of the O-H and O-D bonds not directly participating in the reaction remain unchanged during the transition from the initial to the final state (cf. references 8, 9 where similar treatments have been employed). The results of these calculations show that a wide range of isotope effects can arise and that these effects are strongly dependent upon the nature of the solution employed (ie, acid or alkaline). An inversion of the exchange current ratio is predicted in some instances for the oxygen-peroxide electrode on changing from standard acid to standard alkaline conditions, owing to a solvent isotope effect.

## II. Hydrogen Peroxide Decomposition

The overall decomposition reactions of hydrogen peroxide in acid and alkaline solution are

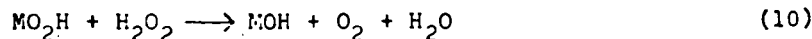


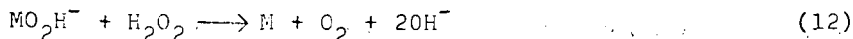
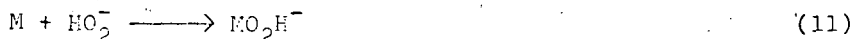
where  $k_h$  represents the heterogeneous chemical rate constant for the surface-catalyzed reaction. As examples of possible reaction mechanisms we consider the following schemes.

### 1) Oxygen Radical Mechanism



### 11) Modified Haber-Willstatter Mechanism



iii) Bimolecular Complex Mechanism

Other possible reaction mechanisms are considered in the final paper.<sup>10</sup>

For a given electrode material, the ratio of rate constants for the heterogeneous decomposition of peroxide in light and heavy water electrolytes is

$$R_{\pm} = \frac{k_h (H_2O_2)}{k_h (D_2O_2)}$$

This quantity may be evaluated from steady state polarization curves for oxygen reduction on a rotating-disk electrode.<sup>6</sup> For the limiting current regions of the current-voltage scans we can make the simplifying assumption that the surface concentration ratios,  $[H_2O_2]/[D_2O_2]$  and  $[HO_2^-]/[DO_2^-]$ , are unity.

Partition function ratios were evaluated as in the preceding section. We shall not present here the total list of expressions for calculation of the isotope effects involving reactions (6)-(12). Two representative calculations are shown below for reactions (6) and (10).

$$R_7 = \frac{q_{DO_2^-}}{q_{HO_2^-}} \cdot \frac{q_H^\ddagger}{q_D^\ddagger}$$

$$R_{12} = \frac{q_{D_2O_2}}{q_{H_2O_2}} \cdot \frac{q_{DO_2^-}}{q_{HO_2^-}} \cdot \frac{q_H^\ddagger}{q_D^\ddagger}$$

Representative rate constant ratios for these and other rate-controlling steps are summarized in Table I.

## DISCUSSION

The predicted kinetic isotope effects vary over a wide range, depending upon the mechanism and rate-controlling step involved. Of particular interest is the prediction of an inverse isotope effect for the oxygen-peroxide electrode. Such an inverse isotope effect has also been found for the oxygen evolution reaction.<sup>4,9</sup>

We have measured the exchange current ratios for the electrochemical reduction of oxygen on gold in acid and alkaline solutions in light and heavy water. In alkaline solutions the kinetic isotope effect is small and normal, but in acid solutions the effect is large and inverse. Small, normal kinetic isotope effects were also observed for the base-catalyzed decomposition of hydrogen peroxide

on gold electrodes and tend to confirm a mechanism involving an ion-molecule complex deduced from studies of pH effects on the kinetics of peroxide decomposition.<sup>12</sup> Details of these experiments will be reported elsewhere.<sup>13</sup>

The fact that predicted isotope effects for several reaction mechanisms are similar may make the assignment of one unique scheme difficult. A similar problem arises in classical electrode kinetic studies when the theoretical Tafel slopes are identical for differing mechanisms. Such results only serve to emphasize the fact that only one type of study is not sufficient to investigate the kinetics and mechanism of complex electrode processes. As with the oxygen and hydrogen evolution reactions, the strength of any conclusion concerning mechanisms lies in consistency of results from all types of studies. The kinetic isotope effect is a powerful tool when used in this sense.

## APPENDIX

For initial state reactants, we have calculated or obtained from the literature, the partition function ratios shown below. All ratios include zero-point energy differences.

$$\frac{q_{D_2O}}{q_{H_2O}} = 1434 ; \quad \frac{q_{D_3O^+}}{q_{H_3O^+}} = 19,023 ; \quad \frac{q_{OD^-}}{q_{OH^-}} = 2615$$

$$\frac{q_{D_2O_2}}{q_{H_2O_2}} = 850 ; \quad \frac{q_{DO_2}}{q_{HO_2}} = 18.9 ; \quad \frac{q_{DO_2^-}}{q_{HO_2^-}} = 14.6$$

The standard potential difference (25°C) of the oxygen-peroxide couple in acidic light and heavy water electrolytes is:

$$\begin{aligned} \Delta\phi^{\circ} &= \phi_{D_2O_2}^{\circ} - \phi_{H_2O_2}^{\circ} \\ &= \frac{RT}{2F} \ln \left[ \left( \frac{q_{H_3O^+}}{q_{D_3O^+}} \right)^2 \left( \frac{q_{D_2O}}{q_{H_2O}} \right)^2 \frac{q_{D_2O_2}}{q_{H_2O_2}} \right] \\ &= + 0.0202 \text{ volt} \end{aligned}$$

Similarly in alkaline solutions:

$$\begin{aligned} \Delta\phi^{\circ} &= \phi_{DO_2^-}^{\circ} - \phi_{HO_2^-}^{\circ} \\ &= \frac{RT}{2F} \ln \left( \frac{q_{H_2O}}{q_{D_2O}} \cdot \frac{q_{OD^-}}{q_{OH^-}} \cdot \frac{q_{DO_2^-}}{q_{HO_2^-}} \right) \\ &= - 0.0198 \text{ volt} \end{aligned}$$

TABLE I

H/D Isotope Effects in the Surface-Catalyzed  
Decomposition of Hydrogen Peroxide

<u>Rate-Determining Step</u>	<u>Rate Constant Ratio, <math>k_h(\text{H}_2\text{O}_2)/k_h(\text{D}_2\text{O}_2)</math></u>
6	1.67
7	1.0
8	1.8
9	5.2
10	1.5
11	1.67
12	2.61

## REFERENCES

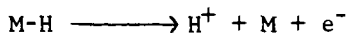
1. J. Bigeleisen and M. Wolfsberg, "Theoretical and Experimental Aspects of Isotope Effects in Chemical Kinetics," in "Advances in Chemical Physics," Interscience, New York (1958).
2. W. H. Saunders, Jr., "Kinetic Isotope Effects," in "Technique of Organic Chemistry, Vol. VIII" ed. A. Weissberger, 2nd ed., Interscience, New York (1961).
3. E. R. Washburn and H. C. Urey, Proc. Natl. Acad. Sci. 18, 496 (1932).
4. B. E. Conway, "Isotopic Effects in Electrode Processes," in "Transactions of the Symposium on Electrode Processes," ed. E. Yeager, p. 267, Wiley, New York (1961).
5. D. J. G. Ives, "Oxide, Oxygen and Sulfide Electrodes," in "Reference Electrodes," eds. D. J. G. Ives and G. J. Janz, p. 322, Academic Press, New York (1961).
6. J. D. E. McIntyre, J. Phys. Chem. (in press).
7. J. D. E. McIntyre and W. F. Peck, Jr., paper presented at the 129th Meeting of The Electrochemical Society, Cleveland, Ohio, May 5, 1966 (Abstract No. 96).
8. M. Salomon and B. E. Conway, Disc. Faraday Soc. 39, 223 (1965).
9. M. Salomon, B. E. Conway, M. Sattar, paper presented at the 127th Meeting of The Electrochemical Society, San Francisco, California, May 12, 1965 (Abstract No. 253).
10. J. D. E. McIntyre and M. S. Salomon, J. Phys. Chem. (to be submitted).
11. W. C. Schumb, C. N. Satterfield and R. L. Wentworth, "Hydrogen Peroxide", Reinhold, New York (1955).
12. J. D. E. McIntyre and W. F. Peck, Jr. (to be published).
13. J. D. E. McIntyre, M. S. Salomon and W. F. Peck, Jr., paper to be presented at the 131st Meeting of The Electrochemical Society, Dallas, Texas, May, 1967.

THE USE OF THE POTENTIAL OF THE HYDROGEN ELECTRODE TO DETERMINE  
THE MECHANISM OF REDUCTION OF COMPOUNDS

T. C. Franklin, D. H. McClelland, P. E. Hudson, J. Barrett

Chemistry Department, Baylor University, Waco, Texas 76703

If the electron transfer reaction at the hydrogen electrode is



where M is the bare adsorption site and M-H is the adsorbed hydrogen atom exchanging electrons with the metal surface, then the equilibrium potential of the electrode should be given by the expression

$$E = E^0 + \frac{RT}{F} \ln \frac{A_H}{(A_{H^+})A_M}$$

If the activity of the adsorbed hydrogen is represented by  $\theta$ , then the activity of the bare metal can be represented by  $1-\theta$ , and at constant hydrogen ion concentration and at 25°C

$$E = E^0 + 0.059 \log \frac{\theta}{1-\theta}$$

The presence of organic or inorganic additives can alter the potential of the hydrogen electrode by changing the hydrogen adsorbed on the electrode. The additive can remove hydrogen by either displacing the hydrogen or reacting with the hydrogen. A study was made of the effect of different additives on the amount of adsorbed hydrogen and the potential of the electrode.

### Experimental

The amount of hydrogen adsorbed on the electrode at equilibrium or under steady state conditions was measured by the coulometric method described previously. (1,2) In the case of the platinized platinum electrodes hydrogen was bubbled over the electrodes until a steady potential was attained. The flow of hydrogen was stopped and sufficient time was allowed for equilibrium to be established between the hydrogen dissolved in the solution and that adsorbed on the electrode. The potential of the electrode was then measured potentiometrically against a reference electrode and the adsorbed hydrogen was removed by polarographic oxidation. The area under the polarographic curve was the number of coulombs needed to oxidize the hydrogen adsorbed on the electrode. This procedure was repeated after the addition of various amounts of the additive.

The experiments on nickel and iron were quite similar except that the hydrogen was electrolytically generated on the surface of the nickel since these metals would not adsorb hydrogen from solution.

The platinum electrodes were platinum wires sealed in glass and plated for three minutes in 3% solution of chloroplatinic acid containing a trace of lead acetate. The electrodes were washed with distilled water and aged for several hours in the solvent to be used in the experiment. Just prior to use these electrodes were polarized anodically for several minutes.

The nickel electrodes were prepared by sealing nickel wire in teflon spaghetti. The iron electrodes were made from iron wires previously etched with nitric acid, washed with doubly distilled water and placed directly in the cell for study. The electrodes were oxidized and reduced several times before the experiments were started.

The temperature was maintained at  $25^{\circ} \pm 0.1^{\circ}\text{C}$ . The p-benzoquinone was purified by sublimation and the acetonitrile was purified by distillation. Other reagents were the purest grade available commercially.

The additives studied were acetonitrile and p-benzoquinone on platinum, 2,7 disodium naphthalenedisulfonate and sodium hypophosphite on nickel, and acetonitrile on iron.

### Data and Results

Figure 1 shows a typical current voltage curve obtained for the oxidation of hydrogen on platinized platinum in two normal sulfuric acid. The shaded area was taken as being proportional to the amount of adsorbed hydrogen. Figure 2 shows a similar plot for iron. The nickel curve was similar to this.

It has been previously reported (1) that a linear relationship exists between the logarithm of the amount of adsorbed hydrogen and the potential when acetonitrile was used as an additive and platinized platinum was the electrode. However, the scatter in the data was very large and an accurate slope was not easily obtained. By not bubbling hydrogen over the electrode during the measurement of potential, it is possible to obtain much more precise data. Figure 3 shows the results obtained in two normal sulfuric acid. It can be readily seen that there is a linear relationship between the potential and the logarithm of the fraction of the surface covered with adsorbed hydrogen. (Logarithm of the amount of hydrogen adsorbed with additive minus the logarithm of the amount of adsorbed hydrogen without additive.) The slope of this line is 0.059 volts. Similarly slopes of approximately 0.059 have been obtained with plots of  $\Delta E$  versus  $\log \theta$  when sodium hypophosphite was used as an additive on nickel (Figure 4) and at low hydrogen coverages when acetonitrile was used as an additive on iron (Figure 5).

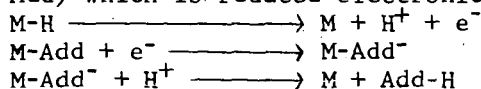
However, if p-benzoquinone is used as an additive in 2N sulfuric acid and platinized platinum is used as the electrode, Figure 6 shows that a plot of  $\Delta E$  versus  $\log \theta$  gives a straight line, but in this case the slope is equal to 0.14. Again if the disodium salt of 2,7 naphthalenedisulfonate is used as an additive in 2N sodium hydroxide solutions with nickel as the electrodes (Figure 7), a plot of the shift in potential against  $\log \theta$  gives a straight line with a slope of 0.12.

### Discussion of Results

The additives can change the amount of adsorbed hydrogen by blocking the surface sites. This merely changes the value of  $\theta$ ; equilibrium is reached at a new point; and the potential will shift in accord with  $\Delta E = 0.059 \log \frac{\theta}{1-\theta}$  or if  $\theta$  is small  $\Delta E = 0.059 \log \theta$ . (1)

The additive can also change the amount of adsorbed hydrogen by reacting with the adsorbed hydrogen. If the reaction occurs directly with the hydrogen atoms, the potential of the hydrogen electrode will

still be calculatable from Equation (I) if the rate of exchange of electrons between adsorbed hydrogen atoms and the electrode is rapid. However, there is a second mechanism of reduction which involves the transfer of an electron from the hydrogen through the metal to the adsorbed additive (M-Add) which is reduced electronically.



In this case the additive behaves like an anodic current and at constant hydrogen ion concentration the shift in potential is given by the equation

$$\Delta E = \frac{RT}{\alpha F} \ln \theta - \frac{RT}{(1-\alpha)F} \ln (1-\theta). \quad (3)$$

At 25°C if  $\alpha$  is assumed to be  $\frac{1}{2}$  this becomes

$$\Delta E = 0.12 \log \frac{\theta}{1-\theta}.$$

If  $\theta$  is small compared to one, this equation reduces to

$$\Delta E = 0.12 \log \theta. \quad (II)$$

The decomposition of the hypophosphite ion on the surface of nickel increases the amount of hydrogen on the surface. This increase undoubtedly is influenced by the presence of adsorbed reactants and products. It can be seen (Figure 3) that, in agreement with theory, the change in potential in this situation follows Equation (I).

The effect of acetonitrile on the potential of the platinized platinum hydrogen electrode has been previously attributed to the blocking action of the nitrile. However, it has been shown that, under the conditions of the experiment, acetonitrile is reduced both on platinized platinum (4) and iron (5). Since the shift in potential (Figure 4 and 5) follows Equation (I), it is evident that this reduction occurs by direct addition of adsorbed hydrogen atoms.

The graphs showing the effect of p-benzoquinone on the potential of the platinum-hydrogen electrode and the disodium salt of 2,7 naphthalenedisulfonate on the nickel-hydrogen electrode indicates that this data follows Equation (II). This shows that these compounds are reduced by the electronic mechanism in agreement with the accepted mechanism (6). The reduction of the sulfonate at nickel electrodes has been discussed by several workers (7,8) and it is probable that it is an electronic mechanism.

In summary it has been shown that the shift in potential of a metal-hydrogen electrode upon the addition of an additive can be used to indicate the mechanism of interaction of the additive with the hydrogen. From the observed data it was concluded that acetonitrile is reduced by direct addition of atomic hydrogen on iron and platinized platinum electrodes. It was also concluded that the reduction of p-benzoquinone on platinized platinum and the 2,7 naphthalenedisulfonate ion on nickel proceeds by an electronic mechanism.

We wish to thank the Robert A. Welch Foundation of Houston for their support of this study.

## References

1. T. C. Franklin and R. D. Sothern, *J. Phys. Chem.* 58, 951 (1954).
2. T. C. Franklin and S. L. Cooke, Jr., *J. Electrochem Soc.* 107, 556 (1960).
3. S. Glasstone, "An Introduction to Electrochemistry", D. Van Nostrand Company, Inc., New York (1942) 448.
4. B. Foresti and S. Musumeci, *Boll. sedute accad. Givonia sci. nat. Catania* 5, 330 (1949).
5. T. C. Franklin and N. F. Franklin, *Plating* 51, 890 (1964).
6. K. J. Vetter, *Z. Elektrochem* 56, 797 (1952).
7. S. E. Beacom and B. J. Riley, *J. Electrochem Soc.* 108, 758 (1961).
8. H. Gotthard and D. Trivich, *Electrochimica Acta* 1, 369 (1962).

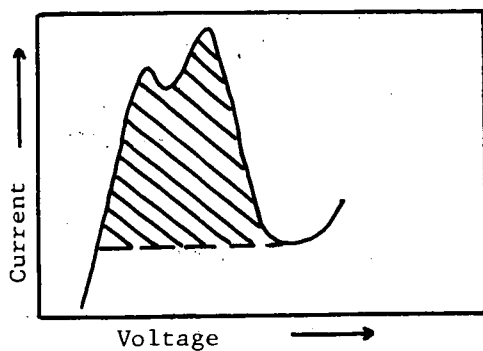


Fig.1. Current Voltage Curve for Oxidation of Hydrogen on Platinum in 2N H<sub>2</sub>SO<sub>4</sub>

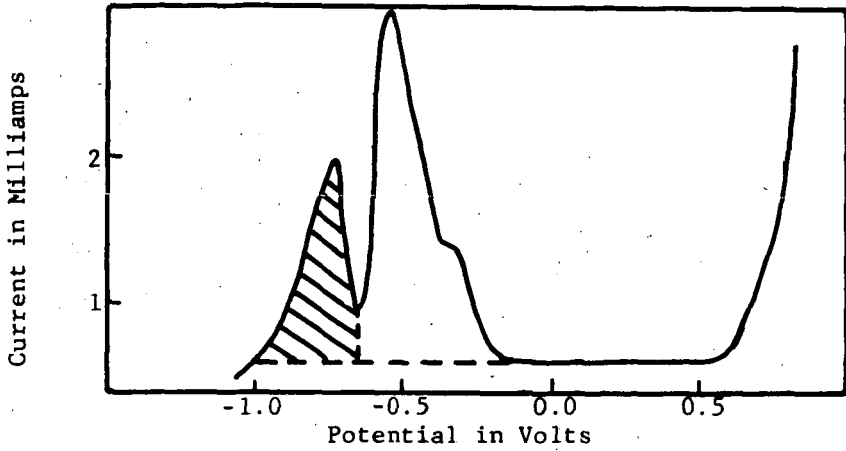


Fig.2. Current Voltage Curve for Oxidation of Hydrogen on Iron in 2N NaOH

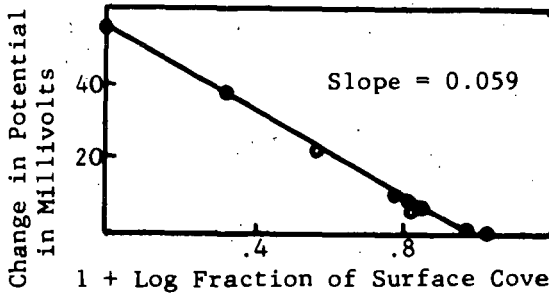


Fig.3. Effect of Acetonitrile on Platinum-Hydrogen Electrode in 2N  $H_2SO_4$

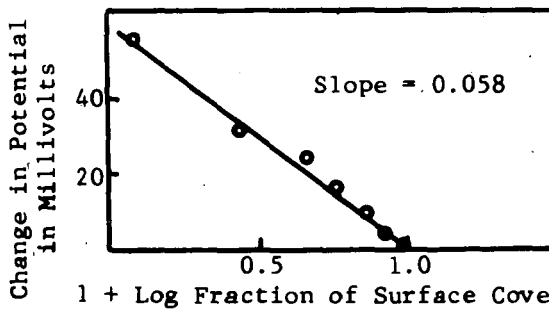


Fig.4. Effect of Sodium Hypophosphite on Nickel-Hydrogen Electrode in 2N NaOH

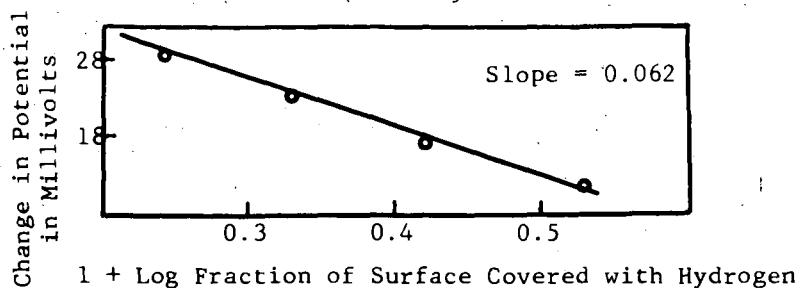


Fig.5. Effect of Acetonitrile on the Iron-Hydrogen Electrode in 2N NaOH

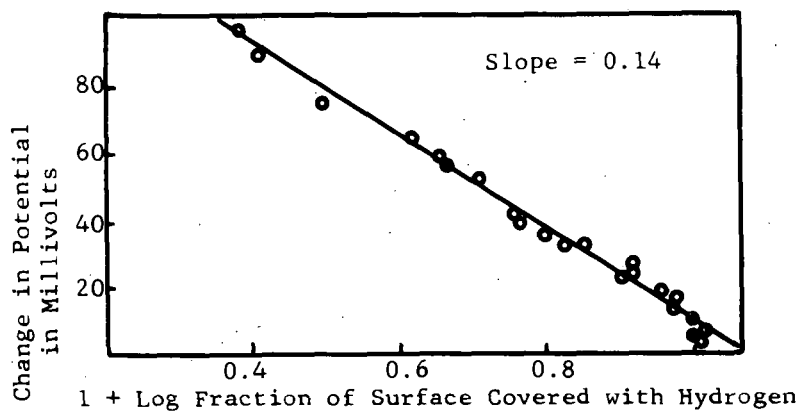


Fig.6. Effect of P-Benzoquinone on the Platinum-Hydrogen Electrode in 2N  $H_2SO_4$

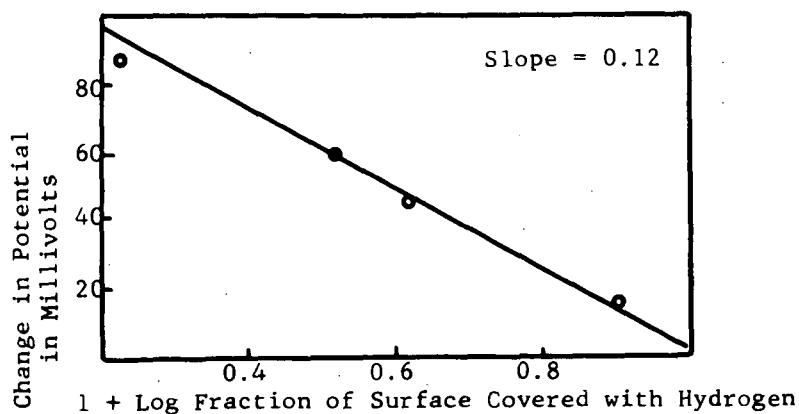


Fig.7. Effect of 2,7 Naphthalenedisulfonate on Nickel-Hydrogen Electrode in 2N NaOH

METHODS FOR DETERMINING THE STRUCTURAL AND STOICHIOMETRIC CHANGES OF  
 $\text{Ni}(\text{OH})_2$  ELECTRODES DURING POLARIZATION IN ALKALINE ELECTROLYTE

Michael A. Aia and Frederick P. Kober

The Bayside Laboratory, research center of  
 General Telephone & Electronics Laboratories Incorporated  
 Bayside, New York

Of the small number of metal oxides that are useful as electrode materials for alkaline batteries, nickel hydroxide combines several desirable characteristics: (1) it is practically insoluble in concentrated alkaline electrolyte, (2) it produces a stable, relatively high potential during discharge, (3) it can be efficiently charged and discharged thousands of times, and (4) it withstands overcharge and overdischarge with relatively little damage. For these reasons, nickel hydroxide is the most commonly used positive electrode material for alkaline cells.

The details of the reactions that occur at the nickel hydroxide electrode in alkaline electrolyte remain poorly defined. It is well established that the starting material has the structure of  $\text{Ni}(\text{OH})_2$  and is gradually converted to some hydrated nickel oxide (usually written  $\text{NiOOH}$ ) during anodic polarization. Some characteristics of the hydrated nickel oxide obtained by electrolysis of nickel hydroxide are black body color, small particle size, and non-stoichiometric composition. These characteristics present a number of analytical problems, for example, absorption spectroscopy is limited to the infrared, and the small particle size causes diffuse x-ray diffraction patterns. Consequently, the crystal structures of the hydrous oxides of nickel have not yet been determined. In the present work, physical, chemical, and electrochemical approaches were used to obtain information on the structure, composition, and hydration states of nickel hydroxide as a function of its oxidation state.

#### Experimental Procedures

Electrodes were prepared by impregnating porous sintered nickel plaques of 80 percent porosity with  $\text{Ni}(\text{OH})_2$ . The plaques were dipped in nickel nitrate solution and then cathodically polarized in concentrated KOH solution.<sup>5</sup> The impregnated electrodes were charged and discharged several times before the nickel hydroxide was anodized to different states of charge. Before analysis, electrodes were washed and dried in nitrogen or vacuum and then ground with a mortar and pestle. Iodometric analysis for active oxygen in the ground powders indicated that the preparative treatment did not significantly decompose the samples. Active oxygen was determined by dissolving 0.1 g of sample in a sodium acetate-buffered solution of acetic acid containing potassium iodide and starch indicator solution; the iodine liberated was titrated with 0.1 N sodium thiosulfate solution. The methods used for further treatment and analysis of the samples, as well as the principal results obtained, are summarized in Table I.

TABLE I

Methods Used and Principal Information Obtained

<u>Technique</u>	<u>Principal Results</u>
X-ray Powder Diffraction	Overall structure and particle size.
Hydrothermal Treatment	Improved crystals for structural studies.
Infrared Absorption	Vibrational spectra of protons.
Thermal Decomposition (DTA and TGA)	Nature of hydration states.
Mass Spectrometry	Analysis of thermal decomposition products.
Chemical Analysis (% Ni, K, $\text{H}_2\text{O}$ , O)	Composition and stoichiometry.
Constant Current Polarization	Electrical capacity and potential.

#### Results and Discussion

Considerable information can be obtained from x-ray powder diffraction patterns, but the results are often ambiguous in the absence of supporting data from single crystal work. In spite of all the compositions and x-ray diffraction patterns that have been reported for oxides and hydrous oxides of nickel, only the structures of  $\text{NiO}$  (rocksalt) and  $\text{Ni}(\text{OH})_2$  (brucite) have

been defined. Even  $\text{Ni}(\text{OH})_2$  has never been studied in detail probably because of the difficulty in obtaining single crystals. Some structural assignments have been made from x-ray powder diffraction analysis:  $\text{Ni}(\text{OH})_2$  has the hexagonal layer structure of brucite,<sup>4, 13</sup> and the space group is  $D_{3d}^3 - P\bar{3}m1$ . The overall structure is composed of complete layers of  $\text{NiO}_6$  octahedra, as shown schematically in Fig. 1. The  $D_{3d}$  site symmetry and layering of the Ni and O atoms in the unit cell can be seen in Fig. 2. Adjacent OH groups are free, i. e., not connected by hydrogen bonds.

The x-ray powder diffraction patterns of nickel hydroxide, as precipitated and in various states-of-charge, are summarized in Fig. 3. The lattice becomes distorted, and the patterns lose some of their features as the oxidation state of nickel hydroxide is increased. A shift to larger values for the  $d_{hkl}$ -spacing of the (001) reflection occurs during oxidation and provides a direct measure of the expansion of the lattice in the  $c$ -direction of the unit cell (Fig. 2). This expansion has also been observed by Harivel and co-workers.<sup>7</sup> A more quantitative explanation of the structural disorder occurring during anodic oxidation of  $\text{Ni}(\text{OH})_2$  was given recently by R. Ritterman and co-workers.<sup>15</sup> As shown in Fig. 3 lattice distortion eventually causes the appearance of a new phase, termed  $\text{Ni}_2\text{O}_3 \cdot \text{H}_2\text{O}$  by Cairns and Ott,<sup>4</sup>  $\gamma$ - $\text{NiOOH}$  by Flemmer and Einerhand,<sup>6</sup> and alpha-phase by Tuomi.<sup>18</sup> A major characteristic of this highly oxidized phase is the diffraction band at  $d = 6.9 \text{ \AA}$ . Sharp x-ray diffraction patterns for  $\text{Ni}(\text{OH})_2$  and  $\text{Ni}_2\text{O}_3 \cdot \text{H}_2\text{O}$  treated hydrothermally in 10 N KOH solution for several days, also shown in Fig. 3, indicate the utility of the hydrothermal method for obtaining materials suitable for structural studies.<sup>1</sup> The crystal structure of the material obtained by hydrothermal treatment of  $\text{Ni}_2\text{O}_3 \cdot \text{H}_2\text{O}$  is still under study.<sup>3</sup> In agreement with crystal field calculations,<sup>12</sup> the overall symmetry is lower than hexagonal.

Infrared spectroscopy was a useful complement to the x-ray diffraction analysis because of its ability to detect changes in the bonding of protons and water in the lattice. As can be seen in Fig. 4, infrared spectra show the OH vibrations characteristic of non-hydrogen-bonded OH groups in both the starting  $\text{Ni}(\text{OH})_2$  and in the discharged electrode. As the oxidation state of the nickel hydroxide is increased, the intensity of the free OH vibrations decrease, while vibrations due to hydrogen-bonded water appear in the spectra.<sup>9, 10</sup>

Differential thermal analysis (DTA) curves, shown in Fig. 5, established that the energy required for thermal decomposition of Ni-OH groups decreases continuously as  $\text{Ni}(\text{OH})_2$  is brought to higher oxidation states.<sup>2</sup> The relative areas under the second peak are indicated. From Fig. 5 it can also be seen that the loosely bound water always found in precipitated  $\text{Ni}(\text{OH})_2$ ,<sup>2, 10</sup> (approximately 0.3 mole  $\text{H}_2\text{O}$  per mole  $\text{Ni}(\text{OH})_2$ ) is more discretely bound in charged electrodes, especially after the structural change to  $\text{Ni}_2\text{O}_3 \cdot \text{H}_2\text{O}$  ( $\gamma$ - $\text{NiOOH}$ ) occurs. For example, compare the first peaks of curves A and J.

Chemical analysis showed that the decrease in hydroxyl water content is accompanied by a corresponding gain in "active oxygen," [O], content. The sum of  $\text{H}_2\text{O}$  and [O] remains essentially constant<sup>2</sup> at 1.3 moles per mole NiO, as shown in Table II.

TABLE II  
Chemical Analysis of Dried Nickel-Hydroxide-Impregnated  
Electrodes in Various States-of-Charge

State-of-Charge	Moles per Mole Ni		
	K	[O]	$\text{H}_2\text{O}$
Over discharged	<0.01	0.10	1.20
68% Charged	0.08	0.41	0.84
100% Charged	0.14	0.55	0.70
660% Charged	0.16	0.81	0.50

The constancy of the total oxygen content of vacuum-dried samples was confirmed by neutron-activation analysis for oxygen which showed 33.6 weight percent in the discharged nickel hydroxide and 33.8 weight percent in the overcharged material. The electrochemical equivalent of the active oxygen found by analysis was in quantitative agreement with that calculated for the amount of charge passed up to about 1.2 Faraday per g. at Ni. For example, after the passage of 1 Faraday per g. at Ni the active oxygen content was 0.5 g. at per g. at Ni.

Table II also shows that the potassium ion content of the nickel hydroxide increases continuously throughout oxidation in KOH electrolyte. The take-up of potassium ions is reversible, and practically no  $K^+$  remains in the lattice after discharge.<sup>2</sup> The sorption occurs, to a lesser degree, in NaOH solution but not in LiOH where only 20 ppm Li was found after extended anodic polarization. The sorption of alkali metal cations, which is apparently contrary to the flow of current, seems to play an important role in the rate and extent of structural transformation of  $Ni(OH)_2$  to  $Ni_2O_3 \cdot H_2O$  ( $\gamma$ -NiOOH). The tendency for structural conversion decreased in the order  $K^+ > Rb^+ > Na^+ > Cs^+ > Li^+$ , as will be described in detail in a subsequent paper.<sup>3</sup> There was no evidence in x-ray patterns for the formation of  $\gamma$ -NiOOH in LiOH solution, which agrees with Tuomi's results.<sup>18</sup> Furthermore, infrared absorption indicates that the OH groups of the solid phase remain free throughout oxidation in LiOH, and there is no evidence for the hydrogen bonding that occurs in KOH and NaOH.

Thermogravimetric analysis (TGA) shows that about 10 percent  $H_2O$  is removed from the charged material up to a heating temperature of  $150^\circ C$ , as shown in Fig. 6(a). Heating to higher temperatures causes the layer lattice to break down, and NiO is observed in the x-ray diffraction patterns (see top of Fig. 6). Above  $250^\circ C$  the surface area of the material begins to decrease rapidly, as shown in Fig. 6(b). The surface areas were calculated from line widths on the x-ray diffraction pattern, using the method described by Keeley.<sup>8</sup> The line at  $d = 6.9 \text{ \AA}$  was used for  $\gamma$ -NiOOH up to  $140^\circ C$ , and the line at  $d = 2.41 \text{ \AA}$  was used for NiO from  $140^\circ$  to  $400^\circ C$ ; line widths were compared to that of the Ni spacing peaking at  $d = 1.762 \text{ \AA}$ . Using gas adsorption, Salkind and co-workers<sup>16</sup> reported values of 61-80  $m^2/g$  for the active material in discharged nickel hydroxide electrodes; in charged electrodes, the surface area was about 10 percent higher.<sup>17</sup> The loss of surface area starts at higher temperatures than the loss of electrochemical capacity stored by the charged material, as shown in Fig. 6(c). Infrared analysis has shown that the capacity loss caused by thermal treatment of charged electrodes is accompanied by a corresponding loss in the intensity of absorption due to "hydrogen-bonded water" at  $580 \text{ cm}^{-1}$ .<sup>11</sup> In discharged electrodes the thermally induced loss of electrochemical activity is directly related to the loss in intensity of free OH vibrations in the infrared spectra.<sup>10</sup> The gases released during thermal decomposition were analyzed with a mass spectrometer.<sup>3</sup> The results for a charged material corresponding to NiOOH show that oxygen, as  $O_2$ , was released from previously vacuum dried, charged material in appreciable amounts only above  $200^\circ C$ ; the rate of evolution of  $O_2$  was fastest at about  $250^\circ C$ . X-ray diffraction data showed that above  $250^\circ C$  the NiO became much better crystallized and the surface area decreased rapidly. From TGA, the amount of  $O_2$  plus residual  $H_2O$  evolved from  $150^\circ$  to  $400^\circ C$  was close to 9 percent of the starting weight; the theoretical [O] content of NiOOH is 8.7 percent.

### Summary

A wide variety of standard methods of analysis were used to study changes that occur in the structure and chemical composition of nickel hydroxide electrodes during anodic polarization in concentrated aqueous solutions of Group I metal hydroxides. X-ray diffraction patterns indicate the general nature of the distortion and expansion of the unit cell, but give no information on the hydration states. Infrared absorption spectra reveal the continuous alteration of hydroxyl sites and the formation of hydrogen-bonded water when  $Ni(OH)_2$  is anodized in 7N KOH. Electrochemical activity was found to be closely related to the quantity of hydroxyl sites in the solid phases. Thermal decomposition analysis shows that the start of loss of electrochemical activity is accompanied by the formation of NiO and the loss of water of constitution, but not the loss of surface area.

## REFERENCES

1. Aia, M. A., *J. Electrochem. Soc.* 113, 1045 (1966).
2. Aia, M. A., Battery Symposium of the Philadelphia Meeting of the Electrochemical Society, Abstract No. 16, October 1966; submitted to *J. Electrochem. Soc.*
3. Aia, M. A., to be published.
4. Cairns, R. W. and Ott, E., *J. Am. Chem. Soc.* 55, 527 (1933).
5. Fleischer, A., *J. Electrochem. Soc.* 94, 289 (1948).
6. Glemser, O. and Einerhand, J., *Z. Anorg. u. Allgem. Chem.* 261, 43 (1950).
7. Harivel, J. P., Morignat, B., Labat, J. and Laurent, J. F., 5th International Power Sources Symp., Brighton, September 1966.
8. Keeley, W. M., *Anal. Chem.* 38, 147 (1966).
9. Kober, F. P., *J. Electrochem. Soc.* 112, 1064 (1965).
10. Kober, F. P., 5th International Power Sources Symp., Brighton, September 1966.
11. Kober, F. P., *J. Electrochem. Soc.*, to be published in early 1967.
12. Kober, F. P. and Aia, M. A., to be presented at Dallas Meeting of the Electrochem. Soc., May 1967.
13. Natta, G., *Rend. accad. Lincei* 2, 495 (1925).
14. Pauling, L., *The Nature of the Chemical Bond*, 3rd ed., p. 557 Cornell University Press, Ithaca, New York (1960).
15. Ritterman, P., Lerner S., Vaughan, P., and Seiger, H. N., Battery Symposium of the Philadelphia Meeting of the Electrochem. Soc., Abstract No. 15, October 1966.
16. Salkind, A. J., Cannin, H. J., and Block, M. L., *Electrochem. Technol.* 2, 254 (1964).
17. Salkind, A. J. and Bodamer, G. W., *Batteries*, 2, D. H. Collins, Editor, pp. 55-62 Pergamon Press, New York (1965).
18. Tuomi, D., *J. Electrochem. Soc.* 112, 1 (1965).

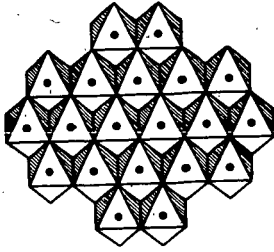


Fig. 1. Schematic diagram of the brucite layer lattice showing the complete layers of  $\text{NiO}_6$  octahedra.

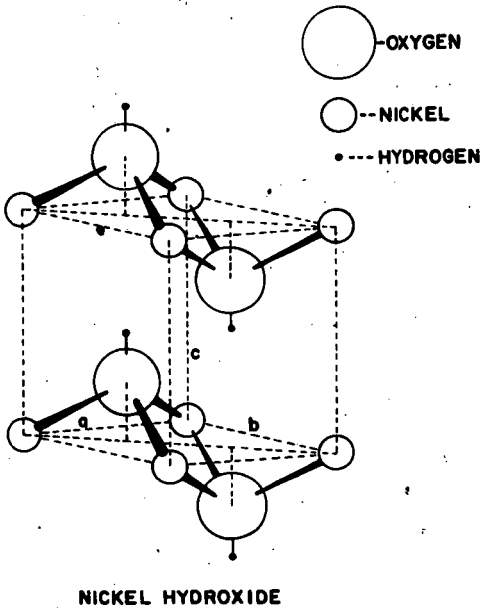


Fig. 2. The unit cell of  $\text{Ni(OH)}_2$  showing the  $D_{3d}$  site symmetry.

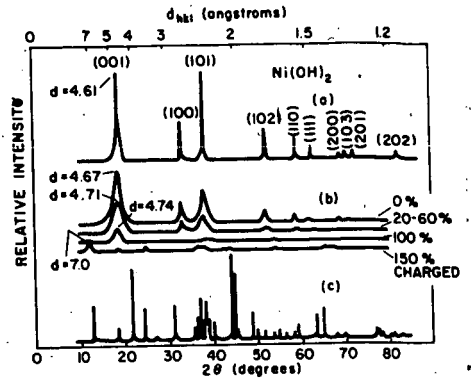


Fig. 3. X-ray powder diffraction diagrams; (a) Hydrothermally treated  $\text{Ni(OH)}_2$ , (b) Electrodes at various states of charge, (c) Hydrothermally treated  $\text{Ni}_2\text{O}_3 \cdot \text{H}_2\text{O}$ .

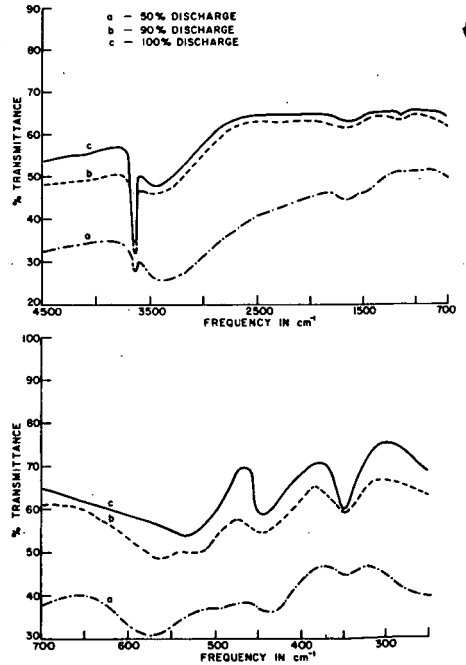


Fig. 4. Infrared absorption spectra of electrodes at various stages of discharge

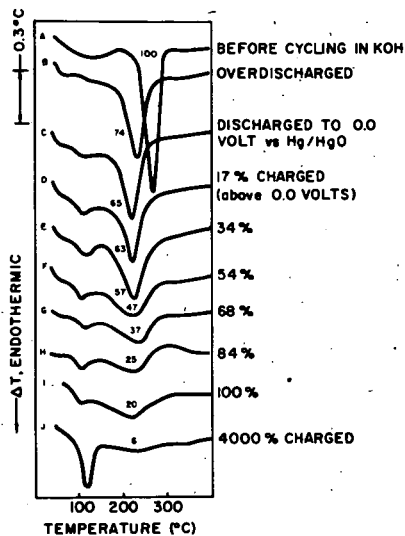


Fig. 5. Differential thermal analysis of electrodes at various states of charge.

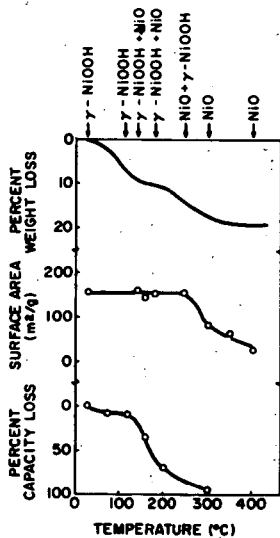


Fig. 6. Weight loss, surface area, and electrical capacity loss as a function of heating temperature.

## THE FINITE CONTACT ANGLE IN POROUS ELECTRODES AND ITS CONSEQUENCES

John O'M. Bockris and Boris D. Cahan

The Electrochemistry Laboratory  
The University of Pennsylvania  
Philadelphia, Pa. 19104

The theoretical solution of the porous electrode has been impeded by two major interrelated problems. The first is the choice of a proper model that is amenable to mathematical treatment, and the second is a solvable mathematical expression compatible with the physical model. The choice of a model has been tackled in several ways.

A number of authors<sup>1,2,etc.</sup> have treated the entire porous electrode as a distributed network of interconnecting pores containing both fuel and electrolyte and, on some statistical basis depending on their exact choice of model, proposed any of several rate-controlling factors, and then set up equations which they then further simplified and linearized to get an analytic solution. This approach ignores the localized nature of the actual three phase region, and can lead to somewhat unrealistic models. For example, to make the mathematics easier, the random network of interconnecting passages between the particles of a sintered porous electrode is frequently 'replaced' by a set of uniform cylindrical tubes running through the porous electrode. Even forgetting that the 'real' porous structure rather resembles a three-dimensional 'string of beads', with relatively large voids interconnected by small non-circular interstices, individual pore behavior may be so dependent on pore size that it is misleading to assign some 'average' value to their diameter. 'Calibrating' factors such as 'tortuosity' can of course always be added to make the solution conform, but they rather tend to obscure the basics involved.

The other approach generally taken is to consider the local question in the meniscus region itself, and to forget the structure of the porous electrode. Thus, for example, Justi<sup>3</sup> proposed a dissociative adsorption on the bare catalyst surface and diffusion of atomic hydrogen to the electrolyte. This treatment, however, yields far too low currents in a practical case.

Will<sup>4</sup> in a paper widely quoted in recent treatments of the subject, suggested that a 'thin film' above the meniscus was the primary active region and showed good agreement with experiments using a partially immersed platinized platinum electrode. Attempts to apply this concept to 'real' electrodes leads to some inherent contradictions. In order to account for the currents produced in his meniscus, Will calculates a .5 to 1.0 $\mu$  film. But in a real porous system, where typical pore sizes are below 1 $\mu$ , this leaves no room for the gas phase, and the electrode would in effect be completely flooded. Further, since many working fuel cells are water-proofed with 'Teflon' or paraffins, a 'thin film' should be inherently unstable.

Experimental: In order to test the various theories, a simulated single pore with two-dimensional symmetry was constructed using closely spaced precision parallel plates (Fig. 1). The electrode is a sputtered Pt film (C) on an optically flat SiO<sub>2</sub> block (D). This block is mounted on a Teflon piston in a Teflon cell so that its spacing to an SiO<sub>2</sub> window (E) can be varied, thus varying the effective slit width. This geometry was chosen rather than that of capillaries because it gave a meniscus length independent of spacing, and permitted direct microscopic observation of the meniscus region.

In most cases, the Pt was in the form of a thin film sputtered onto a sub-film

of Ta, which had been sputtered into the  $\text{SiO}_2$  electrode block. The films produced in this fashion were extremely stable and adherent, and mirror-bright. Electron microscopy showed no structure up to 150,000 X. (One of the electrodes was used for over a year, even though it was accidentally subjected to vigorous  $\text{H}_2$  and  $\text{O}_2$  evolution on several occasions and twice cleaned with concentrated  $\text{HNO}_3$ ). Some experiments (during the initial period) were also run with a Pt foil (.005" thick) sputtered onto the face of the  $\text{SiO}_2$  block, instead of the sputtered (2000 Å) Pt film.

The counter electrode was a thin-walled Pd tube so that any hydrogen evolved on it would diffuse into the metal, rather than be liberated as bubbles which would change the volume of the electrolyte and alter the meniscus level and/or shape. The reference electrode was a Pd-H bead to minimize contamination. This electrode retained a stability of  $\pm 2$  mv over weeks with a  $\text{H}_2$  ambient and for better than a day with  $\text{O}_2$ .

Runs were made both with and without special cleaning precautions. Because of the many close tolerance crevices between parts of the cell, and because of the Pd tube, the usual stringent cleaning regimes ( $\text{H}_2\text{SO}_4$ - $\text{HNO}_3$  mixtures) could not be used. Instead, reagent grade isopropanol was refluxed through the assembled cell for periods up to 10 hours, and then dried for 2-3 days with a stream of highly purified  $\text{N}_2$ . It was then washed with 1-5 liters of conductivity water distilled under  $\text{N}_2$  directly into the cell, and the system dried again. Several additional washings were done with 5-10 cc portions of pre-electrolyzed  $\text{H}_2\text{SO}_4$  and finally filled with fresh electrolyte, after which the cell was sealed off and the desired ambient gas introduced. After this treatment, residual currents were usually much less than  $10^{-7}$  A/cm<sup>2</sup>, and would stay so for long periods of time. A potentiostat was used to follow the voltage-current relationship using  $\text{H}_2$  and  $\text{O}_2$  in 1 N  $\text{H}_2\text{SO}_4$ .

Simultaneously, measurements were made of the meniscus shape using two optical techniques. The first used interferometry with a Na "D" light to measure the thickness of the liquid in the meniscus, and in any 'thin films' which might have been present. The fringes were measured visually and by microphotography and microcinematography.

The second technique used the local curvature of the meniscus to focus the light from a point source of light into a fine line superimposed on the image of the meniscus in a microscope (Fig. 2). From the geometry, the slope of the meniscus at the locus of the line could be calculated down to and including the angle at the meniscus edge, when present. At the same time, this technique permitted an unequivocal determination as to whether a finite contact angle or a thin film continuous with the meniscus existed by the presence or absence of a critical minimum angle for the reflection at the tip.

#### Experimental results:

1. Optical: On the polished metal foil, and on the sputtered films which were not rigorously cleaned, the meniscus edge was always erratic and irregular and showed strong hysteresis on lowering and raising the meniscus level. After cleaning, the meniscus edge was extremely straight, any local variation from linearity usually being less than 25  $\mu$ , the limit detectable with the 60 X microscope which was used. When the meniscus was raised in the slit at a potential  $> 0.8$  V (vs. NHE) and then lowered a 'stable' film was produced above the liquid which slowly drained to a thickness of about .5 to 1  $\mu$ . When the potential was lowered below .6 to .8 V the film split forming a finite contact angle (of between 2-6° depending on conditions), a region with a teardrop shaped cross section above it where the film had been, and a bare space between them (see Fig. 3). Once the thin film was broken, it was not possible to re-establish it except by actual re-immersion at

higher potentials. If the meniscus was lowered slowly at potentials below about .6 V, it always ran down smoothly, maintaining a finite edge, and leaving no film. (Rapid lowering of the meniscus also produced a finite edge but frequently left isolated 'islands' of solution behind.) Variation of potential in the finite edge meniscus increased the contact angle (in accordance with changes of interfacial tension changes), but it never decreased significantly unless disturbed by other causes.

2. Electrochemical: Measurements with  $H_2$  under 'dirty' conditions were generally irreproducible and showed marked decay of current with time at constant potential. The electrode could be 'activated' by cycling it back and forth anodically and cathodically (care being taken not to evolve  $H_2$  or  $O_2$  on the immersed surface) but the currents from electrodes so treated dropped steadily over periods of hours.

In clean systems, erratic behavior was obtained while the 'thin films' drained, but when a finite edge was established, the currents stabilized and were generally reproducible within  $\pm 2-5\%$ . Occasionally, the electrodes were mildly 'activated', but the simple act of measuring the currents at potentials from 0-1 V and back sufficed for hours at a time.

Figures 4 and 5 show typical E-I curves obtained with  $H_2$  and with  $O_2$  at 1 atm in 1 N  $H_2SO_4$ . Both curves show a highly linear 'pseudo-ohmic' behavior over a wide potential region. This apparent resistance (about 1000  $\Omega$  for a 1 cm long meniscus) was independent of the immersed length of the electrode. (The calculated resistance of the solution from the meniscus bottom to the bottom of the slot was only about 25  $\Omega$  in this case.) The oxygen reduction reaction was more sensitive to 'activation' than was that of hydrogen. The value of  $dI/dV$  was constant, but the intercept of I on the V axis varied with activation.

3. Meniscus heating: As reported earlier,<sup>5</sup> at higher polarizations (i.e.  $> \sim .5$  V) a definite activity above the meniscus was observable with the microscope. This activity took two different forms, depending on whether the system was 'clean' or 'dirty'. In the 'dirty' system, both on Pt foil and on the sputtered films, a 'fog' of minute droplets grew, coalesced and drained down into the meniscus, permitting new drops to grow in the drained regions. In 'clean' systems, a band of condensed liquid grew 25-100  $\mu$  above the meniscus edge. As the band grew, it became unstable and drained down locally into the meniscus (never draining 'dry', however) detached, and continued growing again.\* This band was not continuous with the main meniscus except during the drainage, a finite edge being observable at all times.

Discussion: On the basis of the detailed physical description of the system obtained through the optical measurements, a differential equation was set up to describe the system as closely as possible. Figure 6 shows the relevant geometries involved in the 'finite contact angle meniscus'. At small pore sizes ( $< 1$  mm), the surface of the gas-liquid interface can be represented very closely by the surface of a cylinder, the surface of which is shown as the circular arc (in cross section normal to the electrode surface). Let  $x = 0$  be the point of intersection of the meniscus with the surface, the equation for the circle then becomes

$(x - x_0)^2 + (y - y_0)^2 = R^2$ ; at  $x = 0, y = 0, R = (x_0^2 + y_0^2)^{1/2}$ , and  $\theta = \text{contact angle} = \tan^{-1}(x_0/y_0)$ . The gas ( $H_2$ ) dissolves in the electrolyte and diffuses to the

<sup>6</sup>The phenomenon, although difficult to describe verbally, appears very similar, except in scale, to the ring of condensing alcohol observable above the meniscus in a partially filled sherry glass.

electrode. Assuming equilibrium dissolution and steady state diffusion, including a linear concentration gradient ( $\delta$  is much less than .05 cm) the diffusion distance,  $\delta$ , from a point 'x' at the metal lies on a radius of the circle, such that  $\delta = [(x - x_0)^2 + y_0^2]^{1/2} - R$ . (Note: This is not strictly true since  $\nabla \cdot C \neq 0$ , but quite reasonable at small x, where the 'C' is large, and unimportant at large x where 'C' is small.) At the electrode surface the gas reacts giving a local current density  $i_x$

$$i_x = i_0 (C_x/C_0) \exp(\beta \eta_x F/RT) \quad (1)$$

(where  $\beta$  is a non-mechanistically significant constant, but can be varied in the solution to represent the experimental Tafel slope, and  $\eta_x$  is the total potential jump at the metal-solution interface).

In a thin strip 'dx' deep into liquid .1cm (into the plane of the paper) between x and x + dx (see Fig. 7) the total current  $I_x + dx$  has been increased from  $I_x$  by the amount  $i_x \cdot dx \cdot l$ , or

$$-\frac{dI_x}{dx} = i_x \quad (2)$$

(A minus sign is used here because the ion current is produced by pos.  $H^+$  ions, but the same equation results if the opposite sign convention is used.)

Considering the diffusion of gas to the surface (and assuming a linear case as described above)

$$i_x = \frac{DZF(C_0 - C_x)}{\delta} = -\frac{dI_x}{dx} \quad (3)$$

Considering the voltage in the solution, as the current,  $I_x$ , passes through the thin slice there will be an IR drop from x to x+dx of

$$dV_x = \frac{I_x \cdot \rho \cdot dx}{\text{area}} \quad (4)$$

Thus,

$$\frac{dV_x}{dx} = \frac{I_x \cdot \rho}{\delta_x \cdot l} \quad (5)$$

Solving eqn. (3) for  $C_x$ ,

$$\frac{C_x}{C_0} = \left(1 + \frac{\delta_x}{DZFC_0} \frac{dI_x}{dx}\right) \quad (6)$$

and putting (6) into eqn. (1)

$$-\frac{dI_x}{dx} = i_x = i_0 \left(1 + \frac{\delta_x}{DZFC_0} \frac{dI_x}{dx}\right) \exp(\beta \eta_x F/RT) \quad (7)$$

solving (7) for  $dI_x/dx$ :

$$-\frac{dI_x}{dx} = \frac{i_0 \exp(\beta \eta_x F/RT)}{1 + \frac{\delta_x}{DZFC_0} \exp(\beta \eta_x F/RT)} \quad (8)$$

Solving eqn. (5) for  $I_x$ ,  $I_x = -(\delta_x/\rho)(dV_x/dx)$  and differentiating,

$$-\frac{dI_x}{dx} = \frac{\delta_x d^2 V_x}{\rho dx^2} + \frac{1}{\rho} \frac{d\delta_x}{dx} \frac{dV_x}{dx} \quad (9)$$

from geometry (Fig. 5)

$$\frac{d\delta_x}{dx} = \frac{(x - x_0)}{[(x - x_0)^2 + y_0^2]^{1/2}} = \frac{(x - x_0)}{\delta_x + R} \quad (10)$$

and combining (8) and (10)

$$\frac{d^2 V_x}{dx^2} + \frac{1}{\delta_x} \frac{(x - x_0)}{(\delta_x + R)} \frac{dV_x}{dx} = \frac{\rho i_0 \exp(\beta \eta F/RT)}{\delta \left[ 1 + \frac{i_0 \delta_x}{DZFC_0} \exp(\beta \eta F/RT) \right]} \quad (11)$$

Matching the potential in the solution with the potential at the boundary (since the metal is considered to be equipotential),

$$\eta = V_x - E_{(\text{Rev. for } C_0)} \quad \text{and} \quad \frac{dV_x}{dx} = \frac{d\eta}{dx} \quad (12)$$

Thus, finally,

$$\frac{d^2 \eta_x}{dx^2} = - \frac{1}{\delta_x} \frac{(x - x_0)}{(\delta_x + R)} \frac{d\eta_x}{dx} + \frac{\rho}{\delta_x} \frac{i_0 \exp(\beta \eta_x F/RT)}{\left[ 1 + \frac{i_0 \delta_x}{DZFC_0} \exp(\beta \eta_x F/RT) \right]} \quad (13)$$

This equation is not solvable analytically, but it was programmed in Fortran IV for solution on a digital computer. Some typical results of this computer solution are also shown plotted in Figs. 4 and 5 where the curves correspond to the experimental conditions for the experimental curves shown and show  $I_{\text{total}}$  (per cm) vs.  $V_{\text{applied}}$ . Figure 8 is a typical plot of terminal current vs. overpotential produced by the computer in this case showing the effect of variation of  $i_0$  ( $A = 10^{-3}$ ;  $B = 10^{-6}$ ;  $C = 10^{-9}$ ) holding all other 'constants' constant ( $D = 1.8 \times 10^{-5}$ ;  $x_0 = 1.7 \times 10^{-3}$  cm;  $y_0 = 5 \times 10^{-2}$  cm;  $\rho = 4.65 \Omega \text{ cm}$ ;  $\beta F/RT = 60 \text{ mv}$ ;  $Z = 2$ ;  $C_0 = 1.2 \times 10^{-6} \text{ moles/cm}^3$ ).

Figures 9 and 10 are typical combined plots of the local current density ( $D$ ), potential ( $V$ ), the integrated current from the tip to the point 'x' ( $C$ ), the local polarization power loss density, and the  $I^2R$  power loss density in the electrolyte for a particular potential ( $V_{\text{applied}} = .23V$ ) in the case of a gas electrode in 1 N  $H_2SO_4$ , assuming for the constants involved  $D = 1.8 \times 10^{-5} \text{ cm}^2/\text{sec}$ ;  $x_0 = 1.5 \times 10^{-3} \text{ cm}$ ;  $y_0 = 4.3 \times 10^{-2} \text{ cm}$ ;  $\rho = 4.65 \Omega \text{ cm}$ ;  $\beta F/RT = 60 \text{ mv}$ ;  $Z = 2$ ;  $i_0 = 10^{-6} \text{ A/cm}^2$ ; and  $C_0 = 1.2 \times 10^{-6} \text{ moles/cm}^3$  where all of the constants involved are experimentally determined. The values are plotted vs. linear distance from the tip in 9, and vs. the log of the distance in Fig. 10.

The equation has been solved for a number of variations of the experimental constants involved, but the results are too numerous to include here. Of considerable interest is the fact that the solution shows that most of the current at higher polarizations is produced within very short distances ( $10^{-4}$  to  $10^{-5}$  cm from the tip) and that the current per cm of meniscus is relatively independent of the pore size. The obvious conclusion is that any catalyst which is any further than  $10^{-5}$  cm from a meniscus edge is worthless at high polarizations. To test this theory, thin film electrodes have been prepared on microporous substrates which contain only 10-20  $\mu\text{g}$  of Pt per  $\text{cm}^2$  of electrode surface, but yielded currents up to 400  $\text{ma/cm}^2$  without showing any detectable diffusion control with  $H_2$ , and showed 'Tafellian' behavior with  $O_2$  up to 100  $\text{ma/cm}^2$ .

#### References

1. J. S. Newman, C. W. Tobias: JECS 109 1183, 1962.
2. K. Micks; Symposium on Fuel Cell Systems, 145th Nat. Meeting A.C.S., Sept. 8, 1963.
3. E. Justi et al., p. 33, Verlag d. Akademie d. Wissenschaften u.d. Lileratur, Wiesbaden (1959).
4. Will, F. G., JECS, 110 152 (1963).
5. Bockris, L. Nanis, B. D. Cahan, J. Electroanal. Chem., 9, 474 (1965).

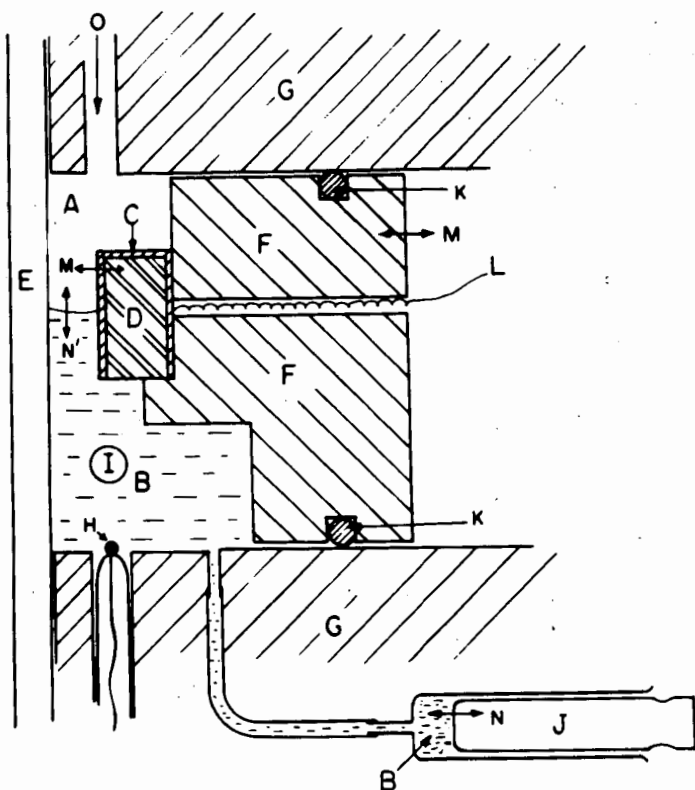


**Figure 1:** Cross section of slot electrode cell:

- A. Gas space
- B. Electrolyte
- C. Pt film on "D"
- D. SiO optical flat block for electrode
- E. SiO optical flat plate for window
- F. Teflon piston
- G. Teflon cell body
- H. Pd-H bead for reference electrode
- I. Pd tube for counter electrode
- J. Piston-micro-burette for changing electrolyte level
- K. O-ring seals for piston
- L. Electrical connection to rear of electrode "C"
- M, M'. In and out translation of piston varies "slot" spacing
- N, N'. Piston "J" varies meniscus level
- O. Gas inlet

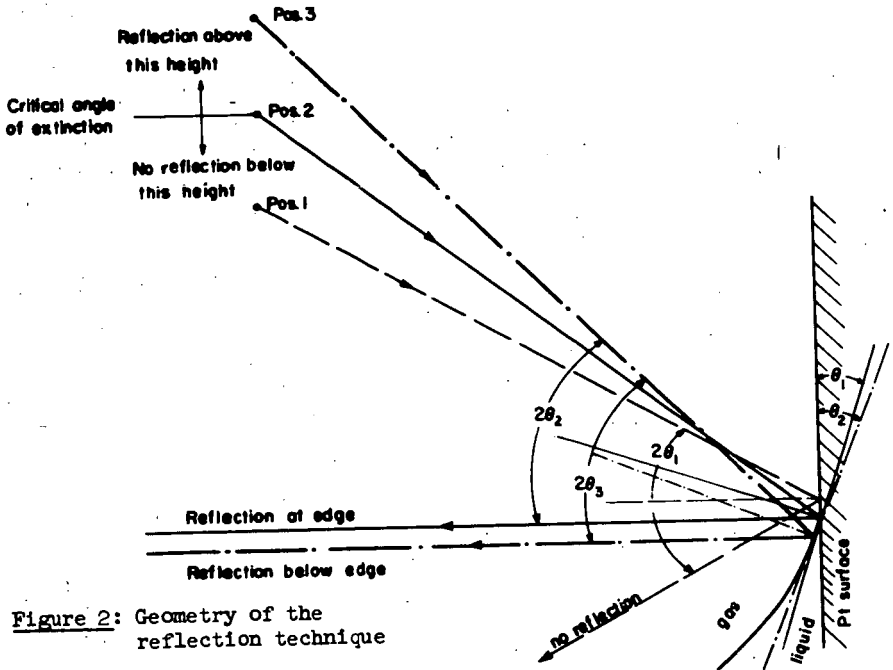


Figure 2: Geometry of the reflection technique

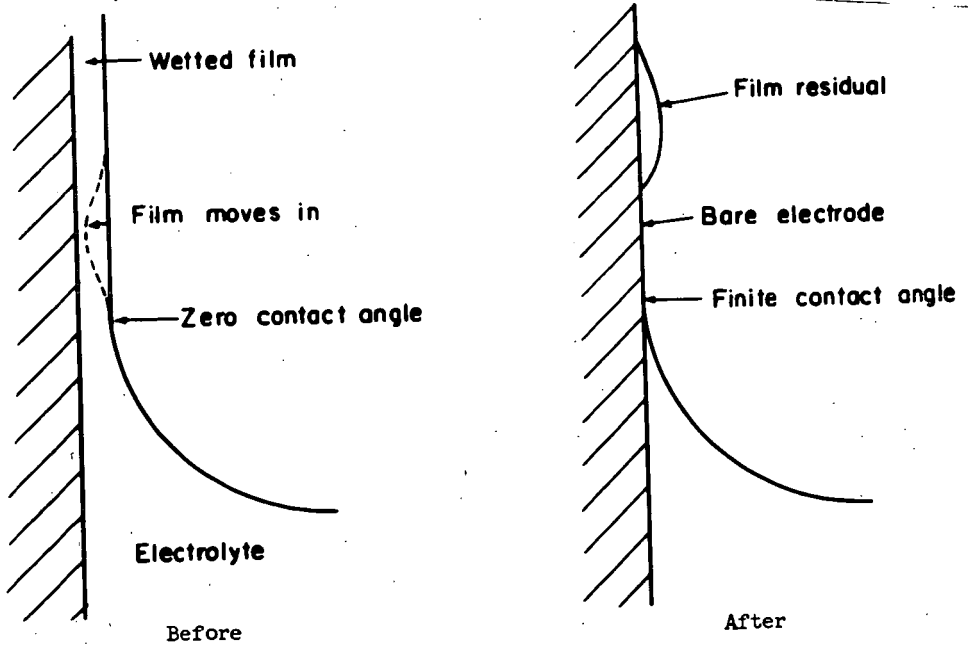


Figure 3: Creation of finite meniscus from wetted film (Horizontal dimension greatly exaggerated)

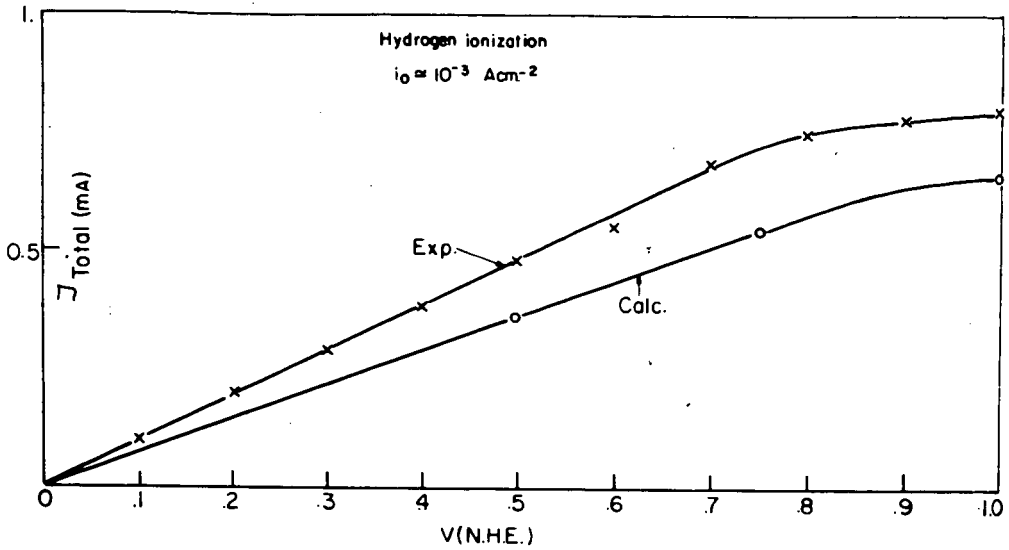


Figure 4: Experimental and calculated values for  $\text{H}_2$

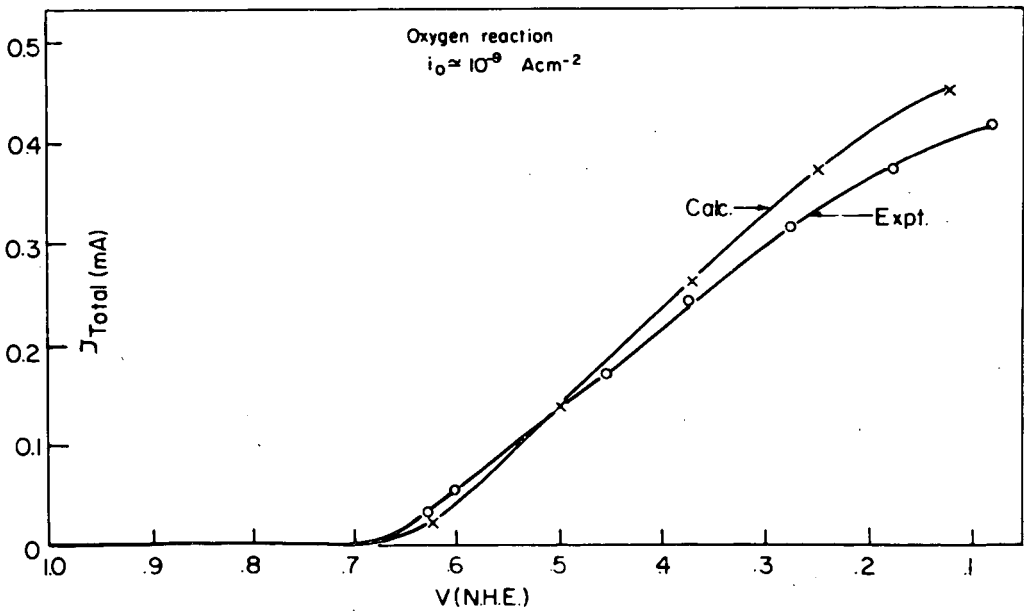


Figure 5: Experimental and calculated values for  $\text{O}_2$



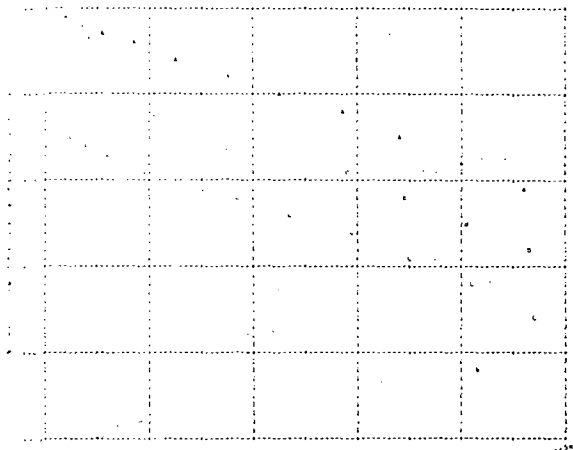
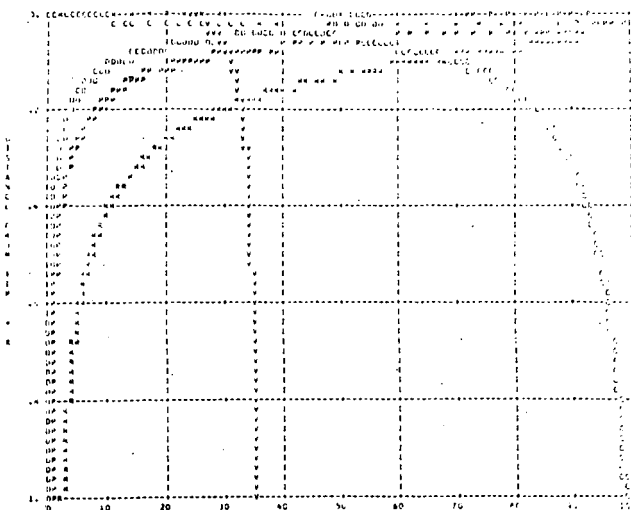
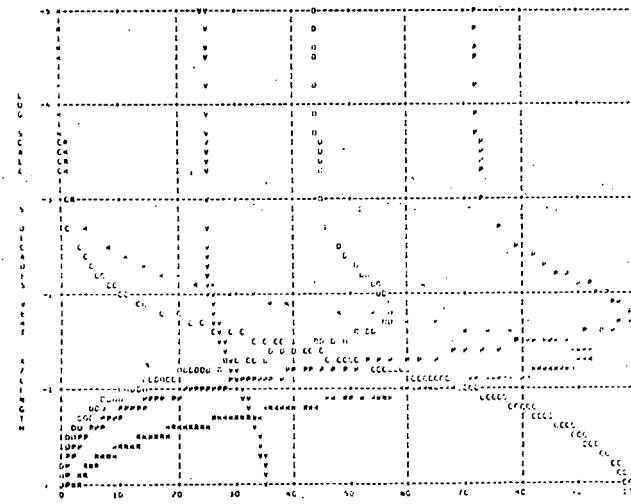


Figure 8: Computer plot of the terminal current-voltage relationship with variation of exchange current.

Curve A:  $i_0 = 10^{-3}$   
Curve B:  $i_0 = 10^{-6}$   
Curve C:  $i_0 = 10^{-9}$



**Figure 9:** Computer plot of the local values of the variables in the meniscus for a given potential plotted with linear distance.



**Figure 10:** Computer plot of the local values of the variables in the meniscus for a given potential plotted with logarithm of the distance.

## ELECTRODEPOSITED PLATINUM AND PLATINUM-LEAD ELECTROCATALYSTS

Hilton A. Roth and William R. Lasko

United Aircraft Research Laboratories  
East Hartford, Connecticut

Finely divided Pt and Pt-Pb black powders have been used for some time as anode catalytic materials for the oxidation of hydrocarbons and hydrocarbons containing oxygen in fuel cells. These blacks have been prepared by a number of different methods with the end result that each preparative method and even variations within a given method yield catalysts of different activity. The subject of this paper is a study of the microstructural and electrochemical surface area characteristics of Pt and Pt-Pb electrodeposited blacks prepared under different electrochemical conditions and is part of an over-all program on electrocatalytic materials.

## EXPERIMENTAL APPROACH

Three important aspects of preparing catalysts by electrodeposition were studied. These were the effects of the electrode surface microstructure upon which the catalyst nucleates and grows, the current density during electrodeposition and the Pb ion concentration in the plating solution. Earlier in the program, it was observed that the electrochemical surface area and activity of electrolytically prepared Pt blacks varied with different surface treatments of the electrode substrate prior to electrodeposition. Replication electron microscopy in conjunction with electrochemical surface area measurements were performed to establish whether or not differences in nucleation and growth of Pt and Pt-Pb blacks could account for such differences. Cross-sections of the electrodeposited layers were also examined.

The extent of electrochemical surface area was investigated in regard to the deposition parameters, current density and Pb concentration of the plating solution. These results were correlated with catalytic activity for the electrode oxidation of hydrocarbon fuels studied in other parts of the program. The surface areas were measured using a charging method which involves the measurement of the number of coulombs required to remove a monolayer of adsorbed hydrogen by electrochemical oxidation from the surface of the catalyst. The influence of the concentration of Pb upon the character of the catalytic deposit was studied both microscopically and electrolytically employing the same methods as mentioned above.

## DISCUSSION OF EXPERIMENTAL RESULTS

Microscopy of the Nucleation and Growth of Pt and Pt-Pb Electrodeposits

Electron Microscopy: Replication electron microscopical techniques were used to study the nucleation and growth of Pt and Pt-Pb electrodeposits on Pt electrodes which were purposely chemically pretreated to alter the electrode topography to ascertain what effects topography had upon structural and physical properties of the deposit. The surfaces examined were, untreated, metallographically

polished, sandblasted and etched by heat, molten sodium carbonate and aqua regia. Figure I contains electron micrographs illustrating the effect of each treatment on the topography. Pt was electrodeposited on a series of 1 cm<sup>2</sup> area pretreated electrodes at different time intervals from a 2% aqueous solution of H<sub>2</sub>PtCl<sub>6</sub> at a current density of 100 ma/cm<sup>2</sup>. Each electrode was electrochemically cleaned and reduced before electrodeposition. Figure II shows the nucleation and growth of Pt on untreated Pt surfaces. The electrodeposit appears first as randomly distributed particles which enlarge laterally with plating time until the electrode surface becomes covered. Further deposition appears to occur primarily in the surface asperities and the deposits become smoother. Deposition on other surfaces follows the same general pattern with minor variations.

Pt-Pb blacks were electrodeposited on untreated, annealed and sandblasted surfaces at current densities of 10 and 100 ma/cm<sup>2</sup> from 0.1 M H<sub>2</sub>PtCl<sub>6</sub>, 2 x 10<sup>-3</sup> M PbOOCCH<sub>3</sub> solutions. The electrodeposits formed at 10 ma/cm<sup>2</sup> on the various surfaces as fine nuclei randomly dispersed over the surface. These nuclei grew laterally into a thin smooth grayish deposit. The electrodeposits prepared at the higher current density were different from those prepared at 10 ma/cm<sup>2</sup> in that the nuclei formed more rapidly and were coarser in appearance. Each pretreated surface showed some difference in mode of nucleation. Figure III shows the nucleation and growth on untreated Pt surfaces. The same general growth pattern persists in this case as those described in the previous experiments. However, these deposits were much more fragile than those previously discussed.

Light Microscopic Surface Analysis: Light microscopic examinations of Pt and Pt-Pb electrodeposits prepared at 100 ma/cm<sup>2</sup> revealed only rough appearing surfaces without any distinguishing features. The same examinations for Pt-Pb blacks deposited at 10 ma/cm<sup>2</sup> did reveal some distinguishing features and are shown in Figure IV. This figure contains a series of photomicrographs for deposits on annealed substrates showing first the smooth deposit followed by cracking defects and some interesting secondary growth phenomena as the electrodeposition time was advanced.

Cross-Sectional Microscopical Analysis: Electron and light microscopic studies show only the topographical features of the deposits. Cross-sections of these deposits were prepared to give some concept as to the structural characteristics of the catalyst interior. Figure V contains cross-sections of deposits prepared at 10 and 100 ma/cm<sup>2</sup> for Pt and Pt-Pb black deposits. Both types of deposits prepared at 10 ma/cm<sup>2</sup> and the Pt deposit prepared at 100 ma/cm<sup>2</sup> appear as solid films with vertical cracks. The Pt-Pb deposit prepared at 100 ma/cm<sup>2</sup> is significantly different and is characteristic of dendritic type structure.

#### Deposit Thickness Growth Rates

Cross-sectional analysis also afforded as a means to obtain information regarding deposit thickness growth rates and the compactness of the deposit from deposit thickness measurements, deposition times and deposit weights. The two types of deposits were prepared on untreated Pt electrodes at time intervals and average film thicknesses and deposit weights were measured.

Linear thickness growth rates were observed for Pt and Pt-Pb deposits prepared at 10 ma/cm<sup>2</sup> and 100 ma/cm<sup>2</sup> respectively. The respective rates are 2 x 10<sup>-4</sup> and 2.8 x 10<sup>-3</sup> mm/sec. Pt discharged at 100 ma/cm<sup>2</sup> was not linear and was found to

obey the relation:

$$\ell' = bt^m$$

where  $\ell'$  is the deposit thickness and  $b$  and  $m$  are constants. The Pt-Pb black deposited at  $10 \text{ ma/cm}^2$  shows an initial rapid thickness growth rate which tapers off and appears to become linear after approximately 200 seconds deposition time.

#### Surface Area of Electrodeposits

Surface Area of Pt Blacks Prepared on Pretreated Electrode Surfaces: The surface area of Pt electrodeposits precipitated at  $100 \text{ ma/cm}^2$  on the pretreated Pt electrodes is shown graphically vs deposition time in Figure VI. These data indicate the influence of surface pretreatment on electrochemical area. An expression was found which relates surface area with deposition time for deposition at  $100 \text{ ma/cm}^2$  for the first 400 seconds of plating time, it is:

$$\theta = m(1 - e^{-\alpha t}) \quad (1)$$

where  $\theta$  is the electrochemical surface area,  $m$  is the slope at high values of time in  $\theta$  vs  $t$  plots, such as Figure VI.  $\alpha$  is obtained by solution of (1) after substitution of  $m$  and an experimental point  $\theta$ ,  $t$ .  $\alpha$  and  $m$  are different for each of the deposits on the differently treated electrodes.

Surface Area of Pt-Pb Deposits on Pretreated Pt Surfaces: The surface area of these deposits was found to increase linearly with time or deposit weight for depositions at  $100 \text{ ma/cm}^2$ . Furthermore, the pretreatment of the substrate electrode did not influence the surface area of the deposit. Surface area vs deposit weight plots have average slopes of  $21.5 \text{ mC/mg}$  deposit. The average weight of deposit which builds up was found to be  $0.05 \mu \text{ g/sec}$ . From this information, the following equation was derived for calculating deposition times to prepare catalysts of approximate desired surface areas;

$$t_{\text{sec}} = \frac{\theta \text{ mC/cm}^2}{1.07} \quad (2)$$

This equation assumes no loss of catalyst due to flaking off from the electrode.

Deposition of this codeposit at  $10 \text{ ma/cm}^2$  did not show any linear relationship between surface area and deposit time or weight. The amount deposited per unit time varied with electrode pretreatment and the rate of increase in surface area was observed to decrease with deposition time. The experimental data were found to obey the following equation:

$$\theta = b\beta (i/t)^{m/2} \quad (3)$$

$b$  and  $m$  are constants dependent upon the nature of the substrate surface and are obtained from graphical plots of experimental data.  $i$  is defined as the current density. Figure VII shows the experimental and calculated surface areas using equation (3).

The Effect of Current Density on Surface Area: Since codeposits prepared at the two current densities varied so widely, experiments were conducted to

determine the effect of variations in current density on the surface area of the codeposit. The same number of Faradays were discharged in the preparation of each codeposit. The results of the experiment on untreated Pt electrodes is shown in Figure VIII. This plot is essentially the same for each of the treated surfaces. A plot of deposit weight vs current density has the same shape as in Figure VIII.

The surface area was found to be related to the current density by the following:

$$\theta / \beta = bt(i/t)^m \quad (4)$$

where each symbol has the same definition as given before. Figure IX shows agreement between experimental and calculated surface areas.

#### Composition of Electrocodeposits

The Effect of Current Density on Deposit Composition: Electrodeposits formed in the same manner as in the previous section were found to give the same shape curve as Figure VIII when %Pb is plotted versus current density. Consequently the form of the equation which related surface area and current density will serve to relate %Pb found in deposit vs current density; it is:

$$\%Pb = bt(i/t)^m \quad (5)$$

Again, b and m are constants and are obtained from linear plots of equation (5) using experimental data.

#### Effect of Pb Ion Concentration in the Plating Solution Upon the Structure and Physical Properties of the Electrodeposit

Effect Upon Surface Area: The electrochemical surface areas were measured for a series of Pt-Pb deposits prepared from plating solutions containing different amounts of Pb ion at a current density of 100 ma/cm<sup>2</sup>. The surface area per unit weight of the electrodeposit was found to decline upon increased additions of Pb ion. The concentrations studied ranged between 1 x 10<sup>-4</sup> and 5 x 10<sup>-2</sup> moles/liter.

Effect on Deposit Structural Properties: Cross sectional and surface photographs were taken of the deposits prepared from solutions containing different amounts of Pb ion at 100 ma/cm<sup>2</sup>. Cross sectional studies revealed a transition from a closely packed deposit prepared from a solution containing 1 x 10<sup>-4</sup> moles/liter Pb ion to a dendritic type deposit from a solution containing 1 x 10<sup>-2</sup> moles/liter Pb ion. Surface photographs show a corresponding transition in texture from fine grains to a coarse open structure for the lower and higher concentrations of Pb ion respectively.

#### CONCLUDING REMARKS

This study has demonstrated that replication electron microscopy in conjunction with cross-sectional optical microscopy can be applied to the characterization of the morphology and mode of nucleation of Pt or Pt-Pb electrodeposits. The analysis has also shown that by closely controlling the microstructure through judicious changes in the cell plating conditions, large variations in the properties of the deposit can be obtained. The quantity of nuclei deposited from solutions containing Pt and Pb was greater than that observed with solutions containing only Pt under similar conditions. An increase in the surface area of the Pt-Pb codeposits was found to be dependent on the weight of the deposit, the electrodeposition time, and the current density.

ELECTRODE SURFACES BEFORE AND AFTER TREATMENT  
MAGNIFICATION: 11,000X

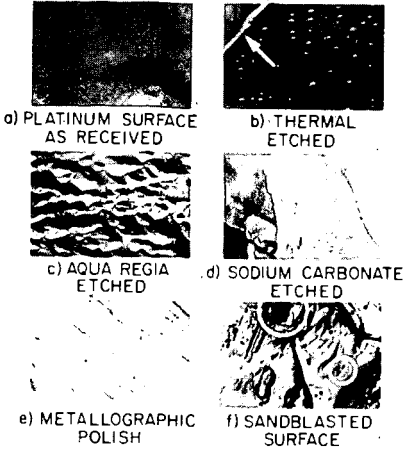


FIGURE 1.

Pt BLACK ELECTRODEPOSITION  
SUBSTRATE: Pt  
MAGNIFICATION: 11,000 X

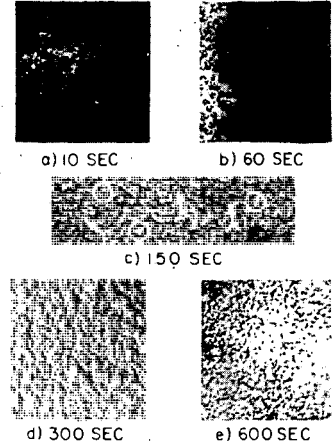


FIGURE 2

NUCLEATION AND GROWTH OF PLATINUM-LEAD CODEPOSITS ON AS RECEIVED PLATINUM SUBSTRATES  
MAGNIFICATION: 11,000X 100 ma/cm<sup>2</sup>

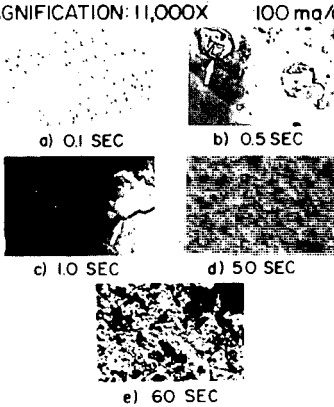


FIGURE 3

GROWTH OF PLATINUM-LEAD CODEPOSITS ON ANNEALED PLATINUM SUBSTRATES  
MAGNIFICATION: 200X 10 ma/cm<sup>2</sup>

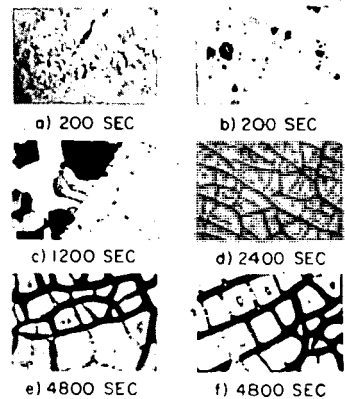


FIGURE 4

CROSS SECTIONS OF ELECTRODEPOSITS

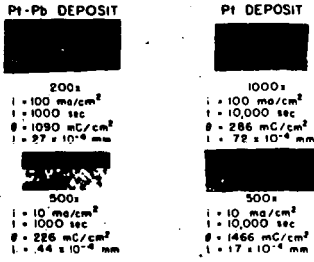


FIGURE 5

SURFACE AREA OF PLATINUM ELECTRODEPOSITS

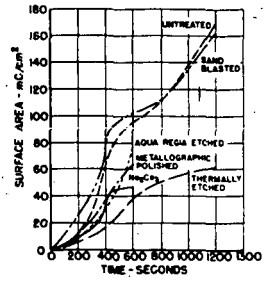


FIGURE 6

SURFACE AREA PER UNIT WEIGHT VS DEPOSITION TIME

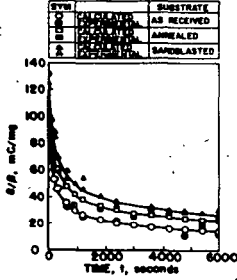


FIGURE 7

EFFECT OF CURRENT DENSITY ON  $\theta$  OF PLATINUM-LEAD DEPOSITS

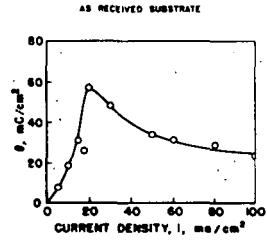


FIGURE 8

EFFECT OF CURRENT DENSITY UPON PHYSICAL PROPERTIES OF ELECTRODEPOSIT

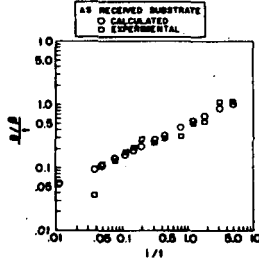


FIGURE 9

## OXIDATION OF MULTI-COMPONENT HYDROCARBON FUELS

Eugene Luksha and Eugene Y. Weissman

General Electric Co.  
Direct Energy Conversion Operation  
West Lynn, Massachusetts 01905

### Introduction

Because of economic necessity, commercial fuels will be used in practical fuel cell devices. Commercially available fuels generally consist of complex mixtures of hydrocarbons, primarily straight and branched aliphatics, olefins, naphthenes, and aromatics. The aliphatic compounds both straight and branched-chained are relatively reactive in fuel cells, while the unsaturated and cyclic compounds are considerably more difficult to oxidize and have been designated as "unreactive." These types of compounds are believed to adsorb on an electrode surface more rapidly than aliphatic compounds, forming an inert ad-layer. For this reason, it is necessary to know the tolerance of an operating fuel cell anode to these "unreactive" compounds.

### Experimental

The model fuel taken into consideration was split into its principal components: paraffins, olefins, naphthenes, and aromatics (Figure 1). Normal octane was chosen as the base fuel and various quantities of single unreactive components were added. The additives were chosen on the basis that they are all found in relatively high concentrations in various types of hydrocarbon fuels (1-3), and have boiling points lower than 350°F, the practical upper temperature limit of the electrodes used in this work. As a result, compounds containing more than 1 ring as, for example, indanes, indenenes, tetralins, and naphthalenes were not considered since they all have boiling points in excess of 350°F. Since hydrocarbons with condensed rings were eliminated, only alkylbenzenes, 1-ring naphthenes, in addition to the olefins and paraffins were studied.

These compounds were added to n-octane in varying concentrations. Polarization curves were taken using the binary solution as a fuel. These curves were measures of the decrease in cell performance caused by the addition of the "unreactive components."

The experimental equipment has been described elsewhere (4). The following conditions apply to the present work:

- 1) The electrodes used were 3 in. x 3 in. (0.05 ft.<sup>2</sup> active geometric area) platinum - Teflon - screen composites of a type previously described (5). The platinum loading was 35 mgms/cm<sup>2</sup> and the composition: 85 wt. % Pt - 15 wt. % TFE. The current collecting screen was generally gold-plated expanded tantalum (5<sup>1</sup>Ta 10 4/0),— and sometimes wire-woven platinum (45 mesh).
- 2) The electrolyte was 95 wt. % phosphoric acid and, as mentioned above, the maximum practical operating temperature compatible with this electrode structure was found to be 350°F.
- 3) The counter-electrodes (cathodes) consisted of platinum - Teflon - platinum screen (woven, 45 mesh) composites with the same composition and loading as the anodes.
- 4) The experimental procedure for obtaining the polarization data was identical for each fuel studied. When the cell reached the desired temperature, the fuel was introduced at a flow rate of 20μl/min. \* and the O. C. V. was allowed to stabilize for approximately 1/2 hour. The fuel flow rate was determined by observing the pressure drop across a calibrated capillary.
- 5) Prior to the start of each run, the anode potential was raised to approximately 1 volt for 30 seconds in order to activate the electrode. The current was then shut-off and the potential was allowed to stabilize. This point was recorded as the O. C. V.
- 6) A Kordesch-Marko bridge was used to control the current through the cell. To determine the initial portion of the polarization curve, small increases in the current were made in the range of 0 to 1 amp (0 to 20 ASF). At each current setting, the anode potential was allowed to stabilize, before being recorded. Above 1 amp (20 ASF) the current changes were made in steps of 1/2 amp until the anode potential reached approximately 0.6 volt. Above this potential, current increases were made in smaller steps as the limiting current was approached. The limiting current was taken as that current at which the anode potential would no longer stabilize. Following each run, the fuel was purged from the anode with nitrogen for 10 minutes. With the nitrogen purge on, the anode potential was brought up to about 1 volt to remove traces of fuel from the electrode surface.

## Results and Discussion

### A. Binary Mixtures

#### 1. Aromatic Additives

Anode performance losses for n-octane with various aromatic additives are summarized in Table 1 and Figure 2.

\* This corresponds to 10 times the theoretical requirement of octane at 30 AS!

Table I  
Anode Performance Loss for Addition of Aromatics to n-Octane

Fuel Composition, mole %	Electrode No.	Anode Performance Loss,* mv					
		0 ASF	20 ASF	30 ASF	50 ASF	70 ASF	11 ASF
99% n-octane + 1% benzene	3515**	15	10	13	25	—	75
97% n-octane + 3% benzene	3515**	30	70	95	80	—	56
95% n-octane + 5% benzene	3515**	40	130	155	—	—	51
99% n-octane + 1% toluene	1050	20	25	35	55	—	67
97% n-octane + 3% toluene	1050	40	60	80	—	—	46
95% n-octane + 5% toluene	1050	65	205	210	—	—	31
99% n-octane + 1% m-xylene	1054	35	30	40	45	60	82
97% n-octane + 3% m-xylene	1054	50	70	90	120	—	63
95% n-octane + 5% m-xylene	1054	50	85	115	—	—	50
99% n-octane + 1% 1, 2, 4-trimethylbenzene	5305	10	30	45	75	—	—
97% n-octane + 3% 1, 2, 4-trimethylbenzene	5305	40	130	190	—	—	27

\* Defined as the increase in anode potential over that measured for pure octane at the same conditions.

\*\* Gold-plated tantalum screens. The other electrodes were supported on platinum screens.

There appears to be an effect on anode performance, in terms of molecular weight and/or degree of complexity of the additive, with the heavier (more complex) additives causing higher anode overvoltages.

The effects are generally small since the concentrations of the additives are small. It is expected that differences may become more pronounced as the concentrations of the additives increase.

In spite of some scatter in the experimental data, certain trends have been observed for the change in anode performance as a function of the additive complexity. This result is indicated in Figures 3 and 4 where the anode performance is shown to decrease with an increase in the number of carbon atoms (methyl groups) on the aromatic molecule. At this time, further comments on this behavior are not warranted.

## 2. Naphthene Additives

The naphthenes that were evaluated can be divided into two classes. The six-membered ring types which, under anode operating conditions, may be dehydrogenated to aromatics, and the five-membered ring types which appear to behave like paraffins.

The anode performance loss for these fuels is shown in Table 2 and Figure 5.

It appears that cyclohexane is more harmful to anode performance than methylcyclohexane possibly because the presence of the electrophilic methyl group in the latter species would make dehydrogenation to an aromatic structure more difficult, and it is the aromatic structure that would cause the higher anode overvoltages.

Probably the most significant result in Table 2 is the high tolerance of a fuel cell anode to rather high concentrations of cyclopentyl naphthenes. This is important since a great many logistic fuels contain high concentrations of this type of compound.

## 3. Olefin Additives

The anode performance loss for various n-octane-olefin fuel mixtures is summarized in Table 3 and Figure 6. There appears to be a relationship between the type of olefin (straight-chained, branched, cyclic) and performance. The straight-chained olefins are apparently the most difficult to oxidize. The chain length of the linear olefin is of little importance to anode performance, except at high current densities, as is evident when one compares octene-1 with pentene-1. Here, at least, the detrimental effect of higher molecular weights is not apparent. The position of the double bond in the olefin molecule also plays a role in determining the anode performance penalty. As the double bond is moved toward the center of the molecule, the anode performance penalty is slightly reduced. This result can be seen by comparing octene-1 with octene-2 in Table 3.

Table 2

Anode Performance Loss for Addition of Naphthenes at 350°F

Electrode Composition Mole %	Electrode No.	Surface Area, m <sup>2</sup> /g	Anode Performance Loss*, mv							i <sub>L</sub> ASF
			0 ASF	20 ASF	30 ASF	50 ASF	70 ASF	90 ASF		
99% n-octane + 1% cyclohexane	3497	9.42	17	20	15	20	20	40	134	
97% n-octane + 3% cyclohexane	3497	9.42	27	50	52	70	80	110	119	
95% n-octane + 5% cyclohexane	3497	9.42	27	60	72	110	120	210	105	
99% n-octane + 1% methylcyclohexane	1052**	—	25	0	0	0	0	—	84	
97% n-octane + 3% methylcyclohexane	1052**	—	55	7	23	35	50	—	75	
95% n-octane + 5% methylcyclohexane	1052**	—	100	23	45	80	—	—	64	
95% n-octane + 5% methylcyclopentane	1058**	—	0	0	0	0	0	0	98	
90% n-octane + 10% methylcyclopentane	3576	9.65	0	0	0	0	0	0	94	
85% n-octane + 15% methylcyclopentane	3576	9.65	0	0	0	0	0	0	90	

\* Defined as the increase in anode potential over that measured for pure octane at the same conditions.

\*\* Electrodes supported on Pt screen.

Table 3  
Anode Performance Loss for Addition of Olefins at 350°F

Fuel Composition, mole %	No. Allylic Hydrogen Atoms	Electrode No.	Surface Area, m <sup>2</sup> /g	Anode Performance Loss, *							
				0 ASF	20 ASF	30 ASF	50 ASF	70 ASF	90 ASF	iL ASF	
99% n-octane + 1% octene-1	2	1051**	—	9	0	0	0	0	0	30	90
97% n-octane + 3% octene-1	2	1051**	—	20	20	25	55	120	—	—	72
95% n-octane + 5% octene-1	2	1051**	—	50	45	75	150	—	—	—	53
99% n-octane + 1% octene-2	5	1059**	—	5	0	0	0	0	0	0	107
97% n-octane + 3% octene-2	5	1059**	—	25	15	20	20	25	20	20	97
95% n-octane + 5% octene-2	5	1059**	—	35	30	35	48	120	—	—	74
99% n-octane + 1% 2-methylbutene-2	9	3543	11.01	0	0	0	0	0	0	—	89
97% n-octane + 3% 2-methylbutene-2	9	3543	11.01	5	0	0	0	0	0	—	86
95% n-octane + 5% 2-methylbutene-2	9	3543	11.01	5	0	0	0	5	—	—	84
99% n-octane + 1% 2-methylbutene-1	5	3497	9.42	20	0	0	0	0	0	0	121
97% n-octane + 3% 2-methylbutene-1	5	3497	9.42	30	0	0	0	0	0	0	114
95% n-octane + 5% 2-methylbutene-1	5	3497	9.42	40	0	0	0	0	0	10	107
99% n-octane + 1% pentene-1		3544	10.22	10	0	0	7	20	34	34	110
97% n-octane + 3% pentene-1		3544	10.22	20	35	50	52	55	73	73	98
95% n-octane + 5% pentene-1		3544	10.22	20	35	50	52	55	98	98	96
99% n-octane + 1% cyclohexene		3515	—	-5	40	47	50	40	—	—	89
97% n-octane + 3% cyclohexene		3515	—	-10	75	80	98	115	—	—	75
95% n-octane + 5% cyclohexene		3515	—	-50	135	127	—	—	—	—	50

\* Defined as the increase in anode potential over that measured for pure octane at the same conditions.

\*\* Electrodes supported on Pt screen.

The branched olefins do not appear to cause any significant performance penalty when present in concentrations up to 5%.

All these facts may be related to the number of allylic hydrogen atoms that the olefins contain (column 2, Table 3). On a qualitative basis, given a series of hydrocarbons containing a single double bond, the olefin containing the largest number of allylic hydrogen atoms will be least harmful to anode performance. This appears to be the case here. An explanation of the phenomenon awaits further clarification.

The cyclic olefins (cyclohexane derivatives) form a separate class of compounds and exhibit higher anode overvoltages than the other types of olefins. These compounds are probably dehydrogenated under anodic conditions (see also, negative values of O. C. V. in Table 3) to aromatics, and as a result behave more like aromatics than like olefins. One point that should be emphasized is that an unsaturated six-membered ring is extremely detrimental to anode performance no matter what may be the degree of unsaturation.

#### 4. Mixtures of Normal and Branched Paraffins

Polarization curves for cells operating on fuels consisting of mixtures of normal and iso-octanes, with 25 to 75 mole % iso-octane show no change in performance as compared to pure n-octane (see Figure 7). This indicates that branched and straight-chained paraffins having the same number of carbon atoms are very similar in reactivity. This is useful result since it increases the flexibility of a choice of multi-component fuels for specific performance requirements.

#### B. Multi-Component Mixtures

The above results were for mixtures of n-octane with single "unreactive" components. Experiments were conducted in which several "unreactive" components were added to n-octane. The polarization curve of an anode operating on a fuel consisting of 89 mole % n-octane, 5 mole % methylcyclohexane, 5 mole % octene-2, and 1 mole % toluene is shown in Figure 8. The concentrations of each of the additives was determined from Figures 3, 5 and 6 so that the anode performance penalty for each of these components is roughly 50 mv at 30 ASF.

The outstanding feature of these results is that the cumulative effect of the "unreactives" does not appear to be additive. In fact, the performance loss is similar to that obtained for the corresponding binary mixtures, meaning that at these concentration levels each ingredient is independent of the others present in the mixture.

This seems to suggest that, should a multi-component mixture be chosen with any combination of ingredients, the performance penalty will be the one roughly corresponding to the "worse offender" in the mixture (as exhibited in a binary mixture with octane).

The main question, then, becomes one of establishing the influence of the other possible performance-determining parameters, such as the fuel flow rate.

### C. Anode Performance at Other Temperatures

In an effort to determine the magnitude of a performance gain that may be obtained by increasing the operating temperature, several cells containing typical "unreactive" compounds were run at 300, 350 and 400°F. The data at 300 and 400°F are given elsewhere (6), while the data obtained at 350°F are given in Tables 1 to 3.

The log of the current at anode potentials of 0.4 volt for various fuels at 300, 350 and 400°F was plotted against  $1/T$ . From the Arrhenius-type relationship shown in Figure 9 an approximate activation energy of 13 Kcal/gmole is obtained; this is indicative of a strong temperature dependence. Although the data does not form a true straight line, probably because a variety of fuels were used, the trend toward significantly increased anode performance is evident. A linear extrapolation to a cell operating temperature of 500°F, for example, indicates the possibility of obtaining about 10-fold increase in performance, assuming, of course, compatible electrode structures are available.

### Conclusions

The performance of a platinum-activated anode oxidizing binary mixture of n-octane and various small amounts (generally 1 to 5 mole %) of hydrocarbon additives in hot concentrated acid electrolytes (95%  $H_3PO_4$  at 350°F) depends on the nature of the additive. Thus:

- 1) For aromatic additives an increase in molecular weight or degree of complexity of the aromatic molecule (e. g., number of methyl groups) will determine a corresponding increase in anode overvoltage.
- 2) For naphthene additives the opposite appears to be true (when comparing methyl cyclohexane to cyclohexane). These findings are, however, in need of further experimental evidence.
- 3) For olefin additives there is a distinct relationship between the type of olefin (straight-chained, branched, or cyclic) and performance; on an overall basis, the number of allylic hydrogens in the non-cyclic additive molecule appears to set a characteristic trend, with the anode overvoltage decreasing as the number of allylic hydrogens increases.

The cyclic olefin is quite aromatic in character due to an apparent dehydrogenation mechanism preceding the oxidation step. Specifically, six-membered cyclic olefins are very harmful to the performance of the anode both on a relative basis (compared to the other types of olefins) and on an absolute basis.

- 4) Iso-paraffins (in any proportion) do not affect the performance of normal paraffins having the same number of carbon atoms.

The detrimental effects of various additives, as obtained from performance data of binary mixtures (with octane), are not cumulative. Therefore, a multi-component mixture will not necessarily contribute more to the rise of the anode overvoltage than the single "worse offender" in the mixture.

Sizeable performance gains can be made by increasing cell operating temperatures. For example, if compatible materials and electrode structures were available so that a cell could be operated at 500°F, as much as a 10-fold increase in cell performance would be possible, based on a linear extrapolation of the existing data.

#### Acknowledgement.

This work was sponsored by the U.S. Army Engineer Research and Development Laboratories, Ft. Belvoir, Virginia under contract number DA 44-009-AMC-479(T).

The authors are grateful for the able assistance of Mr. Lucien Brassard who performed much of the experimental work.

#### References

1. Chemistry of Petroleum Hydrocarbons, Reinhold, New York (1954).
2. Hydrocarbon Analysis, ASTM STP 389, (1965).
3. Y. M. Paushkin, The Chemical Composition and Properties of Fuels for Jet Propulsion, Pergamon Press, New York, (1962).
4. H. J. R. Maget and P. J. Chludzinski, Hydrocarbon Fuel Cell Technology, Academic Press, New York (1965) p. 429 ff.
5. L. W. Niedrach and H. R. Alford, J. Electrochem. Soc. 112, 117 (1965).
6. Technical Summary Report No. 9, Hydrocarbon-Air Fuel Cells, January 1965- 30 June 1965, ARPA Order No. 247, Contract Nos. DA 44-009-ENG-4909, DA 44-009-AMC-479(T), and DA 44-009, ENG-4853, p. 3-11 ff.

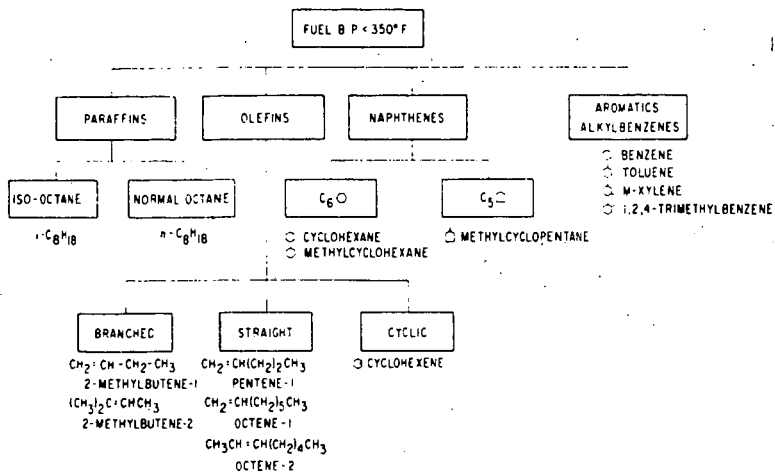


Figure 1. Principal Components of Model Fuel.

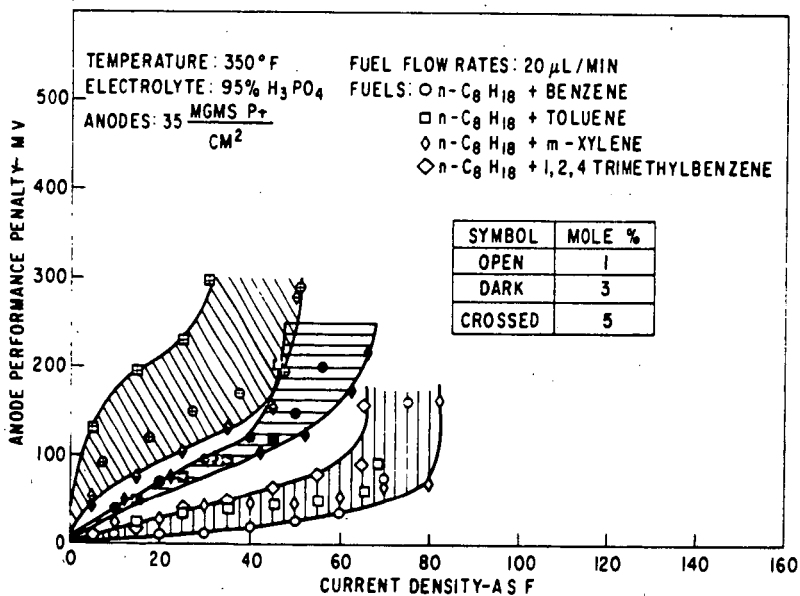


Figure 2. Anode Performance Penalty for Aromatics at 350°F.

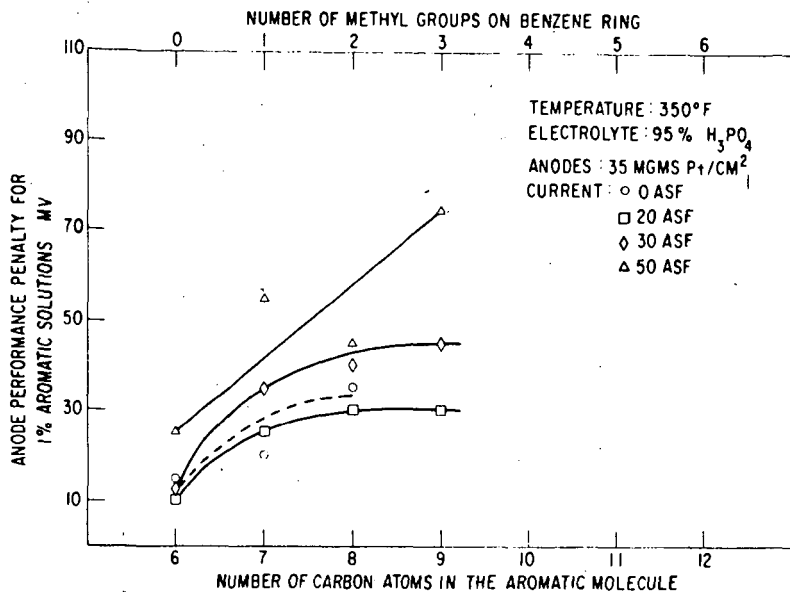


Figure 3 Anode Performance Penalty vs Number of Carbon Atoms on the Aromatic Molecule Additive.

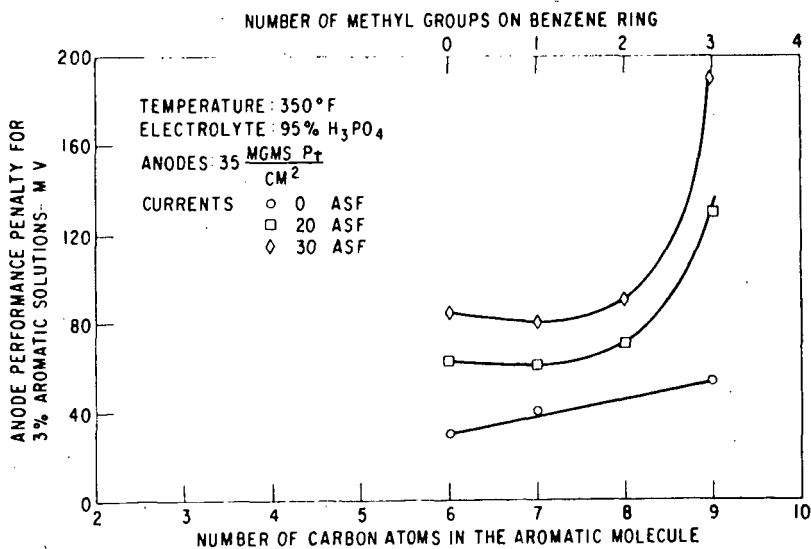


Figure 4 Anode Performance Penalty vs Number of Carbon Atoms on the Aromatic Molecule Additive.

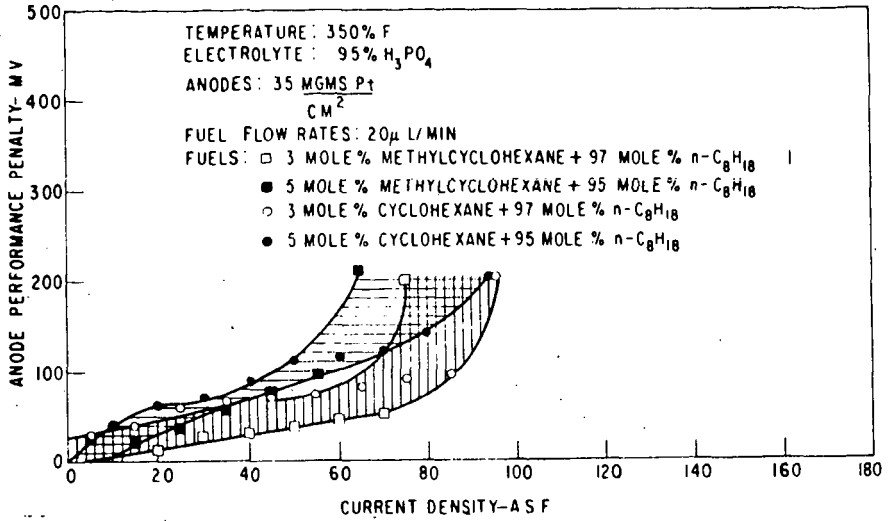


Figure 5 Anode Performance Penalty for Cyclohexyl Naphthenes at 350°F.

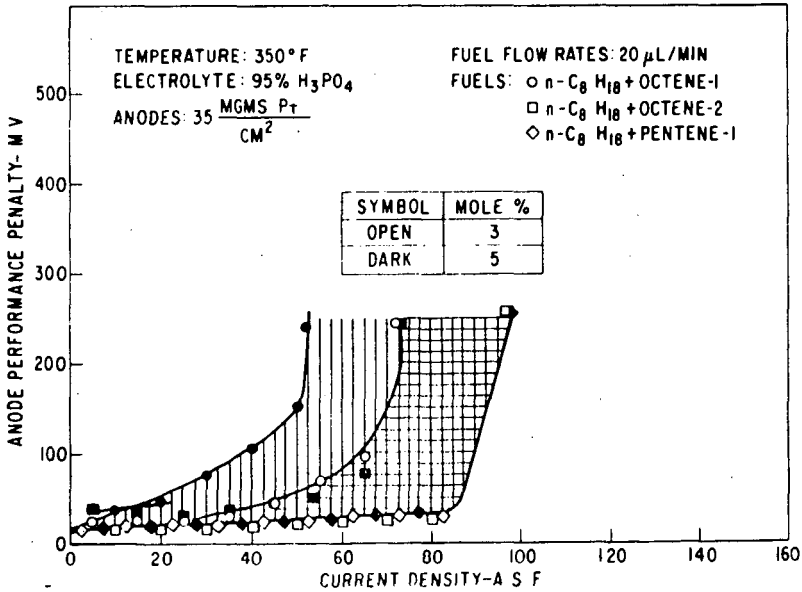


Figure 6 Anode Performance Penalty for Straight Chained Olefins at 350°F.

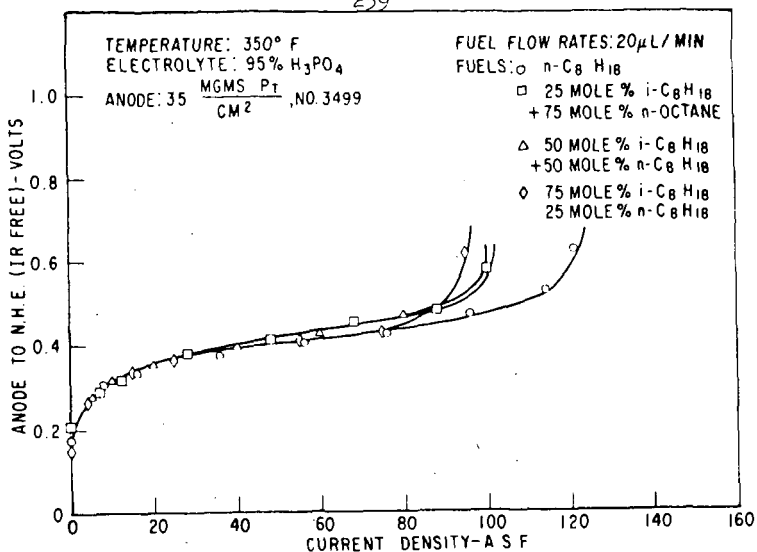


Figure 7 Anode Polarization for n-Octane and iso-Octane Mixtures at 350°F.

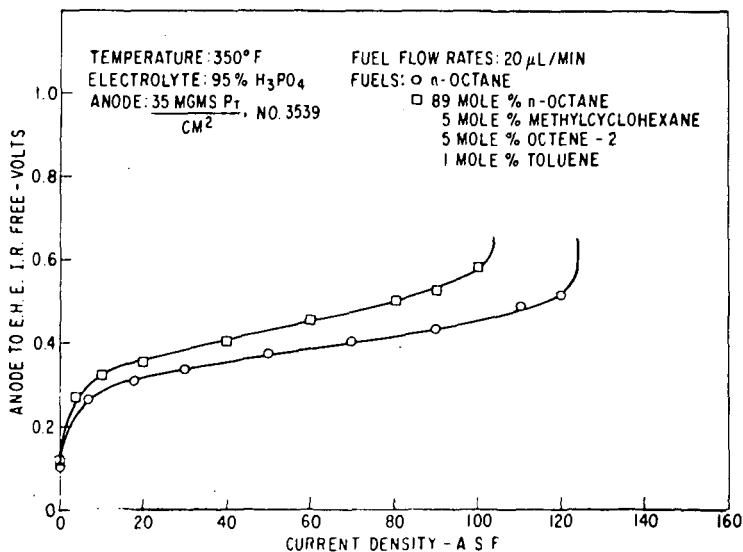


Figure 8 Anode Polarization Curve for a Fuel Mixture Consisting of 89 mole % n-Octane, 5 mole % Methylcyclohexane, 5 mole % Octene-2, and 1 mole % Toluene at 350°F.

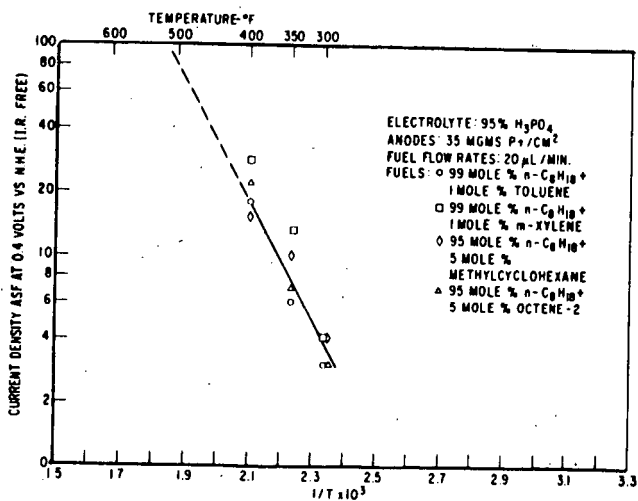


Figure 9 Current at an Anode Potential of 0.4 Volt vs  $1/T$ .

## LONG-TERM ELECTROCHEMICAL OXIDATION STUDIES OF MULTI-COMPONENT HYDROCARBON FUELS

James F. Lennon, Eugene Luksha, and Eugene Y. Weissman

General Electric Co.  
Direct Energy Conversion Operation  
West Lynn, Massachusetts 01905

### Introduction

For the most part, studies of the various aspects of direct hydrocarbon oxidation are based on short-term measurements. It is recognized that long-term anode performance with hydrocarbon fuels may be different from what can be predicted from short-term polarization data. This is due to such time-dependent factors as the accumulation of inert ad-layers on the electrode surface.\* A study of the long term effects that various "unreactive" additives (e. g. aromatics, olefins, naphthenes) may have on the performance of fuel cells operating on n-octane was made in order to determine whether there may be cumulative inhibition of the active sites on the anode as a function of time by these additives.

Other long-term effects of various additives in multi-component, octane-based fuels, are changes in the characteristics of performance cycling, which is present when hydrocarbons are oxidized directly with phosphoric acid electrolytes.

It is the purpose of this study to provide information and shed some light on these time-dependent aspects of anode performance.

### Experimental

The life testing installation has been described earlier (1). The electrodes (both anode and cathode) were of the same types described elsewhere (2) (35 mgms Pt/cm<sup>2</sup>, 85% Pt-15% TFE, gold-coated Ta screen for anodes, Pt screen for cathodes).

The following experimental procedure was used: After establishing the desired gas flow rates (in general: 20  $\mu$  l fuel/min; corresponding to 10 stoichs of octane at 1 amp and 10 stoichs of oxygen supplied in the air stream to the cathode) and isothermal conditions (350°F), the open-circuit potential was recorded. Thereafter, an initial polarization curve was taken.

---

\* Another important contribution to such performance changes is a progressive structural deterioration of the electrode; particularly, where an optimization of the electrode structure is pursued.

After these initial data were obtained, the cell current was maintained in general at 1.5 amp (30 ASF), by means of Electro-Products, Model EFB, D.C. power supply units. The IR-included anode vs  $H_2/H^+$  potential and cell current were continuously recorded with Varian two-channel strip chart recorders. IR-free potential data were also obtained by means of a Kordesh-Marko bridge. These data were logged, together with cell potentials and resistances.

The circulating electrolyte concentration was maintained at 95-98%  $H_3PO_4$  by means of controlled-rate addition of water to the electrolyte sump.

At the end of each test (usually caused by excessive electrolyte leakage through the anode) a final polarization curve was taken. The cell was then disassembled and the anode was cleaned. If desired, its surface area was measured by the B. E. T. method.\*

Whenever necessary, the polarization curve data points were determined after suitably pre-activating the anodes at anode potentials of  $> 0.90$  v vs  $H_2/H^+$ , and subsequently waiting for the output to stabilize at what would have been the average anode potential under cycling conditions for a fixed current density. This wait period was usually of the order of three to four minutes. In this way, cycling disturbances were avoided, without affecting the values to be measured.

#### Interpretation of the Test Data

##### A. Characteristics of Extended Performance - vs - Time Data

As mentioned above, direct hydrocarbon oxidation in phosphoric acid is characterized by spontaneous performance cycling. One of the objectives of the present work was to quantitatively define differences in the behavior of octane and various octane-based binary and multi-component fuel mixtures, in terms of the frequency and/or the amplitude of anode potential fluctuations at constant current. The interpretation of such differences can be refined by noting that in each case the time required for the onset of cycling can be divided into four distinctly different periods. Figure 1 is a graphical representation of these four periods which can be defined as follows:

I. The induction period - a short interval of time, normally one to two hours, during which there is a large increase in anode potential, from its open-circuit value.

---

\* Whenever time permitted, initial surface area measurements on anodes prior to assembly were also made. The method itself, as applied to whole electrodes, has been described earlier.

Technical Summary Report No. 7, Hydrocarbon-Air Fuel Cells, January 1965 - 30 June 1965; ARPA Order No. 247, Contract Nos. DA-44-009-ENG-4909, DA-44-009-AMC-479(T), and DA-44-009-ENG-4853, p. 193 ff.

ibid., No. 8 same contract numbers.

II. The ripple period - follows the induction period and is of short duration; up to two hours. During this time interval, the anode potential starts fluctuating at high frequencies (e.g. several times a minute) and low amplitudes (e.g. 10-20 mv).

III. The onset-of-cycling period - sometimes indistinguishable from the actual cycling mode of operation (IV, below). When it occurs, it lasts a few hours, or less, and is characterized by performance cycling at frequencies that are sometimes higher and sometimes lower than during the actual cycling operation that follows; the corresponding amplitudes are always smaller (e.g. 20-80% of actual cycling amplitudes).

IV. The cycling period - characterizes the onset of steady-state anode operation. Here, the performance fluctuations have been established to their full extent, according to the experimental conditions and the species being oxidized.

The anode potential will change from its minimum to its maximum value according to a set pattern. This pattern can be used to define differences in the behavior of various fuels of interest in terms of frequency and amplitude of performance cycling (see following section: Results and Discussion).

As time goes on, various modes of degradation occur (e.g. progressive catalyst inhibition by a relatively non-reactive ad-layer, or structural degradation of the anode). These may be responsible for observable changes in the characteristics of performance cycling. It sometimes appears that these changes are auto-compensatory in nature; thus, a certain increase in frequency is associated with a decrease in amplitude and vice-versa. This latter observation, however, is only of a tentative nature at our present state of knowledge.

It should be noted that this report summarizes cycling differences, between various species, in terms of the characteristics of period IV and the combined periods (I + II + III) as defined above. Certainly further elaboration is possible, whenever warranted, in terms of individual differences in the characteristics of periods I, II, and III.

#### B. Processing and Significance of the Experimental Data

The high-loading unsupported platinum anodes used in the present work, while sufficiently active catalytically to yield meaningful results, at least on a comparative basis, present the drawback of structural variance with time. This variance is sufficiently severe to make it necessary not to consider the "last-stage" data for comparison purposes since they are often influenced by high rates of electrolyte leakage through the anode.

Two methods of data interpretation were used:

- 1) Use of available polarization curve data to define various performance points (e.g. anode potential at given current densities) at various chronological

stages; say, at the beginning and at the end\* of a run. These are, essentially, extent-of-degradation data.

2) Averaging of cycling data, from recorder traces, and graphical representation of the resulting changes of performance with time. These are the typical life test curves, supplying information on the total life for a set of pre-determined conditions, as well as the individual durations of the various periods of operation (induction, ripple, etc.).

## Results and Discussion

### A. n-Octane

Seven anodes were tested with pure n-octane in order to establish a reliable frame of reference for the results obtained with various fuel mixtures. Table 1 lists a variety of averaged performance data for n-octane; the ranges of values from which the averages were calculated are given in parentheses. The broad band in Figure 2 is a graphical representation of the change in anode potential with time for six of the seven anodes, based on an averaging of the cycling performance as described in the experimental section. The boundaries of the band represent the range of anode performance for the electrodes tested. The abrupt break in the curve after the initial several hours is an indication of the onset of steady-state operation (cycling).

Table 2 summarizes the cycling characteristics observed with n-octane. The numbers marked in parentheses in the fourth column represent the time intervals during which the reported frequencies were observed. The range of frequency values are arranged chronologically with the left-hand figures representing the beginning of the measured period and the right-hand figures, the end. Some resistive load operational data is also included for comparison purposes.

The relationship between current density and time-to-cycle, at constant-current conditions, follows an exponential behavior previously described (2) with the log (time to cycle) decreasing as the current density increases.

The frequency of cycling appears to indicate a trend towards higher values at higher current densities while the amplitude does not exhibit any significant trend. It is interesting to note that, under resistive load conditions, the amplitude does not appear to be different from that at constant current (common basis of comparison: 30 ASF), although the current varies as well. The averaged anode potential is higher, though, indicating that simultaneous current and voltage cycling might have a deleterious effect on performance.

Regarding the time-to-cycle values (Column 3 in Table 2), equivalent to periods I + II + III, it is interesting to note that the ripple period (II)

\* Note that the end-of-run data are not to be confused with the previously mentioned "last-stage" data; the end-of-run data are obtained before the electrode degrades to a point where high rates of electrolyte leakage can occur.

Table 1

Average Life Test Data for n-Octane Oxidation at 350°F

(Ranges of values corresponding to the averages are marked in parentheses.)

Electrolyte: 95-98% H<sub>3</sub>PO<sub>4</sub> Anode: 35 mgms Pt/cm<sup>2</sup>  
Life: 190 hours (150-405)

Cause of test termination:	Excessive anode leakage
Initial anode resistance:	6 mΩ (0.004-0.008)
Initial IR-included anode potential at 30 ASF:	0.436 v (0.380-0.470)
Final IR-included anode potential at 30 ASF:	0.504 v (0.455-0.600)
Rate of decay of potential:	approx. 0.45 mv/hr (0.100-0.870)
Initial IR-included power output at 30 ASF:	12.7 WSF (11.4-13.5)
Initial IR-included power output at 60 ASF:	18.4 WSF (15.6-20.4)
Final IR-included power output at 30 ASF <sup>*</sup> :	11.2 WSF (8.7-11.4)
Final IR-included power output at 60 ASF <sup>*</sup> :	13.3 WSF (7.8-15.6)

\* The pre-activation procedure described in the Experimental Section was used prior to obtaining these data.

included therein was at times negligibly small, while at other times it contributed significant portions to the total reported time interval (e.g. 2-3 hours at 30 ASF). The onset-of-cycling period (III) was often indistinguishable from the actual cycling period (IV).

#### B. Normal Octane with Single Additives

A comparison of the life test summaries in Tables 1 and 3 indicates that there are no significant performance differences in the cycling period for the octane + 1% aromatic and octane + 3% olefin data as compared to pure octane. These similarities can be seen more clearly in Figure 2 where the performance-time curves for the fuels containing olefins and aromatics fall within the n-octane band. It can also be seen that anodes operating on octane + 5% naphthene fuels polarize more extensively during a relatively short initial time interval. Even after this brief interval, the performance-time curve is situated within the upper portion of the n-octane band while the latter has most of its data clustered in its lower portion.

The cycling characteristics of octane plus single additives are summarized in Table 4. The only significant differences, compared to pure octane oxidation, are the increased cycle frequencies, roughly 3 times higher, for the binary fuels.

Table 2

Cycling Characteristics for the Oxidation of n-Octane at 350°F in a  
95-98% Phosphoric Acid System

No. of Anodes Represented	Current Density, ASF	Time-to-cycle, hours	Cycle Frequency, CPH	Amplitude (potential range), mv vs H <sub>2</sub> /H <sup>+</sup> at anode	Average Anode potential vs H <sub>2</sub> /H <sup>+</sup> , mv
2 -	20	7.0	7-3 (24 hrs)	300-720	530
5 -	30	4.0	4-3 (59 hrs)**	363-750**	560
1 -	60	1.2	8-12 (4 hrs)	300-720	560
1 -	100	0.25	40-28 (4 hrs)	370-800	600
1 -	2 (1.8-2.4)	5	12-20 (35 hrs)	450-680	500
1 -	6 (5.8-6.2)	4	20-6 (24 hrs)	400-680	570
1 -	30 (28-33)	5	10	360-750	600

Note: the figures below represent some data collected for a resistive load mode of operation (cell #L.T. 142) with both current and voltage cycling.

\* Corresponding to periods I + II + III (see interpretation of the test data).

\*\* Most of the time at 3 CPH; the amplitude for 4 CPH: 385-680 mv.

Table 3

Life Test Data for the Oxidation of n-Octane with Single Additives  
at 350°F in a 95-48% Phosphoric Acid System

Anode: 35 mgms Pt/cm<sup>2</sup>

Cell No.	Mole % Fuel Additive to n-octane	Time, hours	C. D., <sup>*</sup> ASF	P. D., <sup>*</sup> WSF	Life, <sup>**</sup> hours	Anode Res., <sup>†</sup> ohms	Anode/H <sub>2</sub> Ref Potential, volts
	<u>Olefins</u>						
145	3% 2-Methyl butene-1	1	30	14.4	80	0.009	0.400
		79	60	21.0			0.480
			30	12.9			0.430
			60	15.7			0.505
146	3% Octene-2	1	30	13.8	391	.008	0.440
		382	60	19.8			0.510
			30	12.9			0.410
			60	17.4			0.490
151	3% 2-Methyl butene-1	1	30	12.6	215	.007	0.440
		215	60	15.6			0.460
			30	11.1			0.455
			60	12.9			0.540
	<u>Aromatics</u>						
147	1% 1, 2, 4 Trimethylbenzene	1	30	12.6	94	.003	0.440
		55	60	12.0			0.610
			30	9.3			0.640
			60	0.0	+1.00		
149	1% Toluene	1	30	11.4	387	.006	0.455
		387	60	16.8			0.480
			30	9.1			0.500
			60	10.5			0.580
157	1% 1, 2, 4 Trimethylbenzene	2	30	13.2	242	.007	0.395
		235	60	19.8			0.440
			30	11.7			0.470
			60	18.0			0.490
	<u>Naphthenes</u>						
143	5% Methylcyclohexane	1	30	12.5	144	.003	0.440
		33	60	18.0			0.500
			30	9.0			0.540
			60	0.0			+1.000
156	5% Methylcyclohexane	1	30	12.6	195	.008	0.465
		194	60	18.6			0.510
			30	9.8			0.555
			60	12.0			0.635

\* Data from polarization curves.

\*\* Actual duration of test before excessive anode leakage required shut-down of the cell.

Table 4

Cycling Characteristics for n-Octane with Single Additives at 30 ASF  
at 350 °F in a 95-98% Phosphoric Acid System

Anode: 35 mgms Pt/cm<sup>2</sup>

Fuel	Time-to-Cycle hours	f/(Amplitude)/time <sup>2</sup> CPH/(mv)/hours	Avg. Anode Potential (IR-included), mv vs H <sub>2</sub> /H <sup>+</sup>
<u>Olefin Additives</u>			
3 m/o 2-methylbutene-1	4.0	24/(250-710)/22	505
3 m/o 2-methylbutene-1	3.0	5/(330-730)/23	560
3 m/o 2-methylbutene-1	4.5	5/(340-730)/75	560
<u>Aromatic Additives</u>			
1 m/o Toluene	4.0	5/(400-750)/25	550
1 m/o 1, 2, 4 Trimethyl- benzene	4.5	6/(360-750)/28	590
<u>Naphthene Additives</u>			
5 m/o Methylcyclohexane	4.0	12/(350-720)/15	580
5 m/o Methylcyclohexane	0.6	9/(300-690)/24	580

### C. Normal Octane with Several Additives

It has been shown (3) that there is no cumulative effect for multiple additions of "unreactives" up to a total of 11 mole % additives. It was shown, in fact, that the performance penalty roughly corresponded to the "worse offender."

A summary of the life-test data for fuels containing several additives is given in Table 5. The fuels are listed in order of increasing concentration of additives.

Figure 3 represents performance-time data for four cells operated on mixtures of 50/50 normal and iso-octane\* containing 11 mole % additives (1% aromatic, 5% naphthene, 5% olefin). It is seen that there is first a sharp increase in anode potential to a value of about 0.575 volt where the potential finally stabilizes. Comparison of this curve with the octane data given in Figure 2 indicates that the multi-component fuel data fit within the upper portion of the n-octane band. The approximately 40 mv penalty over the performance of pure n-octane, based on the 5% naphthenes being the "worse offender" under these conditions is substantiated by these graphical representations. This is due to the fact that most of the n-octane results fall within the lower portion of the performance-time band while the multi-component data are clustered close to the upper limit.

The situation appears to become different for higher amounts of additives. Two cells operating on 50/50 n + i-octane containing 26% additives (1% aromatic, 5% olefins, 5% cyclohexanes, 15% cyclopentanes) were life tested. The variation of the anode potential with time is shown in Figure 4. When the data given in this figure is compared with the octane data in Figure 1 it appears that there is at least a 40 mv anode potential increase above the upper limit of the octane data band (i.e. 40 mv higher than what the "worse offender" would normally show). This performance difference could be due either to the presence of methylcyclopentane or to the high total amount of additives. It is expected that these aspects will be clarified in future work.

The balance of Table 5 is a summary of the life test data where increasing amounts of the "unreactive" components were added to the fuel. The data is shown diagrammatically in Figure 4 and 5. Since these concentrations of "unreactives" were not studied on a short term basis the discussion of these results will be deferred until this data is on hand. However, it is evident that sizeable performance penalties are paid when the unreactive concentrations reach such high levels (greater than 11%). It can be seen that when successive amounts of "unreactive" compounds are added the performance penalty increases until the deviation from n-octane reaches about 180 mv\*\* (~50% of the cell output IR included). This performance drop occurs within the first 25 hours of operation, where effects of anode deterioration are minimal. Figure 6 is a graphic representation of the

---

\* It has been previously shown (3) that there are no performance differences between anodes operating on n-octane and on n-octane + i-octane mixtures.

\*\* Note that the detrimental effect of octene-1, as compared to octene-2 particularly obvious with high amounts of additives (30 mole %).

Table 5

Multiple Addition Performance of a 50/50 n + iso-Octane Based Fuel at 350°F  
in 95-98% Phosphoric Acid System

Anode: 35 mgms Pt/cm<sup>2</sup>

Fuel	Time, hours	C.D., <sup>o</sup> ASF	P.D., <sup>o</sup> WSF	Life, <sup>oo</sup> hours	Anode/H <sub>2</sub> Ref Potential, volts	Anode Res., ohms
<u>11% Additive</u> (4 cells)	1	30	11.5	207	0.474	0.007
		60	15.3		0.533	
1 Toluene	174	30	3.9		0.750	
5 Octene-2						
5 M.C.H.		60	0.0		1.00 + (anode polarized)	
<u>24% Additive</u> (2 cells)	1	30	11.6	75	0.477	0.008
		60	16.3		0.538	
1 Toluene	74	30	0.0		1.00 + (anode polarized)	
5 Octene-2			60	0.0		1.00 + (anode polarized)
5 M.C.H.						
15 M.C.P.						
<u>30% Additive</u> (2 cells)	1	30	10.3	165	0.495	0.010
		60	12.3		0.560	
5 Toluene						
5 Octene-2						
5 M.C.H.						
15 M.C.P.						
(Both cells overtemperated > 370°F during initial 24-hour test period)						
<u>30% Additive</u> (1 cell)						
5 Toluene	1	30	6.3	38	0.640	0.010
5 Octene-1			60	4.5		
5 M.C.H.	38	20	4.0		0.680	
15 M.C.P.			30	0.0		1.00 +
<u>36% Additive</u> (2 cells)	1	30	7.6	103	0.628	0.008
		60	6.6		0.708	
1 Toluene	103	30	0.8		0.900	
5 Octene-2			60	0.0		1.00 + (anode polarized)
5 M.C.H.						
25 M.C.P.						
<u>50% Additive</u> (1 cell)	1	30	9.0	190	0.530	0.008
		60	10.3		0.620	
5 Toluene	187	10	3.2		0.610	
5 Octene-2			30	0.0		1.00 + (anode polarized)
10 M.C.H.						
30 M.C.P.						
<u>55% Additive</u> (2 cells)	1	30	7.7	110	0.645	0.006
		60	8.4		0.700	
5 Toluene	110	5	1.25		0.720	
10 Octene-2			10	0		1.00 +
10 M.C.H.						
30 M.C.P.						
<u>35% Additive</u> (1 cell)	1	30	7.8	95	0.585	0.006
		60	10.2		0.610	
10 Toluene	95	0	0.0		1.00 + (anode polarized)	
5 Octene-2						
5 M.C.H.						
15 M.C.P.						

M.C.P. = methylcyclopentane  
M.C.H. = methylcyclohexane

<sup>o</sup> From polarization curves.

<sup>oo</sup> Actual duration of test before excessive anode leakage or performance below 5.0 WSF dictated test termination.

decrease in current density, at a given polarization, with increasing amounts of the "unreactive" components. It should be noted that the current densities are normalized in terms of real B.E.T. surface areas measured on the pure electrodes. The spread of the data increases at higher concentrations of "unreactives."

The cycling characteristics of these multi-component fuels are shown in Table 6. The numbers in parentheses have the same meaning as described for Table 2.

These results were averaged for operation at 30 ASF. The frequency and amplitude of cycling does not appear to exhibit any of the trends reported for n-octane and n-octane with single additive mixtures. In fact, there are no appreciable changes of the frequency of cycling with time.

### Conclusions

Information regarding the influence that various hydrocarbon additives have on the short-term performance of an octane anode, cannot necessarily be applied towards predictions of long-term performance in that any detrimental additive effects noticeable during a short run may become insignificant in the context of real fuel cell operation, proceeding for extended periods of time.

However, while several additives do not necessarily have to affect performance on a cumulative detrimental basis, beyond a certain quantity limit and for extended durations of operation, the overall decrease in anode performance can be intolerably severe.

The cycling characteristics associated with the process of direct electrochemical oxidation of hydrocarbons can be described in terms of several distinct modes of performance fluctuation prior to the establishment of steady-state conditions.

This descriptive refinement can be quite useful as a semi-quantitative tool for the definition of operational differences in the expected oxidation process, as caused by a variety of additives to a base fuel.

### Acknowledgement

The authors acknowledge the financial support of this work by U.S. Army Engineer Research and Development Laboratories, Ft. Belvoir, Virginia.

### References

1. Technical Summary Report No. 5, Hydrocarbon-Air Fuel Cells, January 1964-June 1864, ARPA Order No. 247, Contract Nos. DA-44-009-ENG-009-ENG-479(T).
2. ibid., Report No. 5, p. 4-145
3. ibid., Report No. 9, p. 2-107 ff.

Table 6

Cycling Characteristics for n-Octane with Multiple Additives at 30 ASF  
at 350°F in a 95-98% Phosphoric Acid System

Anode: 35 mgrms Pt/cm<sup>2</sup>

Fuel	Time-to-Cycle, hours	i(Amplitude) CPH/(volts)	Avg. Anode/H <sub>2</sub> Ref. volts
1 Toluene, 5 octene-2, 5 MCH*	5	15(446-662)-11(415-685)	0.595
1 Toluene, 5 octene-2, 5 MCH, 15 MCP	6	19(525-675)-17(500-700)	.640
1 Toluene, 5 octene-2, 5 MCH, 25 MCP	1	12(485-685)-10(435-720)	.655
5 Toluene, 5 octene-2, 5 MCH, 15 MCP	10	10(543-720)-12(445-745)	.645
5 Toluene, 5 octene-2, 10 MCH, 30 MCP	3	11(560-750)-9(420-820)	.710
5 Toluene, 10 octene-2, 10 MCH, 30 MCP	1	10(500-720)-15(450-760)	.725

\* MCH - Methylcyclohexane.

MCP - Methylcyclopentane.

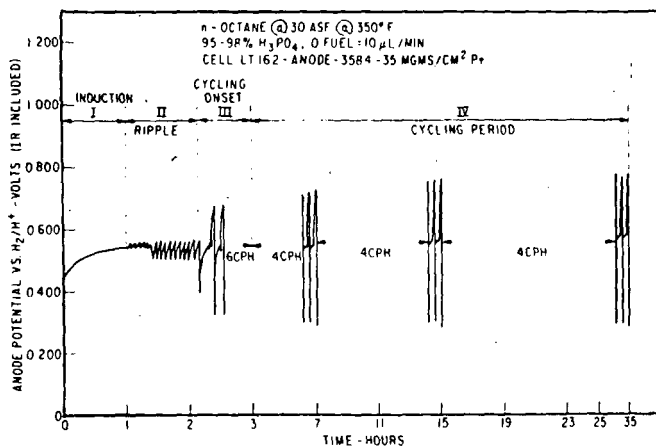


Figure 1 Typical Anode Performance at Constant Current Over Extended Time Periods.

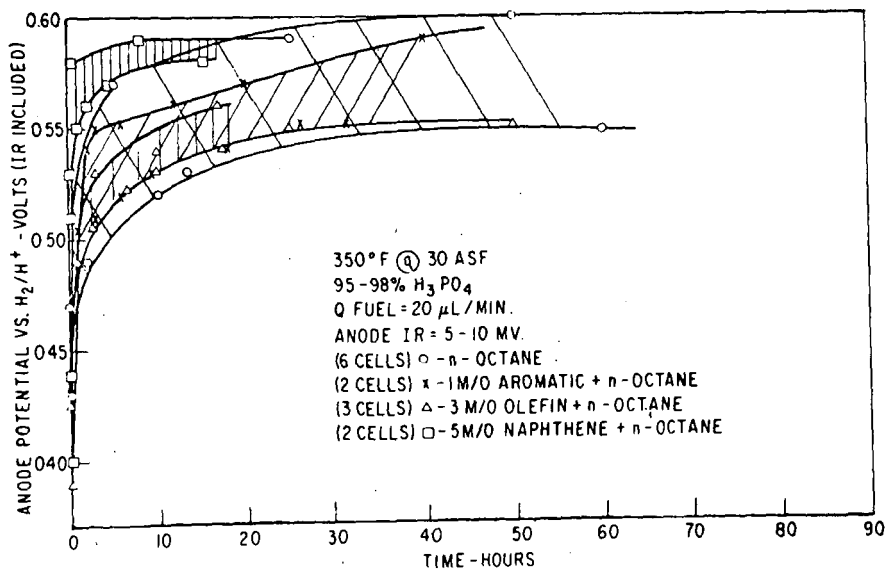


Figure 2 Change of Anode Potential with Time.

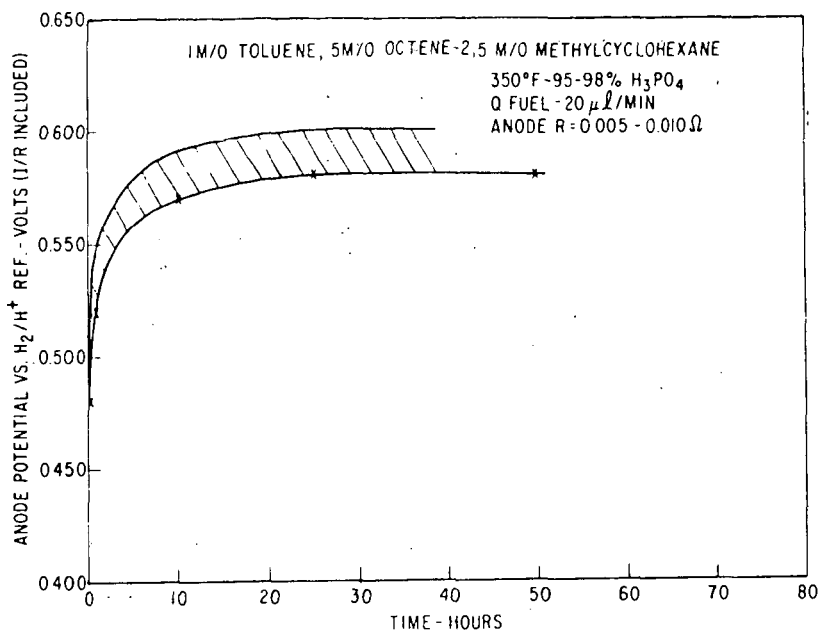


Figure 3 Change of Anode Potential with Time (Unsupported Anode: 35 mgms Pt/cm<sup>2</sup>).

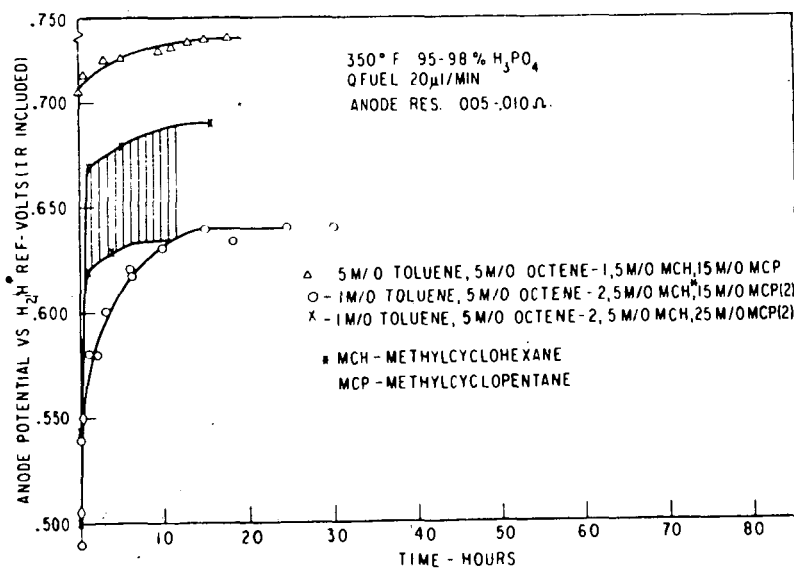


Figure 4 Change of Anode Potential with Time (Unsupported Anode: 35 mgms Pt/cm<sup>2</sup>).

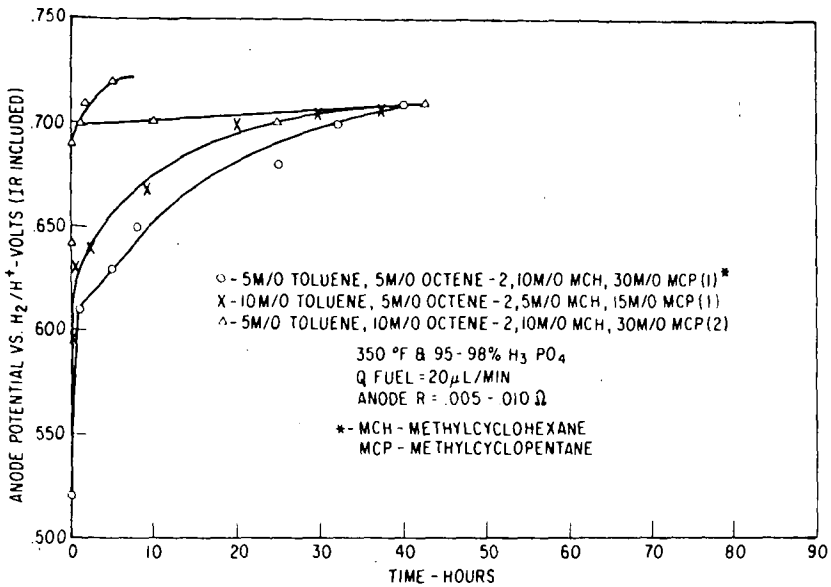


Figure 5 Change of Anode Potential with Time (Unsupported Anode: 35 mgms Pt/cm<sup>2</sup>).

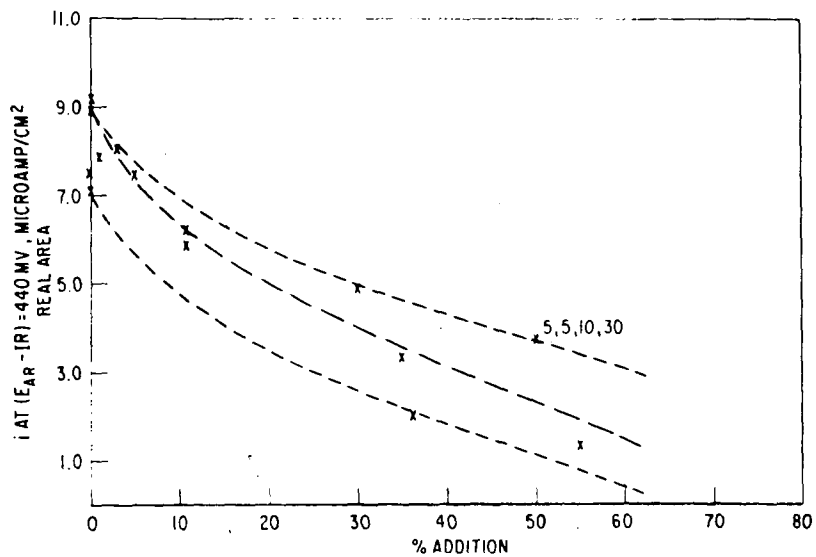


Figure 6 True Current Densities as a Function of the Total Amount of Additives.

ELECTROCHEMICAL STUDIES OF THE SODIUM-BISMUTH SYSTEM\*

M. S. Foster, G. H. McCloud, and E. J. Cairns

Argonne National Laboratory  
9700 South Cass Avenue  
Argonne, Illinois  
60439Introduction

Studies of various thermally regenerative galvanic cell systems have been underway at Argonne National Laboratory for some time. In these systems, thermal energy, as from a nuclear reactor, is used to decompose the products of a power-producing galvanic cell to form into the original reactants for re-use in the cell. Since the cell generally operates at a lower temperature than the decomposition temperature of the cell products, the system is a two-temperature system and is limited to Carnot cycle efficiency.

The search for materials which combine with a large negative Gibbs free energy change at the cell temperature, and yet may be thermally decomposed at a temperature obtainable in a reactor using today's technology, has led to an examination of various alkali metal-containing binary alloys. Many of these alloys have a large negative free energy of formation, as indicated qualitatively by the high melting points of the compounds formed between the lighter alkali metals, and, for example, bismuth.

In order to predict the ideal behavior of a thermally regenerative galvanic cell system, it is necessary to know the thermodynamic properties of the alloy used in the cell. For instance, the chemical potential of the alkali metal in the binary alloy is used to calculate the open-circuit potential of the cell in the system if the cell is a concentration cell without transference. Likewise, the temperature variation of the chemical potential of the alkali metal in the alloy may be used to calculate the partial pressure of the alkali metal over the alloy for various postulated regeneration conditions. The particular alloy which is the subject of this report is the sodium-bismuth alloy.

In a study of the thermodynamic properties of the binary sodium-bismuth alloy, the most obvious method would appear to be an emf technique. This technique corresponds directly to the cell in a regenerative system.

In using the emf technique, one may choose to operate cells which by design are not capable of producing significant electrical currents. For example, several workers in the past have operated cells with sodium anodes in which the electrolyte consisted of a sodium ion-containing glass. Other electrolytes which might be used include mixtures of molten sodium salts or a solid sodium salt. The cell-potential data reported here were taken using electrolytes of solid NaCl.

Although power-producing cells may well use molten salt electrolyte, the solubilities of sodium metal from the anode and of sodium-bismuth intermetallic species from the cathode alloy are sufficiently high to introduce complications when attempting to make thermodynamic measurements<sup>1</sup>. These complications take several forms. First, the sodium metal dissolved in the electrolyte near the anode tends to diffuse toward the cathode. At the cathode, the sodium is extracted from the electrolyte by the cathode alloy. The result is a transfer of sodium from the anode to the cathode without producing any current in the external circuit,

---

\* This work was performed under the auspices of the United States Atomic Energy Commission.

causing a constant change in the cathode composition of the cell. Second, the solution of sodium in the electrolyte is a "mixed" electrical conductor, that is, it has both ionic and electronic conductivity. This results in a lowering of the open-circuit potential by causing an internal short circuit in the cell. Third, there exists the possibility of back-diffusion of bismuth from the cathode alloy to the anode through the solubility of intermetallic species in the electrolyte. For these reasons, solid NaCl electrolytes were used in the cells reported here.

### Experimental Studies

Since the sodium metal itself and the sodium-bismuth alloys are subject to attack by water vapor and oxygen, all of the cells were operated in furnace wells attached to an inert atmosphere enclosure containing helium. The helium was continuously recirculated through a purification system and contained as impurities less than 1.5 ppm water vapor, and less than 5 ppm each of oxygen and nitrogen.

Electrolytes were obtained from Harshaw Chemical Company in the form of cups with 1/8-in. thick walls and bottoms. These were machined from single crystals of NaCl. The sodium anode was contained inside the cup electrolyte, which was in turn lowered into the liquid sodium-bismuth alloy. Tantalum rods were used as electrode contacts. Cell potentials were measured with a potentiometric electrometer having an input impedance of  $10^{13}$  ohms. Forward and reverse current-voltage curves were measured by passing small currents through the cell. The current-voltage relationship so obtained was linear for cell temperatures between 810 and 1050°K. At a cell temperature of 523°K, the internal cell impedance was approximately  $2.2 \times 10^7$  ohms, indicating the requirement of an electrometer or similar device for measuring the cell potential. At higher temperatures, approaching 1050°C, the internal cell resistance dropped to  $\sim 300$  ohms.

### Results

It was found necessary to add a small correction to the raw cell potential-temperature-composition data in order to compensate for the "mixed" ionic and electronic conductivity in the electrolyte. Sodium may dissolve in the solid electrolyte in contact with the sodium anode. These dissolved atoms may dissociate into sodium ions (which may be located in cation vacancies) and electrons, at least some of which are located in F-centers (or anion vacancies). The electronic conductivity could arise from the thermal excitation of electrons in F-centers into conduction bands.

The correction terms was found by comparing the voltage of the experimental cell:  
 $\text{Na}(\ell)\text{NaCl}(\text{s})/40 \text{ a/o Na in Pb}(\ell)$   
 as a function of temperature with both emf data from the literature and with the emf calculated for 700°C from vapor pressure measurements. Previous concentration cell studies using the Na-Pb system have been reported by Hauffe and Vierk<sup>2</sup> (in 1949) and by Lantratov<sup>3</sup> (in 1959). These investigators used glass electrolytes containing sodium oxide. Their results are in agreement with those reported in 1956 by Porter and Feinleib<sup>4</sup>, who used an electrolyte of alumina impregnated with sodium carbonate. A. K. Fischer<sup>5</sup> of Argonne determined the vapor pressure of Na over a 40 a/o Na in Pb alloy held at 700°C. From his measurement, the cell emf was calculated to be  $\sim 8$  mv higher than that reported by Feinleib and Porter. The correction term for the cell potentials observed using solid NaCl as the electrolyte ranged from 4 mv at 400°C to 36 mv at 700°C. The corrected cell potential-temperature-composition data for the sodium-bismuth cells are shown in Figure 1.

### Discussion

The data in Figure 1 clearly reflect that when a cell with a cathode alloy containing 30 to 40 a/o Na in Bi is cooled, a solid starts to precipitate from the liquid alloy as evidenced by the change in slope of the emf vs temperature curves. This is predicted, of course, from the phase diagram. Using the data of Figure 1, the corresponding excess chemical potentials of sodium have been calculated for the liquid Na-Bi alloys. These data were then treated by a least-squares technique

to find an expression for the excess chemical potential of sodium in liquid sodium-bismuth alloys as a function of temperature and composition. The best fit was obtained by assuming a quadratic dependence of excess chemical potential on both temperature and composition -- a subtle way of saying that nine coefficients are necessary to describe the excess chemical potential surface (see Equation 1 and Table 1).

$$\Delta\mu_{\text{Na}}^E = \sum_{i=1}^3 \sum_{j=1}^3 C_{ji} T^{j-1} X_{\text{Na}}^{i-1} \quad (1)$$

Other thermodynamic quantities for sodium-bismuth alloys may be calculated from the equation for the excess chemical potential of sodium, using the standard thermodynamic relationships.

Using the cell potential surface calculated from the equation:

$$E = \frac{-1}{F} \Delta\mu_{\text{Na}} = \frac{1}{F} \left[ RT \ln X_{\text{Na}} + \sum_{i=1}^3 \sum_{j=1}^3 C_{ji} X_{\text{Na}}^{i-1} T^{j-1} \right] \quad (2)$$

one may calculate the composition,  $X_{\text{Na}}$ , at a given temperature, for which E is the same as that observed for cells in which the cathode alloy was saturated with a solid intermetallic compound -- either NaBi or Na<sub>3</sub>Bi. This composition-temperature relationship is the usual phase diagram, and the points calculated are shown in Figure 2, compared with the phase diagram published in Hansen and Anderko<sup>6</sup>. The compositions and cell potentials calculated were used, along with the equation for the excess chemical potential, to calculate the standard free energy of formation of solid NaBi and Na<sub>3</sub>Bi, assuming pure liquid Na and Bi as the standard states. These are compared in Table 2 with those reported previously<sup>7</sup> for solid Li<sub>3</sub>Bi. It is to be noted that the sodium-bismuth interaction is significantly lower in energy than the interaction between lithium and bismuth.

Table 1.  
Coefficients Used in Evaluating  $\Delta\mu_{\text{Na}}^E$  from Equation 1.

$C_{ji}$	$i = 1$	$i = 2$	$i = 3$
$j = 1$	-7454.10	-14928.3	6227.26
$j = 2$	-17.7422	25.5126	37.9301
$j = 3$	.0113414	-.000940211	-.0435859

Table 2.  
Standard Free Energies of Formation of Li<sub>3</sub>Bi, NaBi, and Na<sub>3</sub>Bi

Standard Free Energy of Formation* (kcal/mole) of:			
T (°K)	Li <sub>3</sub> Bi	NaBi	Na <sub>3</sub> Bi
550		-15.4	-
600		-15.0	-
650		-14.7	-
700		-14.4	-
750		-	-36.1
800	-50.5	-	-34.6
850	-49.7	-	-33.4
900	-48.8	-	-32.6

\* Standard states were chosen to be the pure liquid elements and the solid compounds in the cell environment.

#### References

1. M. S. Foster, "Laboratory Studies of Intermetallic Cells", in C. E. Crouthamel, ed., "Thermally Regenerative Galvanic Cells", to be published.
2. K. Hauffe and A. L. Vierk, Z. Elektrochem., **53**, 151 (1949).
3. M. F. Lantratov, Russian J. Inorg. Chem., **4**, 927 (1959).

4. B. Porter and M. Feinleib, J. Electrochem. Soc., 103, 300 (1956).
5. A. K. Fischer, to be presented at the Spring, 1967 ACS Meeting.
6. M. Hansen and K. Anderko, "Constitution of Binary Alloys", McGraw-Hill Book Co., Inc., New York, N. Y., 1958, p. 322.
7. M. S. Foster, S. E. Wood, and C. E. Crouthamel, Inorg. Chem., 3, 1428 (1964).

Figure 1.  
CORRECTED POTENTIALS FOR THE CELL:  
 $\text{Na}(l)/\text{NaCl}(s)/\text{Na}$  in Bi as a Function of Temperature.

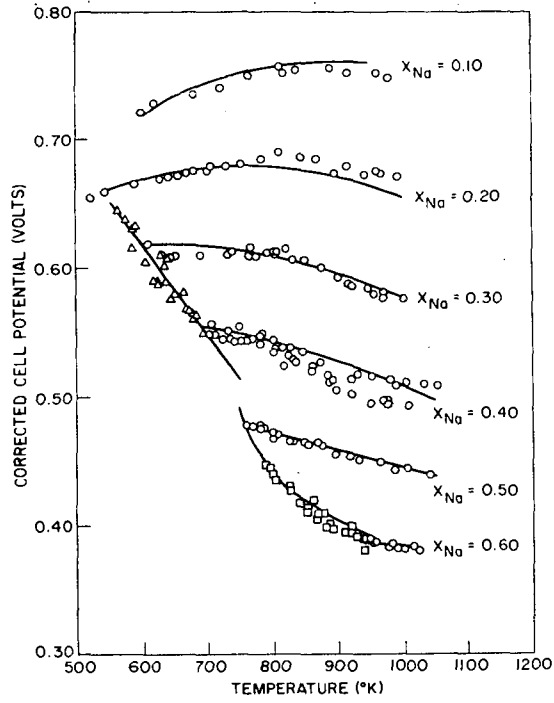
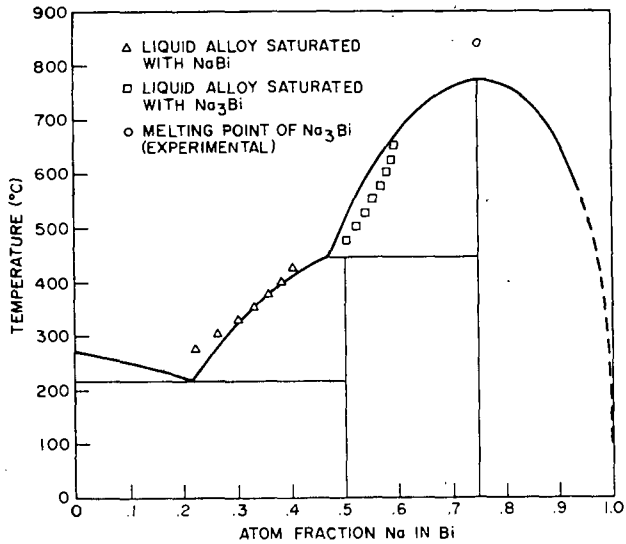


Figure 2.  
COMPARISON OF CALCULATED SATURATION CONCENTRATIONS  
WITH PUBLISHED PHASE DIAGRAM<sup>6</sup>.



## MEMBERSHIP IN THE DIVISION OF FUEL CHEMISTRY

The Fuel Chemistry Division of the American Chemical Society is an internationally recognized forum for scientists, engineers and technical economists concerned with the conversion of fuels to energy, chemicals, or other forms of fuel. Its interests enter on the chemical problems, but definitely include the engineering and economic aspects as well.

Any chemist, chemical engineer, geologist, technical economist, or other scientists concerned with either the conventional fossil fuels, or the new high-energy fuels--whether he be in government, industry or independent professional organizations--could benefit greatly from participation in the progress of the Fuel Chemistry Division.

The Fuel Chemistry Division offers at least two annual programs of symposia and general papers, extending over several days, usually at National Meetings of the American Chemical Society. These include the results of research, development, and analysis in the many fields relating to fuels which are so vital in today's energy-dependent economy. Members of the Division have the opportunity to present papers of their own, or participate in discussions with experts in their field. Most important, the Fuel Chemistry Division provides a permanent record of all of this material in the form of complete preprints.

Starting in September 1959, the biennial Fuel Cell Symposia of the Division have been the most important technical meetings for chemists and chemical engineers active in this field. These symposia have all been published in book form. The recent landmark symposium on Advanced Propellant Chemistry has been published in book form also. Further, the Division is strengthening its coverage of areas of air and water pollution, gasification, and related areas.

In addition to receiving several volumes of preprints each year, as well as regular news of Division activities, benefits of membership include: (1) Reduced subscription rates for "Fuel" and "Combustion and Flame," (2) Reduced rates for volumes in the "Advances in Chemistry Series" based on Division symposia, and (3) The receipt card sent in acknowledgment of Division dues is good for \$1.00 toward a complete set of abstracts of all papers presented at each of the National Meetings.

To join the Fuel Chemistry Division as a regular member, one must also be or become a member of the American Chemical Society. Those not eligible for ACS membership because they are not practicing scientists, engineers or technical economists in areas related to chemistry, can become Division Affiliates. They receive all benefits of a regular member except that they cannot vote, hold office or present other than invited papers. Affiliate membership is of particular value to those in the informational and library sciences who must maintain awareness of the fuel area. Non-ACS scientists active in the fuel area and living outside of the United States are invited also to become Division Affiliates.

Membership in the Fuel Chemistry Division costs only \$4.00 per year, or \$11.00 for three years, in addition to ACS membership. The cost for a Division Affiliate, without joining ACS, is \$10.00 per year. For further information, write to:

Dr. Frank Rusinko, Jr.  
Secretary-Treasurer  
ACS Division of Fuel Chemistry  
c/o Speer Carbon Company  
St. Marys, Pennsylvania 15857  
Telephone: 814 - 834-2801

## TRACERLAB

A DIVISION OF LABORATORY FOR ELECTRONICS, INC.

### EXCITED GAS RESEARCH AND TECHNOLOGY

Tracerlab has pioneered in programs involving generation and utilization of low temperature plasmas employing electrodeless discharges at radio frequencies. This field of research and development is defined as Excited Gas Research and Technology. The programs at Tracerlab have been based on research investigations, and have resulted in many technological applications and the development of specialized instrumentation. The electrodeless method is free of contamination by consumable electrodes, provides a uniform volume of excited reactive gas, and requires only "soft" vacuum engineering design.

Systems studied to date have included both organic and inorganic systems in the following areas:

- Homogeneous gas reactions at discharge conditions.
- Gas-solid reactions.
- Reactions involving solids of different physical disposition, such as ultrafine sub-micron powders.
- Treatment of solid sheets of metals or polymers.
- Reactions producing products in the gas phase.
- Reactions for effecting synthesis.
- Reactions for reducing organic media to residual inorganic ash.
- Flow discharge configurations for spectrographic studies.

IN ADDITION TO RESEARCH AND DEVELOPMENT SERVICES, THE FOLLOWING EQUIPMENT\* IS AVAILABLE:

- RF Generators - 300, 2,000 and 5,000 RMS Watts - Variable Output
- Plasma Activators - Inductive and Capacitive Coupling
- Plasma Research System - 300 RMS Watts - Variable Output
- Low Temperature Asher - LTA-600

\*All equipment operates at FCC - approved frequency - 13.56 megacycles.

For Additional Information, Please Call or Write:

Mr. James Robinson  
Product Manager, Plasma Technology  
TRACERLAB/WEST  
2030 Wright Avenue  
Richmond, California 94804  
Telephone: 415-235-2633

RECENT FUEL DIVISION SYMPOSIA

Volume	Title	Presented At
Vol. 8, No. 1	Symposium on Gas Generation General Papers	Philadelphia, Pa. April, 1964
Vol. 8, No. 2	Symposium on Chemical Phenomena in Plasmas Symposium on Kinetics and Mechanisms of High Temperature Reactions	Philadelphia, Pa. April, 1964
Vol. 8, No. 3	Symposium on Pyrolysis and Carbonization of Coal Symposium on Mineral Matter in Coal	Chicago, Illinois August, 1964
Vol. 9, No. 1	Symposium on Advanced Propellant Chemistry*	Detroit, Michigan April, 1965
Vol. 9, No. 2	Symposium on Fuel and Energy Economics General Papers	Detroit, Michigan April, 1965
Vol. 9, No. 3 Parts 1 & 2	Symposium on Hydrocarbon-Air Fuel Cells**	Atlantic City, N. J. September, 1965
Vol. 9, No. 4	Symposium on Coatings Based on Bituminous Materials General Papers	Atlantic City, N. J. September, 1965
Vol. 10, No. 1	Symposium on Fossil Fuels and Environmental Pollution Joint with the Division of Water, Air, and Waste Chemistry	Pittsburgh, Pa. March, 1966
Vol. 10, No. 2	Symposium on Pyrolysis Reactions of Fossil Fuels Joint with the Division of Petroleum Chemistry	Pittsburgh, Pa. March, 1966
Vol. 10, No. 3	Symposium on Current Analytical Methods for Fuels Symposium on Combustion Reactions of Fossil Fuels General Papers	New York, N. Y. September, 1966
Vol. 10, No. 4	Symposium on Gasification*	New York, N. Y. September, 1966
Vol. 11, No. 1	Symposium on Electrochemical Processes	Miami, Florida April, 1967
Vol. 11, No. 2 Parts 1 and 2	Symposium on Chemical Reactions in Electrical Discharges General Papers	Miami, Florida April, 1967

\* To be published by Advances in Chemistry

\*\* Published by Academic Press Inc.

PROJECTED PROGRAMS

- Symposium on Detonations and Reactions in Shock Waves  
Joint with the Division of Physical Chemistry  
R. W. Van Dolah, Chairman  
Chicago, Illinois  
September, 1968
- Fifth Biannual Fuel Cell Symposium  
B. S. Baker, Chairman  
Chicago, Illinois  
September, 1968
- Symposium on Advances in Spectrometry of Fuels and Related  
Materials  
Joint with the Division of Analytical Chemistry  
R. A. Friedel, Chairman  
Chicago, Illinois  
September, 1968
- General Papers  
Irving Wender, Chairman  
Chicago, Illinois  
September, 1968
- Symposium on Advanced Propellant Chemistry  
R. T. Holzmann, Chairman  
San Francisco  
April, 1968
- Symposium on Oil Shale and Tar Sands  
Joint with the Division of Petroleum Chemistry, Inc.  
J. H. Gary, Chairman  
San Francisco  
April, 1968
- General Papers  
R. T. Struck, Chairman  
San Francisco  
April, 1968
- Symposium on Industrial Carbon and Graphite  
Frank Rusinko, Jr., Chairman  
Atlantic City, N. J.  
September, 1968
- Symposium on Synthetic Fuels from Coal  
E. Gorin, Chairman  
Atlantic City, N. J.  
September, 1968
- General Papers  
R. T. Struck, Chairman  
Atlantic City, N. J.  
September, 1968